# Wind Speed Profiles and Pressure Coefficients Obtained in the Wind Induced Damage Simulator for Silsoe Cube Model

by

Jaskirat Singh

Thesis submitted to the University of Ottawa
in partial Fulfillment of the requirements for the
Masters of Science

in

Civil Engineering

Department of Civil Engineering

Faculty of Engineering

University of Ottawa

Ottawa, Canada

June 2020

# Acknowledgements

I would like to thanks all those who helped and supported me during the experiment in laboratory and writing thesis.

First of all, my deepest and sincere gratitude to my supervisor Dr. Elena Dragomirescu, for giving me this precious opportunity to work under her guidance and it is my pleasure to learn a lot under her guidance. She has always been helpful and encourage me to do the work in appropriate manner.

I would like to acknowledge the help of Dr. Muslim Majeed and Dr. Gamal Elnabelsya during the experiment performed in the structure lab. I am also thankful to Ms. Paula Oppici and Mr. Luc Cloutier, who helped me in getting all the office paperwork done on time. Thanks to Junxin Wang, Ph.d candidate, Southwest Jiaotong University, Zhe Xiao, Ph.d candidate, University of Ottawa and Rajinder Singh Deol, Ph.d candidate, IIT Delhi, I have learned a lot from the knowledge and the experience they shared with me in the field of aerodynamic.

Finally, I would like to thanks my family (parents and brother), who encourage me to pursue my study in such a prestigious University and who continuously helped me during my thesis. They always supported me mentally and financially.

I am blessed to have all these wonderful people in my life.

# ABSTRACT

Hazardous winds, such as tornadoes and hurricanes, have a great impact on civil engineering structures and cause significant social and economic disturbances. The wind speed and pressure tested in the conventional wind tunnel experiments are much smaller than the actual wind speed and pressure measured in the field. Therefore, the Wind-induced Damage Simulator (WDS) was constructed at the University of Ottawa to overcome the wind speed limitations of wind tunnels and to simulate different types of wind speed profiles. WDS is an isolated cubic box with dimensions 3.65m x3.65 m and 3.0 m height, with multiple inlets on the side faces of the testing chamber and an outlet on the top side. This unique equipment creates a controlled environment for studying wind speed profiles in a confined space, by regulating the air flow with the aid of an attached industrial blower. To measure the simulated wind velocities inside the WDS and to obtain the wind speed profile in the testing chamber, Aeroprobe (12- Hole Probe) sensor was used for different combinations of opened inlets and at four different locations. The data collected from the Aeroprobe was processed by the use of the Aeroflow 2.7.5.7346 software, to get the velocity of wind in three different directions (u, v and w) and the mean velocity at a single point. After determining the mean velocity at different heights and RPM values at all four positions, Matlab software was used to determine the wind profile and the spectra of the turbulence intensities and these were compared for different heights at the four investigated locations and for various rotations per minute (RPM) values (400 to 800 RPM) for controlling the blower. Once the flow characterization was completed, the wind-induced pressure for three models of the Silsoe Cube were measured as a part of the second phase of the test. The current experiment employed 3 different scales of Silsoe cube: 1:40, 1:30 and 1:20, while the pressure coefficients were determined at 16 different points along a vertical line crossing the faces of the cube. A pressure taps system with 16 channels and a Scanivale pressure scanner were used to measure the pressure at 16 different positions on the cube. Matlab software was used to determine the pressure coefficients from the data measured by pressure taps. The pressure coefficienst for the Silsoe Cube were plotted and compared for the three different scales. Also, for determining the best scale to be used in future experiments. The pressure coefficients of the 3 different scaled model of Silsoe Cubes was compared with full-scale data reported in the literature for the same structure. Based on the results obtained from the experiments, recommendations for the best location in the testing chamber for the future experiments employing the WDS were formulated.

# Contents

# List of Tables

# List of figures

# Chapter 1 – Introduction

## 1.1 Background

The low-rise, mid-rise and high-rise buildings are designed and built in atmospheric boundary layer, thus the effects of the wind acting on such buildings are estimated as the wind-induced pressure. The wind-induced pressure varies with the wind velocity, which can be as low as to produce an insignificant effect on the structure, or it can reach extreme values that can destroy the civil engineering structures. The wind is classified based on its velocity on the scale of 0 to 12 on the Beaufort scale, which is discussed in detail in Chapter 2. Hazardous winds such as tornadoes, cyclones and hurricanes can reach up to 500 km/h and are very harmful for civil engineering structures and human lives. The impact caused by highly turbulent wind velocities can be mitigated if the civil engineering structures are designed according to the guidelines given in the building codes. The design codes for wind loads are usually estimated based on the data provided from the experiments performed in wind tunnels, which do not simulate extreme winds effects. Wind engineering experimental facilities have evolved in the recent years and their capabilities expanded towards better replicating the wind speeds profiles and turbulence characteristics encountered in the field measurements. Comparing the experimental results recorded for scaled models, with the field measurement data will always give the best indication on the wind-induced pressures acting on civil engineering structures.

## 1.2 Motivation of research

The building design codes for wind load are based on the data provided by the experiments performed in conventional wind tunnels, according to Jafrai et al, (2019). Multi-directional wind speed effects on structures are difficult to simulate in laboratory conditions, due to the lack of experimental facilities with capabilities of simulating complex wind velocity profiles. Moreover, Jafrai et al, (2019) also stated that it is very difficult to scale the low-rise civil engineering structures in conventional wind tunnels, due to which there could be a mismatch of turbulence spectra as shown in . At the University of Ottawa a new Wind-induced Damage Simulator (WDS) was constructed as part of the structures lab, to simulate the multi-directional wind velocities and to replicate complex wind flow turbulence characteristics, thus complementing the capabilities of the conventional wind tunnels. The WDS outlet/inlets arrangement is

unique, therefore careful calibration must be conducted before performing extreme winds tests on civil engineering building models.

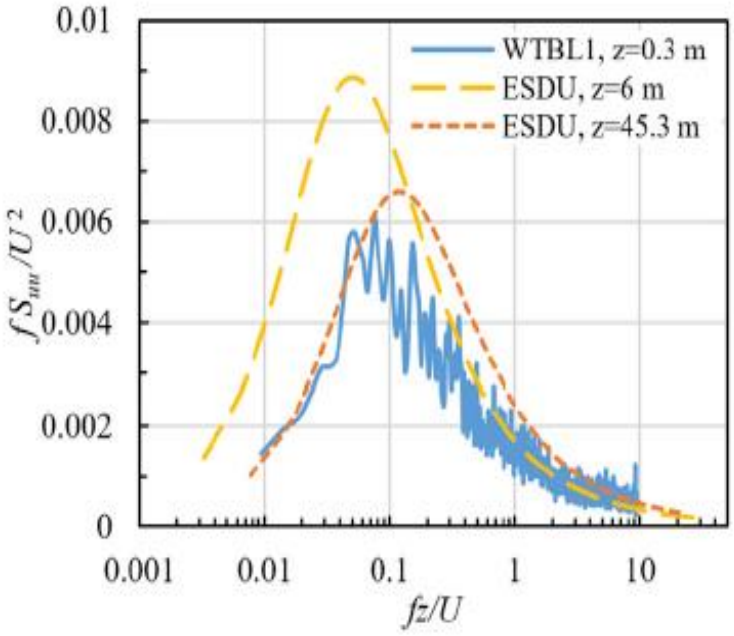


Figure 1. 1 Mismatch of turbulence spectra (Jafrai et al, 2019)

## 1.3 Research objectives

The new WDS facility is used to study the effect of multi-directional winds on civil engineering models, however the test conditions must be identified and validated before performing extensive experimental programs. The WDS facility can operate at low wind speeds, for nondestructive tests and at high wind speeds, when damage of structural models is studied. The objective of the current research is to investigate the WDS testing conditions for low wind speeds range and to validate the pressure coefficients induced by the WDS simulated winds on a standard shape model.

Therefore, to configure the WDS and to characterize the wind flows and pressure coefficients obtained in the testing chamber, the following research objectives were identified:

- Measure the vertical wind speed profiles and the turbulence spectra for different locations in the WDS, for low wind speeds range, determined by up to 800 RPM values.

- Determine the vertical wind speed profiles and the pressure coefficients for different combinations of opened inlets on the front and lateral walls.
- Compare the measured wind speed and turbulence characteristics with the field data reported in the literature and recommend the wind profile to be used for future experiments.
- Build models of three different scales for the Silsoe Cube and measure the surface pressure along the vertical center line.
- Compare the results of the current experiment with the full-scale Silsoe Cube's results, and determine the best location to place the scaled test models.
- Recommend the optimum WDS configuration for future experiments to be performed in low range wind speeds to be used for future experiments.

To achieve these research objectives, the experiments were divided into two stages, as listed below:

1. Stage A: Determination of vertical wind profiles at different locations in WDS.
2. Stage B: Determination of pressure coefficients on three different scales of Silsoe Cubes.

## 1.4 Methodology

The Wind Induced Damage Simulator (WDS) is a new wind testing facility, which was constructed at the University of Ottawa, structure lab, to complement the experimental results provided by conventional wind tunnels, with pressure coefficients induced by multi-directional winds. The current research was performed by the aid of the WDS which comprises of an isolated cubic steel box with dimensions of 3.65 m x 3.65 m and height of 3.0 m, and can simulate multi-directional wind flows by using an industrial blower. The wind flow is ensured by extracting air from the WDS box through a duct and an outlet installed on the rooftop, which produces injections of high-speed wind flows through the multiple inlets on the lateral faces. The WDS facility has five inlets on each of the lateral faces and an outlet on the roof top, connected to an industrial blower. The 12-holes Aeroprobe was employed to measure the wind speeds for 12 different directions at a point and the data provided by the Aeroprobe was processed in the Aeroflow 2 software to determine mean wind velocity and the three different components of velocity: longitudinal velocity (u), vertical velocity (w) and transverse velocity (v). The pressure coefficients at 16 different points on a vertical

central line were determined for three different scales 1:20, 1:30 and 1:40 of the Silsoe Cube model, which were computed with the help of the pressure tap system and the 1 PSID DSA3217 pressure Scanner.

The experiment was conducted for five different RPM values (400, 500, 600, 700 and 800), at five different heights (0.14 m, 0.24m, 0.34m, 0.44m and 0.54m), at four different locations and three different combinations of opening of inlets, which are discussed in Chapter 3. After the determination of the wind velocities, the vertical wind speed profiles for different locations at different RPM values were compared for determining the appropriate testing conditions. The pressure coefficients at 16 different positions for the three different scales of the Silsoe Cube model were measured for five different RPM values and were compared with each other and also with the results reported for the full-scale Silsoe Cube, constructed on a smooth flat area in Silsoe Research Institute (Richards, 2001). All the comparisons and results interpretations are discussed in Chapter 4.

## 1.5 Thesis layout

The thesis consists of five chapters, each chapter has its own significance for the research program. The Chapter 1 consists of a brief introduction of the damage caused by the wind load to the human lives and the civil engineering structures. The motivation, objective and methodology of this research are also described in Chapter 1. The detailed knowledge of the impact of wind on the civil engineering structures along with the related building design code are listed in Chapter 2. The Various previous studies related to wind load or pressure coefficients estimation on full-scale or scaled Silsoe Cube are also described in Chapter 2.

The Chapter 3, which introduces the experimental setup and configurations describes all the equpiment used during this experimental investigation in detail. The new wind testing facility the Wind Induced Damage Simulator (WDS) constructed at the University of Ottawa, structure lab, is described in detailed in Chapter 3 as well, along with the 12-hole Aeroprobe sensor which was employed to determine the wind speed profile within the WDS testing chamber. Other instruments such as pitot tubes, pressure taps, pressure scanners are also discussed in Chapter 3. The various software which were employed during the research are listed and described in Chapter 3. This chapter also includes the description of the experimental program in detail, the cases performed for the two different stages of the experimental investigation.

The Chapter 4 presents the results of all the experimental cases done as a part of this research. The vertical wind profiles of mean wind velocity at different RPM values and different cases are compared in Chapter 4. The three different components of wind velocity were also determined during the experiment, based on which the turbulence spectra were determined and compared for different locations and height in the WDS, as discussed in Chapter 4. The pressure coefficients for 16 different points and for 3 different scales (1:20, 1:30 and 1:40) of the Silsoe Cube were discussed and compared in this chapter. Chapter 4 also includes comparison of the results on the current research with the previous researches done related to this study.

The Chapter 5, which is the last chapter of the thesis, consists of all the conclusions drawn from the experiments performed during this research. The future works related to this study are also mentioned in this chapter.

# Chapter 2 – Literature Review

## 2.1 –Introduction to wind engineering

The moving air is known as wind and it is generated when there is a difference in air pressure at a place. The air tends to blow from the area of high pressure to low pressure. The velocity of the wind depends upon the difference between air pressure. Higher the difference of air pressure, higher will be the wind speed. The fastest wind speed recorded till date is 231 miles per hour (mph) in 1934 in Mount Washington during the spring storm. The Beaufort scale is employed to categorize the wind speed in 13 different categories which ranges from less than 0.5 m/s to more than 29 m/s. The Beaufort scale is described in Table 2- 1.

Table 2- 1 – Beaufort Scale (Yamaguchi,2000)

| Scale | Wind speed (m/s) | Wind Description |
|---|---|---|
| 0 | <.5 | Calm |
| 1 | 0.5-1.7 | Light airs |
| 2 | 1.7-3.3 | Light breeze |
| 3 | 3.3-5.2 | Gentle breeze |
| 4 | 5.2-7.4 | Moderate breeze |
| 5 | 7.4-9.8 | Fresh breeze |
| 6 | 9.8-12.4 | Strong breeze |
| 7 | 12.4-15.2 | Light gale |
| 8 | 15.2-18.2 | Moderate gale |
| 9 | 18.2-21.5 | Fresh gale |
| 10 | 21.5-25.1 | Strong gale |
| 11 | 25.1-29 | Destructive gale |
| 12 | >29 | Hurricane |

The wind engineering was introduced to study the effect of wind on the natural and the human built environment with the aim of minimizing the damage caused by the wind. The field of wind engineering is making use of a multitude of principles from mechanical engineering, structural engineering and applied physics. The wind engineers developed the wind design code for wind loads to minimize the damage due to heavy winds.

## 2.2 Characteristics of wind speed

The atmospheric boundary layer, where all the structures can be found, involves different wind characteristics, which are employed in wind engineering, such as vertical profile of the wind speed, the mean wind velocity and its components, direction of wind speed and turbulence and spectra of wind flow as detailed below.

### 2.2.1 Vertical profile of wind speed

The vertical profile of the wind speed or wind speed profile is the comparison of wind speeds at different heights in vertical direction. The vertical profile of wind in neutral conditions is shown in Figure 2. 1. The wind velocity at greater heights (500 or above) is almost steady and wind flows in geostrophic manner. The earth's surface exerts frictional drag on motion of air for height 50 m or less which reduces the wind speed to zero. The height between 50 m and 500m is known as transition zone, which is between the smooth geostrophic flow at greater height and turbulent flow near the ground.

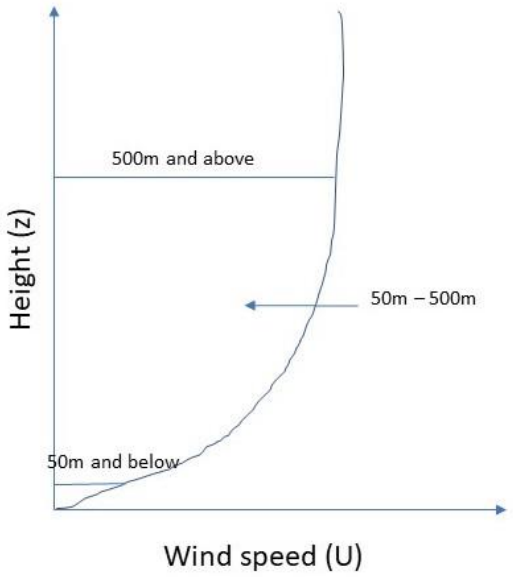


Figure 2. 1 Vertical profile of wind

### 2.2.2 Mean wind velocity and its components

Mean wind velocity (U) is the arithmetic mean of the components of wind speed in three different directions. The three components of wind velocity are longitudinal velocity (u) which is in the direction of flow of wind, vertical velocity (w) which is vertical to the flow of the wind and transverse velocity (v) which is perpendicular to flow of wind in horizontal direction. The power law is employed to estimate the wind velocity at a given height, as given by Eq (2. 1) (Yamaguchi,2000).

$$\frac{Uz}{U_R} = \left(\frac{Z}{Z_R}\right)^{\alpha} \qquad (2.\ 1)$$

where $U_Z$ is the wind velocity at height Z and $U_R$ is the known wind velocity at reference height $Z_R$. The topography of the land affects the value of α, which is an empirically derived coefficient. The values of α are as follow:

- For open terrain $\alpha = \frac{1}{10} \sim \frac{1}{7}$
- For countryside $\alpha = \frac{1}{6} \sim \frac{1}{4}$
- For forest land $\alpha = \frac{1}{4} \sim \frac{1}{2}$

### 2.2.3 Direction of wind speed

The direction of the wind speed plays a significant role in the effect on wind on structure. The angle at which the wind approaches the civil engineering structure is known as the wind angle of attack. The angle of attack affects the wind load or pressure on the structure, due to the nominal area exposed to the wind and the shape of the structure.

### 2.2.4 Turbulence and spectra of wind flow

The turbulence is produced due to unsteady flow of wind caused by vortices and large eddies, which cause the fluctuation in wind velocity with time. An example of wind velocity fluctuation recorded during this experiment is shown in Figure 2. 2. Different intensities can be associated with the turbulence and the effect they have on structures.

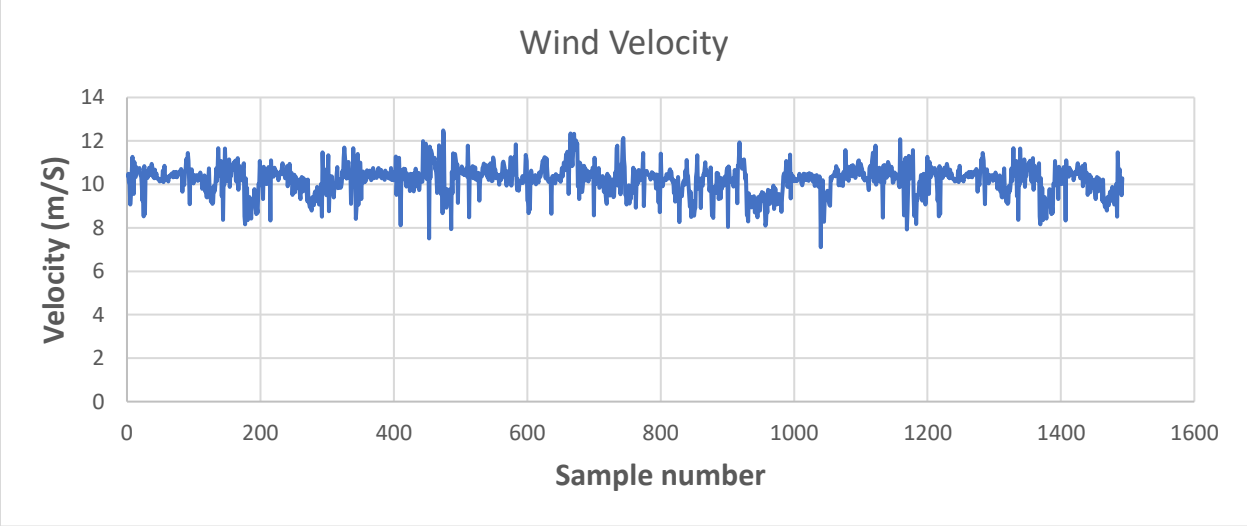


Figure 2. 2 Fluctuation of wind velocity

#### 2.2.4.1 Categories of turbulence

The turbulence is divided in 4 categories which are described below (NOAA,2020):

1. Light turbulence – which does not have much impact on airplane and passengers will not be able to feel anything due to light turbulence.
2. Moderate turbulence - It is more intense than light turbulence. Airplane passengers will feel strain around their seat belts.
3. Severe Turbulence – The altitude of the airplane may change due to this type of turbulence and the fluctuation in wind velocity is very large.
4. Extreme turbulence – During extreme turbulence it is difficult to control the airplane and it will cause the damage to the structure.

2.2.4.2 Causes of turbulence

The phenomena and causes due to which turbulence is produced are listed below (NOAA, US Dept of Commerce):

1. Thermal turbulence – Turbulence can be caused whenever a surface gets warmer than the other surface and the air starts moving from surface with high temperature towards surface with low temperature. This type of turbulence is known as thermal turbulence.
2. Mechanical turbulence- Whenever the turbulence is produced due to the interaction of wind and land, this is known as mechanical turbulence. It depends upon the topography of the land. The turbulence will have higher intensity if the degree of roughness of the land is denser and the air will be more unstable.
3. Wind shear – Turbulence can also be produced due to change in wind direction or wind velocity in adjacent layers of air.
4. Frontal turbulence- The sloping frontal land sometimes lifts the warm air producing turbulence in frontal zone due to friction between two opposite wind flows.

2.2.4.3 Characteristics of fluctuation of wind velocity

1. Turbulence intensity (I(z))– It is defined as the standard deviation of fluctuating wind velocity divided by the mean wind velocity. Turbulence intensity is given by Eq (2. 2) (Yamaguchi,2000):

$$I(z) = \frac{\sqrt{Ui^2(z)}}{U(z)} \qquad (2.\ 2)$$

2. Integral scales of turbulence ($Lu^x$) – it is the length scale at which the eddies are the largest. Integral scale of turbulence is given by Eq (2. 3) (Yamaguchi,2000).

$$Lu^x = \frac{1}{U^2}\int_0^\infty R\mathrm{u}_1\mathrm{u}_2(x)dx \qquad (2.\ 3)$$

where $Ru_1u_2(x)$ is the cross-covariance of the longitudinal velocity components, $u_1=U(x_1, y_1,z_1,t)$ and $u_2=U(x_1+x,y_1,z_1,t)$. The integral length scale of turbulence can be calculated for all the three components of velocity in x, y and z direction, determining Lu, Lv and Lw.

3. Spectra of velocity fluctuation–Spectrum of wind velocity compares the wind energy with respect to frequency as shown in Figure 2. 3. The spectra of longitudinal velocity (u) is given by Davenport, (1961) and is drawn by Eq (2. 4)(Yamaguchi,2000); the spectra of vertical velocity (w) fluctuations is given by Panofsky and McCormick, (1960) and is drawn by Eq (2. 5)(Yamaguchi,2000) and the spectra of transverse velocity (v) given by Kaimal, (1972) as drawn by Eq (2. 6)(Yamaguchi,2000).

$$f.\frac{Su(f)}{U*^2} = Z\frac{X^2}{(1+x^2)^{4/3}} \qquad (2.\ 4)$$

$$f.Sw(f) = w^2\frac{2X}{(1+4x)^2} \qquad (2.\ 5)$$

$$f.\frac{Sv(f)}{U*^2} = \frac{15X}{(1+9.5x)^{5/3}} \qquad (2.\ 6)$$

where $U*$is the frictional velocity and X is non-dimensional frequency.

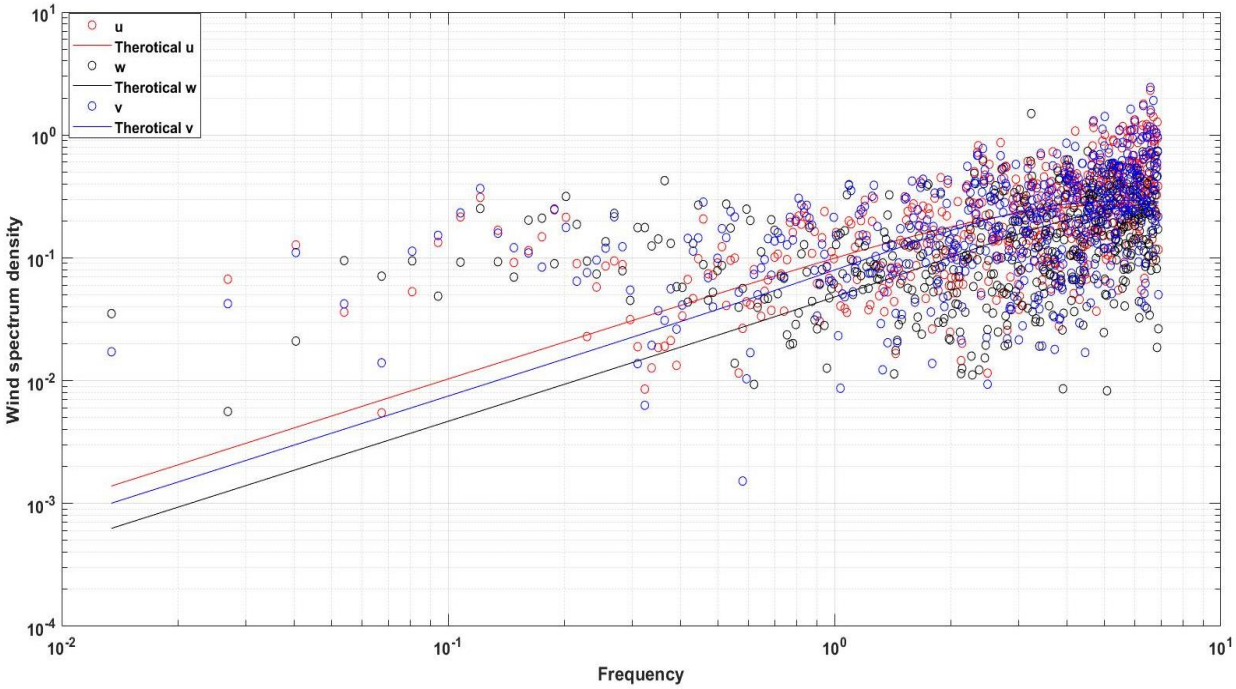


Figure 2. 3 Wind velocity spectra for the three components, vertical, longitudinal and transversal wind speeds

The full lines in the Figure 2.3 represent the turbulence spectra determined by equations (2. 4), (2. 5) and (2. 6), while the dots represent the data measured in the current experiment.

## 2.2 Effect of wind on civil engineering structures

### 2.2.1 Interaction of wind with structure

The wind flow, formed by the transition between the high pressure areas to low pressure areas, exert pressure on the surface of the civil engineering structures and the failure of these structures depends upon the response of the building to the wind pressure. If the exerted wind load is greater than the load carrying capacity of the structure or the members of the structure, then the structure, or its elements, could collapse. The failure in the structure tends to start when the building materials are stressed to their strength limit, which cause the deformation or fracture in the structure. The flowchart diagram of interaction between the wind flow and the civil engineering structure is shown in Figure 2. 4.

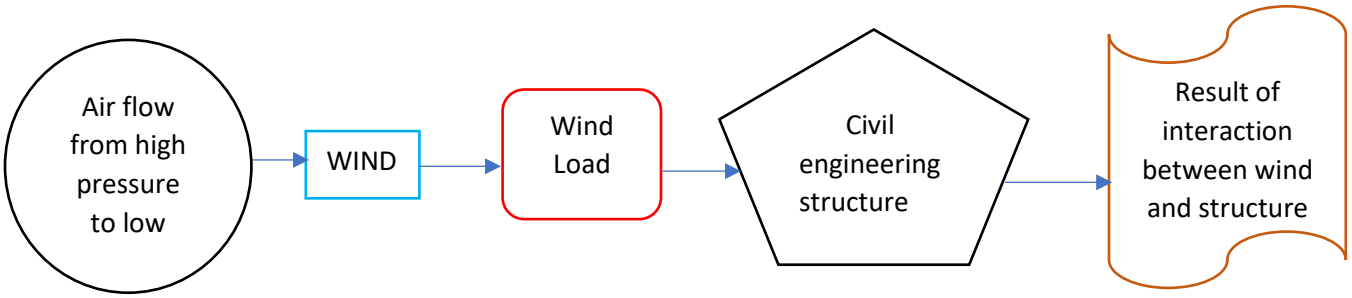


Figure 2. 4 Diagram of interaction of wind with civil engineering structure

## 2.3 Building design code for wind load

The building codes are designed by the civil engineers to construct a safer and economical structure. The minimum requirements are provided to construct, use or maintenance of a civil engineering structure by building codes. The wind design building codes are different for every country due to environmental and climatic condition. These codes are updated every 2 to 5 years, to improve the design procedure by new researches. The primary goal of these codes is to provide a safer and healthier design of structures, whereas to make the construction cost efficient is also one of the goals of the design. Moreover the wind design building codes provide only minimum criteria to construct a safe structure, however the owner can opt to invest additional resources for achieving the higher degree of safety for the structure ( Liu, 1991).

### 2.3.1 American National Standards Institute (ANSI) approach

The North American design code for wind and other loads on civil engineering structure is ANSI A58 had several revisions along the years converting into ASCE7 - 05. The ANSI gave the accreditation to the American Society of Civil Engineers to write and revise the standards related to civil engineering in 1977. The types of loads which are included in this code are the dead load (D), live load (Lr), load of roof and

other parts (L) earthquake load (E), wind load (W), rain load (R), snow load (S), self-straining load due to contraction or expansion (T) and other loads which may affect the design of a building. The design load is decided from the worst load combination

### 2.3.2 Comparison of wind load determination procedure of ANSI/ASCE and NBCC

American National Standards Institute (ANSI) and American Society of Civil Engineers (ASCE) used a procedure for wind load determination which depends upon the type of building and the location where the building will be constructed. The procedure includes the following steps.

1. The first and foremost step is to categorize the exposure of the building location. The exposure is categorized into 4 types. The centers of big cities is denoted as exposure A, exposure B includes urban, suburban or wooded cities, open terrain is denoted as exposure C and exposure D category includes beach areas.
2. The 2$^{nd}$ step is to compute the basic wind speed (V) from the Figure 2. 55.The range of wind speed given in this map spans from 70 mph to 110 mph.

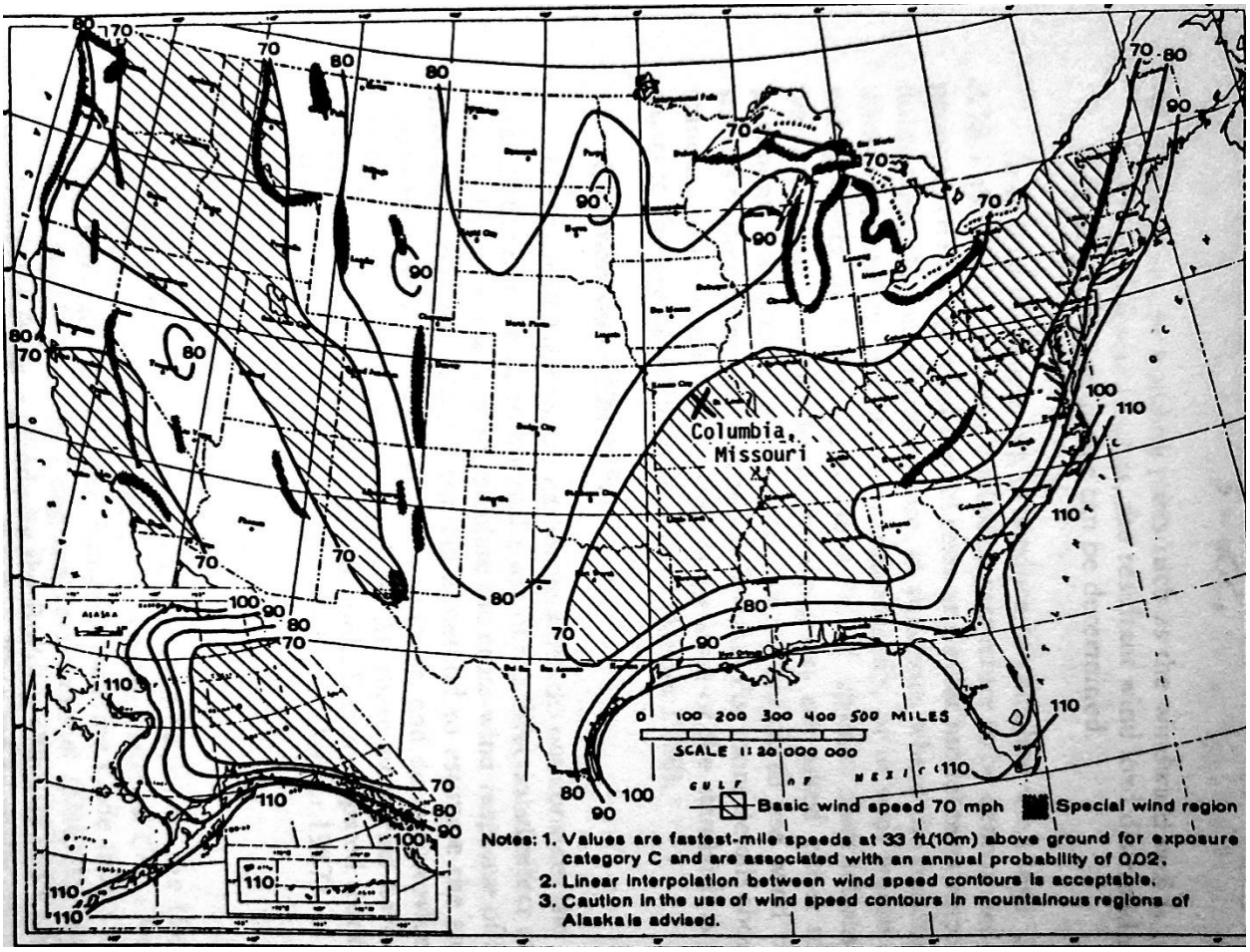


Figure 2. 5 Basic wind speed map of ANSI Standard A58.1

3. Depending upon the location and the type of the building, the velocity V is multiplied by an importance factor I. Importance factor is equal to 1 for ordinary building constructed away from hurricane oceanline, where importance factor 1.11 is for hospitals near hurricane oceanline.
4. The velocity pressure is determined at height z from Eq (2. 7)

$$q = 0.00256K_z(IV)^2 \qquad (2.\ 7)$$

Where q is the wind-induced pressure in pounds per square foot and V is in miles per hour. $K_z$ is known as exposure coefficient.

5. Determine the height to width ratio and the natural frequency of a building to check whether it is a flexible or a rigid building. If the height to width ratio is greater than 5 or the natural frequency is less than 1 Hz then the building is considered to be flexible, otherwise it is a rigid building.
6. The gust response factor G for rigid structure is calculated by employing Eq (2. 8), whereas the Solari's method is employed for determination of G coefficient for flexible structures.

$$G = 0.65 + 8.58 Do^{1/2} \left(\frac{30}{z}\right) \alpha \qquad (2.\ 8)$$

where α is the power-law exponent, z is the height in feet and Do is the surface drag coefficient.

7. The pressure coefficient $C_p$ and the force coefficient $C_f$ tables and graphs for different categories of structures are provided by ANSI and ASCE07-5, from which $C_p$ and $C_f$ can be determined for a structure.
8. The wind pressure at any point on a building is the product of velocity pressure, gust response factor and the pressure or force coefficient as shown in (2. 9)

$$p = qGC_p \qquad (2.\ 9)$$

The wind design procedures of ASCE and National Building Code of Canada (NBCC) have some similarities but also they have several differences, which are listed below.

1. There are 3 exposure categories A, B and C in NBCC. Exposure A is for smoothest terrain, exposure B is for the modest areas and C is for the roughest, whereas ANSI/ASCE uses 4 exposure categories.
2. NBCC employs the basic wind speed V (m/s) as the hourly average of the fastest winds, whereas ANSI and ASCE's procedure to determine the wind load is based on the fastest mile wind speed.
3. The velocity pressure in NBCC design procedure is determined by employing Eq (2. 10)

$$q = \frac{1}{2}\rho V^2 \qquad (2.\ 10)$$

4. The wind pressure at any point on a building is determined by the product of velocity pressure (q), exposure factor ($C_e$), gust effect factor ($C_g$) and pressure coefficient ($C_p$) as given in Eq (2. 11) below:

$$p = qC_eC_gC_p \qquad (2.\ 11)$$

## 2.4 Wind loads and Pressures on Silsoe Cube structure

The full-scale SilsoeCube with width, depth and height of 6m, was constructed in the Silsoe Research Institute in late 1990s, to study the interaction of the wind flow and the basic civil engineering structures. The aim of studying the wind-induced pressure on Silsoe Cube is to relate the study of external wind loads to the study of building frame response. The Silsoe Cube, as shown in Figure 2. 7, is placed on a smooth flat surface to avoid the terrain effect on the wind speed profile. The mean, peak and area average pressures on the roof of the Silsoe Cube were determined by Richard and Hoxey (2008) whereas the pressure coefficients(cp) were measured along the vertical as well in the horizontal centerlines of the cube, through the tapping points by Richard and Hoxey (2012). There were 18 tapping points (V1-V18) for the vertical direction whereas 24 tapping points (H1-H24) were used for the horizontal direction and several additional tapping points were placed on the quarter of the roof. The differential pressure transducer and pitot tube were employed to measure the dynamic pressure around the Silsoe Cube. Ultrasonic anemometers were also used to measure the wind velocity of the surroundings of the cube. The wind conditions were not controlled as the measurements were recorded in an open area. The maximum suction was experienced by the taps which were closer to the edges of the roof, due to the vortex wind flow. When a strong wind gust developed simultaneously along the wind direction associated with highly negative pressure coefficient then the peak suction pressure was experienced at that location according to Richard and Hoxey (2004). The results of the field measurements carried out in 2008 depict the strong agreement between the instantaneous pressure distribution during an extreme event and the mean pressure coefficients distribution. Earlier it was difficult to calculate the pressure coefficient as there was confusion whether cp should be ratio of mean pressure to the mean dynamic pressure or dynamic pressure computed from the mean wind velocity. Richard and Hoxey (2012) considered their calculation of cp normalized to the measure pressures and the dynamic pressure, in order to determine the mean, standard deviation, maximum and minimum values for the pressure coefficients represented in Figure 2. 6. They state that in order to reduce the uncertainty of the results it was important to normalize the pressure coefficient in the similar way Richard and Hoxey (2004) have done.

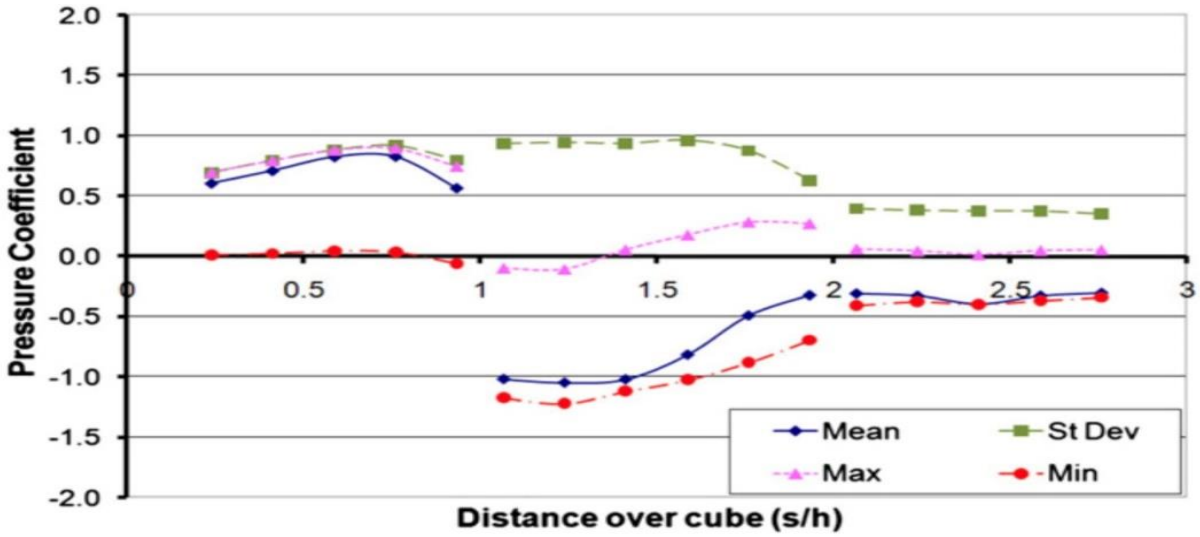


Figure 2. 6Pressure coefficients for the Silsoe Cube (Richard and Hoxey 2012)

Figure 2. 7 The full-scale Silsoe Cube building (Richard and Hoxey, 2012)

## 2.5 Comparison of wind spectra for the full-scale and Silsoe Cube models

The experiments performed for models of building tested in wind tunnels, are extremely important for understanding the impact of the wind-induced pressure on the civil engineering structures, such as low-rise buildings. Basic structure as the Silsoe Cube building serve as a reference for wind design based on the data provided from the field measurements and from the wind tunnel experiments. The wind design building codes rely on the experiments performed in wind tunnels, more than the field measurements, due to cost efficiency and because the full-scale measurements cannot be performed in controlled wind conditions like in a wind tunnel, due to open area, thus sometimes inducing errors. The comparison of data of wind tunnel experiments performed by different researchers (Richardson and Surrey (1992)) shows that there is a difference of 15%-20% in the results due the following reasons:

1. Difference in method of acquisition.
2. Different scales of models were used in different experiments.
3. Position of the reference static and dynamic pressures might be different.
4. The instruments used during experiments might be different.
5. Experiments were performed in different season for example in winter or summer or fall season.

Surrey and Johnson (1986) concluded that there might be fundamental differences between full-scale and model results on comparing the wind loads on mobile home. The experiments on full-scale wind loading on Silsoe Cube building began in 1987 and in 1992, a wind tunnel experiment was performed for a 1:100 scale model of the Silsoe Cube (Richardson and Surrey, 1992) for comparing the results with the full-scale data reported for an open environment (Richard and Hoxey, 1987). Richardson and Surry (1992) used the floor mounted static reference pressure, whereas during full-scale experiment (Richard and Hoxey, 1987) static reference probe was placed on a mast at the ridge. Richardson and Surrey (1988) employed Statham 2.5 transducers and Scanivalve to measure the pressure at different points on scaled model, but in full-scale experiment ((Richard and Hoxey, 1987) differential transducer and pitot tube were employed. The time, velocity and measurements length are the 3 interdependent factors used for the scaling of the model. The horizontal separation in power spectra of any 3 components of wind velocity can be observed if there is error in determination of scaling factor. Richardson and Surrey (1988) also calculated the pressure coefficient, CP by taking the square root of the ratio of tapping point pressure to the reference dynamic pressure. They were successful in scaling the 1:100 model in the wind tunnel and in comparing the pressure coefficient results of the full-scale field test with the 1:100 experimental model, for determining the

accuracy of their analysis. The vertical profile of the longitudinal wind speed of the 1:100 scale model was the same as for the full-scale model, as shown in Figure 2. 8 (b), however there was a slight decrease in energy in power spectra of 1:100 scale in transverse velocity, as shown in Figure 2. 8(a), which shows potential error in considering the scaling of the experimental conditions. The power spectra comparison of the 1:100 scale and of the full-scale measurements also confirms that 1:100 frequency scaling of the full-scale results has been accurate over a wide bandwidth.

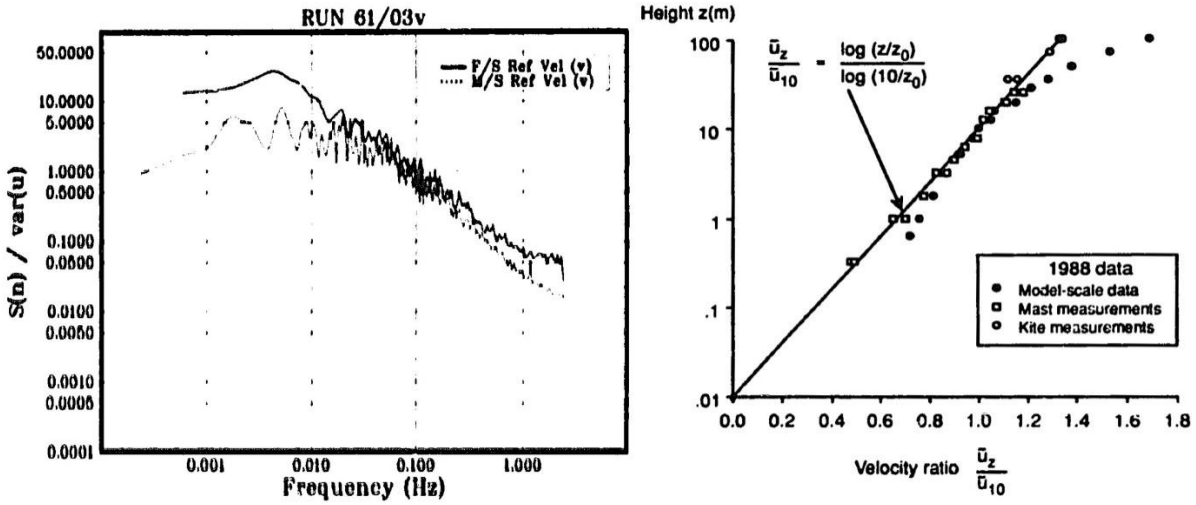


(a) Transverse velocity spectra comparison (b) Vertical profile of longitudinal velocity comparison

Figure 2. 8 Results of Richardson and Surrey (1988)

Usually the turbulence spectra measured in the field for smooth wind velocities in atmospheric boundary layers are characterized by an initial increase, at small frequencies, followed by a gradual decrease for high range frequencies as noticed in Figure 2. 9 (Morfiadakis et al, 1996) and also represented by Davenport (1960) in Figure 2.10.

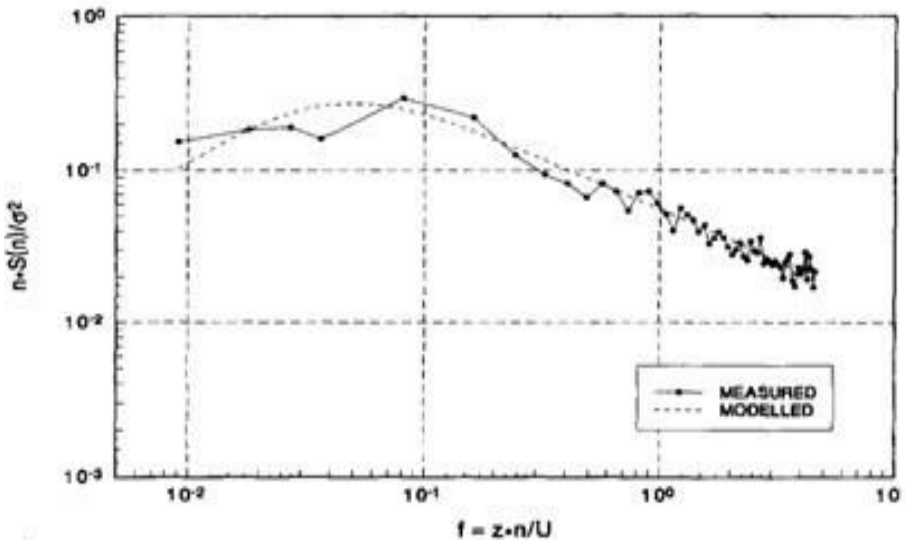


Figure 2. 9 Turbulence spectrum of Morfiadakis et al, (1996)

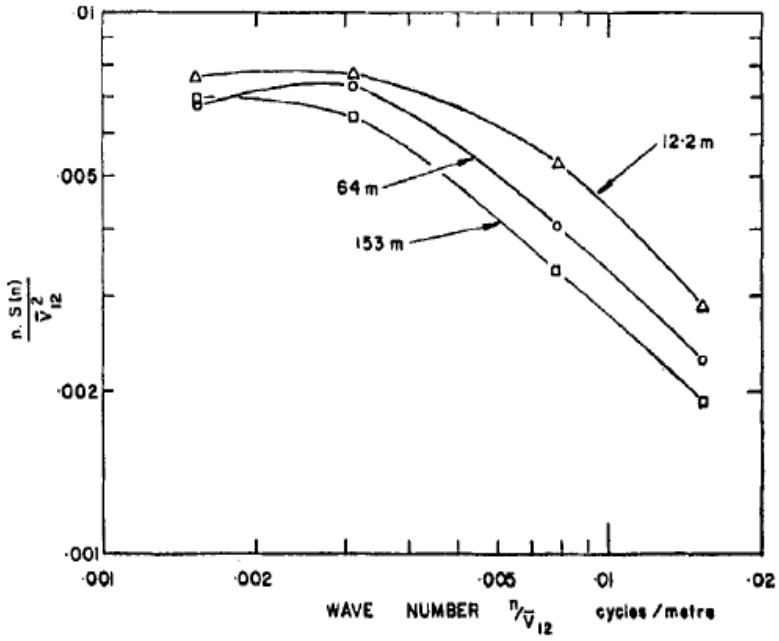


Figure 2.10 Turbulence Spectrum of Davenport (1960)

For higher turbulence intensity however the measured data shows an increment for the high frequencies range , while the models slightly underestimate the turbulence, as it can noticed in Figure 2. 11.

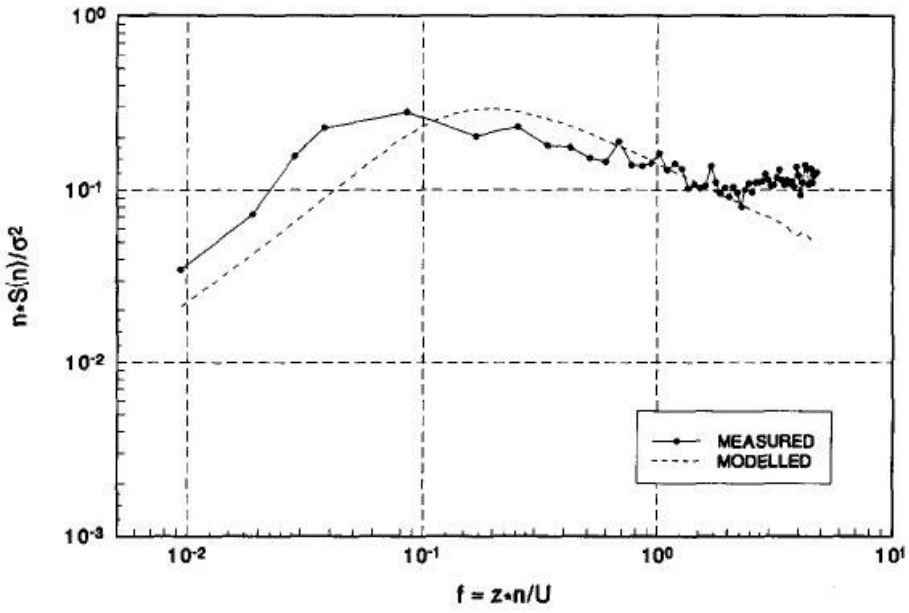


Figure 2. 11 Turbulence spectrum of Morfiadakis (1996)

The turbulence power spectra measured in wind tunnel experiments are similar to the ones reported for smooth stationary flow (Jafari et al, 2019) and as reported by Richards (2007), the turbulence spectra obtained from the wind tunnel simulated flows reproduce better the low-frequency turbulence, and due to the chamber dimensions limitations, the eddies cannot fully develop, thus it fails short of replicating the high-frequency turbulence reported by in-situ measurements. The Figure 2. 12 (a) and (b) represent the normalized longitudinal velocity spectrum and normalized vertical velocity spectrum respectively plotted by Jafrai et al, 2019 during their research.

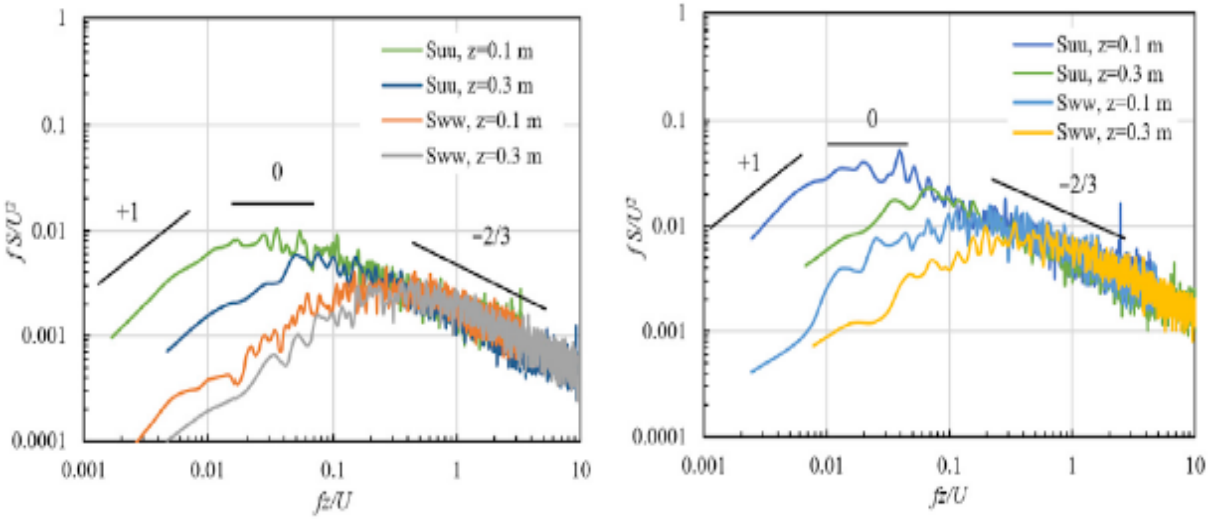

(a) (b)

Figure 2. 12 Longitudinal and vertical velocities spectra obtained by Jafrai et al, 2019

Morrison and Kopp (2018) have compared the turbulence spectra they obtained when performing a wind tunnel full-scale experiment at IBHS Research center with the several field experiments and ESDU full-scale data. The Figure 2. 13 (a) and (b) depict the longitudinal velocity spectrum and vertical velocity spectrum respectively obtained during the experiment performed by Morrison and Kopp (2018). As it can be noticed, even a full-scale wind tunnel facility fails to reproduce the high-frequency range turbulence existent in the field data.

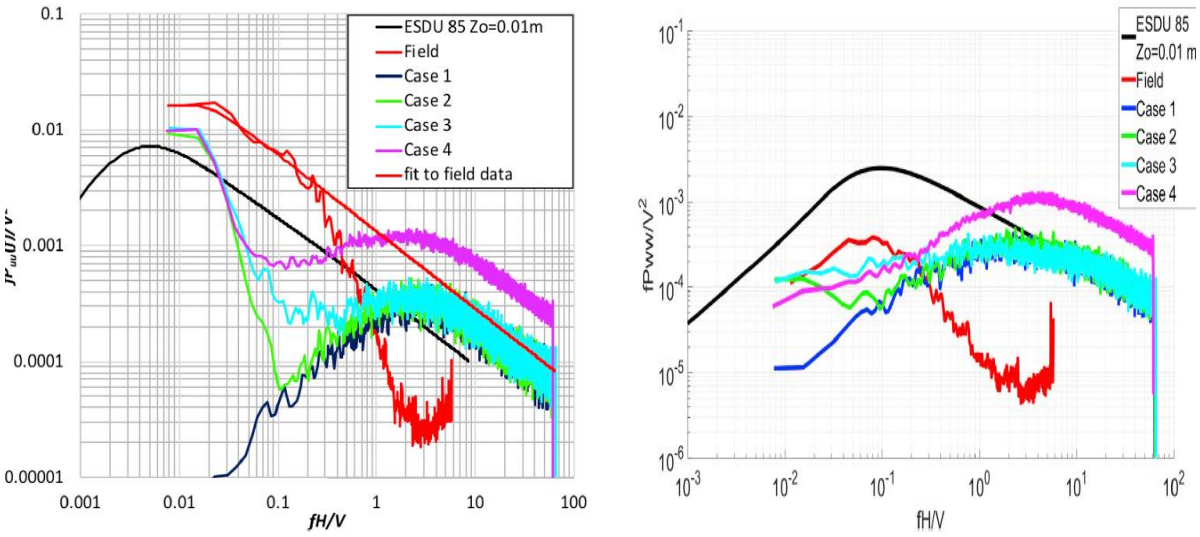


(a) (b)

Figure 2. 13 Longitudinal and vertical velocities spectra obtained by Morrison and Kopp (2018)

Liao et al (2020) had measured the wind speed characteristics in the mountain-valley relief, using and comparing data from different recording instruments, to determine the complex properties of the wind turbulence, The measured turbulence spectrum compared well with the Von Karman formulation, as it can be noticed in Figure 2. 14 below.

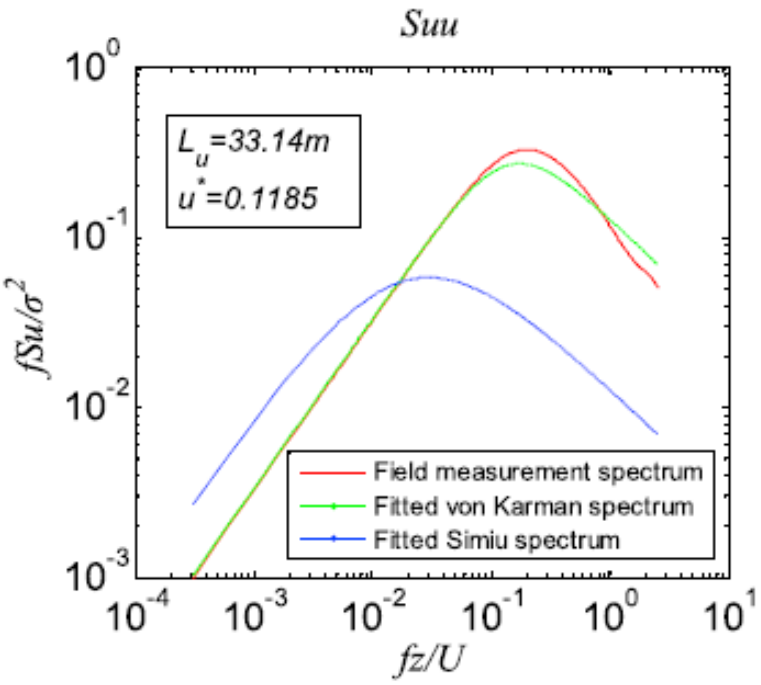


Figure 2. 14 Turbulence spectrum obtained by Liao et al, 2020

## 2.6 Computational Fluid Dynamics technique (CFD)

### 2.6.1 Background of CFD techniques

Computational Fluid Dynamics (CFD) is a numerical technique which is used before performing any experiment in wind tunnel. CFD is employed to simulate the wind flow around the civil engineering and to determine their aerodynamic characteristics. CFD was not much popular several years ago, however due to the advancement in technology andhigh speed digital computer technology, CFD has been widely employed to compute the interaction of wind and civil engineering structures. Also, CFD techniques were not employed in earlier stage due to the lack of powerful computers and limitation in modelling techniques. There are five common turbulence model namely Standard k-ε, RNG k-ε, Realizable k-ε, Reynolds Stress method, RANS, RSM and Large Eddy Simulation. Launder and Spalding(1972) proposed a standard k-ε turbulence model to compute the wind flow and conditions around the structures before performing the experiment on them in wind tunnel. There were some limitations in this model and to overcome these limitations Yakhot and Orszag (1986) developed RNG k-ε turbulence model. The renormalization group theory was employed to derive the RNG k-ε model. For the boundary layer under adverse pressure gradient,

Realizable k-ε model better predict the wind-induced pressure (Irtaza et al, (2013)). The complex unsteady turbulent flows can be easily simulated with theLarge Eddy Simulation (LES) algorithm.

### 2.6.2 Wind pressure measurement comparison between full-scale data, wind tunnel experiments and CFD techniques

A research performed by Irtaza et al, (2013) compared the wind pressure measurement on the Silsoe experimental building from the full-scale data, with the 1:30 scale model in wind tunnel and with the results obtained from CFD simulations. The main objective of the study was to determine the most appropriate turbulence model for the computational wind engineering (CWE) approach. The results reported by Irtaza et al, (2013) as shown in Figure 2. 15, proved that none of the turbulence models was able to predict with accuracy the wind-induced pressure coefficients for the investigated structure, however the cp evolution was somehow consistent along the measured lines. A structured mesh was required for Reynolds Stress Method (RSM) to determine the pressure coefficient, while the pressure coefficients determined by Standard k-ε were 20-25% overpredicted. Out of all the turbulence models, LES showed the best performance in computing the accurate results. Thus, Irtaza et al, (2013) concluded that a better turbulence model is required to predict the pressure coefficient and wind-structure interaction more accurately.

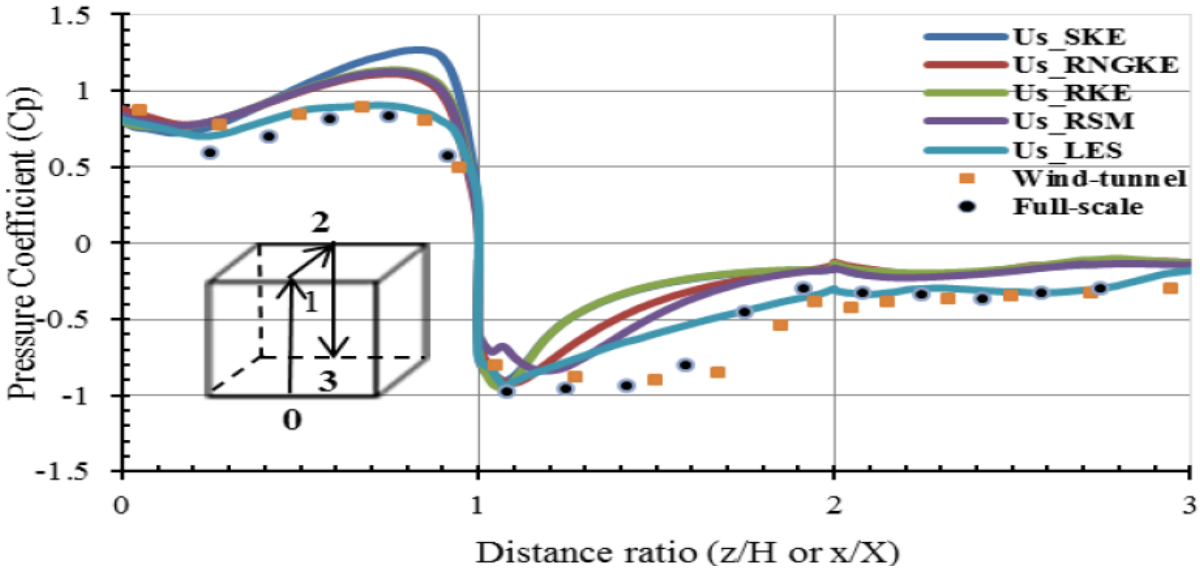


Figure 2. 15 Pressure Coefficients from Irtaza et al, (2013)

## 2.7 Wind Induced Damage Simulator (WDS)

### 2.7.1 Introduction of WDS

The conventional wind tunnels have controlled wind experimental conditions, which encompass the smooth and turbulent unidirectional boundary layer velocities, which cannot simulate however hazardous winds, like tornados and hurricanes. Extreme wind effects on structures are difficult to simulate in laboratory conditions due to the lack of experimental facilities. At the University of Ottawa a new Wind-induced Damage Simulator (WDS) as shown in

Figure 2. 16 was constructed as part of the structure lab. The WDS comprises of an isolated cubic steel box with dimensions of 3.65mx3.65m and height of 3.0m, which can simulate extreme wind flows by using an industrial blower which extracts the wind flow from the WDS box through a duct and an outlet installed on the roof top , and produces injections of high-speed wind flows through the multiple inlets on the lateral faces.

Figure 2. 16 Wind Induced Damage Simulator at UOttawa

## 2.7.2 Determination of pressure coefficients in WDS

The pressure coefficients at 42 different points were determined for 1:30 and 1:40 scaled Silsoe Cube in WDS by Xiao and Dragomirescu, (2019) when the WDS was still installed in the CBY in structure lab of University of Ottawa and the enclosure did not have doors. The instruments used to determine the pressure on the surface of the cubes were pressure taps and DSA3217 pressure Scanner. The results of the research done by Xiao and Dragomirescu (2019) were compared with the full-scale data reported by Richards et al (2001). The pressure coefficients results presented in Figure 2. 17 shows the cp at some locations of scaled models did not match the cp of full-scale Silsoe Cube and the reason stated by them for this mismatch was that " the cross-section area of the generated shear flow was not large enough to cover the entire scaled model at designated locations".

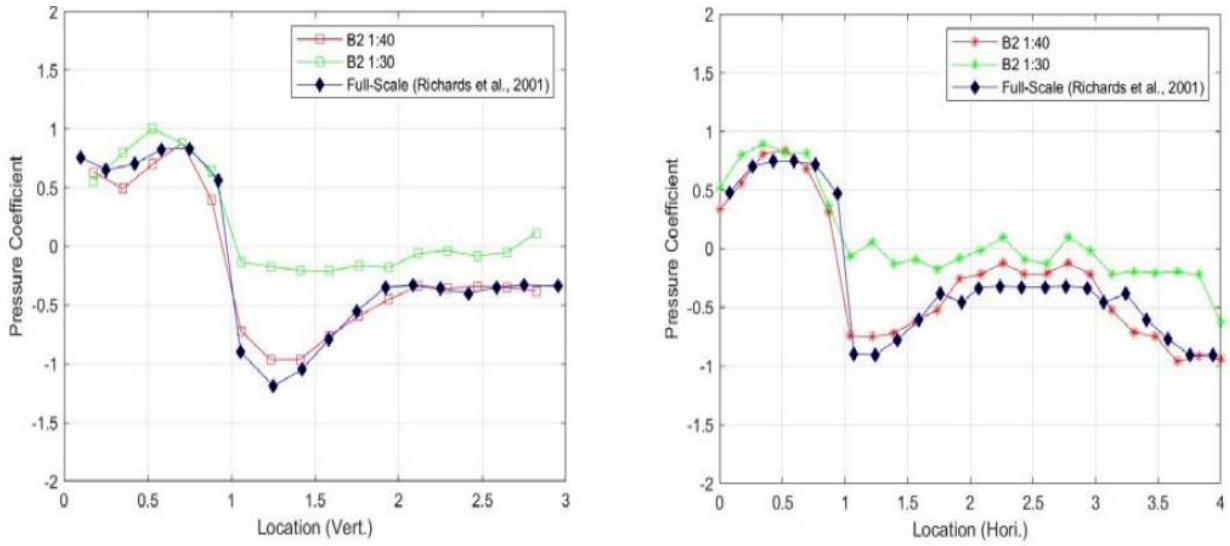

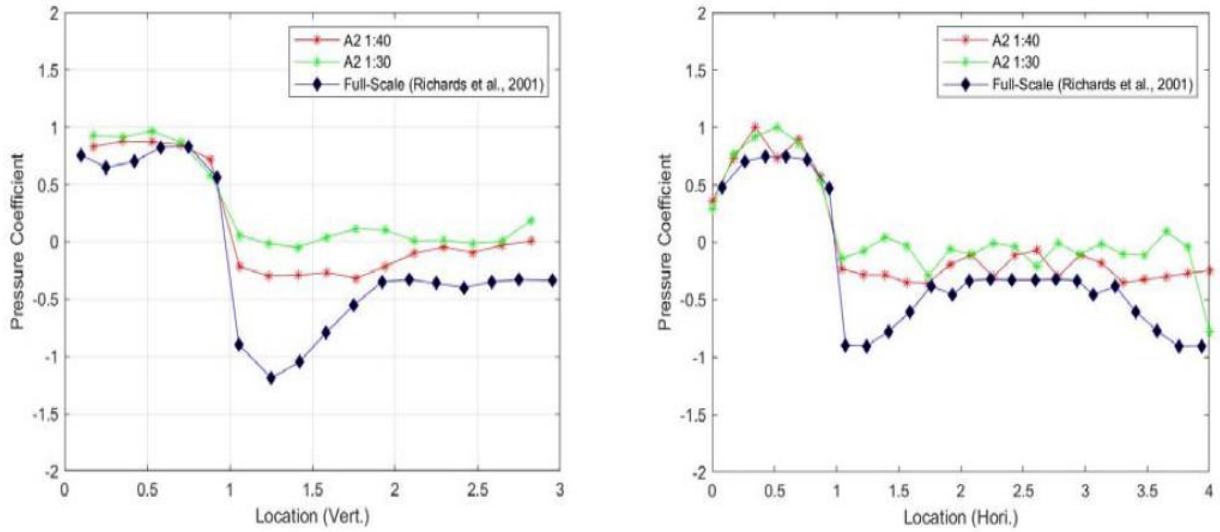


Figure 2. 17 Pressure Coefficients of experiment done by Xiao and Dragomirescu (2019)

### 2.7.3 Difference Between Current experiment and Xiao and Dragomirescu (2019) Experiment

The experiment performed by Xiao and Dragomirescu (2019) were conducted in the initial WDS facility, which had different floor configuration, thus a wooden artificial floor was installed during the experiment as shown in Figure 2. *18* to elevate the floor height of the WDS; therefore the bottom edge of the inlet of WDS was at the level of wooden artificial floor, whereas, for the current experiment the floor level was lower than the bottom edge of the inlet. This installation conditions affected directly the flow approaching the tested models, leading in different pressures recorded on the windward face of the models, as explained in Chapter 4 below. A system of insulated hydraulic doors were installed in WDS for the current experiment but during Xiao and Dragomirescu's (2019) experiment the entire WDS box was used to lift up to access the models and the equipment inside the testing chamber. Thus a good insulation of the WDS chamber was not possible in the previous experiments.

Figure 2. 18 Experimental setup of Xiao and Dragomirescu (2019)

## 2.8 Unsteady wind loads measurements

### 2.8.1 Background of unsteady wind loads

The measurement of the unsteady wind loads should be accurate as the durability and serviceability of the civil engineering structure depends on it during the extreme conditions (Jafri et al, (2019)). However, it is very difficult to measure it correctly as there is a significant challenge in matching the turbulence spectra of the corresponding full-scale conditions with the spectra obtained in the wind tunnel modeling of unsteady wind loads on small scale structures (Holscher and Niemann,1998),). The boundary layer wind tunnels are generally designed to perform the experiment on large-scale civil engineering structures. The error in the calculation could be due to the large difference between the dimensions of the structure and the atmospheric surface layer height. It is not an easy task to scale the prototype to a small-scale model, without proper scaling ratios which can be used in turbulent conditions and it is also difficult to measure the pressure and forces on the small-scale models. The wind load data from different experiments performed in wind tunnel

shows a great variation due to the mismatch of the turbulence spectra. The difference in the model dimensions and the ratio of the turbulence length scales led to the large variation of peak pressure coefficient between the different experiments. The unsteady wind loads can be easily computed from the wind tunnel measurements, if the scaling of the model is properly applied. The shifting of the power spectra to the higher frequency can be done to match the turbulence intensity of full-scale in wind tunnel experiments. The accurate estimation of the unsteady wind load is necessary, therefore it is important to develop a standard method to determine it accurately.

### 2.8.2 Measurement of unsteady wind loads in a wind tunnel

A research was done by Jafri et al, (2019) regarding the measurement of unsteady of wind loads in wind tunnel, with higher accuracy for the Silsoe Cube model. The main objective of their study was to determine the correlation of the unsteady wind loads determined in the wind tunnel, and their turbulence spectra. The three different components of wind velocity, the longitudinal velocity (u), vertical velocity (w) and transverse velocity (v) respectively, were determined using a multi-hole pressure probe, which was further used to generate the turbulence spectra of that model. The most of the unsteady wind loads measured on the flat plates during the experiment were exerted by the turbulent eddies within a frequency range of 0.01Hz and 1HF. The results of this study, as shown in Figure 2. *19* , depict that a discrepancy of turbulence spectra can be seen when an experiment is performed on a small-scale model in the wind tunnel. Jafri et al, (2019) state in their results that “when the turbulence length scale is much larger than the characteristic length of the structure, free-stream turbulence acts like a correlated unsteady mean flow and the flow behavior around the body is quasi-static.”

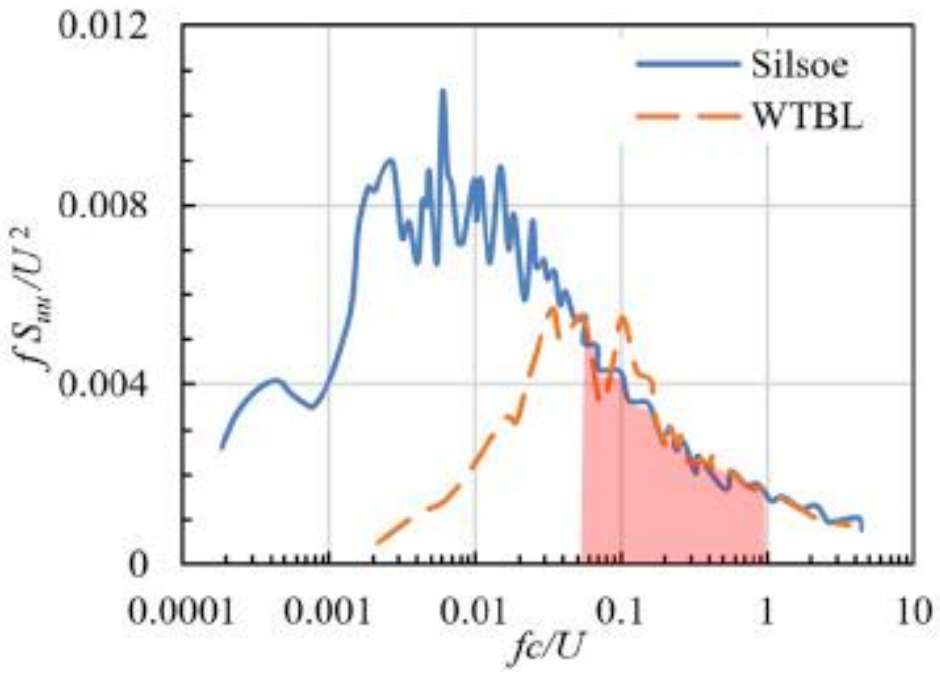


Figure 2. 19 Turbulence spectra results of Jafri et al, (2019)

## 2.8 Other related Studies

Richards et al, (2007), performed wind characteristics experiments on 1:40 scale of SIlsoe Cube in wind tunnel at the University of Auckland, and recommended that turbulence-independent normalizing parameter should be employed for the spectral comparison. They also concluded that the values of longitudinal and transverse turbulence were lower than the full-scale because of the size of the tunnel. Tieleman (2003) suggested that the scale of the model for the low-rise buildings should not be less than 1:50. An experiment was performed by Wu et al, (2017) to study the effect of turbulence on the mean pressure field, to determine the pressure gradient from planar particle image velocimetry data ,Wu et al, (2017) employed the time-averaged Navier-Stoes equations. They found that increased convention and turbulence-contributed pressure gradients resulted in the decreasing minimum mean roof surface pressure coefficient where as according to Akon and Kopp (2016), the decrease in the minimum mean roof surface pressure coefficient is related to the increased of upstream turbulence intensity. Richardson et al, (1997), did a research to compare the pressures measured at Silsoe Structures Building and scaled Silsoe Cube models in different wind tunnels. They suggested that the transient flow characteristics could be more accurate if surface pressure data is normalized using the local reference pressure and the direction data.

Richardson et al, (1997), also found that the under-estimation of the high negative pressure in the wind-tunnel data is related to the Reynolds number effect.

## 2.9 Difference between experiment performed in WDS and Wind Tunnels

Most of the previous studies related to the Sisloe Cube have employed full-scale, wind tunnels and CFD simulations mimicking the wind flow in a wind tunnel. The current WDS simulator is using a different approach by simulating wind flow through an outlet suction-inlets injection system, thus naturally creating flow perturbations. Such system was attempted before for studying the Sisloe Cube model by Xiao and Dragomirescu (2019), however, since then the WDS facility has been modified and the experimental conditions were altered. Therefore to clarify the WDS capability of replicating wind – induced pressure on building models, several Silsoe Cube scaled models were tested and were compared with other available studies, as presented in Chapter 4.

The pressure coefficients results obtained in the WDS are expected to be disparate from the other wind tunnel studies, reported for the same models, because there are fundamental differences between these two types of facilities, as follows:

- The wind flow can enter the WDS box from all the four faces of the box whereas in conventional wind tunnels, the wind flow is unidirectional.
- Most of the wind tunnels use the fan to push wind flow through the testing section, while the WDS is using the fan (industrial blower) to create a strong suction at the ceiling, which pulls the wind flow from the inlets and through the testing section.
- Additional filters are employed in the conventional wind tunnels to achieve the turbulence but in WDS no filters are required to have turbulence in the wind flow.
- The wind speed turbulence spectra determined in WDS is closer to the spectra determined in the field measurements, which means the energy is increasing with increase in the frequency, while for the wind tunnels this is decreasing with the frequency.
- The wind tunnels have a longer section before the test section, to allow the wind flow to smoothen, however the WDS doesn't have such a dedicated space in front of the test section. Thus, the wind tunnels can simulate smooth flow, but the WDS can simulate only mixing layers, multi-directional, tornadic and turbulent flows.

# Chapter 3 - Experimental Setup and Configurations

## 3.1 Wind induced damage simulator (WDS)

Multi-directional wind effects on structures are difficult to stimulate in laboratory conditions due to the lack of experimental facilities capable of replicating complex flows. Conventional wind tunnels can simulate only boundary layer wind speed of up to 30 m/s - 35 m/s, which do not resemble any of the multi-directional windstorm events. At the University of Ottawa a new Wind-induced Damage Simulator (WDS) was constructed as part of the structures lab. The WDS comprises of an isolated cubic steel box with dimensions of 3.65 m x3.65 m and height of 3.0 m, which can stimulate extreme and multi-directional wind flows by using an industrial fan running up to 3,560 RPM. The industrial fan extracts the wind flow from the WDS box through a duct and outlet installed on the rooftop and produces injections of high-speed wind flows through the multiple inlets situated on the lateral faces, as schematically presented in Figure 3. 1(a). Figure 3. 1 (b) represent the actual WDS facility mounted in the structures laboratory. The WDS equipment creates a controlled environment for studying wind profiles in a confined space, by regulating the air flow with the aid of the attached industrial blower. The five circular inlets have a diameter of 200 mm each; also four, out of five inlets are situated on the lower row, which is 140 mm from the ground, with spacing between them of 915 mm, while the fifth inlet is located on the right hand side of the upper row, which is 540 mm above the ground. The top outlet has a diameter of 300 mm located at the center of the roof of the WDS, which is connected to an industrial blower that extracts the air from the WDS. The speed of the blower engine varies from 356RPM to 3,560RPM, thus producing wind speeds of up to 40m/s at the top outlet. The wind speed at the lateral inlets always depends on the number of inlets in use for each test case. A filter is installed on the outlet duct to secure the blower from any debris, foreign objects or dust particle released from the experimental chamber and entering in its engine. Also, the testing section of the wind box is accessed through two doors which can be operated by hydraulic jacks controlled by the levers located on the right-hand side of the WDS. The doors have bolts on the bottom side and a clip on the upper side, to ensure that the door closes hermetically and there is no air leakage between the box and the exterior environment. The doors are very heavy, approximately 500kg, and it can be hazardous if opened or closed manually, thus due to this safety reason only the hydraulic system is employed for operating the doors. A small rectangular exit, which is covered during the experiment, was designed at the back of the testing chamber, as a safety exit. Various equipment used during the experiments are discussed below.

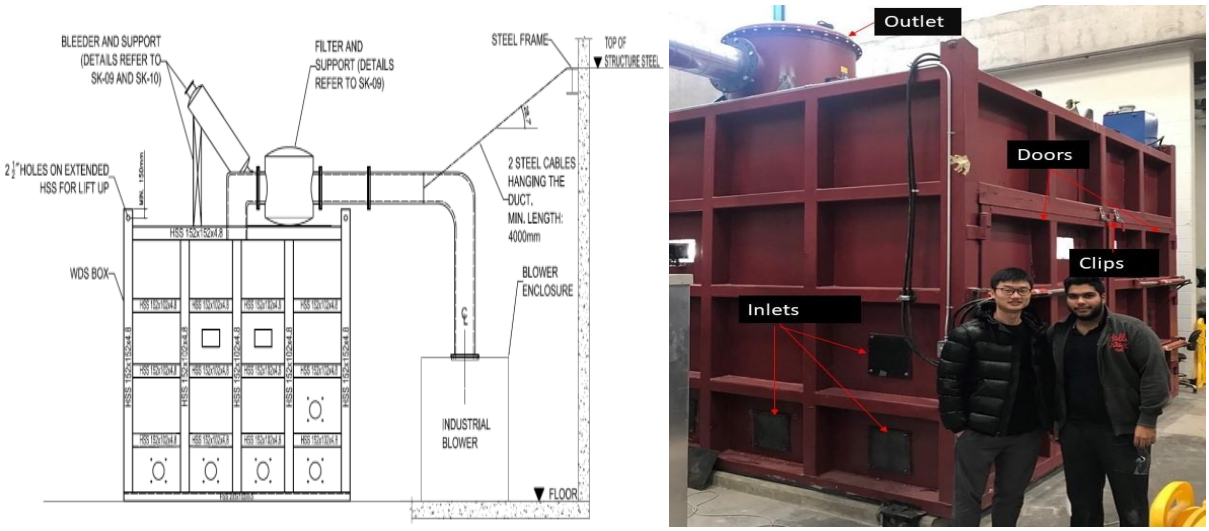


(a) Schematic representation of the WDS (b) Actual WDS facility

Figure 3. 1 Schematic representation of WDS and the laboratory WDS image

## 3.2 Equipment employed for the WDS experiment

When an experiment is carried out in the WDS facility, several parameters must be measured to determine the wind effect on the tested models. The incoming wind speed at the lateral inlet and on a vertical height describing the wind speed profile at the location of the model are necessary; for these measurements, the 12-holes Aeroprobe sensor and Pitot tubes were employed. Also, once the model is installed the pressure induced by the wind flow is recorded along certain lines on the surface of the model; these measurements were recorded through a system of 12 pressure taps and a pressure scanner as detailed below.

1. The 12-holes Aeroprobe device a sensor with spherical tip, as shown in Figure 3. 3 (b), measures the wind speed on 12 different directions at a single point and using an associated software, Aeroflow (v2.7.1), the wind velocities on 3 directions are determined. Aeroprobe sensors of different configuration are available with different number of holes (3, 5,7 or 12) for this experiment 12 holes Aeroprobe was selected for better data acquisition. The three dimensional flow velocity field can be measured with the help of 5 basic system components which are listed below :
    - The multi-hole probe
    - Aerodynamic calibration data
    - Pressure sensors

- Data acquisition system
- Pressure to velocity conversion software

2. Pitot Tube is another instrument as shown in Figure 3. 3 (a), which is used to determine wind flow velocity at one point, but this is an unidirectional instrument. Traditional method employing Pitot Tube was used for validation check during the experiments. Pitot Tube measures the pressure of the airflow entering the tube, which can be used in Bernoulli's equation as shown in Eq 3.1 to determine the wind velocity.

$$\text{Bernoulli's equation} = \; Pe + \frac{1}{2}\rho V^2 = P_0 \quad (3.1)$$

Where, Pe is the static pressure, $P_0$ is the stagnation pressure, V is the flow velocity

During the current experiment, two Pitot tubes were employed to determine the wind flow velocity in longitudinal and transverse directions.

3. A pressure taps system was employed to connect the Aeroprobe sensor with DSA3217 Scanivalve pressure scanner as shown in Figure 3. 3 (a) for data acquisition. The number of pressure taps that were employed for measuring the wind speed during the current experiment was 16, out of which 12 were used for the Aeroprobe sensor and 4 were used for the two Pitot Tubes respectively.

4. A DSA3217Scanivalve pressure scanner of 1.0 PSID, as shown in Figure 3. 3 (a), was used to determine the pressure output from the Aeroprobe sensor and to provide the raw data for evaluating the wind-induced pressure. This scanner had 16 channels and it was important to connect all the respective holes of the Aeroprobe sensor with the correct channels of the scanner, which otherwise can create difficulties during the data analysis and derivative parts of this work.

5. Silsoe Cube model was employed to study the effects of wind on the basic architectural structures. The length of the prototype Silsoe Cube was 6.0m and was built and instrumented for wind-induced pressure measurements at the Silsoe Research Institute (Richard and Hoxey, 2001). For the current experiment, the prototype of the Silsoe Cube was used as an example and three different scaled models of the Silsoe Cubes were built 1:40, 1:30, and 1:20, with widths of 15m, 20cm and 30cm respectively. The Silsoe Cubes model with scale 1:40 is shown in Figure 3. 3(d).

6. An industrial blower was used as part of the WDS facility, to regulate the wind speeds inside the WDS testing chamber, with controlled engine rotations of 356 RPM to-3,560 RPM.

7. A simple iron rod was used to support the Aeroprobe sensor at 5 different heights and 4 different locations in the WDS testing chamber, as shown in Figure 3. 3 (c).

8. The software Aeroflow (v2.7.1) was used to generate 2D spatial plots, time series data graphs, summary statistics and other analyses of the raw and reduced data recorded by the Aeroprobe sensor. Various parameters which were calculated by this software are show in Figure 3. 2 and are also listed below.
    - u(m/s) – Longitudinal velocity ( X- component of the velocity)
    - v(m/s) – Transverse velocity (Y- component of the velocity)
    - w (m/s)– Vertical Velocity (Z- component of the velocity)
    - V(m/s) – Mean Velocity
    - Mach number
    - Density of the wind (kg/m3)
    - Total Pressure (Po)
    - Static Pressure (Ps)
    - Yaw angle in degree (β)
    - Cone angle in degree(θ)
    - Pitch angle in degree(α)

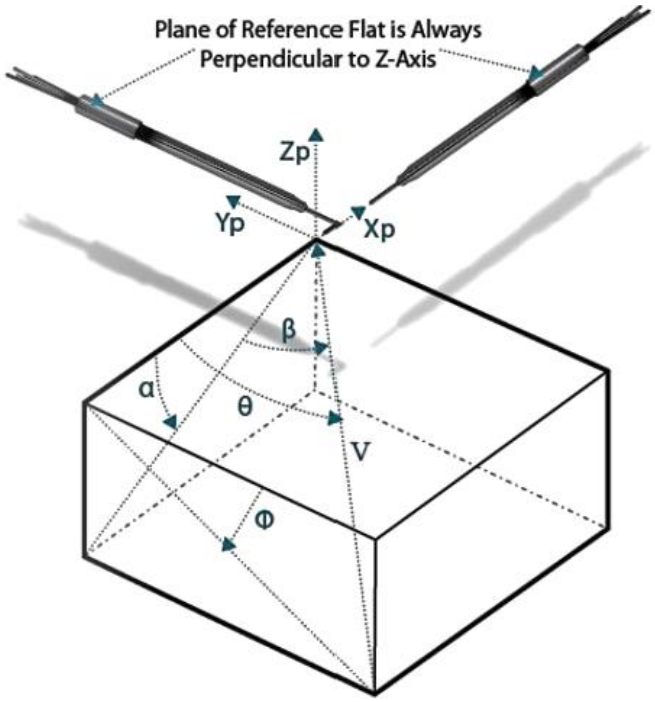


Figure 3. 2 Plane of reference of Aeroprobe (Aeroflow v2.7.1 manual, Aeroprobe Corporation)

9. Scanivalve DSALink ver. 4.01 software was used to interpret the raw A/D counts from DSA3217 pressure scanner. Also, the settings of the scanner can be changed by using this software. Different parameters to configure the DSA scanner functions are discussed below (DSA3217/3218 Operational and Service Manual).
    - Average (Avg)- sets the number of raw samples to acquire before producing an averaged output. Its value varied from 1 to 24.
    - Binary Data (BIN)- sets the format of the data packet output. The value of BIN can be 0 or 1, where 1=Binary and 0 = ASCII
    - Unit Conversion Factor (CVTUNIT)- converts the calibrated units to the requested scan units. The value for CVTUNIT can be any real number.
    - Engineering Units (EU)- sets the output format for temperature and pressure units. The EU value can be 0 or 1, where 0 is for raw units and 1 is for engineering units.
    - Data Format (Format)- determines if data is to be scrolled on the display. The value of Format can be 0, 1 or 2, where 0 = data is scrolled, 1= data is displayed in place, formatted for a VT100 terminal and 2= data is displayed in CSV format.
    - Frames Per Scan (FPS)- sets the number of averages frames to send to the host computer when a scan command is issued. Averaged frames will be sent to the host computer until the value of FPS is met. At the time the DSA will exit the scan mode and wait for another command. The value of FPS can range between 0 to 2147483648, if 0 is entered, the scan will continue until a STOP command is received.
    - Page (PAGE)- When set to 1, the DSA will accumulate 10 frames of data before the data is sent over the network. If FPS is set to a number less than 10, the data will be sent over the network when FPS is completed. When a Stop command is issued, the frame acquisition will stop on a 10 frame boundary. The value of PAGE is either 0 or 1.
    - Period- sets the interval between channel samples in microseconds. The value of period can vary between 73.5 to 65535.
    - QPKTS- this switch controls the action the DSA will take when the data buffer is full. The valid values for QPKTS is 0 or 1, where 0 means frames will be discarded when the data buffer is full. The DSA will continue to scan and 1 means no frame will be lost. The DSA will stop scanning and log an error if the data buffer is filled.
    - Data Sample Source (SIM)- determines the source of the data samples. The value of SIM is either 0 or 1, where 0- data are taken from the sensors and 1- data are generated internally.

- Time Stamp (TIME)- determine the format of the Time Stamp. The value of TIME ranges from 0 to 3, where 0- no time stamp, 1- time stamp data are in microseconds, 2- time stamp data are in milliseconds and 3- time stamp data are in PTP time.
- Scan Unit (UNITSCAN)- sets the scan units for the DSA. UNITSCAN will also affect the value of CVTUNITS.
- Enable External Trigger (XSCANTRIG)- sets the external trigger as the frame trigger. The value of XSCANTRIG can be either 0 or 1, where 0- internal clock is in the frame trigger and 1- external trigger is the frame trigger.
- Zero Correction (ZC)- set zero correction on or off. If ZC=0, there is no correction and if ZC=1, there is zero correction.

The values selected during the current research for the configuration variables described above, are listed in Table 3- 1 below.

Table 3- 1 : Settings parameters for the pressure scanner

| | |
|---|---|
| Period | 500 |
| Avg | 10 |
| FPS | 0 |
| XSCANTRIG | 0 |
| FORMAT | 0 |
| TIME | 0 |
| EU | 1 |
| ZC | 1 |
| BIN | 1 |
| SIM | 0 |
| QPKTS | 1 |
| UNITSCAN | PA |
| CVTUNIT | 6894.76 |
| PAGE | 0 |

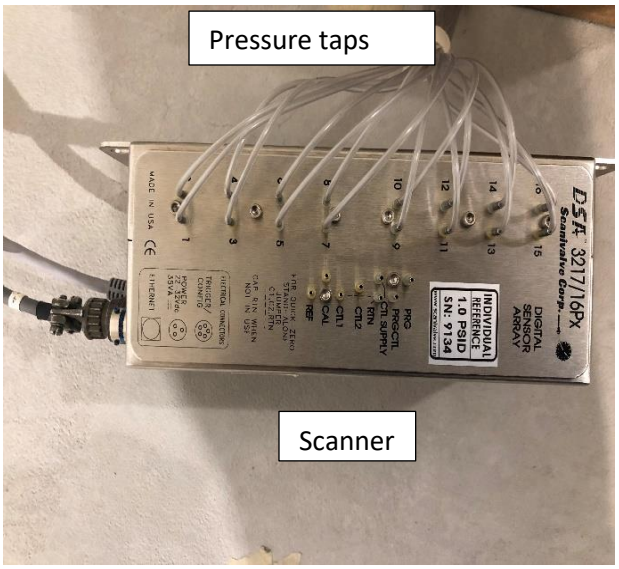


(a) Pressure Scanner and Pressure taps

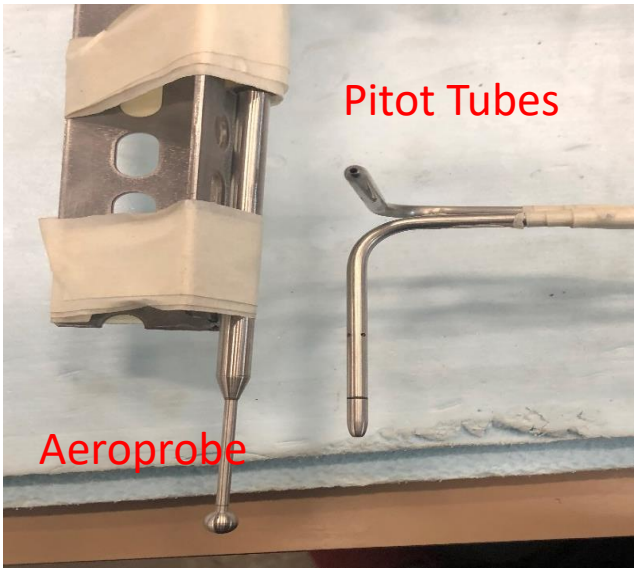


(b) Aeroprobe and Pitot tubes

(c) Steel rod setup

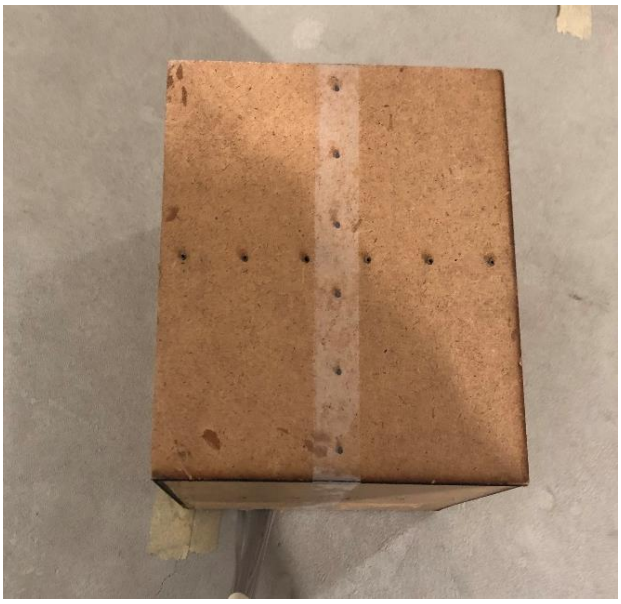

(d) Silsoe Cube Model (scale 1:40)

Figure 3. 3 – Equipment used during experiment

## 3.3 Experimental Setup

The Wind-induced Damage facility is relying on the lateral inlets for achieving the wind flow required for the experiments, however because the inlets have small circular section ($0.125m^2$), the wind speed profile will be much different, when compared with the conventional wind tunnel facilities, which employ large rectangular cross sections for incoming flow. Therefore, the results from the WDS experiments are not comparable with the wind tunnel tests, but are more compared with the field measurements, as it will be shown in the following chapters. Also, due to the impinging jet created by the WDS inlets, these experiments focus on replicating the intensity of the wind speed and the turbulent components of the wind velocities, encountered in the field and not the entire boundary layer profile.

The current experiment was designed and performed in two different stages as listed below:

1. Stage A- the Aeroprobe sensor was installed successively at four different locations inside the WDS test chamber for determining the wind speed characteristics. These four locations were selected along the middle lines of the inlets, or the intersection of these when lateral inlets were also used, because the effect of incoming flow was considered to be more intense at these locations due to the proximity to the open inlets. To avoid the bouncing back of the flow from the back walls of the WDS, the sensors and the models were installed in the first half of the testing chamber. The measurements for wind speeds were performed at different heights, between the ground and 54cm, for determining the wind speed profiles and the turbulence parameters. The heights range of 0 to 54cm was chosen, in order to capture the effect of the inlets; also, the biggest height of the tested models was 30cm, thus the wind velocity at much bigger heights was not necessary for the current test. Moreover, it was noticed that there was not much variation in wind speed beyond the height of 54cm height.
2. Stage B- For determining the pressure coefficients at the four locations where the wind profiles were measured, three Silsoe Cube models, of scales 1:20, 1:30 and 1:40 were installed at the same locations and wind-induced pressures were measured by the pressure taps system, along vertical lines at the surface of the models. The pressure taps were installed on vertical lines, to be compatible with the same pressure taps arrangement used by Richards and Hoxey (2001) for their field measurements performed on full-scale Silsoe Cube structure.

### 3.3.1 Stage A Experiments: Wind speed profiles at four different locations in WDS

The wind profiles were determined at four different locations inside the WDS chamber, as shown in Figure 3. 5 (a) for five different RPMs (400, 500, 600, 700 and 800 RPM). The experiments were not performed for larger wind speeds, as this project was a non-destructive project and if RPM was increased beyond 800,

it would have damaged the models, the Aeroprobe sensor and the DSA3217Scanivalve pressure scanner as only1.0PSID pressure scanner was used during the experiments. Moreover, there was no filter installed in the outlet, thus if some elements break during the experiment and become debris, it would have damaged the blower. The default frequency of 750 readings per minute, given in the DSA3217 Scanivalve pressure scanner manual, was employed as the sampling frequency. The reference pressure was considered at the location of the DSA3217 Scanivalve pressure scanner. At each location wind velocities on 12 different directions were measured by the Aeroprobe device and through the Airflow 2.0 software, three main components, longitudinal velocity (u), vertical velocity (w) and transverse velocity (v) and the mean velocity (V) were determined. The measurements were taken for five different heights 14cm, 24cm , 34cm, 44cm and 54cm as shown in the Figure 3. 5(b), spanning the opening of the inlet and the height above this. Thus, the height of the lower point of the inlet circumference is 14cm and height of the upper point on the circumference is 34 cm, whereas the height of the center of the inlet is 24cm. For investigating the wind profiles and turbulence characteristics for different simulated wind conditions, this experiment was conducted for three different combination of opened inlets as listed below.

- In Case 1- Inlets A and B were opened and all the remaining inlets were closed.
- In Case 2 -Inlets A, B and C were opened and all the remaining inlets were closed.
- In Case 3- Inlets A, B, C and D were opened and all the remaining inlets were closed.

The Aeroprobe sensor used to determine the wind speeds on 12 directions at each point is a very sensitive instrument, therefore when installing it in the wind-box, it was very important to ensure that there was no vibration of the Aeroprobe support during the experiment. A Scanivalve pressure scanner of 1.0 PSID was used to obtain the data from Aeroprobe. The pressure scanner has 16 different channels, out of which 12 were used by Aeroprobe and remaining 4 channels were used by the two Pitot Tubes. Pitot tubes were installed on x and y wind direction, at the same location with the Aeroprobe sensor, to verify the positive and negative directions of the results drawn from Aeroprobe. The wind flow was simulated for 2 min for each RPM, at each location and for every height tested. The number of readings that were recorded in 2 mins were 1,500 which leads to a frequency of the pressure scanner of 750 readings in 1 minute.

After recording all the measurements with the aid of Aeroprobe sensor, the raw data was processed in Aeroflow (v2.7.1) software which provides the time history values and graphs for the three different components of velocity (u, v and w) and for the mean velocity (V). Thereafter, the measured parameters were processed in Matlab (2018) to represent the wind speed profile graphs at different locations, for different heights and for 400 RPM to 800 RPM. Because of the injection flows coming into the box from several inlets concomitantly, the mixing layers would cause a highly turbulent wind flow. Therefore the turbulence spectra were calculated and plots were also generated in the Matlab (2018) for each height for

all locations, at each RPM tested, as part of cases presented in this section. The three main velocities component (u, v and w), were employed to generate the spectra plots and were compared with Von-Karman formulation for turbulence spectra.

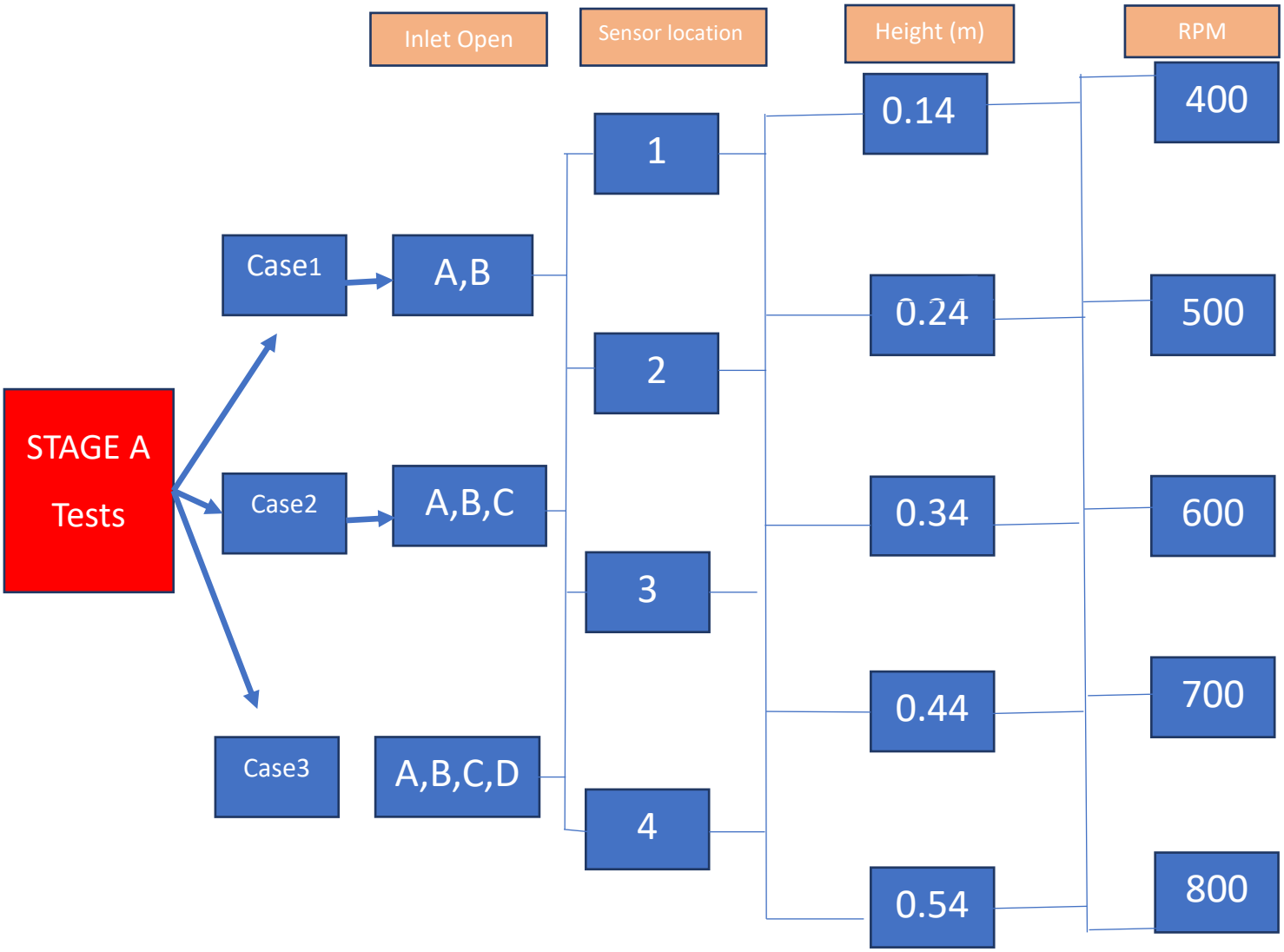


Figure 3. 4- Schematic of combination of experiments in stage A

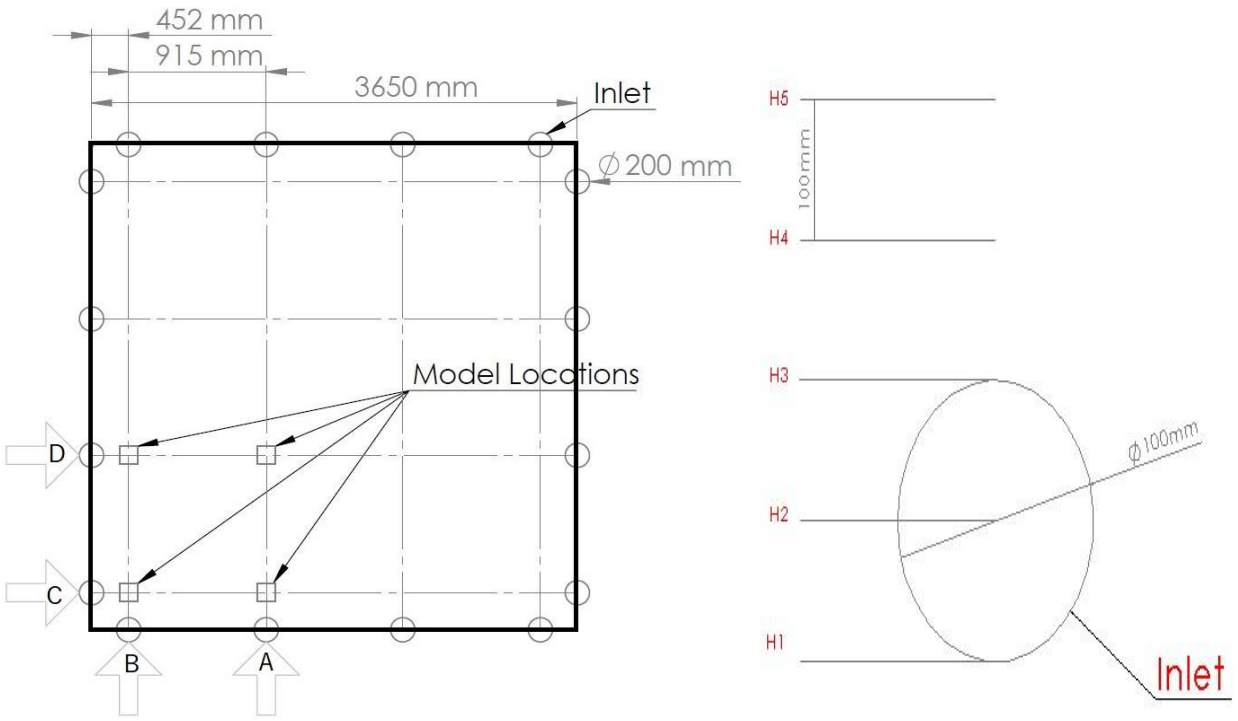


(a) Schematic representation of WDS locations layout (b) Schematic of inlet and heights of Aeroprobe

Figure 3. 5- Schematic representation of the WDS layout and inlet with the heights of the Aeroprobe

### 3.3.2 Stage B experiments - pressure coefficients for Silsoe Cube models

For the stage B experiments, the same three combinations of inlets were employed, as described in section 3.3.1. During this stage, the pressure coefficients were measured on models of three different scales (1:20, 1:30 and 1:40) of the Silsoe Cube, for five different RPM (400, 500, 600, 700 and 800 RPM) and at four different locations in the WDS chamber, as shown in Figure 3. 5 (a). Similar to stage A experiments, wind-flow was circulated within the WDS chamber for 2 minutes when recording the pressure measurements. Pressure taps were installed on16 points along a vertical line on the Silsoe Cube models, spaced at 0.173L between them, as shown in

Figure 3. *6*, where L is the side of the cube. The first pressure tap was situated at 0.29L from the ground and the last pressure tap on the front face was at a distance of 0.066L from the edge. Pressure data was processed in Matlab software for all three scales models, to determine the pressure coefficients. After determining the pressure coefficients, these were represented in graphs at 16 positions for all the experiments. Schematic of stage B experiments is shown in

Figure 3. *7*.

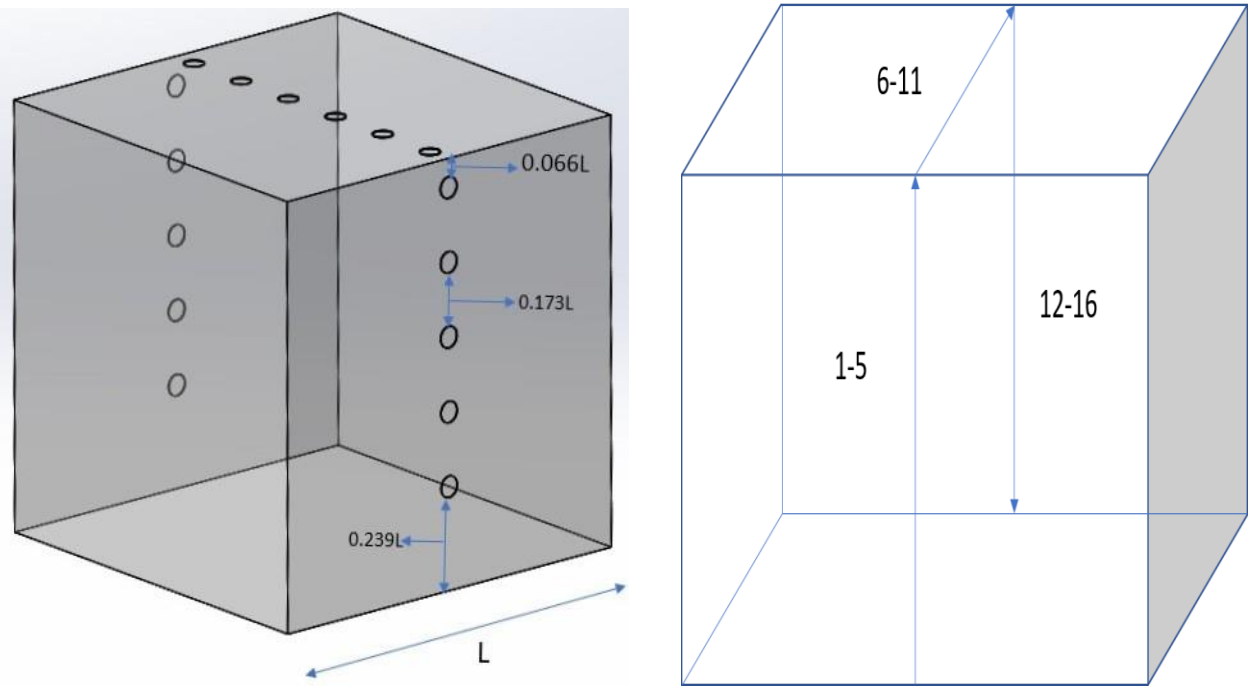


Figure 3. 6- Positions of pressure taps on the Silsoe Cube models

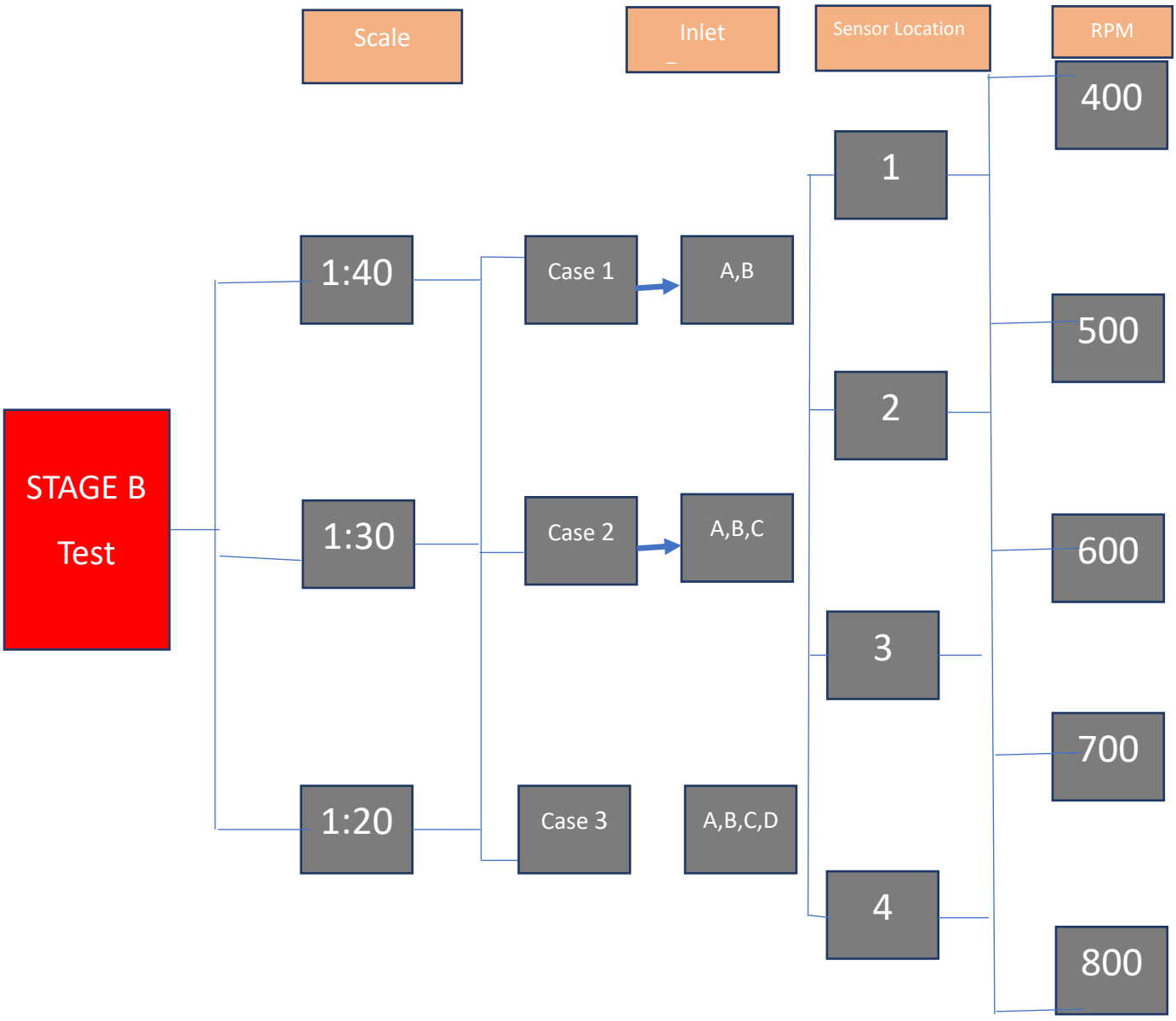


Figure 3. 7- Schematic of cases combinations for experiments in stage B

From the stage A experiments, the adequate wind speed profiles and the best location inside the testing chamber will be determined and these will be proposed for performing the pressure coefficients measurements the Silsoe Cube models, as presented in Chapter 4. The stage B experiments will conclude with the pressure coefficients for the three Silsoe Cube models and these will be compared with the pressure coefficients available in the literature from the field experiments results reported for the full-scale Silsoe Cube.

# Chapter 4 -Experimental Results

The wind effect on structures can be evaluated for different types of wind speed profiles, which will give an indication on type of wind phenomena that is simulated. For a boundary layer wind profile, the wind flow simulated in experiments should match the power law or logarithmic law profile, as detailed in Chapter 2. Turbulent wind profiles are described by the wind speed averages along with the frequency contained in the wind speed fluctuations measurements. The Wind-induced Damage Simulator (WDS) is a new experimental facility, which is capable of replicating several wind profiles, however detailed analysis of the measured wind speeds is required for each tested case, as wind speed profiles data collection is just in incipient phase for this facility.

Once the wind speed profiles and the turbulence properties are determined, the wind-induced pressure for the standard shape Silsoe Cube structure is quantified by determining the pressure coefficients, for different locations inside the testing chamber and different types of wind speed profiles. The wind speed intensity was controlled by adjusting the RPM values for the blower, while the wind speed angles of the attack were not investigated in the current research, as the objective was to determine the effect of using different inlets arrangements, from the two adjacent walls, which would create both a wind speed inclination angle and a turbulent profile.

## 4.1 - Stage A experiment- Wind speed profile results

### 4.1.1 – Wind speed profiles comparison

In this section the wind speed profiles are compared for different RPM values, at different locations and for different inlets opening arrangements, for determining the best location for conducting the wind-induced pressure experiments within the WDS facility. The wind speed profiles depict the three different components of velocity which are: the longitudinal velocity (u), which is in the direction of the wind flow, the transverse velocity (v), which is in the direction perpendicular to the longitudinal velocity in horizontal direction - the vertical velocity (w), which is in the direction perpendicular to the longitudinal and transverse velocities in vertical direction, and the mean velocity (U),which is the resultant of the above

discussed velocities. Figure 4. 1 and Figure 4. 2 represent the wind speed profile for different locations in the test chambers, at 600 RPM for case 1 and case 3 respectively. The mean velocity (U), is the resultant of the longitudinal, the vertical and the transverse velocities, however because the values of the transverse and vertical velocities are not significant, the value of the mean velocity depends mostly on the magnitude of the longitudinal velocity. The highest value of the mean velocity, of 10 m/s was attained at 2$^{nd}$ height (0.24 m) for all tested locations, where the strong incoming flow from the inlets is dominant, except for location 4 in Case 1, which is influenced by the suction produced by the WDS outlet, as shown in Figure 4. 1. Actually, the entire wind speed profile is different for location 4, due to the proximity to the ceiling outlet, which induces a higher vertical suction, associated with a higher vertical wind speed component ("outlet effect"), but also due to the longer distance from the active inlets, which involves lower longitudinal and transverse velocity components. Most of the variation registered in the wind speed profiles occurred at the heights up to 0.34m, covering the diameter of the inlet, while for the heights above the inlet, from 0.44 m and above, the longitudinal and the transverse velocity components stabilized towards values close to 0, and the vertical components approached negative values of up to -1.0 m/s as the effect of wind flow above 0.34 m was not significant. For case 3, the maximum mean velocity is registered at 2$^{nd}$ height as well, for all the tested locations, except for the location 1, as shown in Figure 4. 2. The wind speed profile for location 1 is different for case 1 and case 3, because of the mixing wind flows entering the WDS from inlets C and D (lateral wall) in case 3, thus producing higher variation at the inlet levels and smaller magnitude for all components. The reason for attaining the maximum value of mean velocity at the 2$^{nd}$ height is that this is at the center of the inlet and the maximum wind velocity will be at the center of the enclosed circular section of the inlet. The maximum mean velocity due to the inlet can be defined as the "inlet effect". The mean velocities at 4$^{th}$ (0.44 m) and 5$^{th}$ (0.54 m) heights are the same for all the locations, as there is no effect of the wind flow from the inlets, at these heights. When comparing the transverse velocities of case 1 and case 3, from Figure 4. 1and Figure 4. 2, it can be found that the transverse velocity increases when opening the C and D lateral inlets. The negative transverse velocity indicates that wind flow is redirected in the opposite direction. The wind entering from inlets C and D not only contribute to increase the transverse velocity but also neutralizes the effect of the wind entering from inlets A and B and thus decreases the longitudinal velocity. The negative vertical velocity indicates that the wind flow is directed in the upward direction, because of the outlet on the top of WDS. The maximum mean velocity is at location 3 for all the RPM values and for all the cases, so the best location for conducting the experiment is location 3. In this section only 2 cases (case 1 and case 3) are discussed but in later section wind profile graphs for all three cases are compared. Also, the detailed data for the wind profiles measured for the second case is provided in Appendix A.

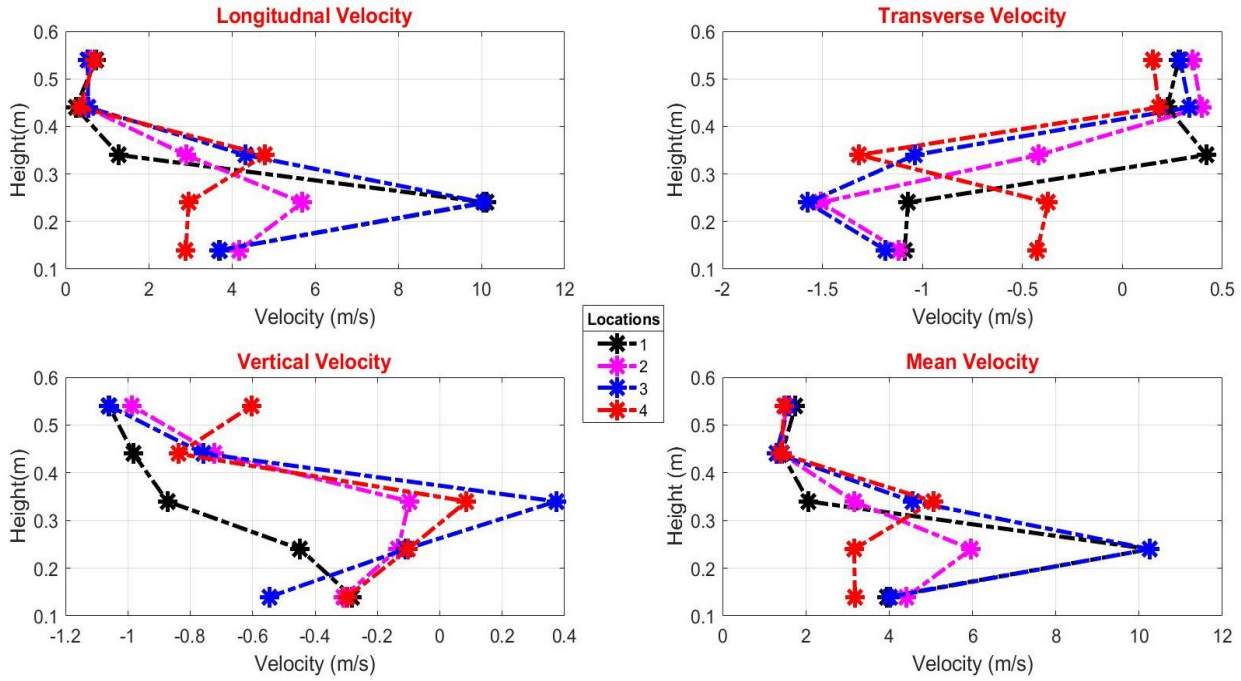


Figure 4. 1 Wind speed profile at different locations for case 1 at 600 RPM

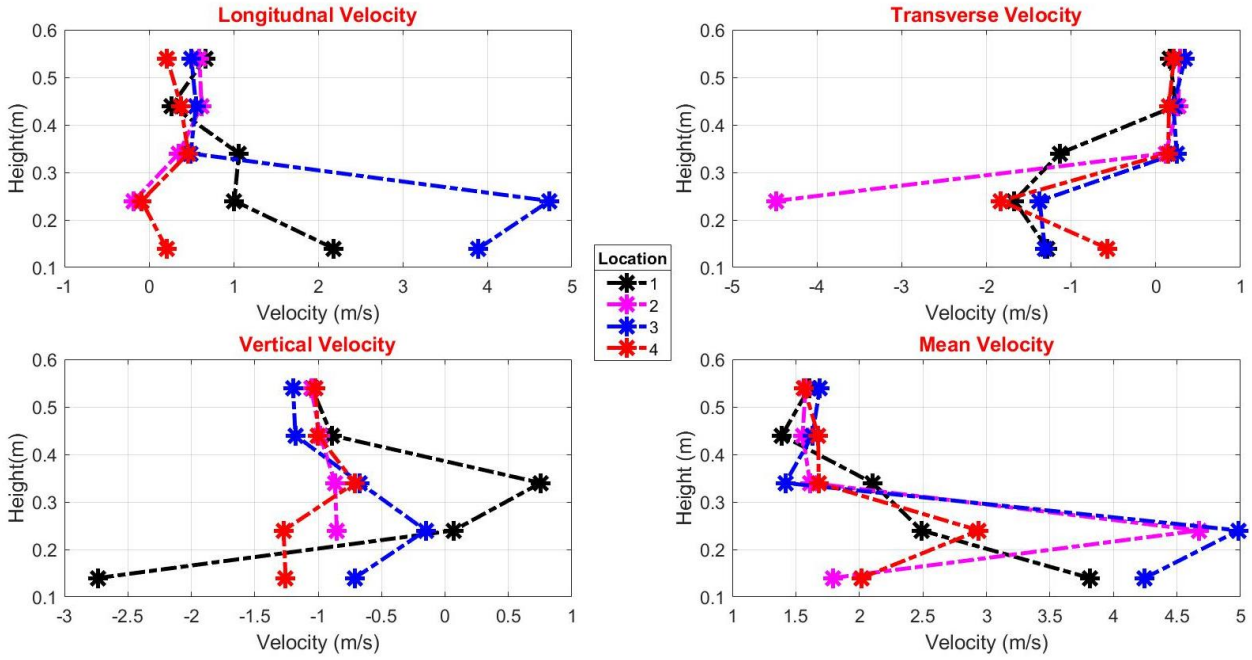


Figure 4. 2 Wind speed profile at different locations for case 3 at 600 RPM

Location 3 is considered to be the best location for wind-induced pressure test on models, because the wind speed profiles are more stable than for other locations, but also because the influence of the outlet and the bouncing back of wind flow from the lateral wall can be avoided. Moreover, the intensity of the wind speed could affect the wind flow regimes inside the box, thus in this section the wind speed profiles for all the RPM values (400, 500, 600, 700 and 800) at location 3 are discussed and compared. For the other cases, the results are included in Appendix B. Figure 4. 3 and Figure 4. 4 represent the wind speed profile for all the RPM values at location 3 for case 1 and case 3 respectively. In general, the measured wind speed increased gradually with the increase of RPM values, as expected. The maximum mean velocity is at 2$^{nd}$ height for both the cases, due to the inlet effect. The wind flow entering from the C and D inlets for case 3, does not have significant effect on the wind speed profile measured at location 3, because there is still a dominant inlet effect. For the case 3, but at location 1 there is no inlet effect, which can be seen in Figure 4. 2, because the wind flow entering in WDS chamber from the inlet C is neutralizing the effect the wind flow entering the WDS from inlet B, and as a result the maximum mean velocity for the wind profile at location 1 is registered at 1$^{st}$ height (0.14 m). The wind speed profiles are similar for both cases 1 and 3, which can be noticed in Figure 4. 3 and Figure 4. 4. The mean velocity is increasing from 1$^{st}$ height (0.14m) to 2$^{nd}$ height (0.24m), where it attains the maximum velocity then starts decreasing till 3$^{rd}$ height (0.34m) and has same value for 4$^{th}$ (0.44m) and 5$^{th}$ (0.55m) heights, for both the cases 1 and 3 and for all the locations investigated. Also, the values of mean velocities increased with the increase in RPM for both cases 1 and 3. The transverse and vertical velocities have very small negative values for almost all the cases, thus they do not contribute much to the mean velocity. Therefore mean velocity mostly depends on the longitudinal velocity and has similar wind speed profile as of the longitudinal velocity profile.

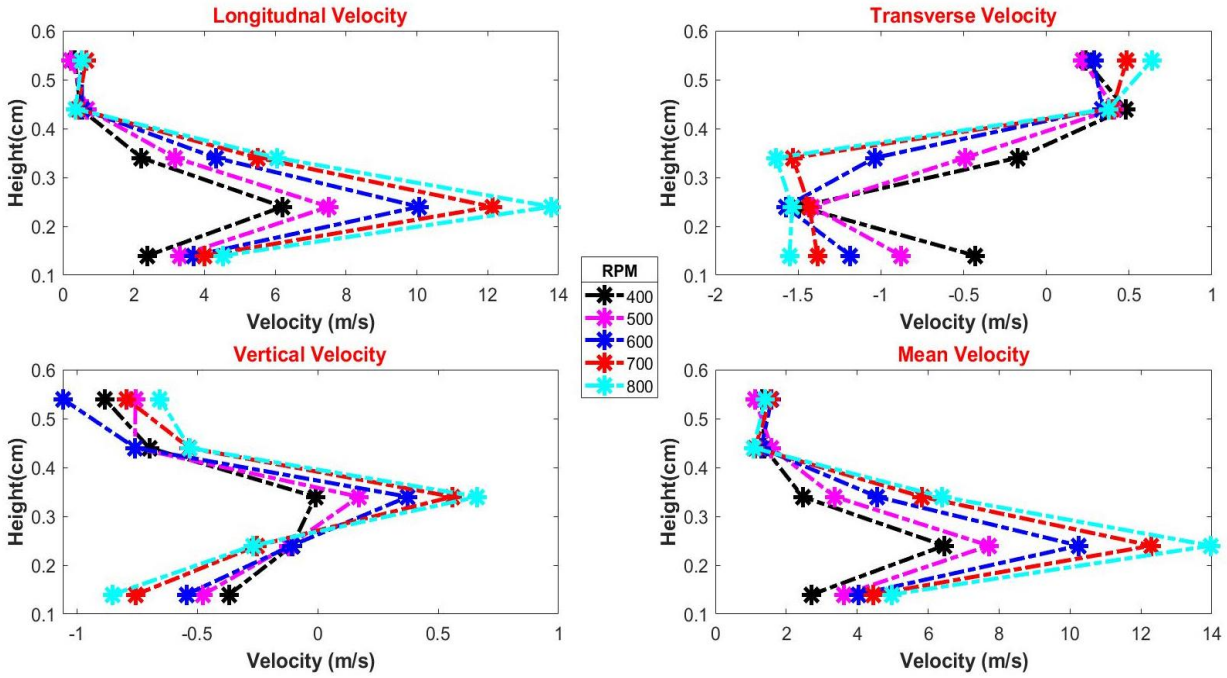


Figure 4. 3 Wind speed profile for Location 3 (case 1)

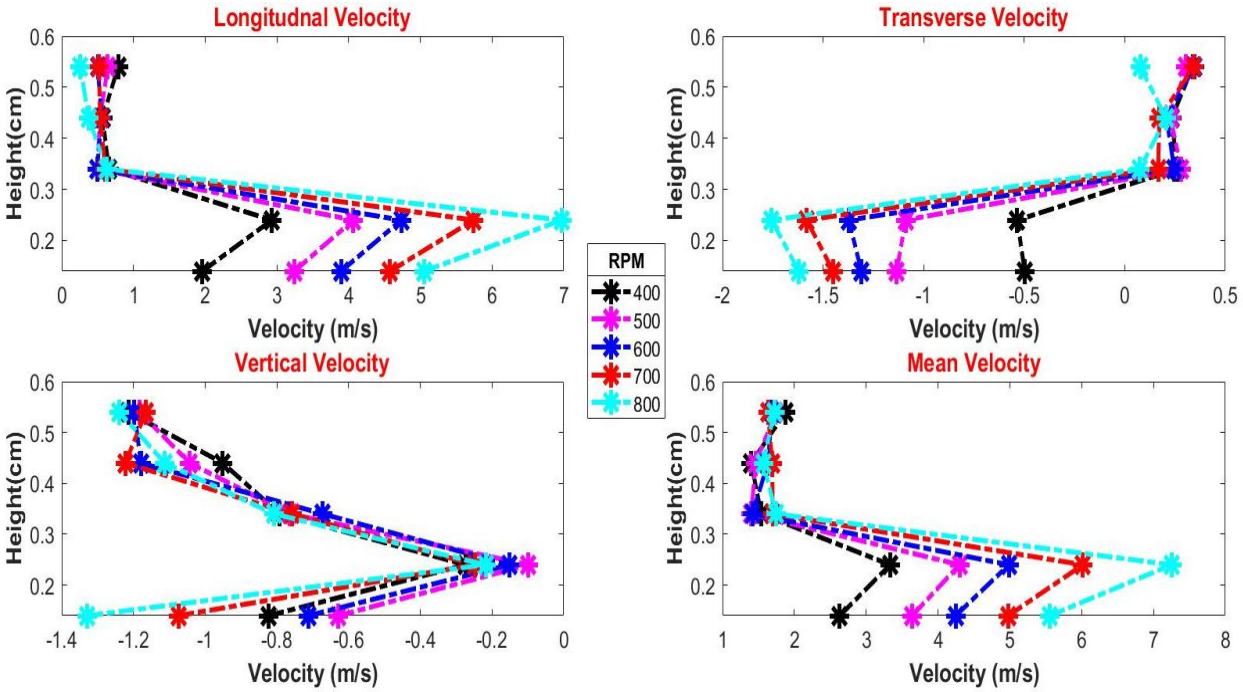


Figure 4. 4 Wind speed profile for location 3 (case 3)

Furthermore, Figure 4. 5 compares the wind speed profiles for all three cases at four different locations, for 600 RPM. From Figure 4. 5 it can be noticed that, wind flow velocity decreases when the number of open inlets increases, as the maximum velocity is attained during the experiment for case 1. The incoming wind flow is only in one direction because only two inlets (inlets A and B) are open on the same wall in case 1, and there is no mixing of wind flow entering from any other direction. The wind velocity decreased by opening more inlets and thus, the case 3 when 4 inlets (A, B, C and D inlets) are open, has the lowest value of wind velocity for all the locations, except for location 2. The maximum velocity for all the cases is at location 3, which also has the most consistent wind profile, thus it can be concluded that the best location for conducting the experiment in WDS is location 3.

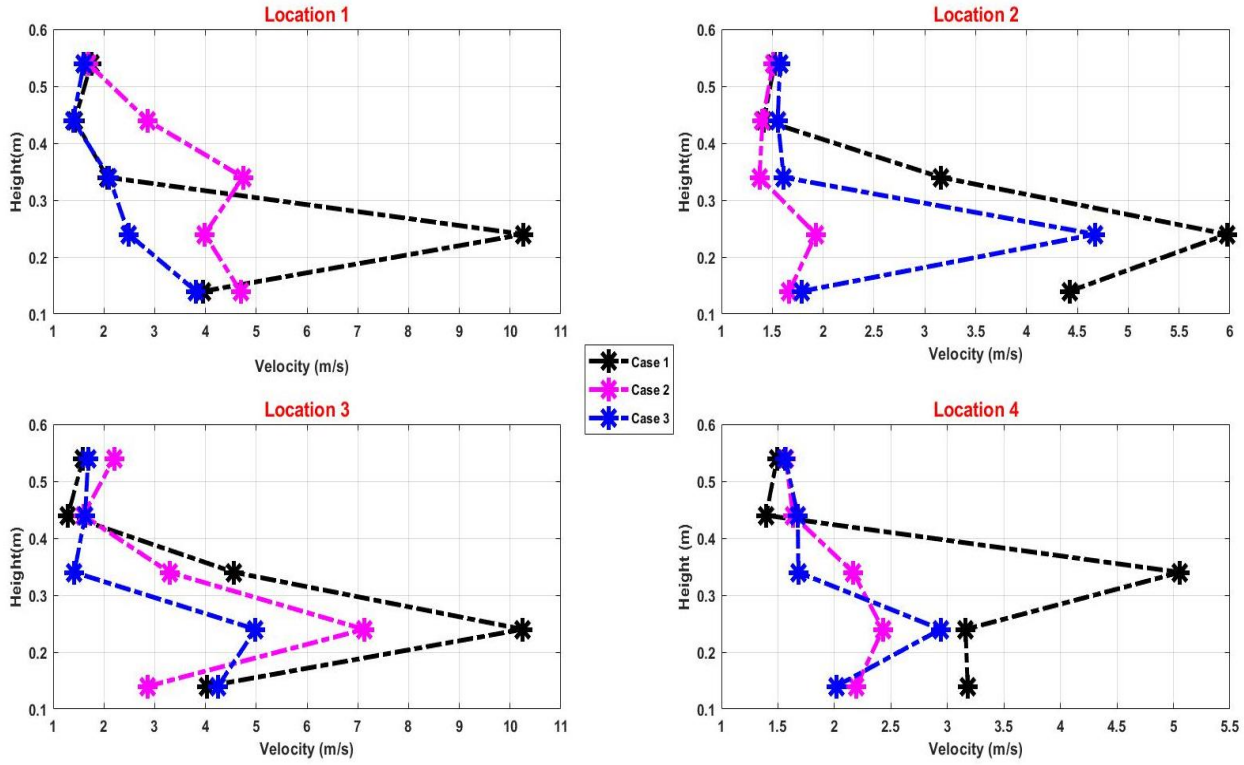


Figure 4. 5 Comparison of wind speed profile for all 3 cases at 4 different locations

### 4.1.2 – Wind turbulence and spectra

The wind speed profile simulated in the current experiment is different than the boundary layer wind profiles described in the design codes by the logarithmic or power laws (ASCE'07, NBCC'15), however it

is closer to a turbulent wind profile. Therefore, a description of the turbulence generated is attempted for better clarifying the experimental conditions induced by the new WDS facility. The power spectra for turbulence, measured at specific points in the wind flow were determined based on the time histories and the fluctuations of wind velocities (m/s) in longitudinal (u), vertical (w) and transversal (v) directions measured simultaneously at the same point with the help of the 12-holes Aeroprobe sensor. The importance of determining the turbulence frequency component in the wind flow is dictated by the wind-structure interaction and the wind-induced pressure at the surface of the investigated structure. Once measured, the experimental values of turbulence on u, v and w directions were compared to the calculated Von Karman turbulence. Figure 4. 6, Figure 4. 7 and Figure 4. 8 show the time history of the wind velocity in longitudinal, transversal and vertical directions respectively, for case 1 (A and B inlets were open) at 0.24 m height, for location 1 tested at 600 RPM. It can be noticed that the highest wind speed magnitude, of up to 12.2 m/s, was registered for the longitudinal wind speed component, u, which is directly impacted by the two lateral inlets opened during the experiment. For the lateral v, and the vertical w, wind speed components, smaller velocities were measured; also the fluctuations in the velocity time histories were higher for the longitudinal velocity component, when compared with the lateral and the vertical ones, due to the concomitant use of two open inlets, which produce mixing layers and due to the circular shape of the inlets, which induce an impinging jet. The time history for the other cases were included in Appendix B. A first measure of the velocity fluctuations for wind flow is the turbulence intensity, which represents the ratio between the standard deviation and the mean wind speed measured at a certain point (Peng et al., 2018). Figure 4. *9* represents the comparison of wind intensities in longitudinal (Iu), transversal (Iv) and vertical (Iw) directions, for five different heights (0.14 m, 0.24 m, 0.34 m, 0.44 m and 0.54 m) at location 1 for 600 RPM for case 1. It was noticed that the turbulence intensity was the highest in the longitudinal direction (Iu) for all the heights, except at height 0.44 m, located just above the inlet, where the turbulence intensity in the vertical direction (Iw) was higher than the longitudinal turbulence intensity (Iu). This might be caused by the mixing layers incoming from the inlets and spreading into the WDS testing chamber. The maximum turbulence intensities of 1.2%, 3.1% and 6% were attained at 0.44 m for Iv, Iu and Iw respectively, whereas turbulence intensity was minimum at 0.24 m, representing the middle of the inlet, due to the consistent wind flow incoming from the inlet at constant value. Higher turbulent intensities can be achieved in the WDS for destructive tests, which employ higher RPM values of up to 2,800RPM.

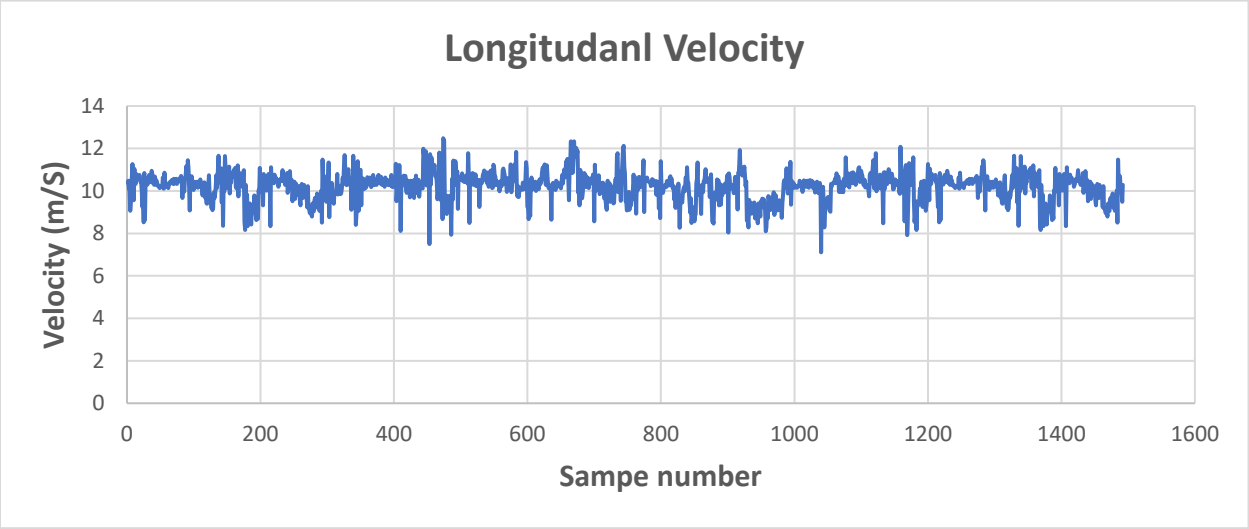


Figure 4. 6 Time history of longitudinal velocity (u)

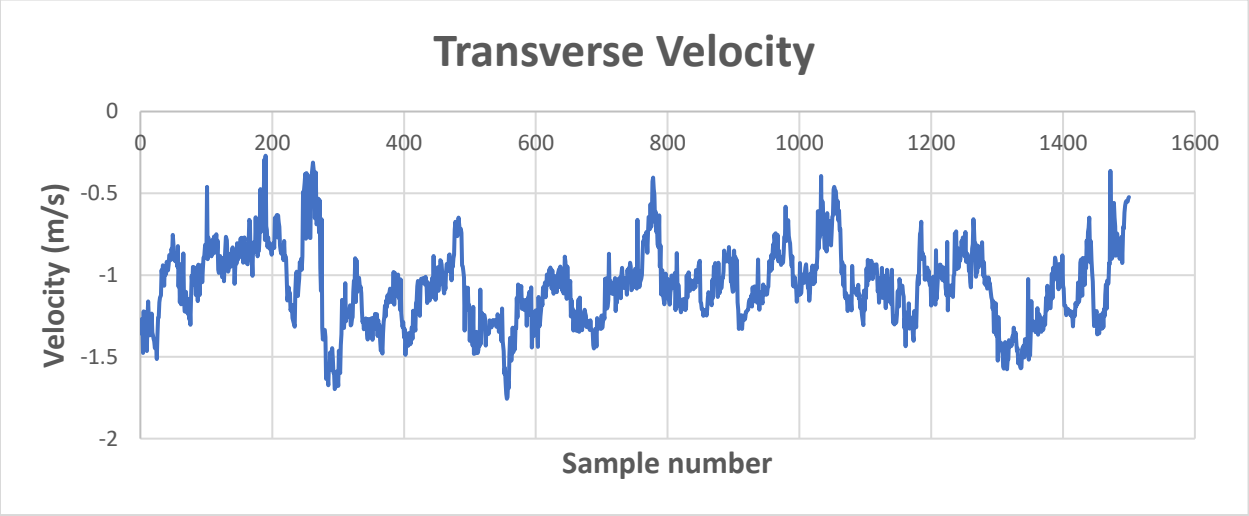


Figure 4. 7 Time history of transversal velocity (v)

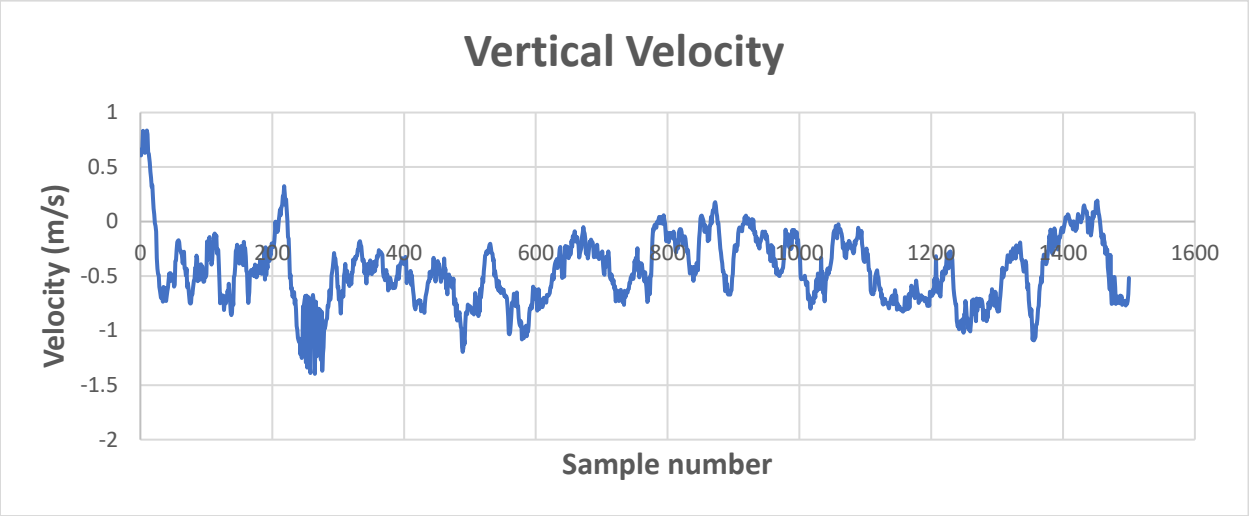


Figure 4. 8 Time history of vertical velocity (w)

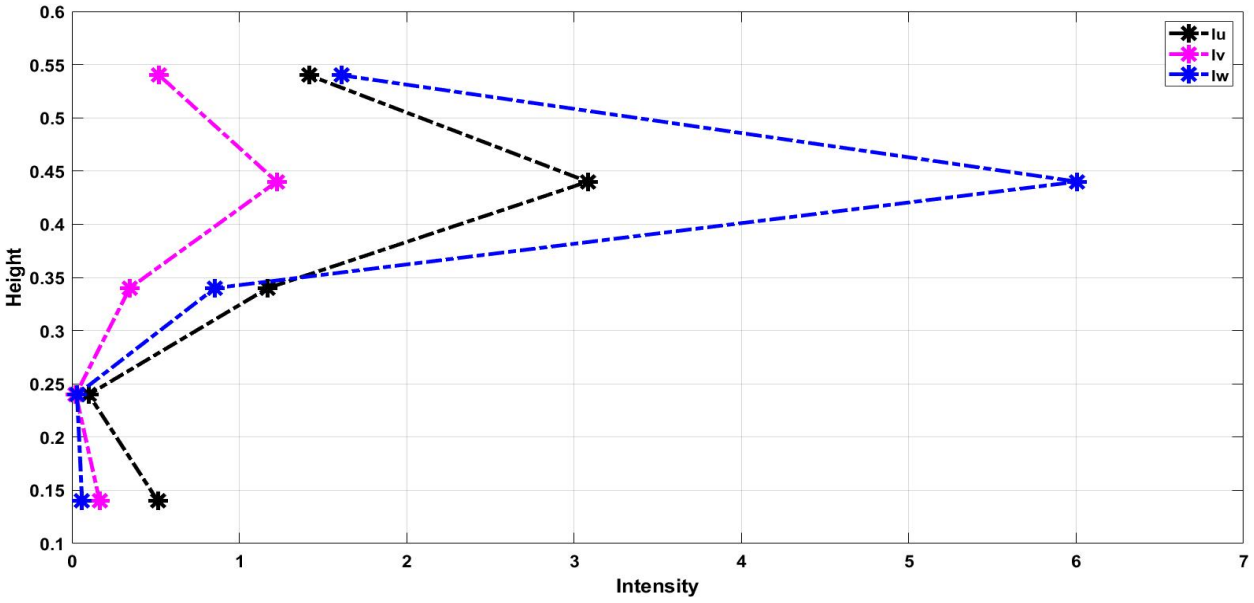


Figure 4. 9 Wind turbulence intensity in longitudinal (Iu), transversal (Iv) and vertical (Iw) directions, 600 RPM, Case 1

The current experiment simulated a wake-like flow, for which the high frequency component is dominant in the turbulence power spectra for all the directions, however the height where this is measured can influence this property. Von Karman spectrum was used for modelling and was compared with the measured turbulence data, as the WDS facility replicated wind flows in the vicinity of the ground, for which Von Karman formulation has showed a better agreement than Bush-Panofsky and Davenport spectra (Teunissen, 1971), however all these formulations are for boundary layers flows, thus some differences between the measured and theoretical turbulence spectra will be noticed. Moreover, no other facilities were capable to simulate high frequency turbulence with good accuracy (Morisson and Kopp, 2018), thus a better comparison is not available.

In general, it was noticed that the turbulence in the wind flow is mostly due to the longitudinal velocity, as depicted in the spectra plots given below. The main feature of all the spectra plots was that there was an increasing trend for the energy content with the increase in frequency, whereas in most of the previous researches for simulated wind turbulence, the energy decreased towards the high-frequency range (Davenport,1960, Morfiadakis, 1996,1999). However, the field measurements clearly indicate a higher turbulence component in the high frequency range (Liao et al, 2020, Morisson and Kopp,2018). In the graphs below, the red, black and blue lines in the turbulence spectra plots represent the theoretical values of u, w and v obtained by Von Karman formulation, whereas the red, black and blue dots represent the experimental values of u, w and v turbulences respectively, measured during the current tests.

Figure 4. 10 (a) and (b) show the turbulence spectrum at 0.24 m and 0.34 m respectively for location 1 at 600 rpm, for case 1 (inlets A and B open). The wind flow was turbulent at 0.24 m height and it became less turbulent at 0.34 m height. Thus, it can be concluded that the wind flow turbulence shifted towards a high-frequency dominant component with the increase in height. The turbulence in the vertical and transversal wind velocities at location 1 showed an increase for lower frequency, followed by a decrease in the high frequency range as depicted in Figure 4. 10 (a), which is similar to the turbulence generated in the boundary layer wind tunnels; the turbulence spectra for the longitudinal wind velocity was higher for the higher frequency range, which is similar to the field measured turbulence intensities (Liao et al, 2020).

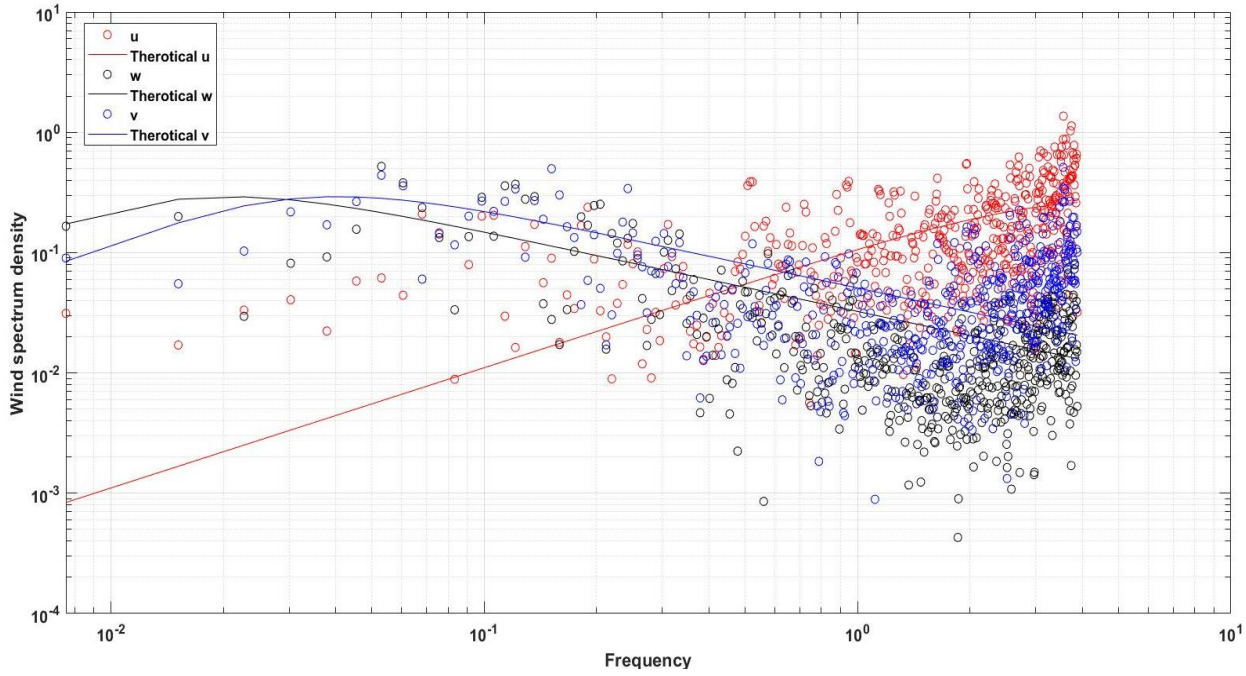


(a) Turbulence spectra at 2nd height (0.24m), at location 1 for 600 rpm

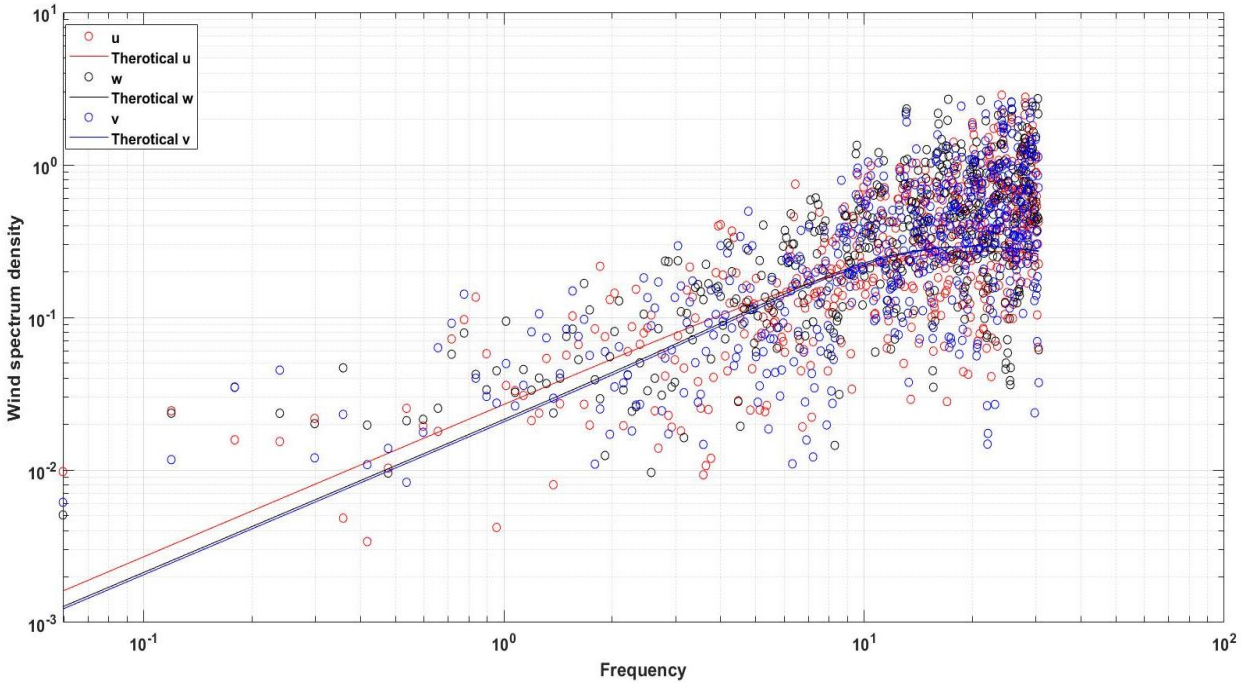

(b) Turbulence spectra at 3rd height (0.34m) at location 1 for 600 rpm

Figure 4. 10 Turbulence spectra for location 1 for 600 RPM

For location 2 and case 1, the spectra plots are consistent with each other for all the heights investigated and these are more similar to the field turbulence spectra. The spectrum plots of 0.24 m and 0.34 m at location 2 were shown in Figure 4. 11 (a) and (b), where it can be noticed an increase in the wind flow turbulence with increase in frequency, for all the 3 directions investigated. Also, the wind velocity at location 2, which is on the second row, thus further away from the open inlets, registered lower values when compared with location 1, due to the fact that the wind flow was more stable at location 2 and there is not much scatter in the turbulent spectrum measured data.

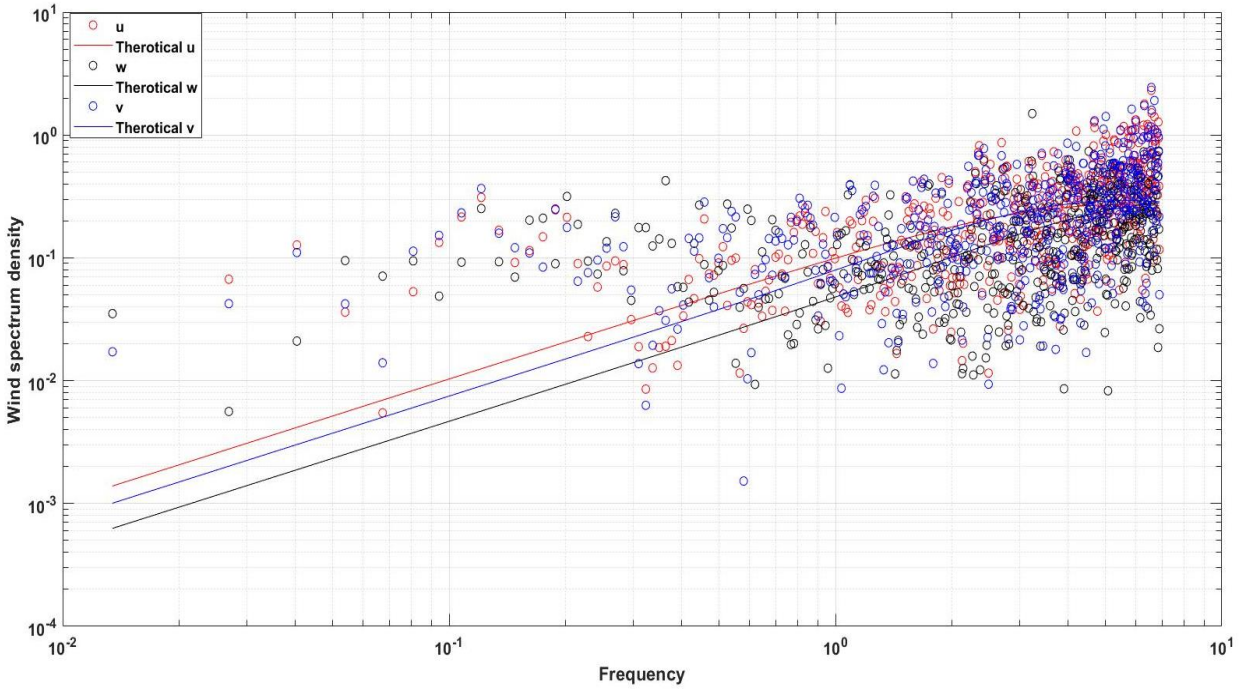


(a) Turbulence spectra at 2nd height at location 2 (0.24m) at 600 rpm

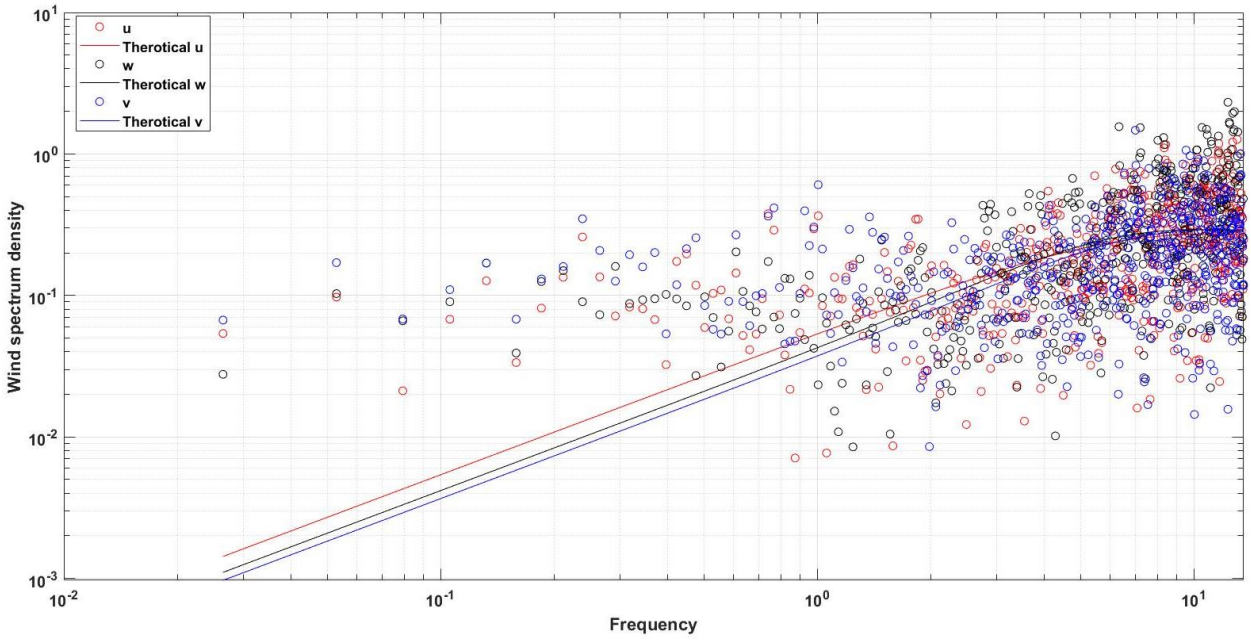


(b) Turbulence spectra at 3rd height (0.34m) at location 2 for 600 rpm

Figure 4. 11 Turbulence spectra for location 2

The Figure 4. 12 (a) and (b) represent the turbulence spectra for 0.34 m and 0.44 m at location 3, for 600 RPM and case 1. At location 3, which is in front of the inlet A, the turbulence measured for the vertical component of wind showed a decreasing trend towards the high frequency range, for 0.44 m, as shown in Figure 4. 12 (b), which is consistent with the turbulence spectra simulated in wind tunnels. For the longitudinal and transversal wind velocities however, the turbulence spectrum showed an increased energy with the increase in frequency, as per the evolution of the turbulence spectrum measured for field data (Liao, 2020, Morisson and Kopp, 2018). The wind flow turbulence energy in the spectrum of the vertical velocity component decreased with the increase in frequency, whereas for the longitudinal and transverse velocity components, energy was increasing at 0.34 m. The wind flow turbulence energy in the spectrum increased with the increase in frequency for all three components, when the flow reached 0.44 m height.

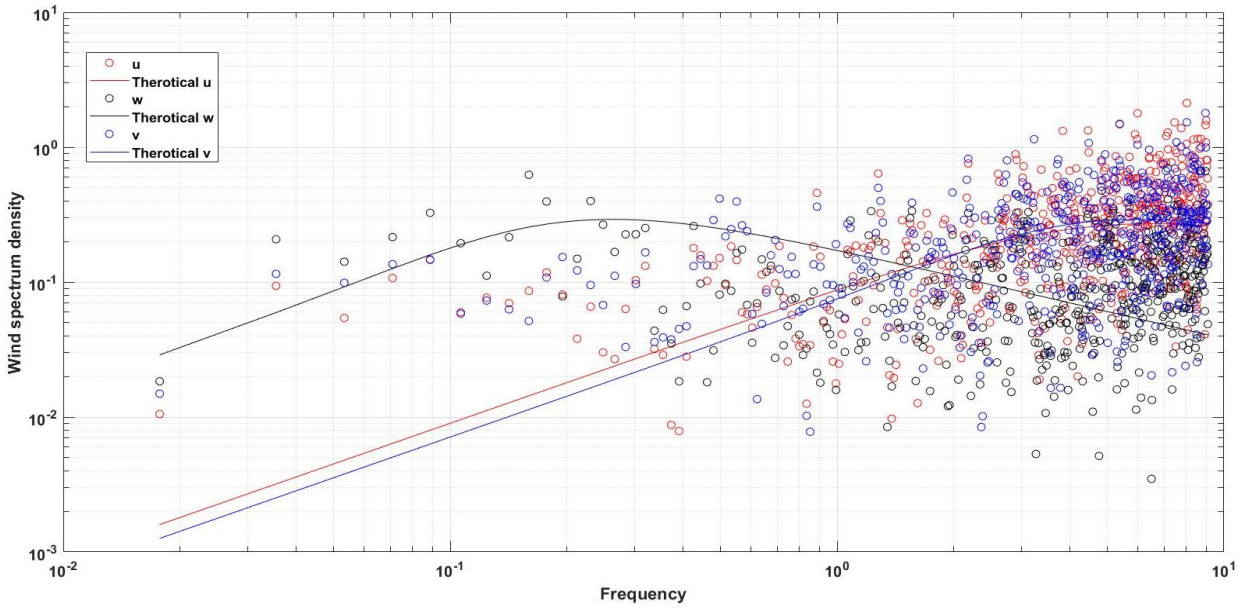


(a) Turbulence spectra at 3rd height (0.34m) at location 3 for 600 rpm

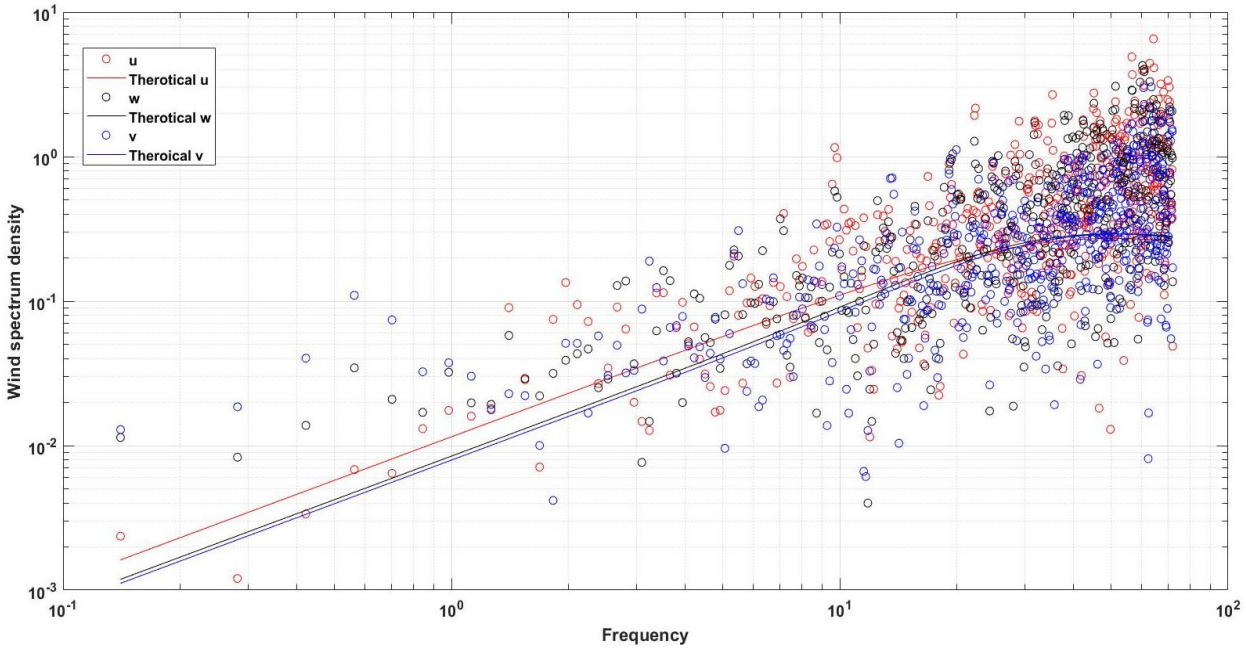


(b) Turbulence spectra at 4th height (0.44m) at location 3 for 600 rpm

Figure 4. 12 Turbulence spectra for location 3

For location 4, which is the closest to the center of the WDS testing chamber, and thus might experience influence from the upper outlet, the wind flow was highly turbulent, with much scatter in the measured data, until the height 0.34 m, but the turbulent spectrum data became more consistent at 0.44 m. The vertical component of wind velocity showed higher energy for low range frequency, as depicted in Figure 4. 13 (a). The wind flow energy was increasing with increasing frequency for longitudinal and transversal component where energy was decreasing for vertical component at 0.34 m height. The Figure 4. 13 (b) shows that the wind flow turbulence energy increased with the increase in frequency, at 0.44 m for location 4, which is more similar to the filed measured turbulent spectra (Liao et al, 2020, Morisson and Kopp, 2018)

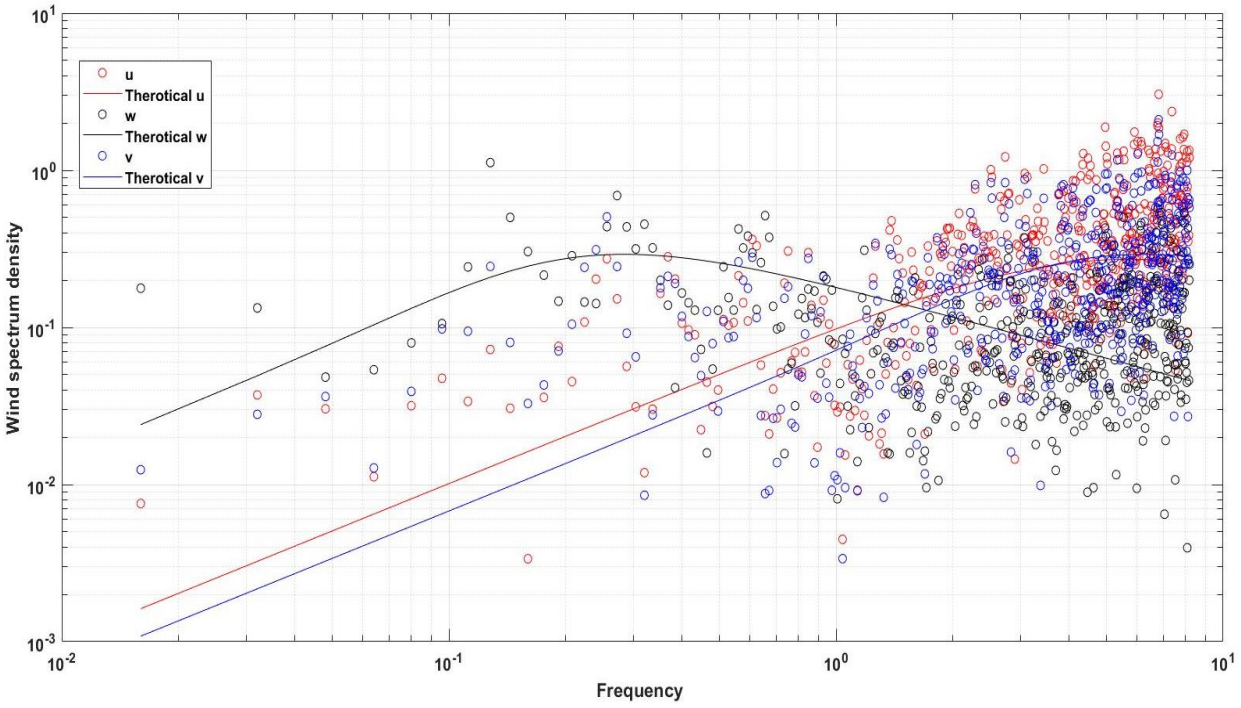


(a) Turbulence spectra at 3rd height (0.34m) at location 4 for 600 rpm

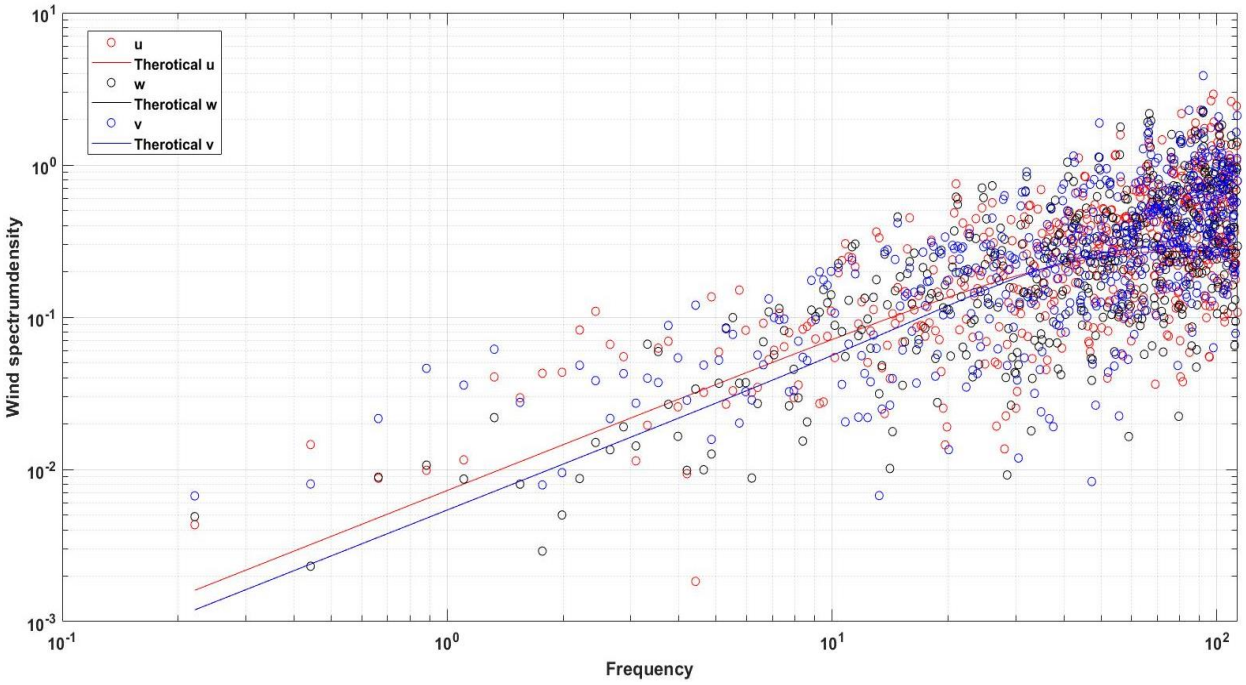


(b) Turbulence spectra at 4th height (0.44m) at location 4 for 600 rpm

Figure 4. 13 Turbulence spectra for location 4

For all the investigated cases the wind speed data measured during the experiment was different then the theoretical Von Karman formulation, mostly due to the fact that the theoretical expression was developed for stable air flow applicable to boundary layer, however the wind flow developed in the WDS is more turbulent and is based on mixing layers of wind flow incoming from the inlets and re-directed towards the outlet. Still Von Karman spectra was found to fit the experimental data better than other wind speed spectra formulations used in wind engineering. Moreover, while in the conventional wind tunnels the wind speed spectra would peak at low frequencies (synoptic peak) and would show a low energy component for high frequencies, the wind speed spectra determined from the WDS experiments registered higher energy components for high wind frequency, thus making the data more compatible with the wind speed spectra measured in the field experiments.

## 4.2 - Stage B experiment- Pressure coefficients for Silsoe Cube models

The wind flow characteristics investigated in the first phase of the experiments showed that the simulated wind profiles and the wind flow turbulent spectra are more similar to the wind velocities and turbulences reported by field data measurements, than those simulated in the standard boundary layer wind tunnels. Therefore the wind-induced pressure coefficients are measured in the WDS for a basic shape Silsoe Cube, for 3 different scales, 1:20, 1:30 and 1:40, and are compared with the field pressure measurements reported for the same structure (full-scale) by Richards et al, (2001) and with a previous wind-box study reported by Xiao and Dragomirescu (2019).

### 4.2.1- Pressure coefficients comparison

In this section pressure coefficients at four different locations, for five different RPM values (400, 500, 600, 700 and 800) are represented in Figure 4. 14 (a), (b), (c) and (d), while for different combinations of opening inlets these are compared in Figure 4. 15 and Figure 4. 16. The reported pressure coefficients were measured along a vertical line crossing the front wall of the Cube (points 1 to 5), the roof of the Cube (points 6 to 11) and on the back wall of the Cube (points 12 to 16), because it is considered that this path is the most impacted by the incoming wind flow. The increase of the RPM values is associated with the increase of incoming wind speed, however because the pressure coefficient CP is non-dimensional, this should not be affected by the change in velocity or by the change in RPM values; when performing experiments, this condition should be verified for the given testing conditions. For location 1, case 1, the pressure coefficient for the model scaled at 1:20, were consistent with each other, for the tested RPM values, expect for the 400 RPM, where higher CP values were determined on the front wall of the Silsoe Cube, as it can be seen in Figure 4. 14. For location 2, case 1 (Figure 4. 14 (b)), when the model is placed in front of the second open inlet, the pressure coefficients started from higher values on the front wall, which receives the full wind speed impact incoming from the inlets, but for the roof and back regions, the coefficients decreased to values closer to 0, as in the previous case (location 1,case 1). When the model was placed at location 3, the pressure coefficients trend was similar to the one for location 1. For location 4, case 1, which bears the effect of the outlet on the ceiling of the WDS, very high CP values were recorded on the front wall, followed by a sudden increase to negative values, towards the first part of the roof as depicted in Figure 4. 14 (d). Also, the pressure coefficients for the front wall and for the roof, were slightly different for different RPM values, which implies a variation of wind speed in this region. Therefore, it can be concluded that the pressure coefficients were not affected by increasing the wind speed for location 1 and 3, while for location 2 and 4 small discrepancies were noticed. In the later part of this section CP plots for 3 different scales of

the Silsoe Cube at 4 different locations and 2 different combination of opening inlets are discussed only for 600 RPM, as the reported CP was not affected by the change in wind speed.

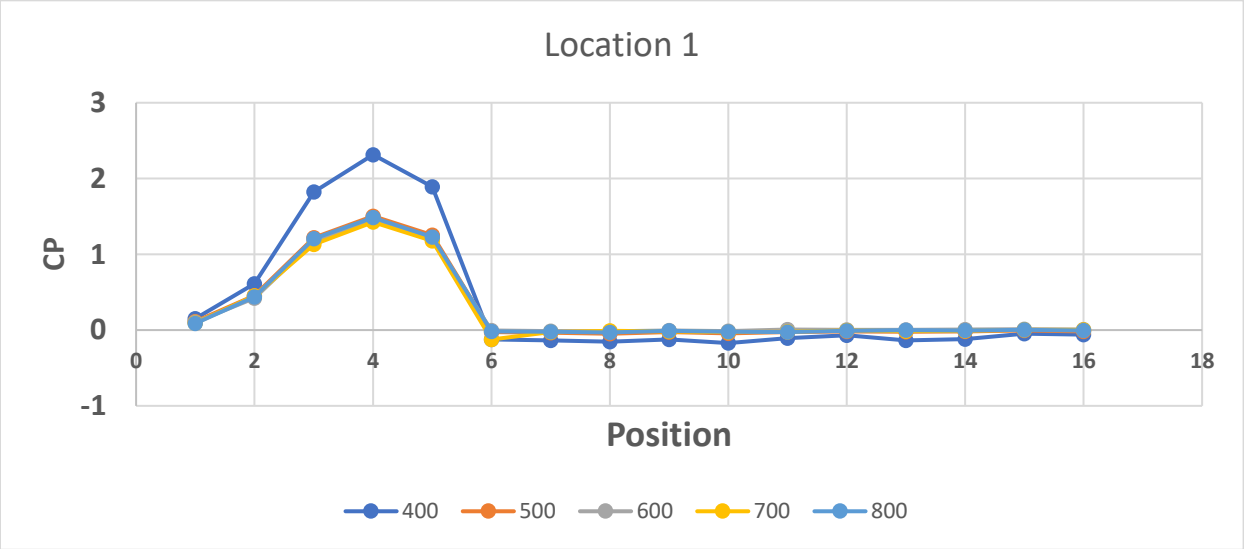


(a) Pressure coefficients at location 1 for case 1

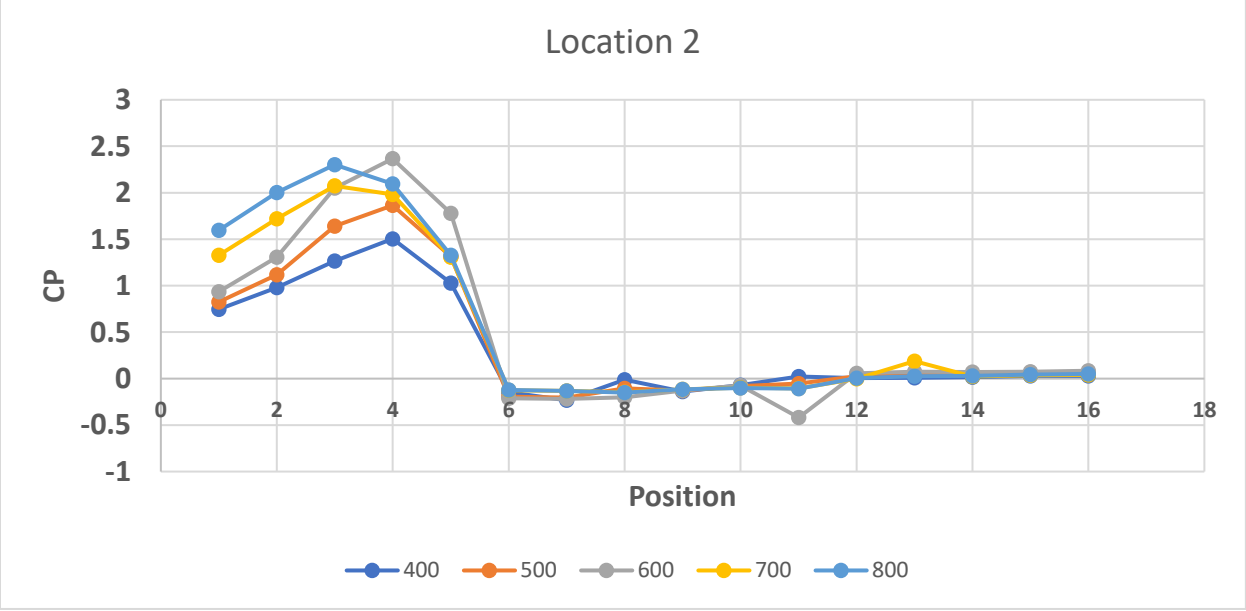

(b) Pressure coefficients at location 2 for case 1

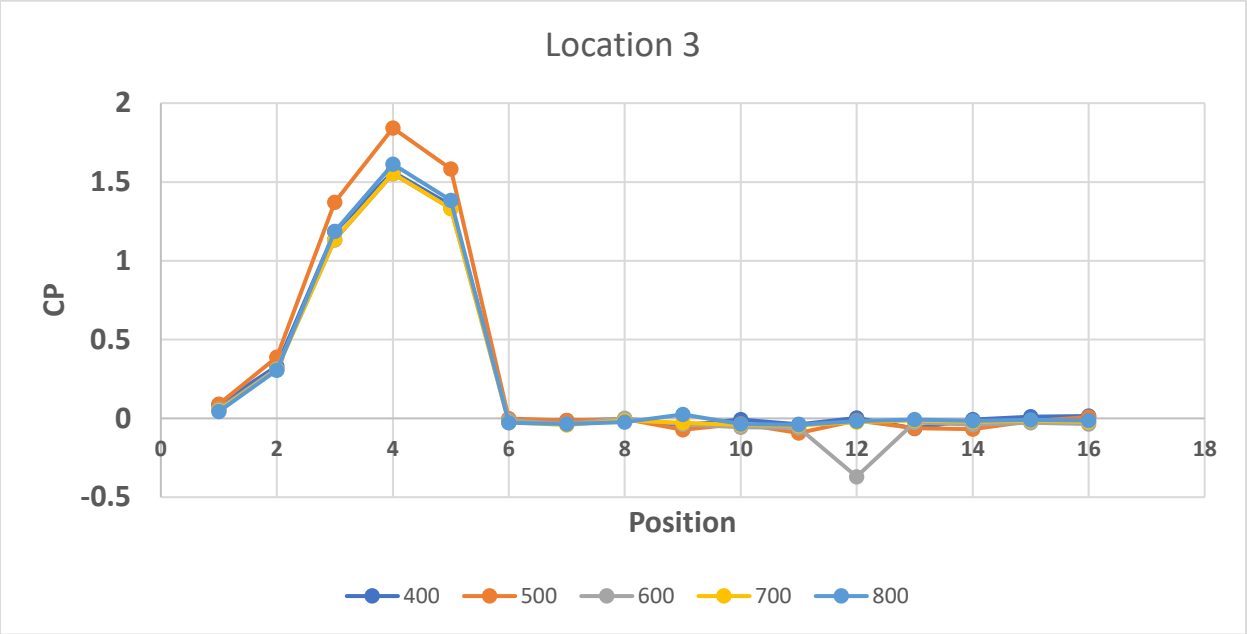


(c) Pressure coefficients location 3 for case 1

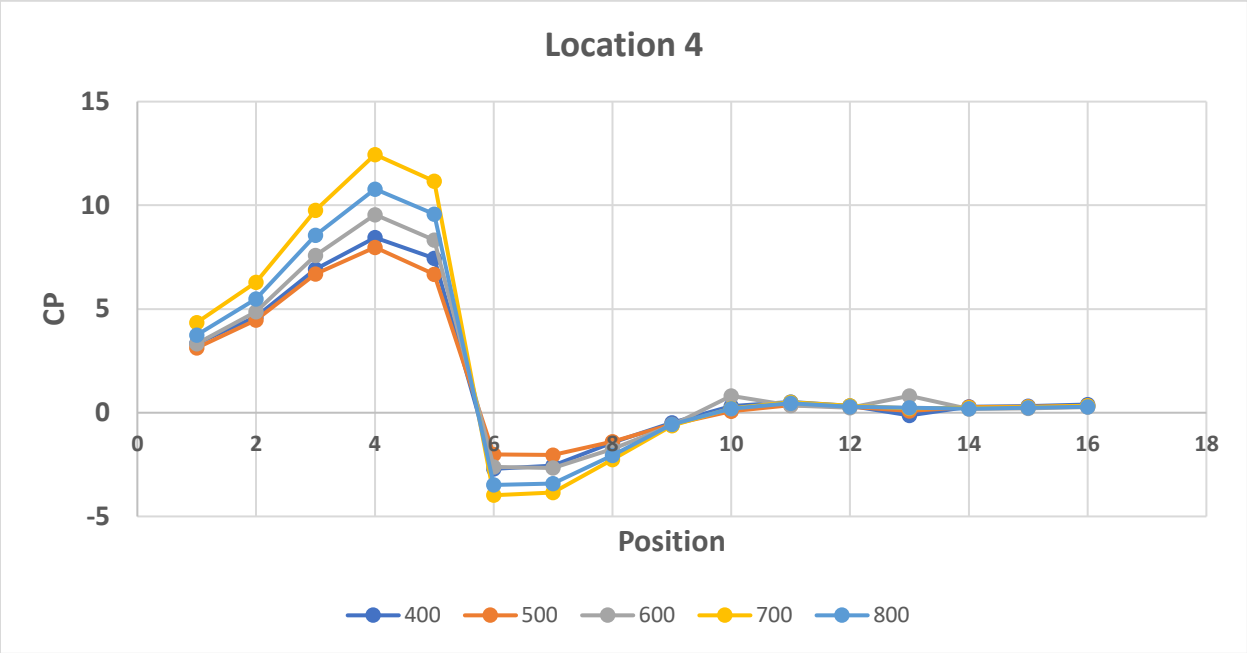


(d) Pressure coefficients at location 4 for case 1

Figure 4. 14 Pressure coefficient for 1:20 Silsoe Cube at 4 different location for 5 different RPMs

As the inlet diameter, thus the longitudinal incoming flow, had the hights between the 1st (0.14 m) and the 4th (0.44 m) heights, the Silsoe Cube model dimensions were chosen to be in the vicinity of these figures, therefore the scales 1:20, 1:30 and 1:40 were tested. Figure 4. 15 (a), (b), (c) and (d) show the comparison of the CP measured for the 3 different scales of Silsoe Cube, placed at locations 1, 2, 3 and 4 and tested for 600 RPM for case 1 (2 inlets opened). For all 4 locations, the CP for the 1:20 Silsoe Cube model increased from points 1 to 4 as these ponits were located on the cube face towards the wind flow, as it can be noticed in Figure 4. 15, however CP gradually decreased from point 5 and became negative from point 6 until 16. Usually at the roof of a structure with sharp edges, a vortex is created, thus the negative CP registered from point 6 to 11 can be attributed to the vortex flow determined by the wind on the top of the

Silsoe Cube. The CP was negative or almost null from point 12 to 16, located on the backside of the Silsoe Cube where there was less or negligible impact of the incoming wind flow due to the suction experienced by the rear face of the cube. The CP for 1:30 Silsoe Cube at all the 4 locations decreased from point 1 until 3 and increased suddenly thereafter until point 5, where it attained the highest value. The CP became negative from point 6 till point 11, because of the roof vortex flow. Similar to the previous case (1:20 scale), the CP was negative or almost null from point 12 to 16, as these points were on the backside of the Silsoe Cube. The smallest CP of the three compared Silsoe Cubes was recorded for the 1:40 model, which was almost 0, because the size of the 1:40 Cube is very small and it was well below the inlets that affect the incoming wind flow. Considersing the pressure coefficients results and the wind speed profiles presented above, the most approriate scale for the testing the Silsoe Cube is 1:20 as the CP plot for the 1:20 scale is more consistent than other two scales, for all the four locations.

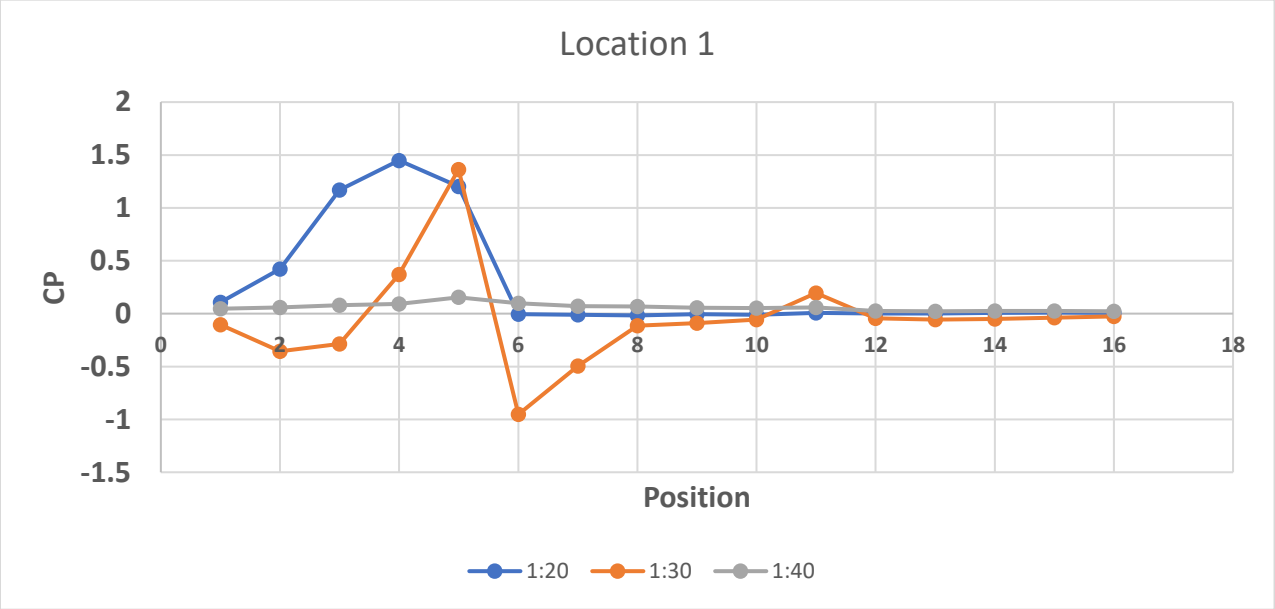


(a) Pressure coefficients for 3 different scales of Silsoe Cube model at location 1, 600 RPM

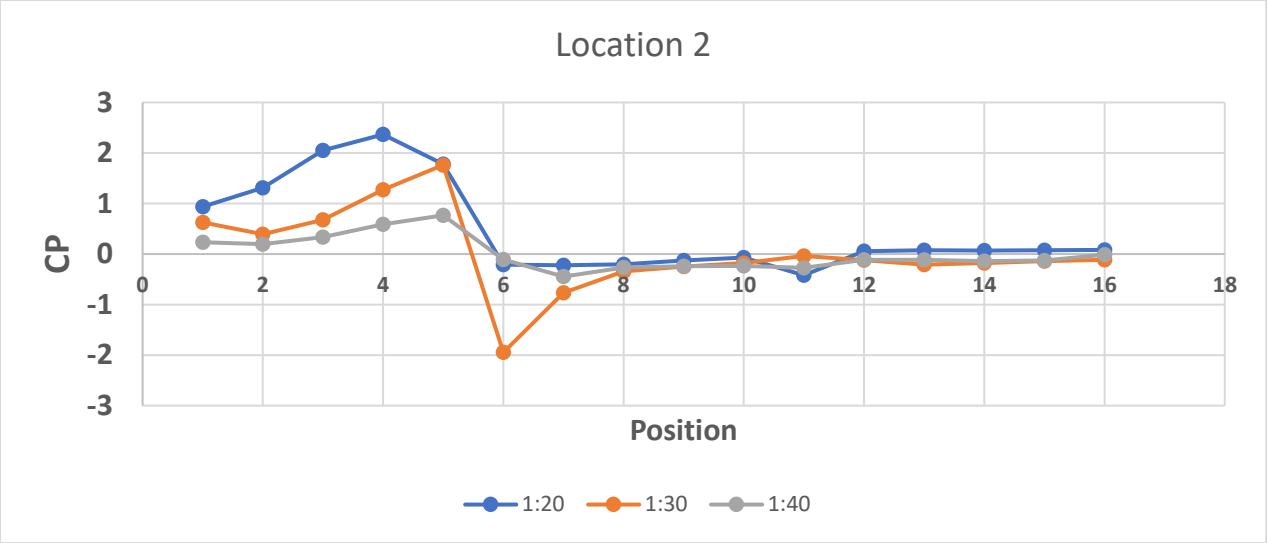


(b) Pressure coefficients for 3 different scales of Silsoe Cube model at location 2, 600 RPM


(c) Pressure coefficients for 3 different scales of Silsoe Cube model at location 3, 600 RPM

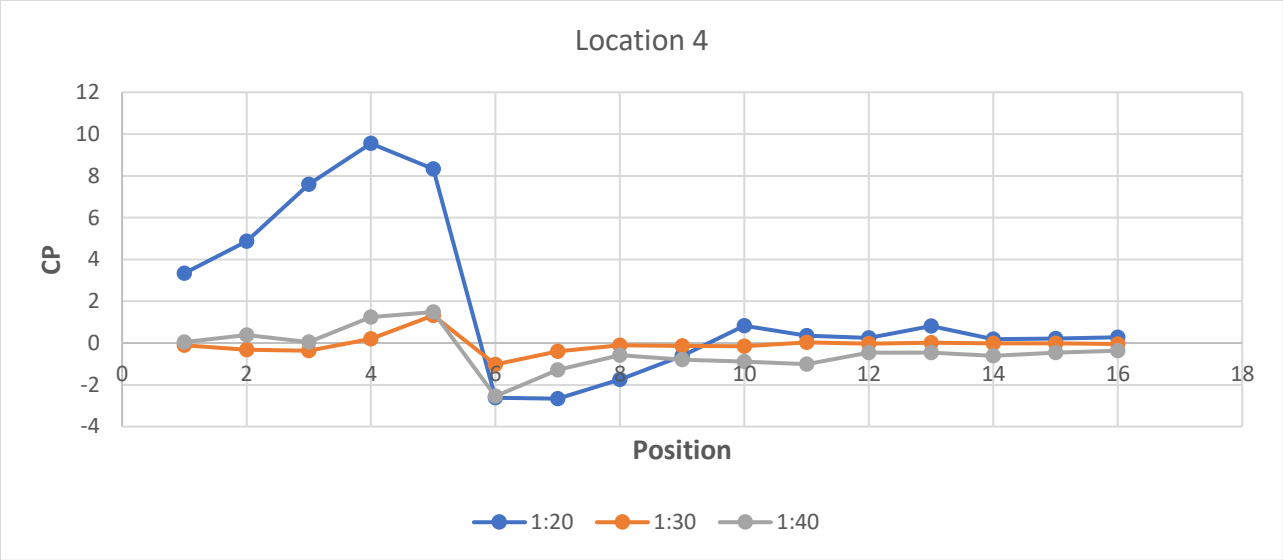


(d) Pressure coefficients for 3 different scales of Silsoe Cube model at location 4, 600 RPM

Figure 4. 15 Pressure coefficient for 3 different models of Silsoe Cube at 4 different location for 600 RPM for case 1

For case 3, when all the four inlets were opened, the pressure coefficient are compared in Figure 4. 16 (a), (b), (c) and (d), for the three different scales of the Silsoe Cube, at four different locations, for 600 RPM. The CP plots for location 1 and location 3, case 3 as shown in Figure 4. 16 (a) and (c) respectively, did not show much variation from the CP plots for location 1 and 3 for case 1, as noticed in Figure 4. 15 (a) and (c). The CP for 1:20 scale Silsoe Cube at location 1 and location 3 increased from points 1 to 4, as these points were on the cube face towards the wind flow and started decreasing from point 5 which is near the front edge if the model. The CP registered negative values from point 6 to 11, located on the roof, because of the flow separation from the edge and the vortex formation on the roof of the Cube, while from points 12 to 16, CP was almost zero as these points were on the backside of the Silsoe Cube, where the wind flow from the inlets does not have much impact. However, there was a significant difference between CP measured for location 2 and 4 for case 3 and those measured for case 1 at the same locations. The reason for this CP variation for locations 2 and 4 might be the mixing of the wind flow incoming from two directions perpendicular on each other and the effect outlet had for location 4. The Silsoe Cube of 1:40

scale had the highest value of CP coefficients for location 2 and location 4, whereas for locations 1 and 4 the Silsoe Cube of 1:20 scale had the highest value of CP. The most consistent in terms of CP coefficients, was location 3 for the scale of the Silsoe Cube of 1:20; thus future research should consider this arrangement by comparing the CP plots for all the locations and scales of basic shapes, low-rise models such as the Silsoe Cube.

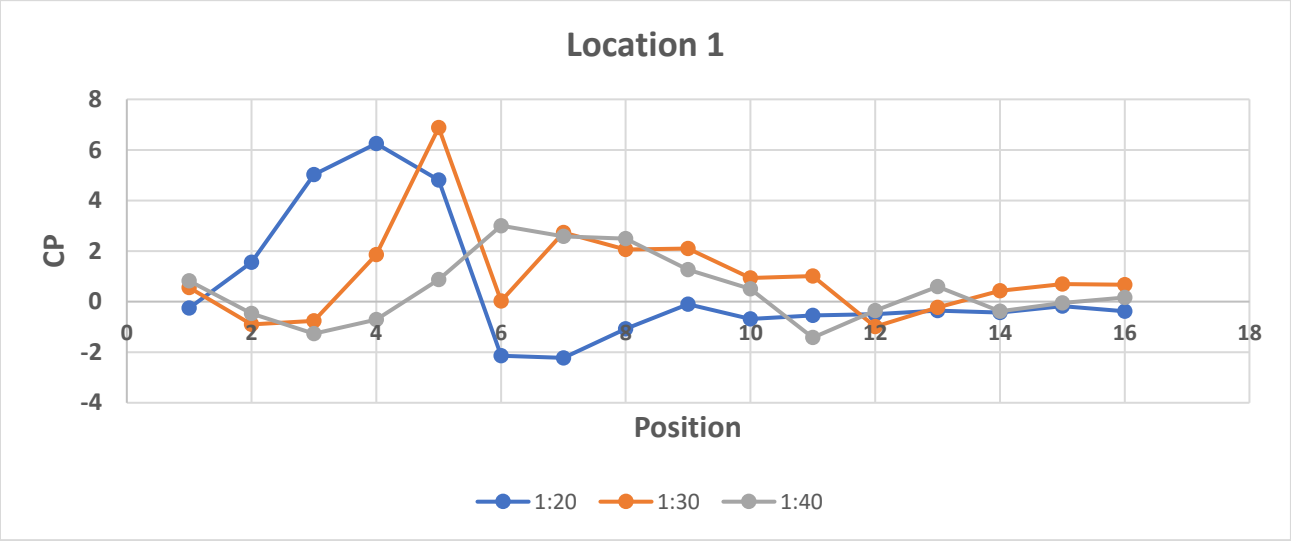


(a) Pressure coefficients (CP) for 3 different scales of Silsoe Cube model at location 1 for 600 RPM

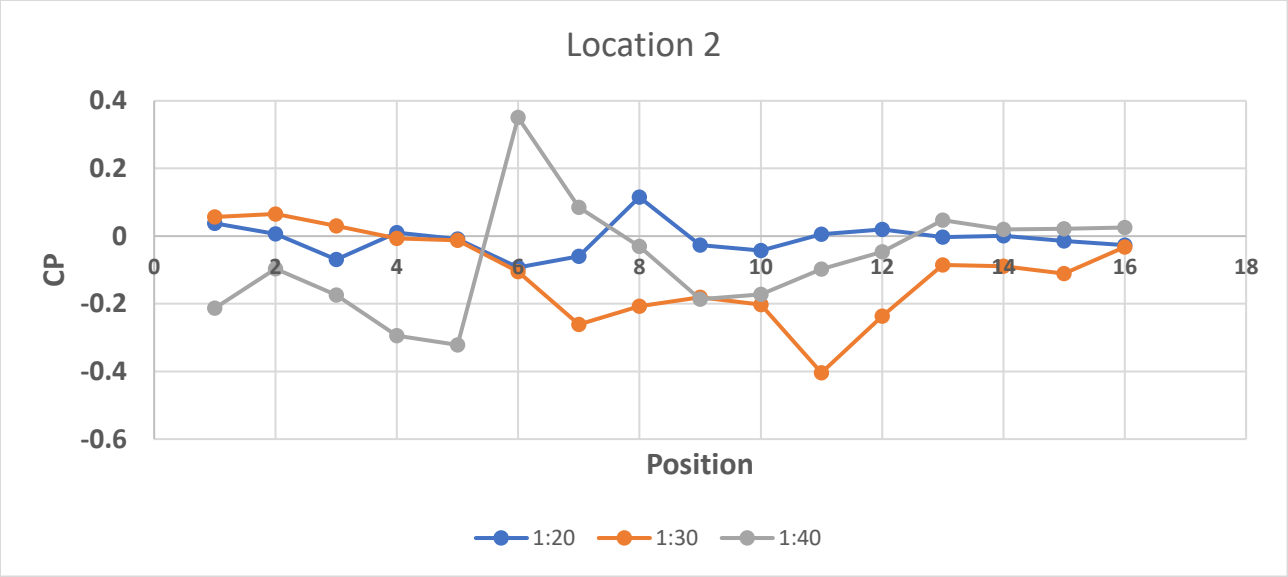


(b) Pressure coefficients (CP) for 3 different scales of Silsoe Cube model at location 2 for 600 RPM

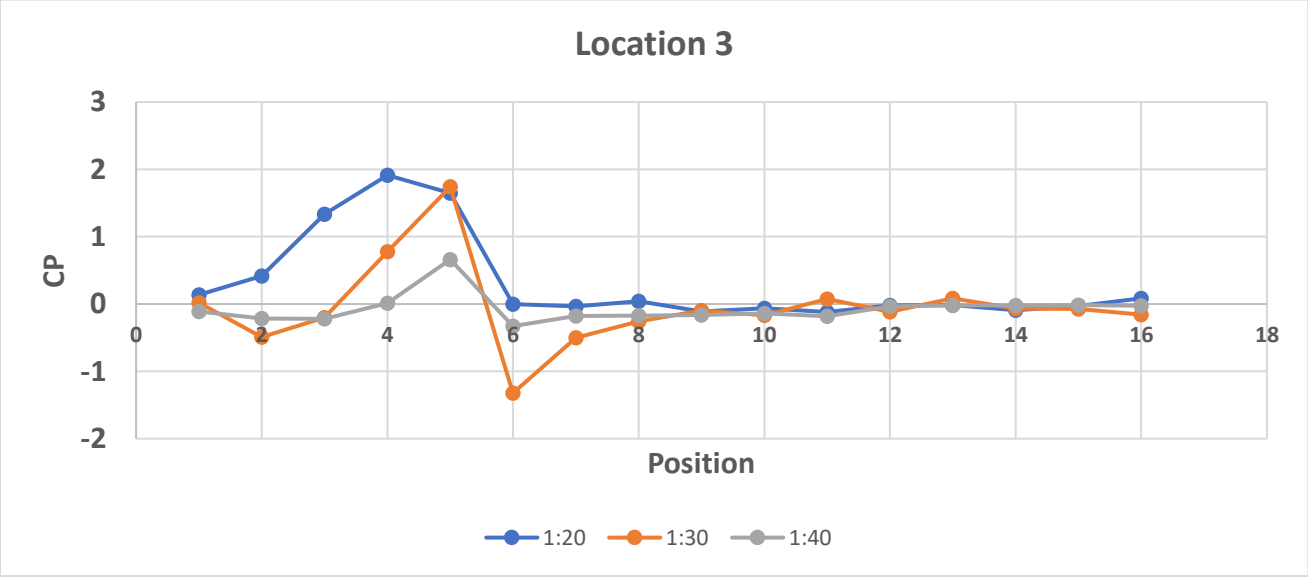


(c) Pressure coefficients (CP) for 3 different scales of Silsoe Cube model at location 3 for 600 RPM

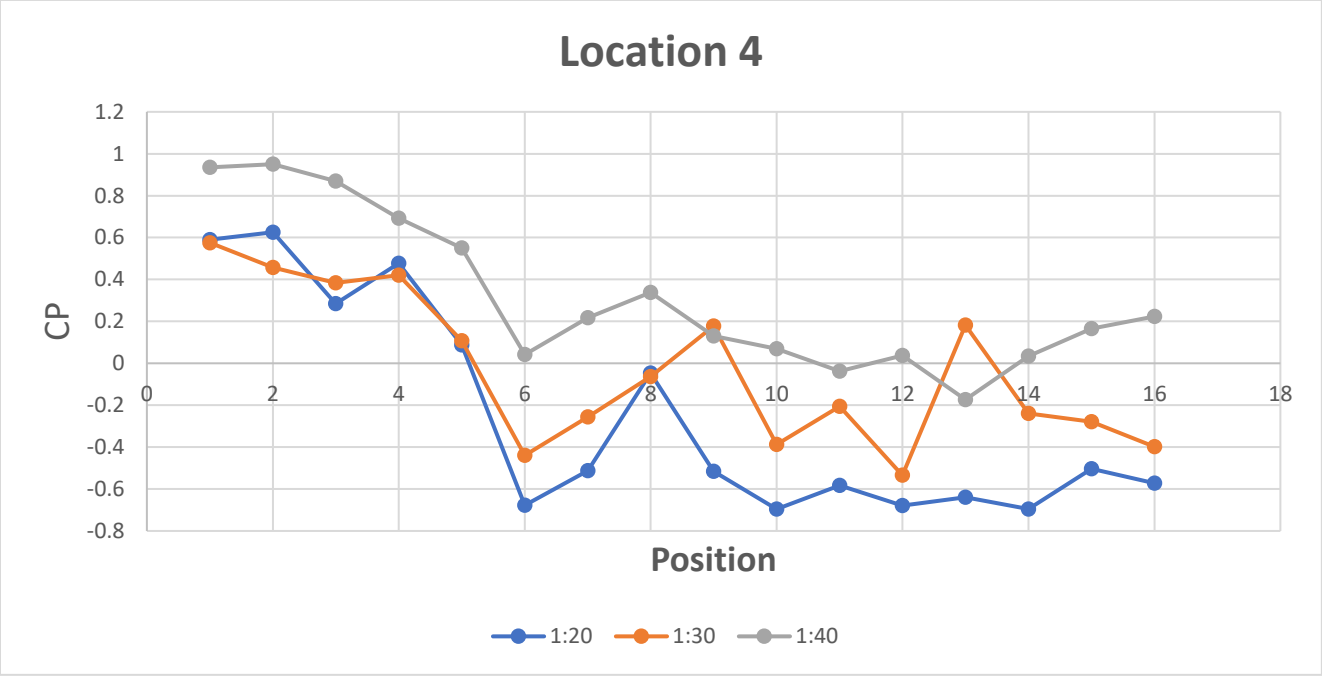


(d) Pressure coefficients (CP) for 3 different scales of Silsoe Cube model at location 4 for 600 RPM

Figure 4. 16 Pressure coefficient for 3 different models of Silsoe Cube at 4 different locations for 600 RPM for case 3

# Chapter 5- Discussion and results comparison

## 5.1 Comparison with previous studies

The measurements taken in the WDS for the wind speed profiles, the turbulence spectra and the pressure coefficients for the basic shaped structure, the Silsoe Cube, have unique characteristics, due to the new method of simulating wind flow in the testing chamber, through suction at the top and combination of opened inlets at the base of the facility. Therefore, comparison with previous studies is very important to clarify the applicability of the testing conditions employed by the WDS facility.

### 5.1.1 Turbulence spectra comparison

The turbulence spectra provide the wind speed frequency information, thus when this is calculated with the theoretical formulations, such as Von Karman spectrum, the values might be different from the measurements registered in the field tests and in the wind tunnels. In general the turbulence spectra measured in the wind tunnel experiments tend to have a decreasing intensity towards the high frequency components, as indicated by Jafari et al, (2019) for the longitudinal and vertical turbulence spectra for two different wind tunnel experiments (Figure 5. 1). As noticed in the current experiment however, the WDS would not simulate wind turbulent profiles with the same characteristics as the wind tunnels as depicted in Figure 5. 3. Instead, the WDS wind speed profiles are closer to the turbulent spectra reported for the field measurements by Morfiadakis (1996) for 12.4 m/s and 10.4% turbulence intensity (Figure 5. 2). Thus, it can be concluded that the turbulent wind simulated in the WDS is closer to replicating the turbulent wind conditions exiting in the open field areas.

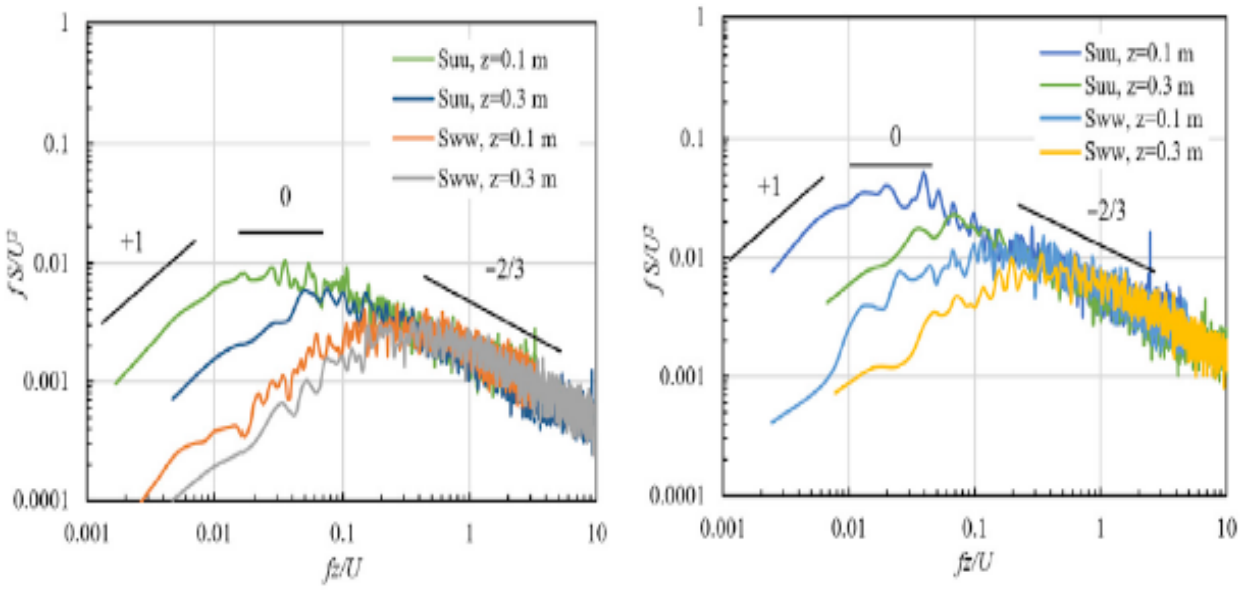


Figure 5. 1 Longitudinal and vertical spectra (Jafari et al, (2019)

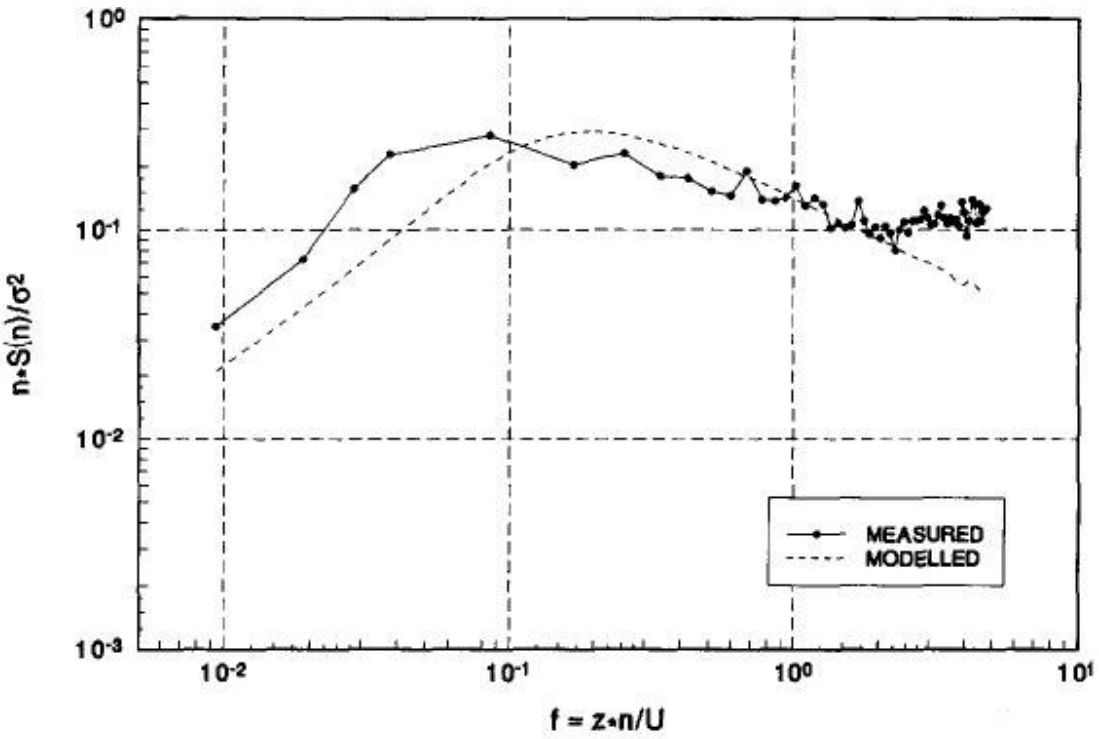


Figure 5. 2 Turbulence spectra for field measurement (Morfiadakis (1996))

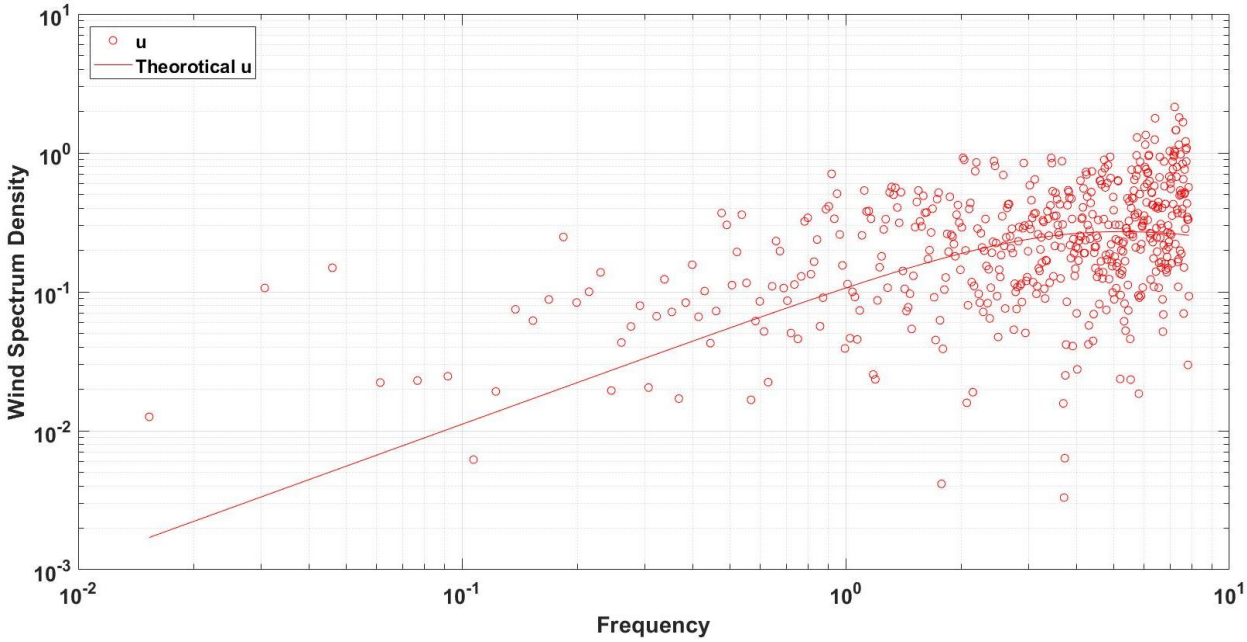


Figure 5. 3 Turbulence spectra of current experiment

### 5.1.2 Pressure coefficients comparison

The pressure coefficients for three different scales of Silsoe Cube (1:20, 1:30 and 1:40) determined during the current research were compared with the results of the previous research performed by Zhe and Dragomirescu (2019), using a similar Silsoe Cube model and scales, but tested in the unaltered Wind-box facility located in CBY structure laboratory of the University of Ottawa. The testing conditions were not identical with the ones employed in the current experiment, because since then the Wind-box facility was moved to STEM building, doors were added and the testing chamber floor was raised by 160 cm. Figure 5. 4 and Figure 5. 5 represents the CP coefficients determined in the current research under unidirectional incoming flow (case 1) and bidirectional flow (case 3) at location 2 and location 3 respectively; these were compared with the experimental CP obtained by Xiao and Dragomirescu (2019) under unidirectional wind flow conditions and with the full-scale CP data reported by Richard and Hoxey (2001). Pressure coefficients started from lower values in the current experiment when compared with the other studies, because of the level of the floor on which the model was installed, which was 140 cm under the level of the inlet. Thus, the pressure coefficients of first point of the current experiment are relatively lower than the other experiments, because this point is situated below the inlet of the WDS box, and the impact of the wind is not significant on the first point of the vertical line for the scaled Silsoe Cube models. This modification however allowed for higher suctions at the roof of the models as detailed below. On the front face of the

cube, from point 1 to point 5 the CP increased gradually but suddenly decreased to negative values at point 6, especially for the full-scale (Richards and Hoxey, 2001) and for the current experiment scale 1:30, case 1, after encountering the edge of the model. The CP became negative on the top of the Silsoe Cube, because of the flow separation at the edge of the model, which produces a vortex flow associated with negative pressures on the roof face, near the front edge, as usually occurs for flat roofs structures (Figure 5. 4). On the backside of the cubes, the pressure coefficients reached almost null values, as there was not much impact of the wind flow on the back wall of the Silsoe Cube. The pressure coefficient data of the 1:20 scale Silsoe Cube data is similar to the data of Xiao and Dragomirescu (2019), excluding the first couple of points. Also, for location 3, as it can be seen in Figure 5. 5, the current study yielded CP values closer to zero for the first three points, as the bottom edge of the cubes was lower than the inlet, and the wind flow bouncing from the floor might have some effect; the floor effect was noticed especially for models 1:30 and 1:40, where negative pressure coefficients were registered, whereas in the experiment performed by Xiao and Dragomirescu (2019) and in the full-scale experiments (Richards and Hoxey, 2001) the bottom edge of the Silsoe cube was at the level of the inlet, thus higher values for the CP coefficients were noticed. On the other hand, for both locations, the 1:30 model tested in the current experiment registered CP magnitudes closer to the CP coefficients reported for the full-scale measurements (Richards and Hoxey, 2001) however it did not capture very well the negative pressure on the roof of the models, caused by the flow separation from the sharp edge of the of the cube.

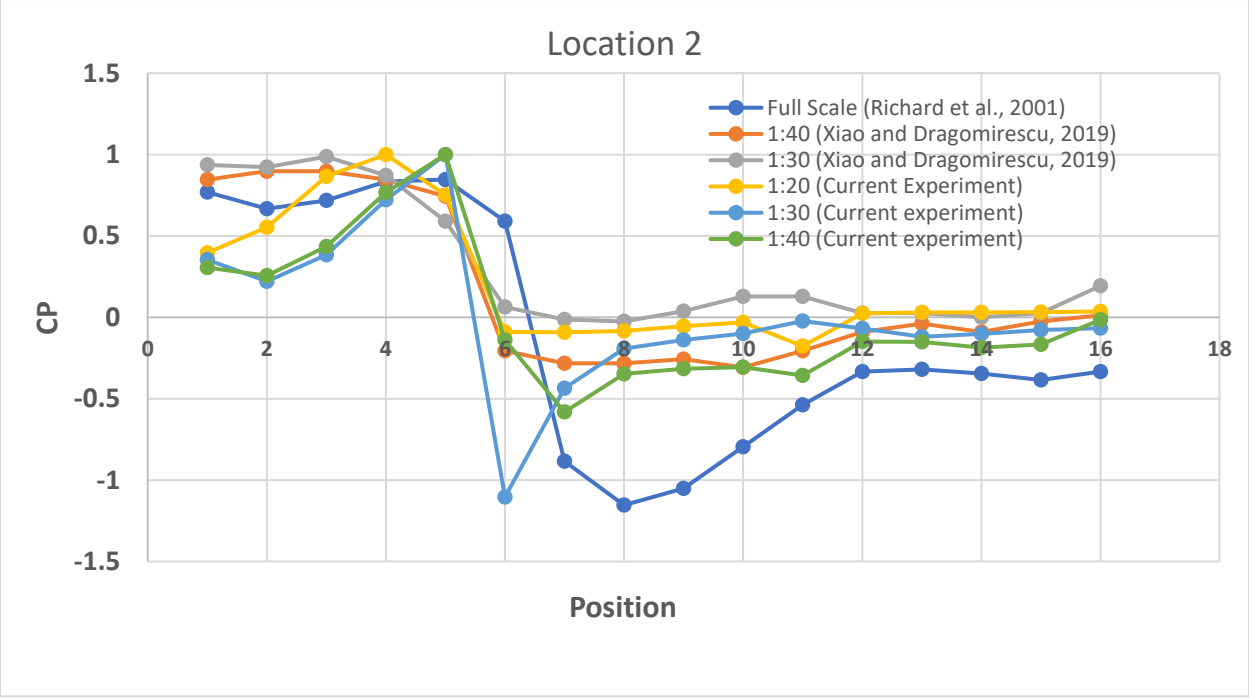


Figure 5. 4 Pressure coefficients comparison with previous studies at location 2, 600RPM, case 1


Figure 5. 5 Pressure coefficients comparison with previous studies at location 3, 600RPM, case 1

Figure 5. 6 and Figure 5. 7 compares the same data but for case 3, location 2 and location 3, respectively, when the incoming flow is bidirectional, because two inlets from the front wall and two inlets from the lateral wall were open. Similar trend was observed in all the cases, except for the CP measured at location 2, case 3. The CP coefficients measured for location 2 used in the current study (Figure 5. 6), showed bigger discrepancies when compared with both Xiao and Dragomirescu (2019) and Richards et al, (2001) probably due to the proximity of the model to the inlet D on the lateral wall and the longer distance from the rest of the open inlets (A, B, C), which would cause an attenuation of flow pattern on the front wall and on the roof of all tested models (1:20, 1:30 and 1:40). Location 3 (Figure 5. 7), which is situated in front of the inlet A, in the proximity of inlet B and further away from lateral inlets C and D, has a very similar CP pattern with the location 3, case 1 (Figure 5. 5), with slight variations for the first part of the monitored line of the Silsoe Cube models. Therefore, it can be concluded that actually the flow conditions for location 3 are closer to unidirectional incoming flow, than the bidirectional flow conditions, while the stronger bidirectional flow determined for location 2 has the effect of attenuating the suction on the roof of the models.

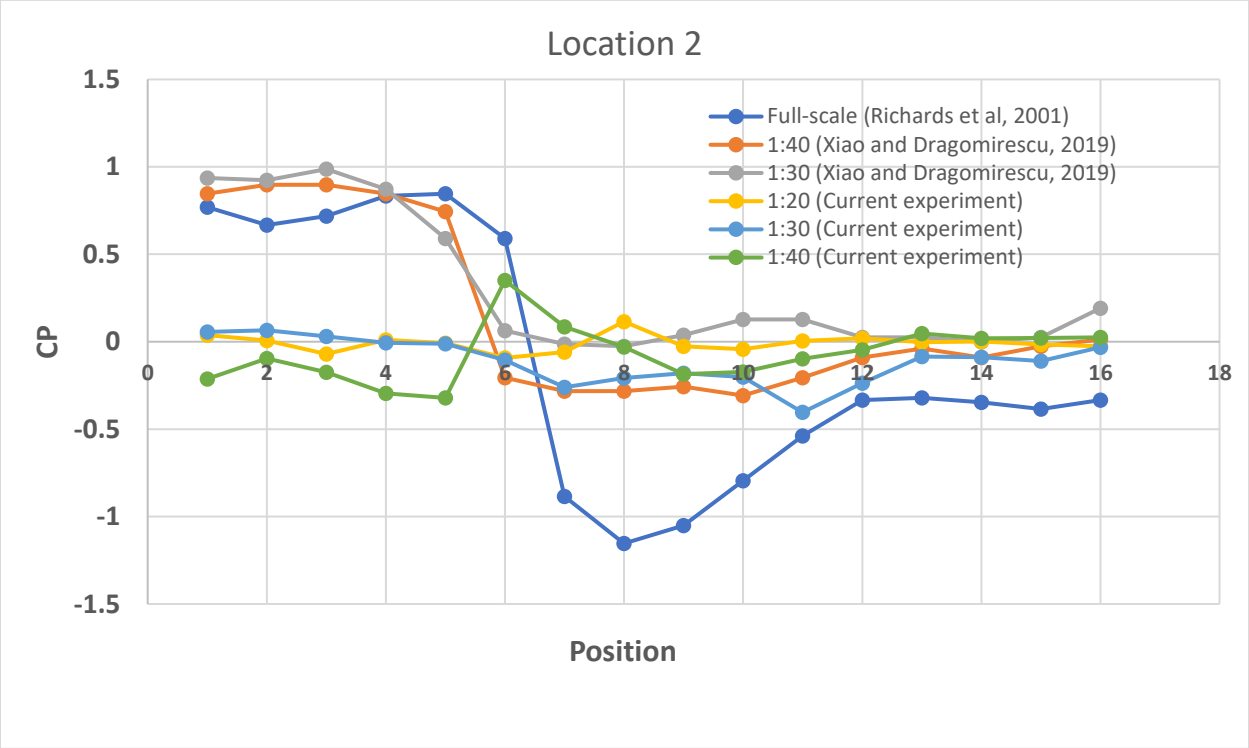


Figure 5. 6 Pressure coefficients comparison with previous studies at location 2, 600RPM, case 3

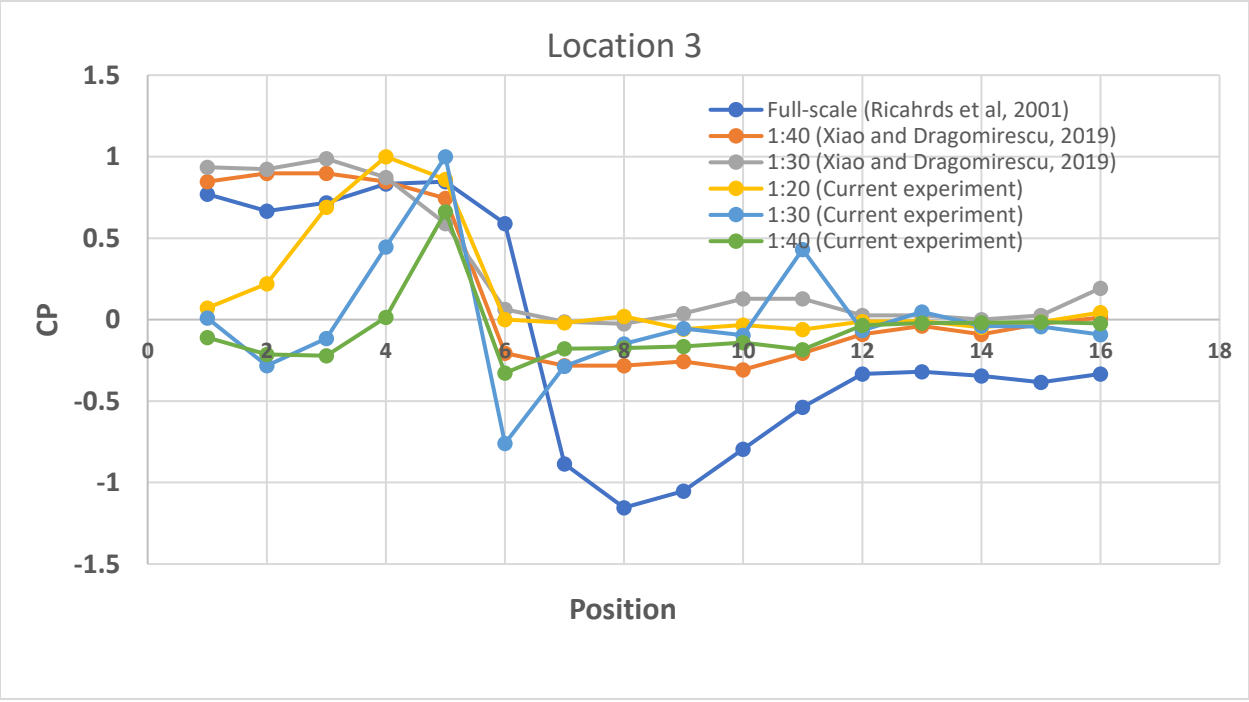

Figure 5. 7 Pressure coefficients comparison with previous studies at location 3, 600RPM, case 3

## 5.2 Discussion of experiment results

Various researches have been performed to study the wind characteristics and their application to civil engineering structures and for determining the parameters to be used in the building design codes for wind loads. The applicability of the data determined from the conventional wind tunnels was always debated because these facilities can simulate only unidirectional boundary layer, which does not characterize the hurricanes, tornadoes and other windstorms. Therefore, to overcome these limitations, the Wind-Induced Damage Simulator was employed for several experiments, to compare the wind characteristics of the scaled model of Silsoe Cube with the full-scale data reported by other researchers (Richards and Hoxey, 2001, Richards and Surrey, 1992). Proper scaling of the Silsoe Cube models used for the determination wind characteristics should be done, as mismatch of the wind flow turbulence spectra could be noticed if the model is not scaled properly (Holscher and Niemann, 1998). The Silsoe Cube model should be scaled in respect to the similarity conditions used for the low-rise buildings models, which should not use scales higher than 1:50 (Tieleman, 2003). When presenting the determination of the pressure coefficients for the current the experiments, proper normalizing procedure should be followed for more accurate results.

From the results for the first experiment phase, it can be stated that some of the locations ($1^{st}$ and $3^{rd}$ ) were more affected by the incoming flow from the inlets (inlet effect), other were affected by the strong suction of the outlet situated at the ceiling of the WDS box (outlet effect). The main feature of the wind speed profiles is that the maximum velocity for locations 1 and 3 was attained at the $2^{nd}$ height (0.24 m) because of the inlet effect because this height was situated at the center of the inlet. At $4^{th}$ height (0.44 m ) and $5^{th}$ height (0.54 m), the value of the velocity was not significant, thus it can be concluded that the wind flow does not have a high impact on height 0.44 m or above in WDS facility. The maximum velocity was observed at the location 3 out of all the four locations tested in the WDS testing chamber for all cases. The turbulence spectra generated through the experiments performed in the wind tunnels usually show a decreasing trend towards the higher frequency as depicted by Jafari et al, (2019), whereas in the current research the turbulence spectra is similar to the turbulence spectra determined in the open areas as represented by Morfiadakis, (1996). The vertical wind speed profile is the most consistent for the location 3 and the maximum velocity was also observed at location 3, therefore it can be concluded that location 3 is the best location within the WDS testing chamber for the future experiments.

The pressure coefficients were determined for the three different scales (1:20, 1:30 and 1:40) models of Silsoe Cube, on the basis of which the best scale for low-rise models was recommended for the future studies in the WDS. The measured pressure coefficients for 1:20 Silsoe Cube for different RPM values (400, 500, 600, 700 and 800) (Case 1) were compared and it was observed that, as expected, increasing the wind velocity does not effect the values of pressure coefficients. Therefore, it can be concluded that increasing in the wind velocity does not affect the pressure coefficients, in spite of using bidirectional turbulent flow. The measured pressure coefficients for 1:40 scale Silsoe Cube were close to zero for almost all the locations and for all the cases because the size of 1:40 scale Silsoe Cube was very small and the inlet was much higher than the top of this model, thus there was no significant effect of wind flow in that region. For 1:20 and 1:30 scaled Silsoe Cube models, a general trend was observed for the measured pressure coefficients of increasing CP from point 1 to 5, then to decrease to negative values for the points on the top of the cubes, while reaching negligible magnitudes for the points on the backside of the cubes. The negative pressure coefficients were observed on the top of the models of Silsoe Cube, due to flow detachment from the sharp and vortex formation. The pressure coefficients determined during the current experiments were compared with full-scale data (Richards and Hoxey, 2001) and the research done by Xiao and Dragomirescu (2019). The pressure coefficients of 1:20 scaled Silsoe Cube model of the current experiments showed a reasonable agreement with the pressure coefficients reported by Xiao and Dragomirescu (2019), except the first couple of points. The reason for not matching the CP of the first points on the front face is that during the experiments performed by Xiao and Dragomirescu (2019), the bottom edge of the Silsoe Cube models were in front of the inlet, whereas in the current experiment, the bottom edge of the Silsoe Cube models was 14cm below the inlets. When comparing the measured pressure coefficients of all the three scales of Silsoe Cube, with the full-scale data reported by Richard and Hoxey (2001), it can be concluded that 1:20 scaled Silsoe Cube model had a better agreement for the first, however it did not capture well the negative pressure on the roof of the model, while the scale 1:30 Silsoe Cube captures better the edge effect and the negative values on the roof region of the Silsoe Cube, thus CP values were closer to the full-scale data (Richard and Hoxey, 2001). Thus for the future models of low-rise building scales 1:20 and 1:30 should be considered, depending on the type of wind phenomena sought to simulate.

For bidirectional wind flow simulated in the WDS for case 3, at locations 2 and 3, shows much smaller the CP coefficients when compared with both Xiao and Dragomirescu (2019) and Richards and Hoxey (2001), because the flow effect on the face and on the roof of the models is attenuated when inlets from both front and lateral walls are used for the experiments.

The experiment done by Xiao and Dragomirescu (2019) cannot be replicated anymore as permanent modifications were performed for the initial WDS facility in which wooden floor was employed to elevate

the floor height of the WDS as a result of which the bottom edge of the inlet of WDS was at the level of the wooden artificial floor. Also, during the experiment performed by Xiao and Dragomirescu, the system of insulated hydraulic doors were not installed, due to which the WDS box was required to lift up to access the models and the equipment inside the testing chamber. As a result, there was chance of leakage of air from the WDS, which might have affect the results of the experiment.

# Chapter 6 – Conclusions and Recommendations

## 6.1 Conclusions

The current research aimed at clarifying the testing conditions employed in the newly built WDS experimental facility, to be employed for models of low-rise structures under unidirectional and bidirectional wind speeds of average magnitude. The experimental program was conducted in two phases: in the first phase of the experiment was carried out for determining the vertical wind speed profiles and the turbulence spectra for unidirectional and bidirectional flow conditions. Also the first phase of the tests focused on determining the best location where the models should be placed for the current and the future WDS experiments. The second phase of the experiment was performed for determining the pressure coefficients on a standard shape model, for which Silsoe Cube was selected, also because full-scale measurements for this structure are available in the literature (Richards and Hoxey, 2001) and a comparison can be drawn. Three scales 1:20, 1:30 and 1:40 of the Silsoe Cube were investigated through a system of 16 pressure taps and 1.0 PSID pressure scanner, for the determining the pressure coefficients CP. The best scale to be employed for low-rise structures of basic shapes such as the Silsoe Cube, were recommended for the future WDS experiments based on the second phase of the performed tests. The main findings drawn from the two phases of the experimental program performed as part of the current research, are listed below.

- The WDS facility cannot be used for simulating smooth atmospheric boundary layer, due to the inlet geometry and their configuration during the tests, thus the results obtained in the WDS facility cannot be compared with the results obtained from conventional wind tunnels.
- The WDS induces an “inlet effect” by producing the maximum wind velocity at a height of 0.24 m above the floor, where the center of the inlet is located.
- For up to 800 RPM, the wind speed does not have a significant impact at heights higher than 0.44 m in the WDS testing chamber.
- The optimum testing location was found to be on the first row in front of the open inlets; for models placed further away, the effect of the wind bouncing back from the back walls could affect the results. For models placed more towards the center of the testing chamber, the “outlet effect” will induce a strong uplift and this will influence the pressure results.
- Two scales were recommended for low-rise standard shape models: 1:20 scale, which had better CP consistency for the WDS experiments and 1:30 scale, which had good agreement with other results reported in the literature.
- Increasing the wind velocity in the WDS velocity, does not affect the pressure coefficients.

- Comparison with field data showed that the suction on the roof of the Silsoe Cube models was underestimated, therefore the flow detachment at the front edge of the model is not well captured under the studied experimental conditions.
- High frequency turbulence spectra was obtained. The turbulence spectra was similar to the turbulence spectra determined for wind speeds recorded in the field measurements for the open area.

## 6.2 Recommendations and future work

As the Wind induced Damage Simulator is a new wind testing facility, there is a vast research work that can be done in the future within the WDS testing chamber. Some of these potential research projects are listed below:

- The current research was done only for low RPM values, as this experiment was non-destructive experiment. For the future experiments the RPM values can be increased slowly. The maximum value of RPM that can be achieved in the WDS facility is 3,560 RPM.
- In the current experiment up to four inlets were opened, however for the future work, researches can be done for the wind flow similar to tornadoes by opening the appropriate inlets.
- The wind characteristics of different models can be determined, such as for a model of an urban area with multiple building models tested simultaneously.
- Experiments can be carried out for a wind flow mixed with artificial smoke, to study the effect of the fog dispersion in wind flow, or to determine the flow pattern around the tested models.
- Further high-frequency and low-frequency turbulence patterns should be studied.
- The scale of the models should be calibrated for each new model tested in the WDS experimental facility.

# Reference


Ahmad, Shakeel, and Krishen Kumar. “Effect of Geometry on Wind Pressures on Low-Rise Hip Roof Buildings.” *Journal of Wind Engineering and Industrial Aerodynamics*, vol. 90, no. 7, 2002, pp. 755–779., doi:10.1016/s0167-6105(02)00152-6.

Castro, I. P., and A. G. Robins. “The Flow around a Surface-Mounted Cube in Uniform and Turbulent Streams.” *Journal of Fluid Mechanics*, vol. 79, no. 2, 1977, pp. 307–335., doi:10.1017/s0022112077000172.

Charuvisit, Songpol, et al. “Wind Tunnel Experiment on Wind Pressures Acting on the Scaffolds in Strong Winds.” *Journal of Wind Engineering*, vol. 32, no. 1, 2007, pp. 1–10., doi:10.5359/jwe.32.1.

Chay, M.t, and C.w Letchford. “Pressure Distributions on a Cube in a Simulated Thunderstorm Downburst—Part A: Stationary Downburst Observations.” *Journal of Wind Engineering and Industrial Aerodynamics*, vol. 90, no. 7, 2002, pp. 711–732., doi:10.1016/s0167-6105(02)00158-7.

Cook, N.j., and J.r. Mayne. “A Novel Working Approach to the Assessment of Wind Loads for Equivalent Static Design a Refined Working Approach to the Assessment of Wind Loads for Equivalent Static Design.” *Journal of Wind Engineering and Industrial Aerodynamics*, vol. 8, no. 3, 1981, pp. 299–301., doi:10.1016/0167-6105(81)90028-3.

Dalley, Sam. “Surface Pressure Spectra on a Model of the Silsoe Structures Building and Comparison with Full-Scale.” *Journal of Wind Engineering and Industrial Aerodynamics*, vol. 60, 1996, pp. 177–187., doi:10.1016/0167-6105(96)00032-3.

Goliber, Matthew Robert. “Pressure Distribution on the Roof of a Model Low-Rise Building Tested in a Boundary Layer Wind Tunnel.” doi:10.31274/etd-180810-1371.

Gough, H., et al. “Effects of Variability of Local Winds on Cross Ventilation for a Simplified Building within a Full-Scale Asymmetric Array: Overview of the Silsoe Field Campaign.” *Journal of Wind Engineering and Industrial Aerodynamics*, vol. 175, 2018, pp. 408–418., doi:10.1016/j.jweia.2018.02.010.

Hoxey, R.p., et al. “A 6 m Cube in an Atmospheric Boundary Layer Flow -Part 1. Full-Scale and Wind-Tunnel Results.” *Wind and Structures*, vol. 5, no. 2_3_4, 2002, pp. 165–176., doi:10.12989/was.2002.5.2_3_4.165.

Hu, J., et al. “Study of Wind Flow over a 6 m Cube Using Improved Delayed Detached Eddy Simulation.” *Journal of Wind Engineering and Industrial Aerodynamics*, vol. 179, 2018, pp. 463–474., doi:10.1016/j.jweia.2018.07.003.

Hölscher, Norbert, and Hans-Jürgen Niemann. “Towards Quality Assurance for Wind Tunnel Tests: A Comparative Testing Program of the Windtechnologische Gesellschaft.” *Journal of Wind Engineering and Industrial Aerodynamics*, vol. 74-76, 1998, pp. 599–608., doi:10.1016/s0167-6105(98)00054-3.

Hölscher, Norbert, and Hans-Jürgen Niemann. “Towards Quality Assurance for Wind Tunnel Tests: A Comparative Testing Program of the Windtechnologische Gesellschaft.” *Journal of Wind Engineering and Industrial Aerodynamics*, vol. 74-76, 1998, pp. 599–608., doi:10.1016/s0167-6105(98)00054-3.

Irtaza, H, et al. “Comparison of Wind Pressure Measurements on Silsoe Experimental Building from Full-Scale Observation, Wind-Tunnel Experiments and Various CFD Techniques.” *International Journal of Engineering, Science and Technology*, vol. 5, no. 1, 2018, p. 28., doi:10.4314/ijest.v5i1.3.

Irtaza, H, et al. “Comparison of Wind Pressure Measurements on Silsoe Experimental Building from Full-Scale Observation, Wind-Tunnel Experiments and Various CFD Techniques.” *International Journal of Engineering, Science and Technology*, vol. 5, no. 1, 2018, p. 28., doi:10.4314/ijest.v5i1.3.

Jafari, Azadeh, et al. “Measurement of Unsteady Wind Loads in a Wind Tunnel: Scaling of Turbulence Spectra.” *Journal of Wind Engineering and Industrial Aerodynamics*, vol. 193, 2019, p. 103955., doi:10.1016/j.jweia.2019.103955.

Jaw, S. Y., et al. “Measurement of Pressure Distribution from PIV Experiments.” *Journal of Visualization*, vol. 12, no. 1, 2009, pp. 27–35., doi:10.1007/bf03181940.

Johnson, Eric V., et al. “Development of Hurricane Resistant Traffic Signal Structures.” *Engineering Structures*, vol. 33, no. 2, 2011, pp. 357–367., doi:10.1016/j.engstruct.2010.10.016.

Levitan, M., and K.c. Mehta. “Texas Tech Field Experiments of Wind Loads. Part 1: Building and Pressure Measuring System.” *Journal of Wind Engineering and Industrial Aerodynamics*, vol. 43, no. 1-3, 1992, pp. 1615–1616., doi:10.1016/0167-6105(92)90569-v.

Lewellen, W.s., et al. “Wind And Pressure Distributions In A Tornado.” *Wind Engineering*, 1980, pp. 121–131., doi:10.1016/b978-1-4832-8367-8.50017-6.

Li, Q.s., and W.h. Melbourne. “An Experimental Investigation of the Effects of Free-Stream Turbulence on Streamwise Surface Pressures in Separated and Reattaching Flows.” *Journal of Wind Engineering and Industrial Aerodynamics*, vol. 54-55, 1995, pp. 313–323., doi:10.1016/0167-6105(94)00050-n.

Liao, Haili, et al. “Field Measurement Study on Turbulence Field by Wind Tower and Windcube Lidar in Mountain Valley.” *Journal of Wind Engineering and Industrial Aerodynamics*, vol. 197, 2020, p. 104090., doi:10.1016/j.jweia.2019.104090.

Lobotka, Peter, and Juraj Žilinský. “Determination of the Wind Pressure Coefficients on the Model of the Silsoe Cube by the Measurements Made in Wind Tunnels.” *Advanced Materials Research*, vol. 1057, 2014, pp. 89–96., doi:10.4028/www.scientific.net/amr.1057.89.

“Measurement of Wind Pressure Coefficients of Single-Span Greenhouses Using Wind Tunnel Test.” *2015 ASABE International Meeting*, 2015, doi:10.13031/aim.20152190521.

Morrison, Murray J., and Gregory A. Kopp. “Effects of Turbulence Intensity and Scale on Surface Pressure Fluctuations on the Roof of a Low-Rise Building in the Atmospheric Boundary Layer.” *Journal of Wind Engineering and Industrial Aerodynamics*, vol. 183, 2018, pp. 140–151., doi:10.1016/j.jweia.2018.10.017.

Ogawa, Yasushi, et al. “Field and Wind Tunnel Study of the Flow and Diffusion around a Model Cube—II. Nearfield and Cube Surface Flow and Concentration Patterns.” *Atmospheric Environment (1967)*, vol. 17, no. 6, 1983, pp. 1161–1171., doi:10.1016/0004-6981(83)90339-6.

Oudheusden, B. W. Van, et al. “Evaluation of Integral Forces and Pressure Fields from Planar Velocimetry Data for Incompressible and Compressible Flows.” *Experiments in Fluids*, vol. 43, no. 2-3, 2007, pp. 153–162., doi:10.1007/s00348-007-0261-y.

Paterson, David A., and Colin J. Apelt. “Simulation of Flow Past a Cube in a Turbulent Boundary Layer.” *Journal of Wind Engineering and Industrial Aerodynamics*, vol. 35, 1990, pp. 149–176., doi:10.1016/0167-6105(90)90214-w.

Richards, P.j., and R.p. Hoxey. “Appropriate Boundary Conditions for Computational Wind Engineering Models Using the k-ε Turbulence Model.” *Computational Wind Engineering 1*, 1993, pp. 145–153., doi:10.1016/b978-0-444-81688-7.50018-8.

Richards, P.j., and R.p. Hoxey. “Flow Reattachment on the Roof of a 6m Cube.” *Journal of Wind Engineering and Industrial Aerodynamics*, vol. 94, no. 2, 2006, pp. 77–99., doi:10.1016/j.jweia.2005.12.002.

Richards, P.j., et al. “Wind-Tunnel Modelling of the Silsoe Cube.” *Journal of Wind Engineering and Industrial Aerodynamics*, vol. 95, no. 9-11, 2007, pp. 1384–1399., doi:10.1016/j.jweia.2007.02.005.

Richards, P.j., et al. “Wind-Tunnel Modelling of the Silsoe Cube.” *Journal of Wind Engineering and Industrial Aerodynamics*, vol. 95, no. 9-11, 2007, pp. 1384–1399., doi:10.1016/j.jweia.2007.02.005.

Richards, P.j., and R.p. Hoxey. “Wind Loads on the Roof of a 6m Cube.” *Journal of Wind Engineering and Industrial Aerodynamics*, vol. 96, no. 6-7, 2008, pp. 984–993., doi:10.1016/j.jweia.2007.06.032.

Richards, P.j., and R.p. Hoxey. “Pressures on a Cubic Building—Part 1: Full-Scale Results.” *Journal of Wind Engineering and Industrial Aerodynamics*, vol. 102, 2012, pp. 72–86., doi:10.1016/j.jweia.2011.11.004.

Richardson, G.m., et al. “The Silsoe Structures Building: Comparisons of Pressures Measured at Full Scale and in Two Wind Tunnels.” *Journal of Wind Engineering and Industrial Aerodynamics*, vol. 72, 1997, pp. 187–197., doi:10.1016/s0167-6105(97)00274-2.

Saathoff, P. J., and W. H. Melbourne. “Effects of Free-Stream Turbulence on Surface Pressure Fluctuations in a Separation Bubble.” *Journal of Fluid Mechanics*, vol. 337, 1997, pp. 1–24., doi:10.1017/s0022112096004594.

Tieleman, Henry W. “Wind Tunnel Simulation of Wind Loading on Low-Rise Structures: a Review.” *Journal of Wind Engineering and Industrial Aerodynamics*, vol. 91, no. 12-15, 2003, pp. 1627–1649., doi:10.1016/j.jweia.2003.09.021.

Turbulence. Accessed June 21, 2020. https://www.weather.gov/source/zhu/ZHU_Training_Page/turbulence_stuff/turbulence/turbulence.htm#:~:text=Turbulence,from eddies and vertical currents.&text=Turbulence is associated with fronts, wind shear, thunderstorms, etc.

Wu, Chieh-Hsun, et al. “Effects of Turbulence on the Mean Pressure Field in the Separated-Reattaching Flow above a Low-Rise Building.” *Journal of Wind Engineering and Industrial Aerodynamics*, vol. 171, 2017, pp. 79–92., doi:10.1016/j.jweia.2017.09.013.

Wyngaard, J. C. “Book Review: Atmospheric Turbulence. Models and Methods for Engineering Applications by Hans A. Panofsky and John A. Dutton.” *AIAA Journal*, vol. 23, no. 12, 1985, pp. 2008–2009., doi:10.2514/3.48643.

Šimiček, Jozef, and Olga Hubová. “Numerical Analysis of the Effects of Wind on Building Structures.” *Slovak Journal of Civil Engineering*, vol. 20, no. 4, 2012, pp. 28–34., doi:10.2478/v10189-012-0019-2.

Yamaguchi, Classnotes,2000

Zhe, X. and Dragomirescu E., ““*Wind-induced Pressure for Silsoe Cube Tested in Wind-induced Damage Simulator”,* CSCE’19, Montreal, Canada, 2019.

# Appendix A: Wind flow turbulence spectra and wind speed profiles

Case 2

Same Location Different RPMS

Location 1

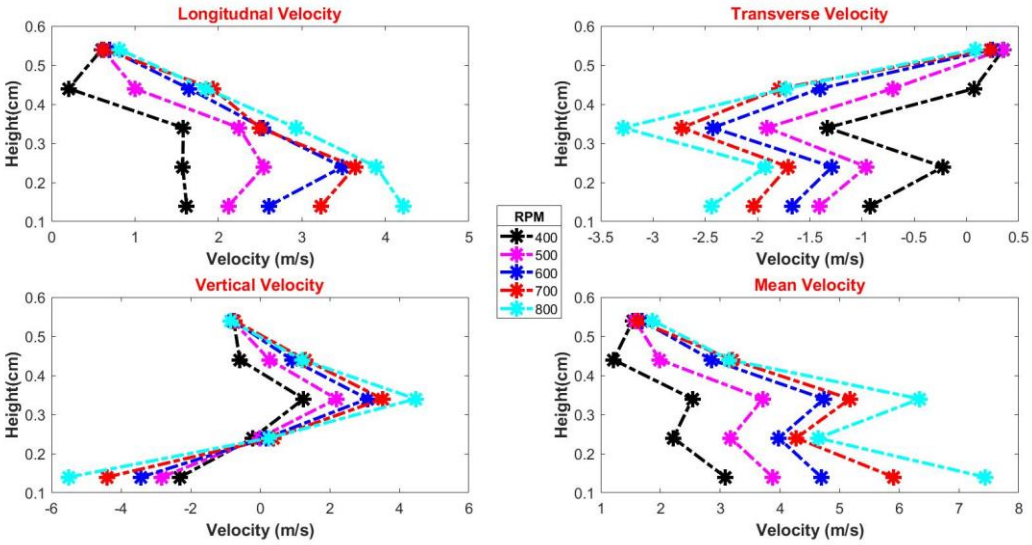


Location 2

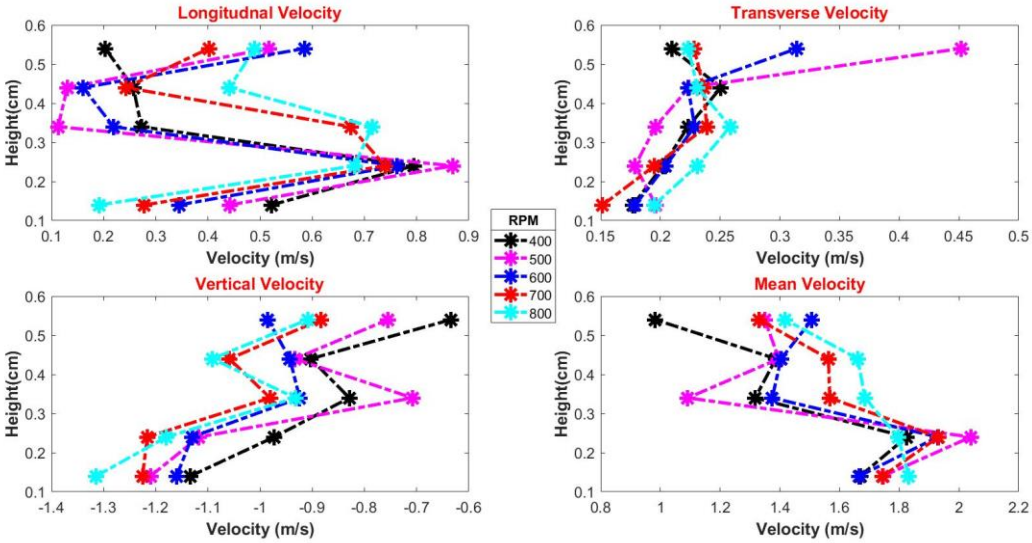

Location 3

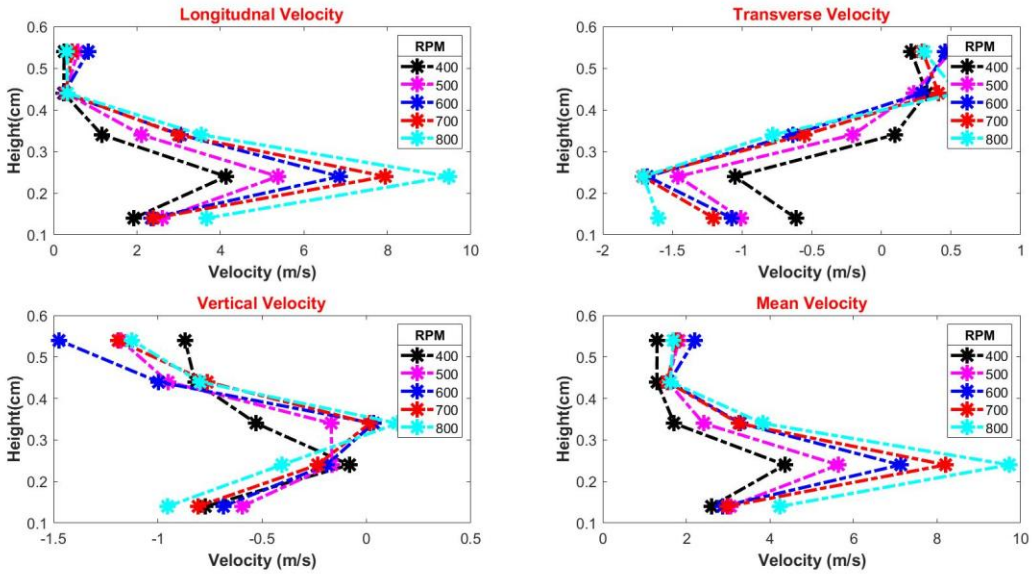


Location 4

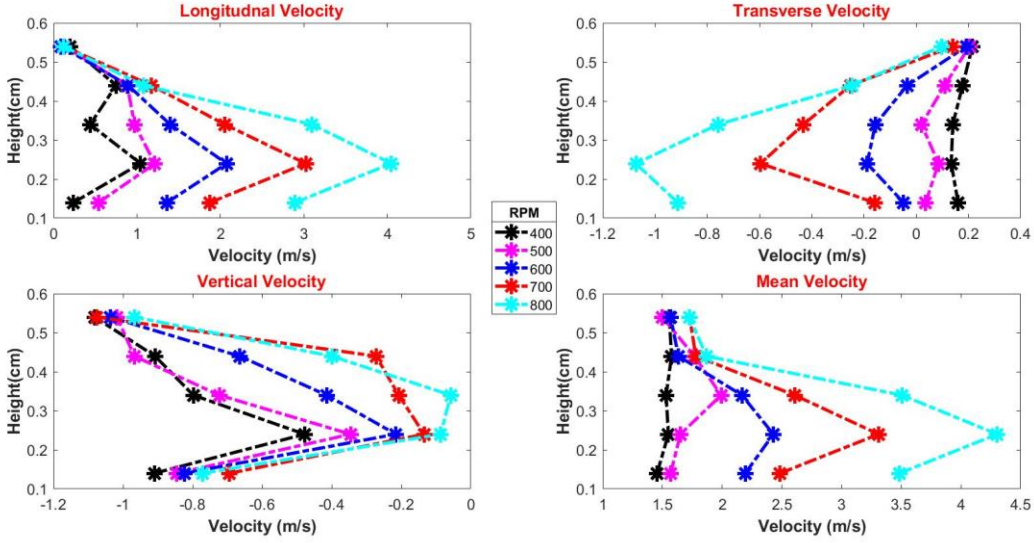


Case 2

Same RPM different Locations

400 rpm

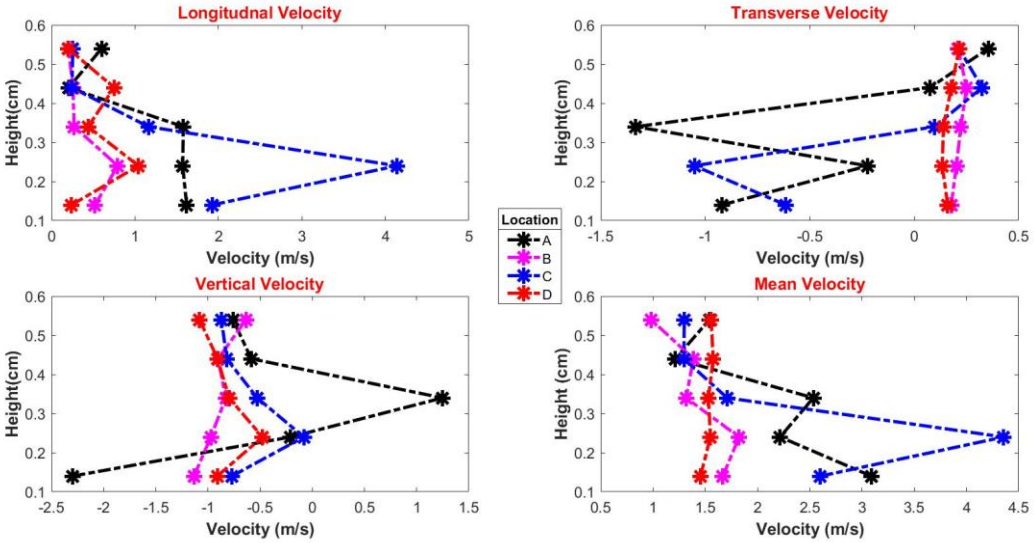


500 RPM

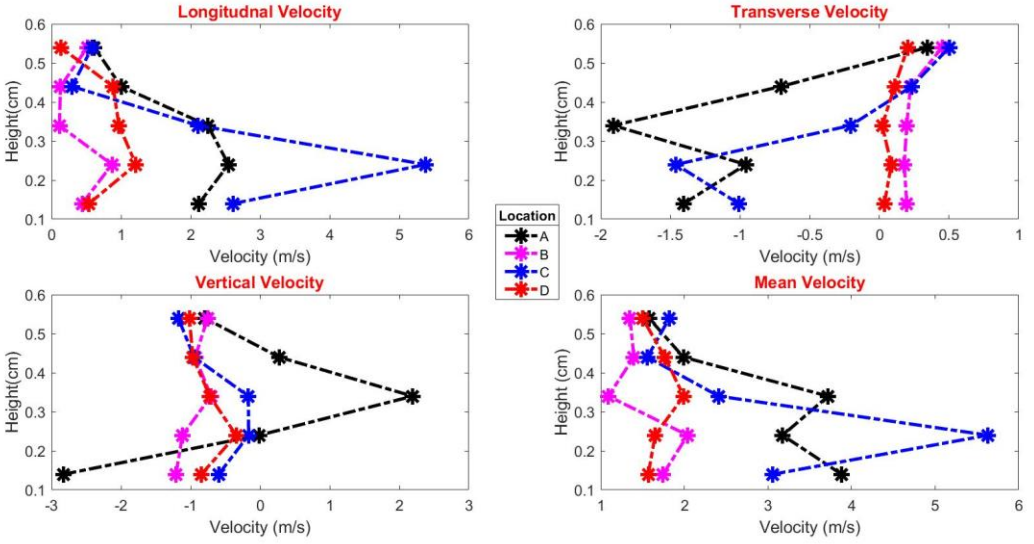


600 RPM

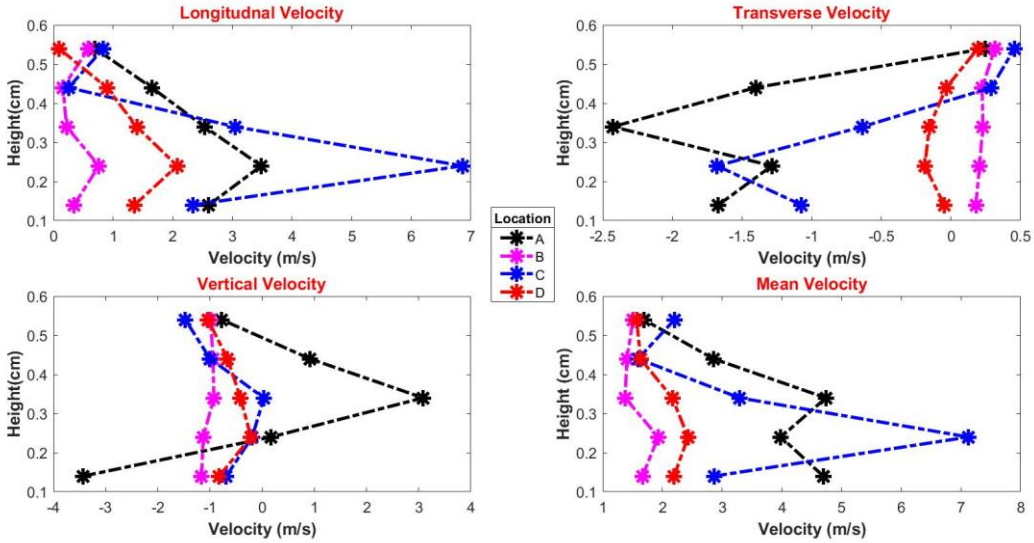


700 RPM

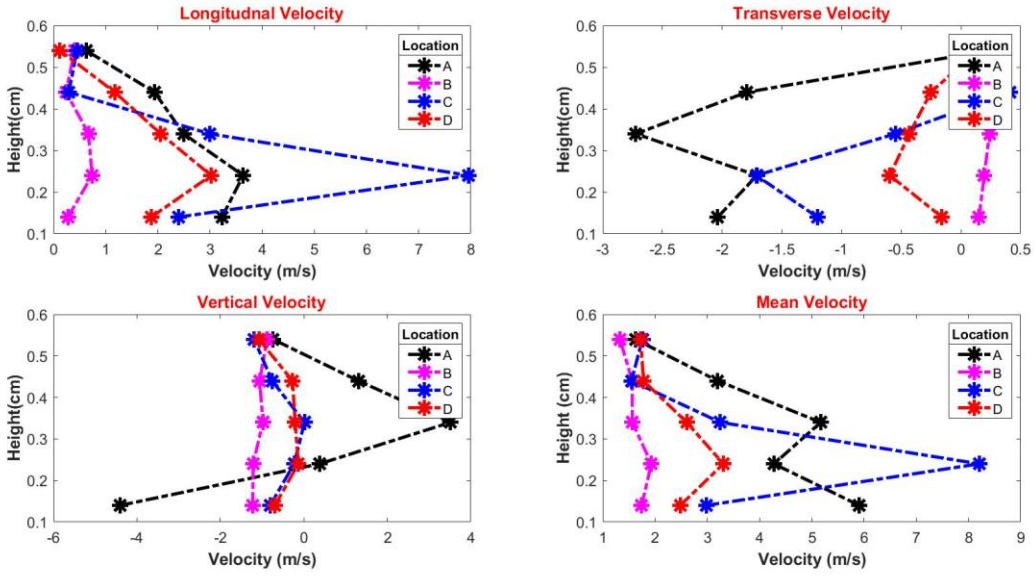


800 RPM

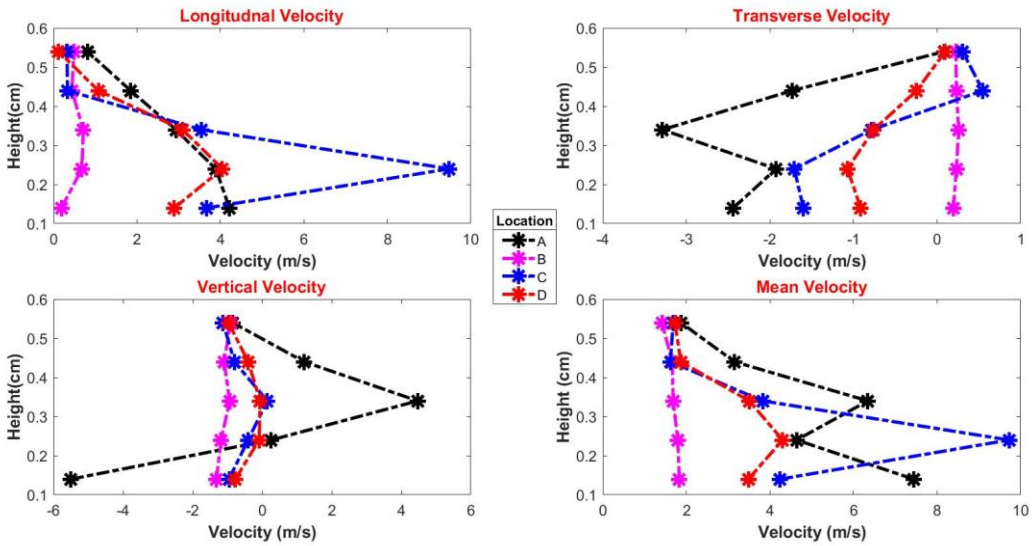


Spectra

Case 1

a-b-c-d

a=case number, b=location, c=height, d=RPM

Location 1

1-1-1-400

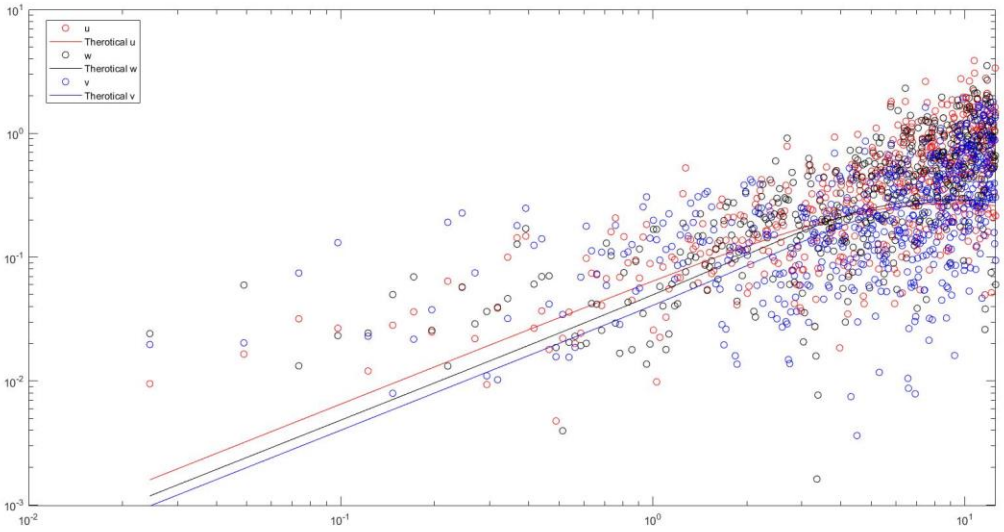


1-1-2-400

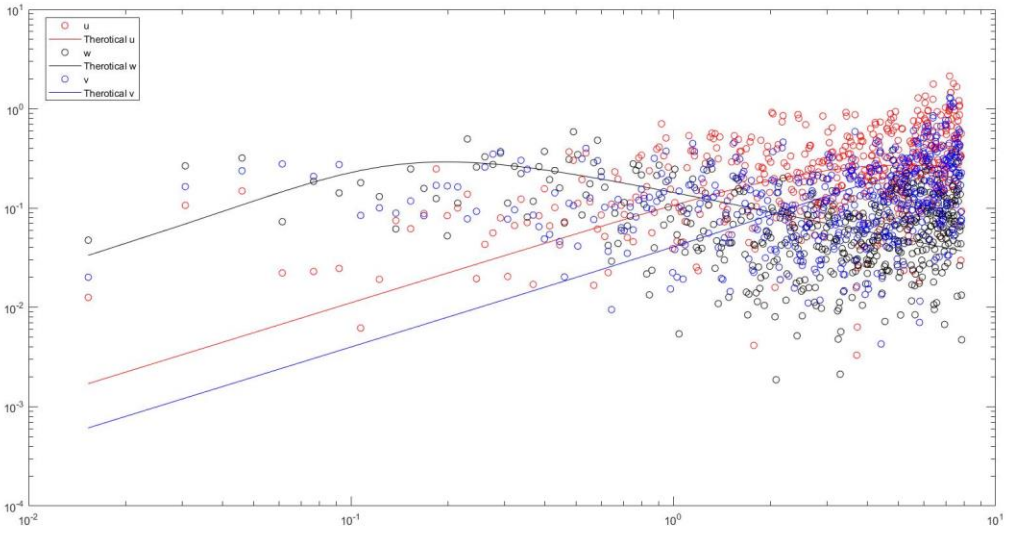


1-1-3-400

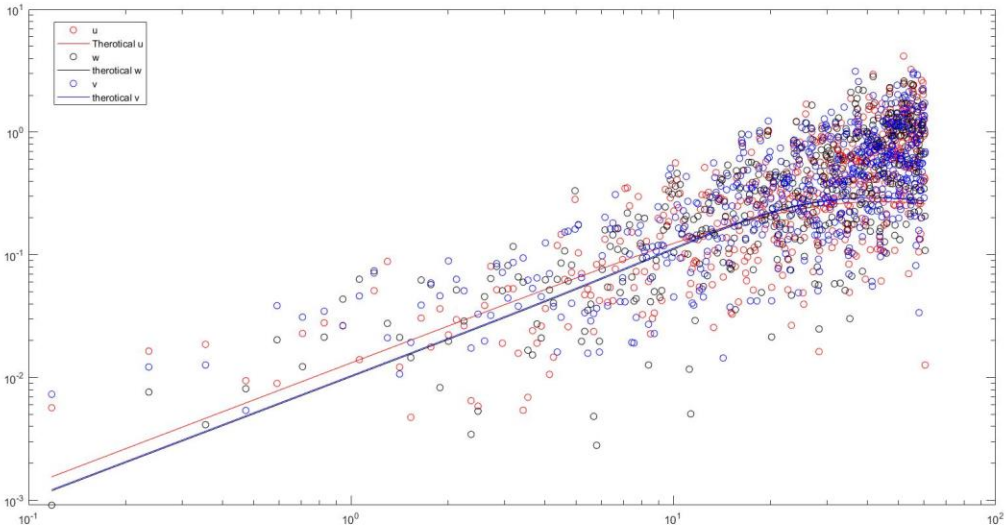


1-1-4-400

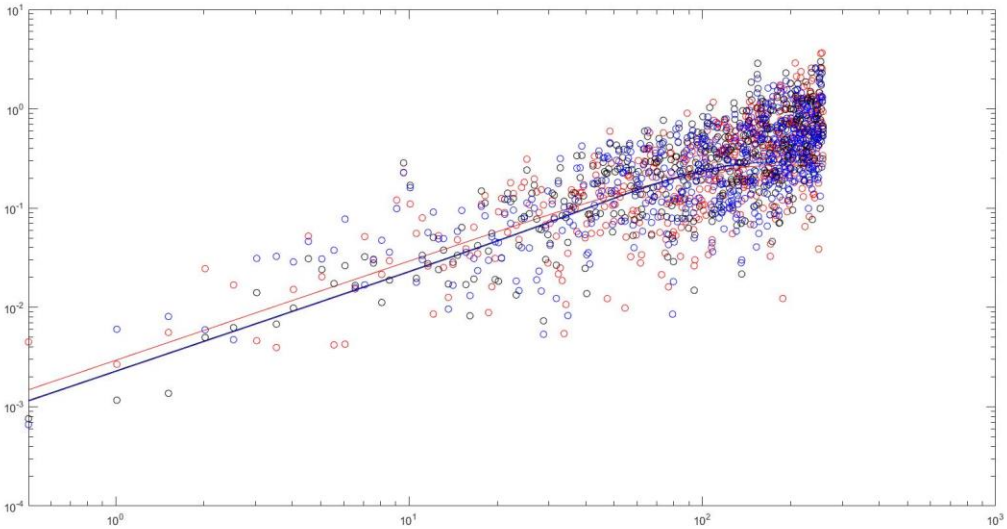

1-1-5-400

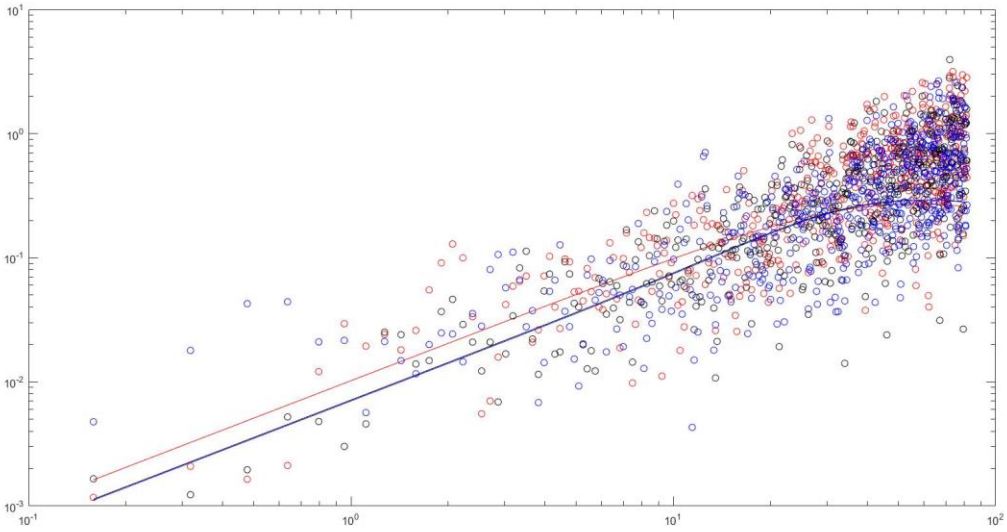

1-1-1-500

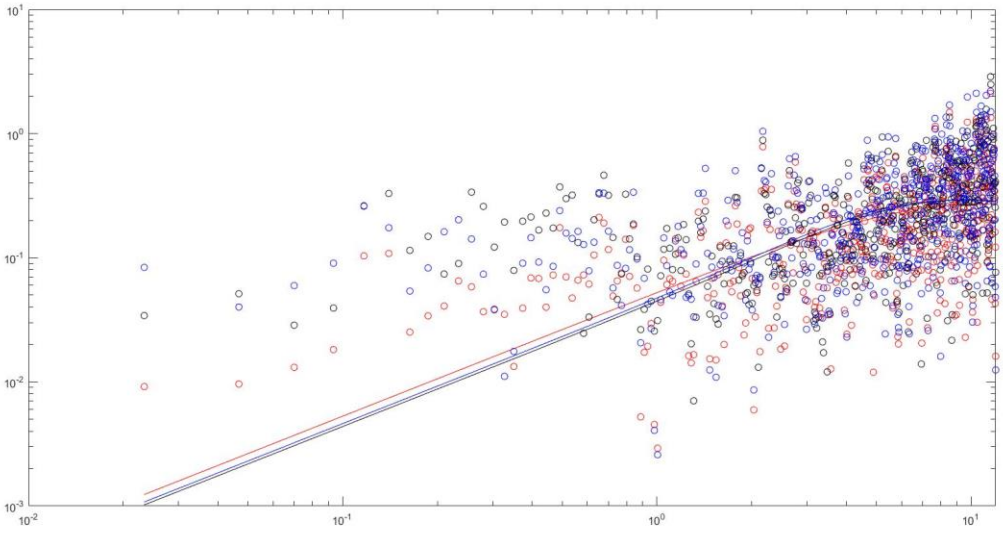

1-1-2-500

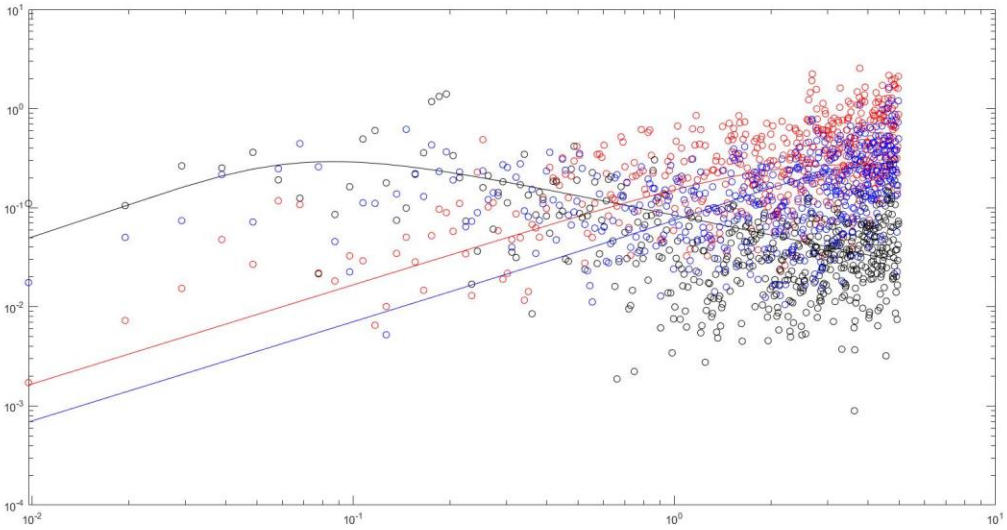

1-1-3-500

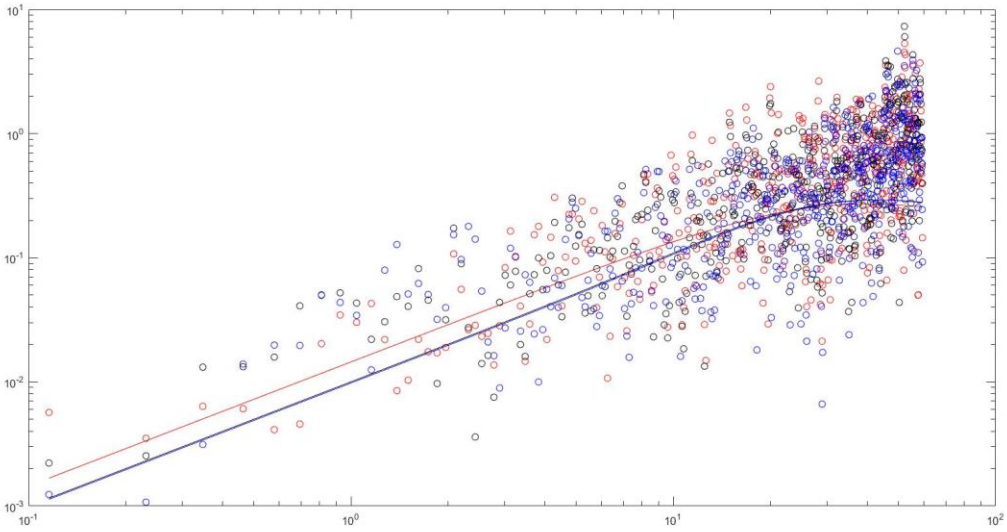

1-1-4-500

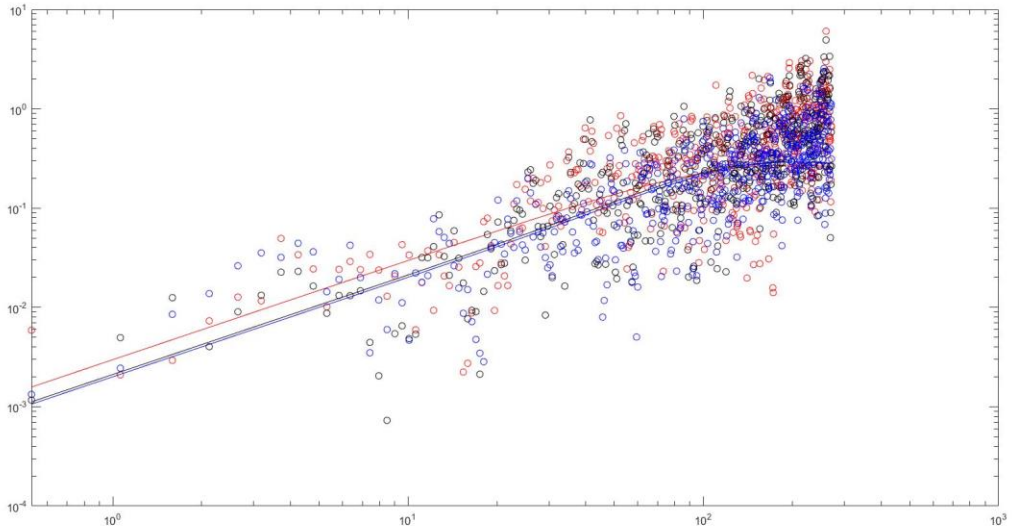

1-1-5-500

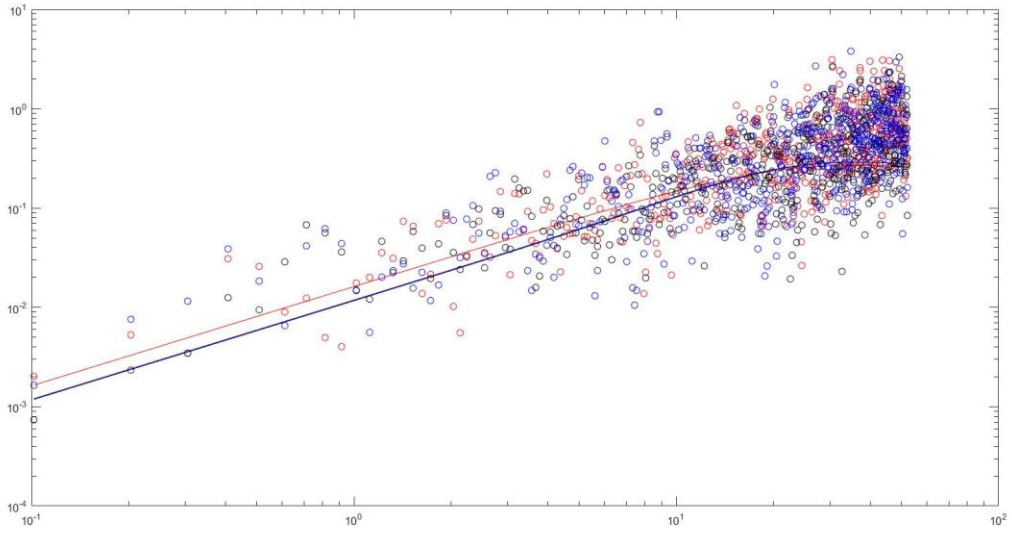

1-1-1-600

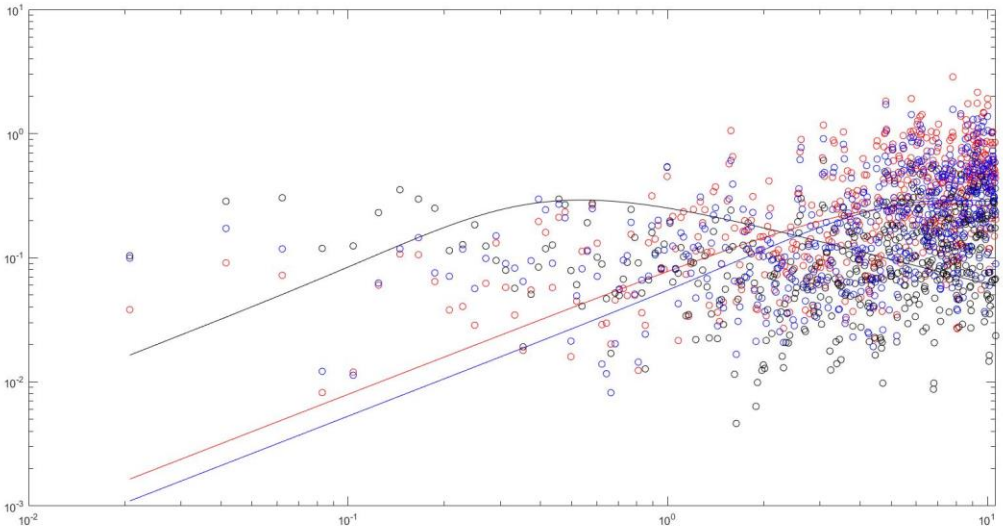

1-1-2-600

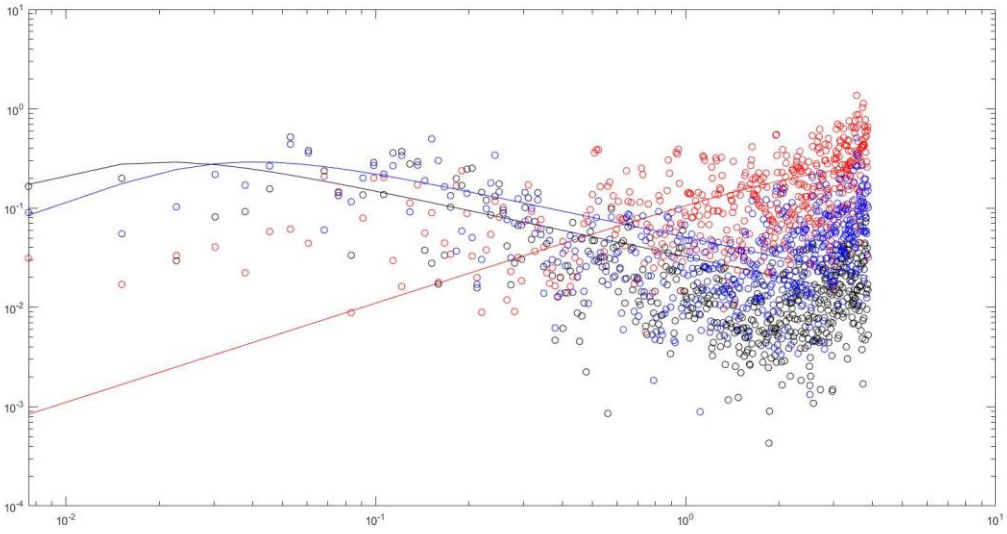

1-1-3-600

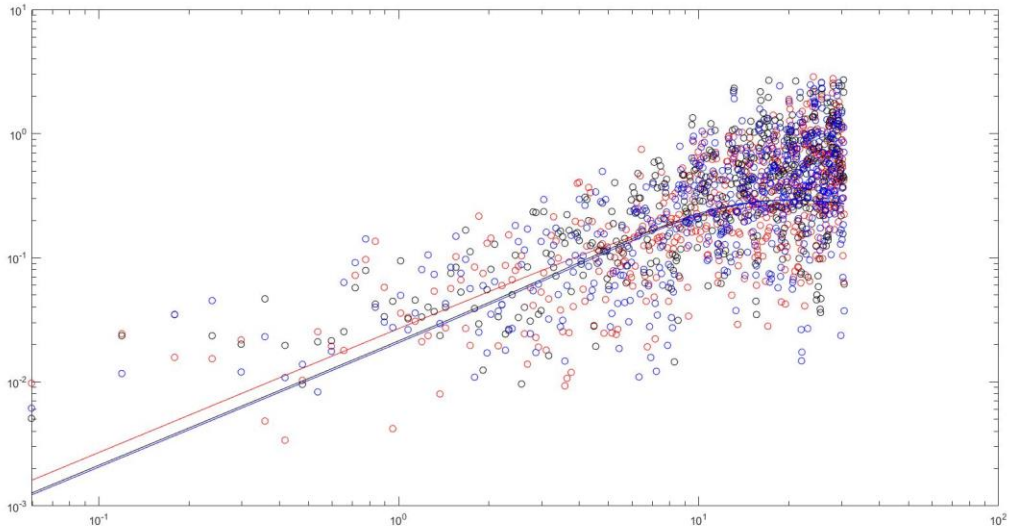

1-1-4-600

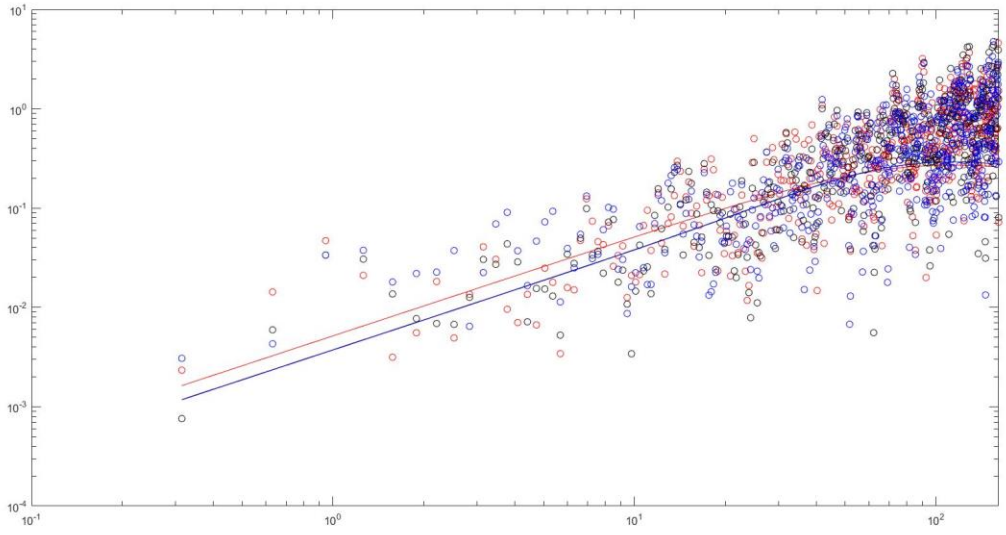

1-1-5-600

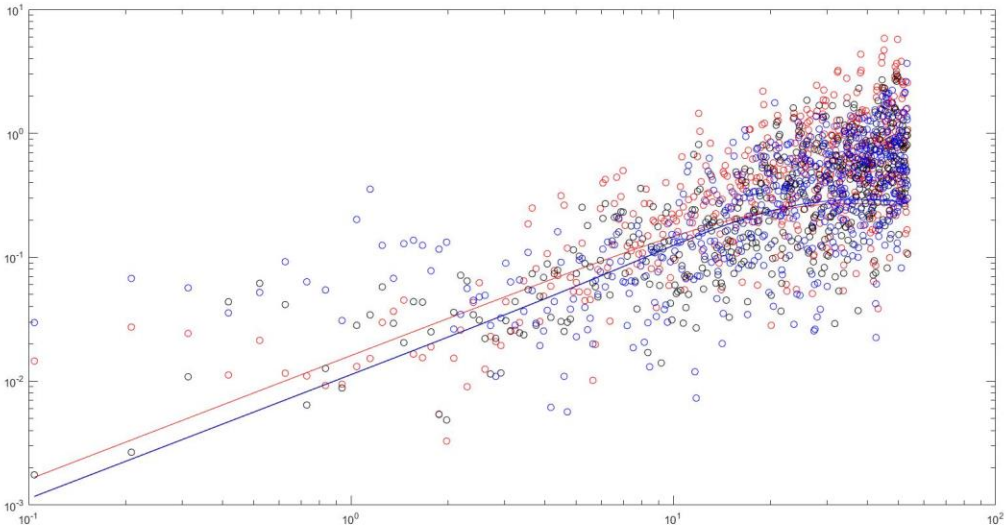

1-1-1-700

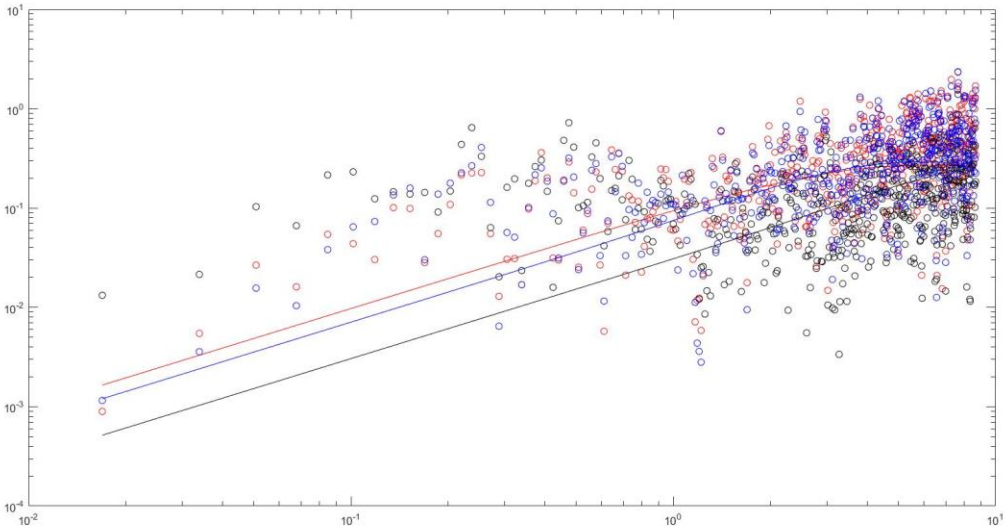

1-1-2-700

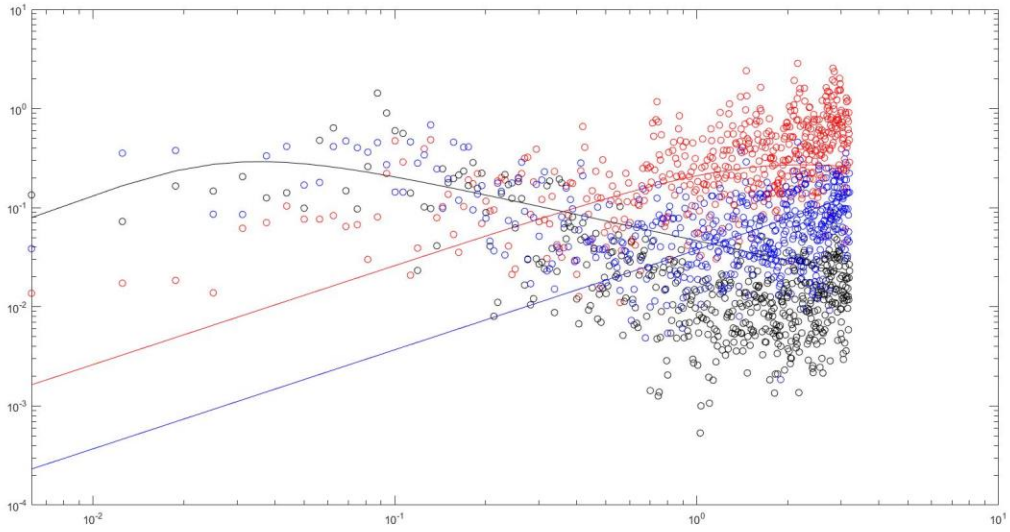

1-1-3-700

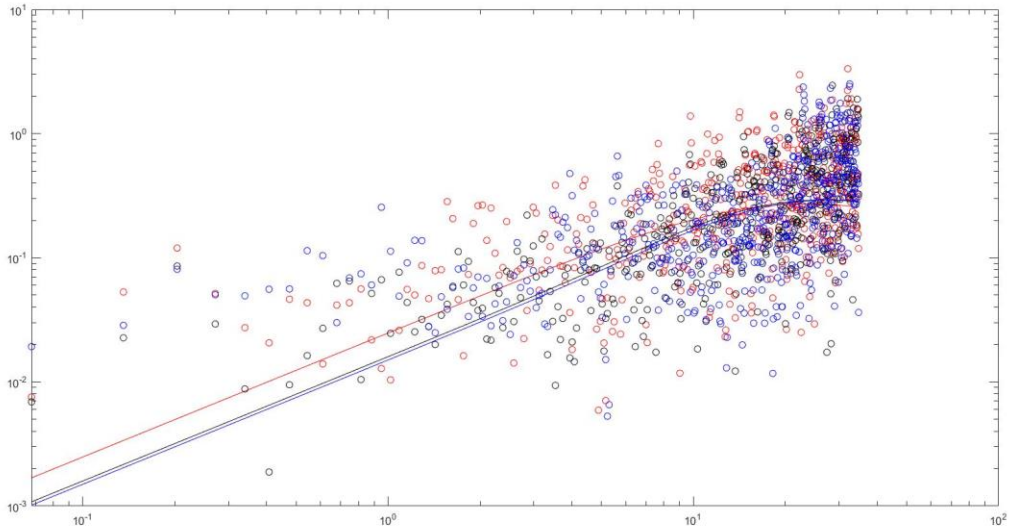

1-1-4-700

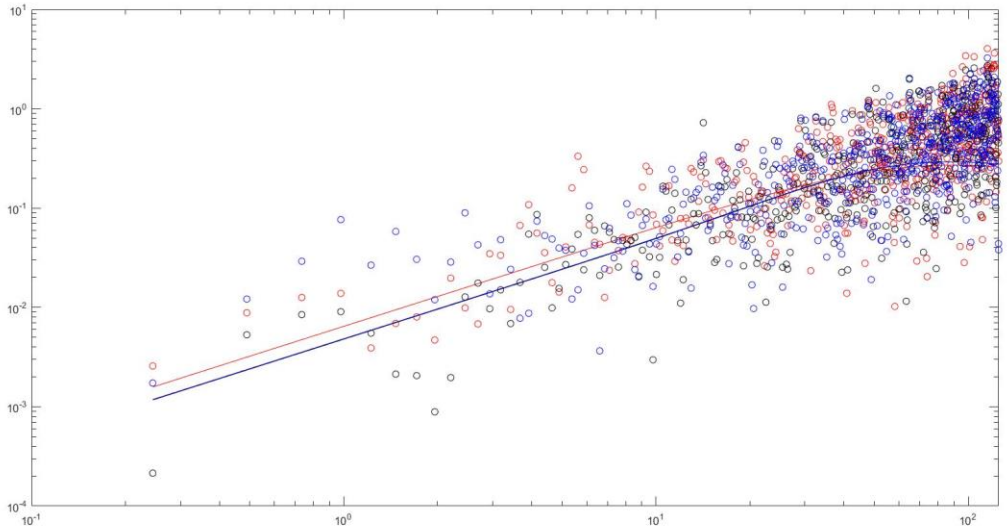

1-1-5-700

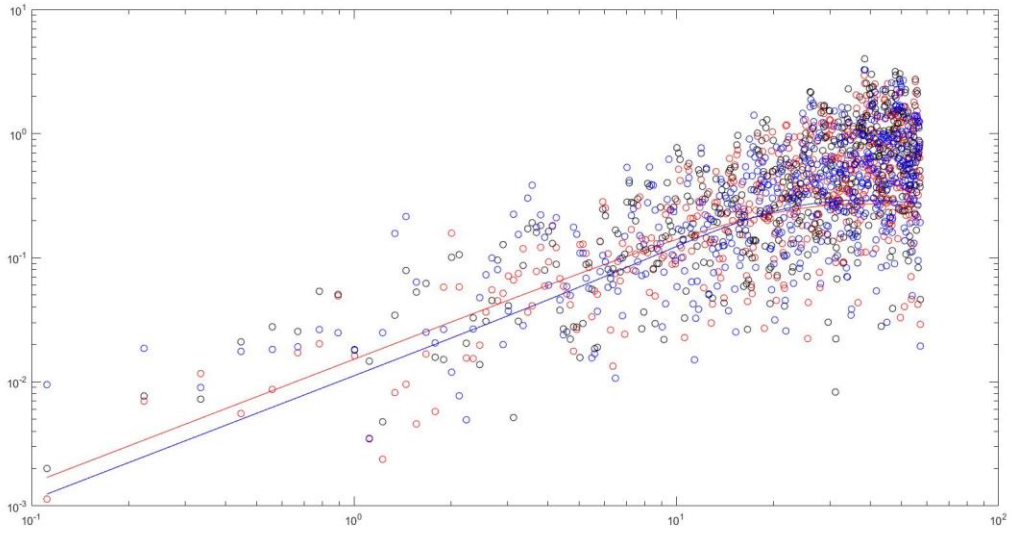

1-1-1-800

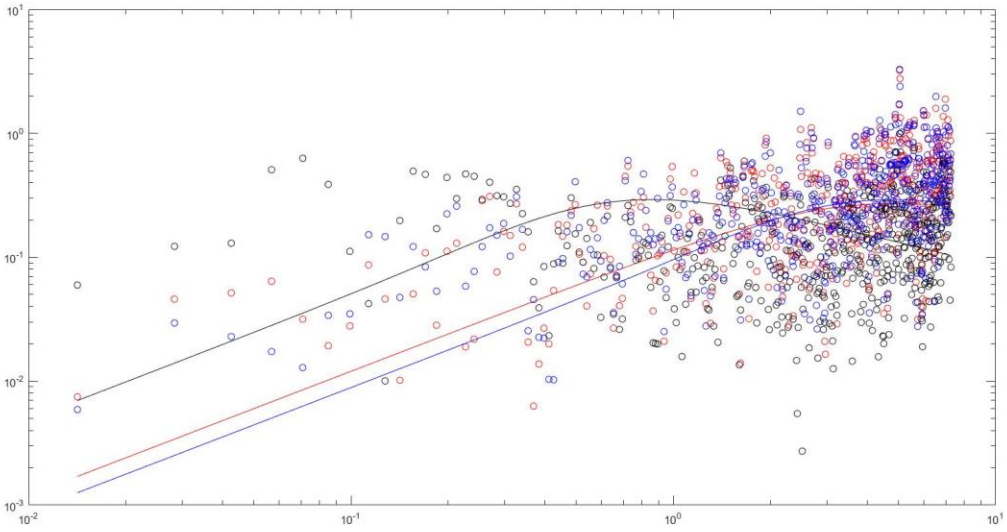

1-1-2-800

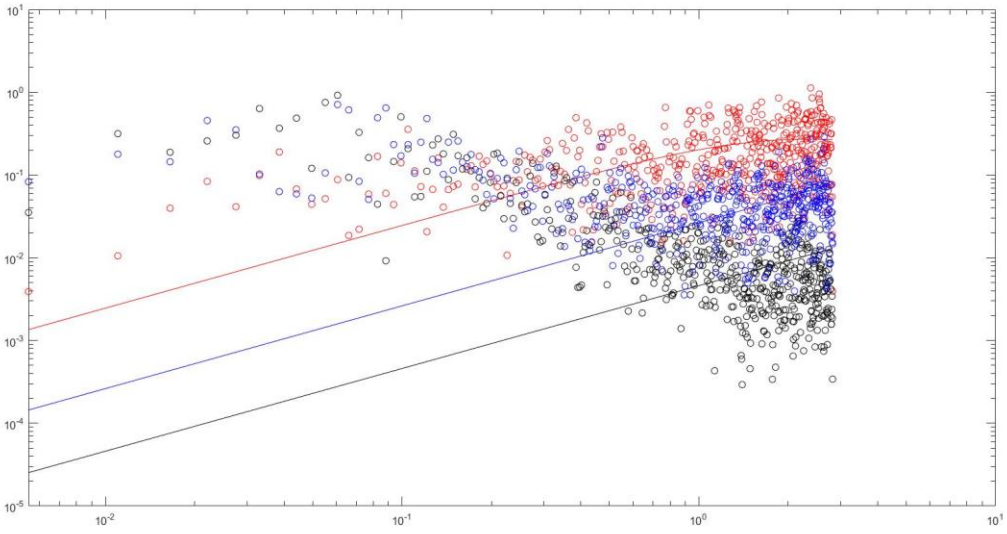

1-1-3-800

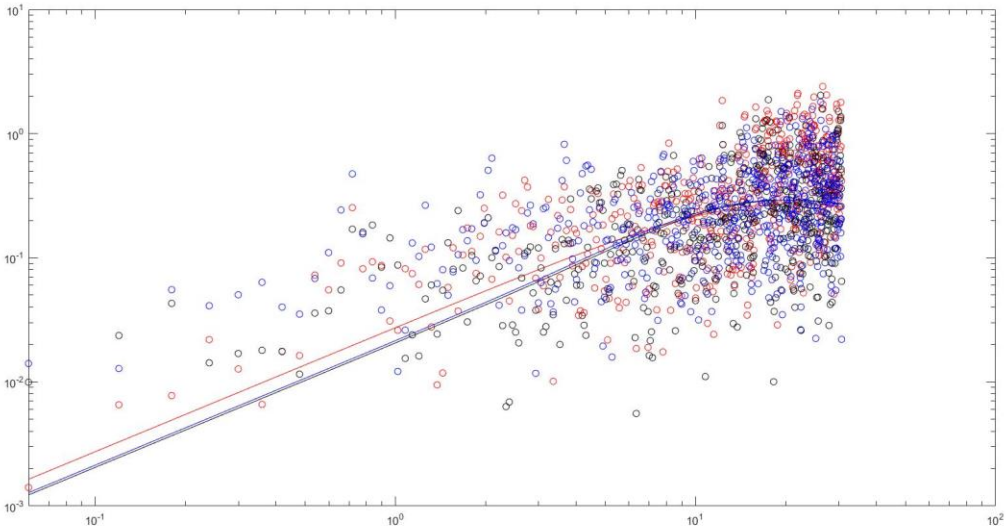

1-1-4-800

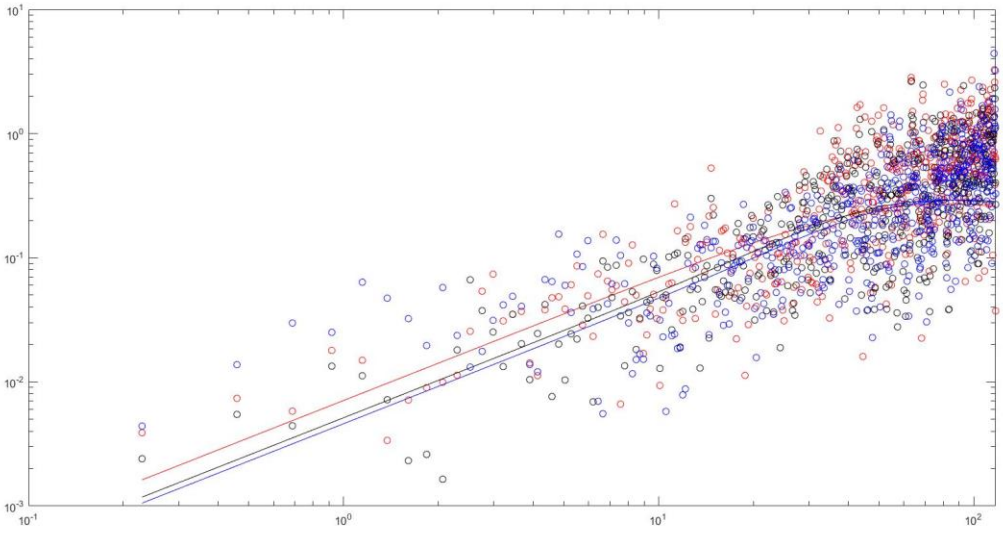

1-1-5-800

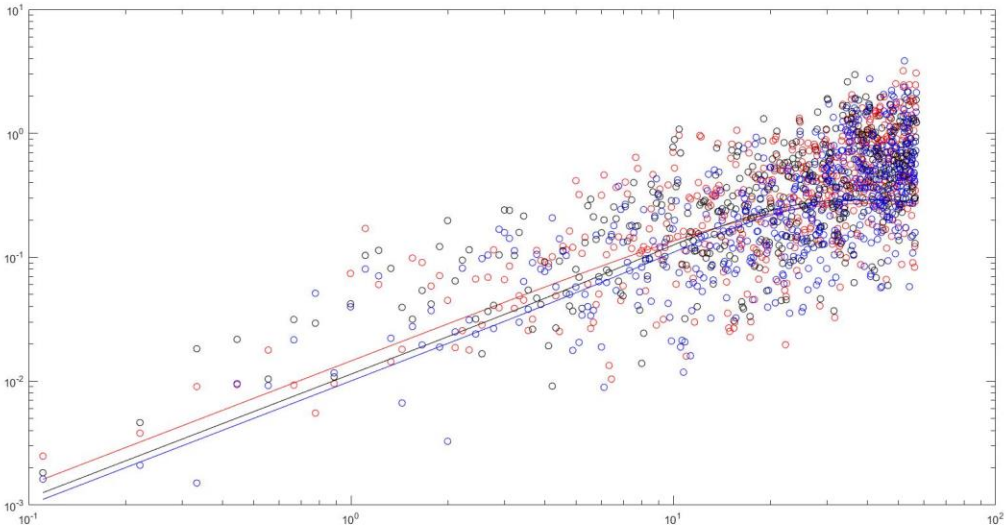

Location 2

1-2-1-400

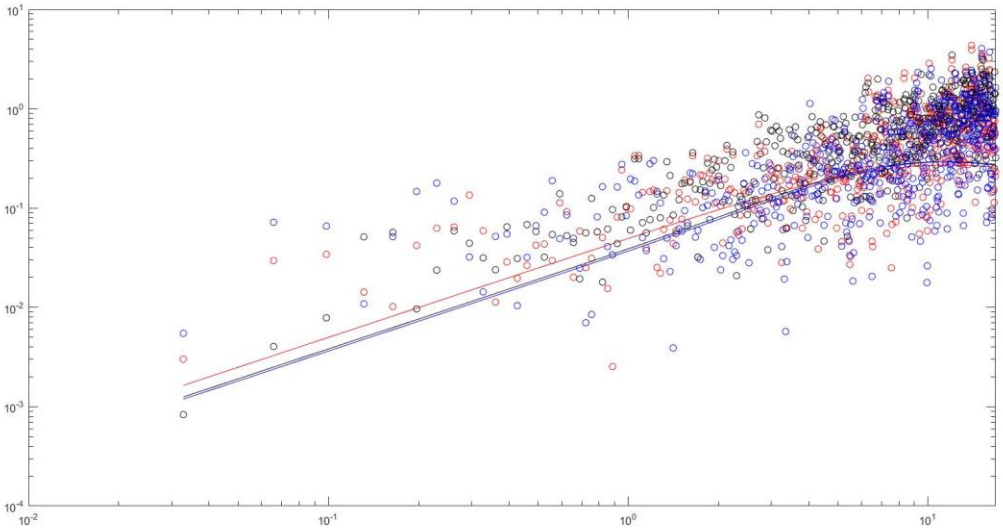

1-2-2-400

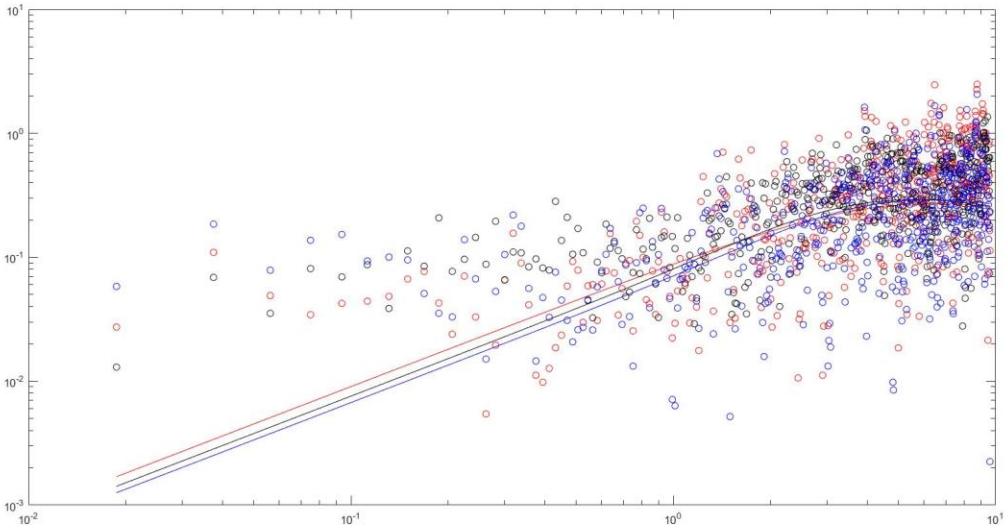

1-2-3-400

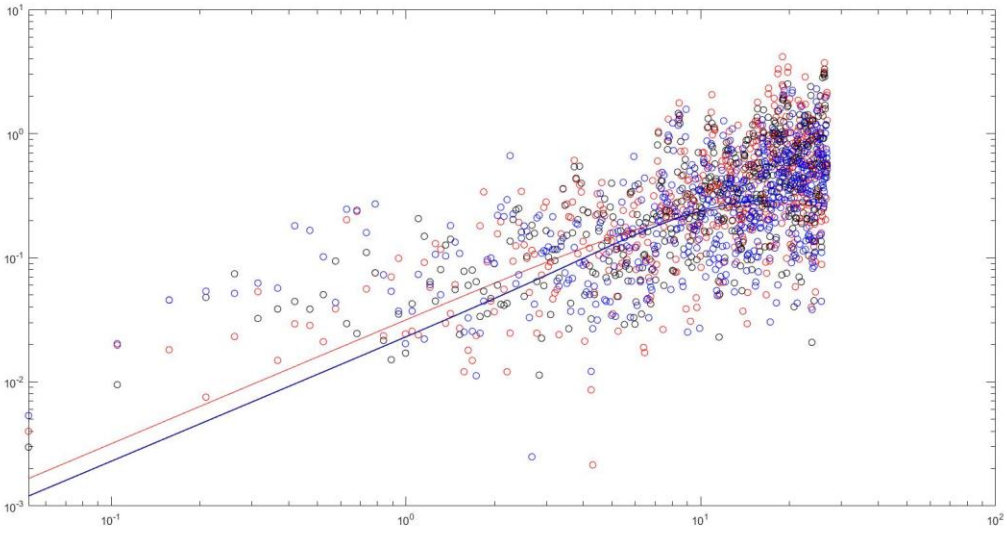

1-2-4-400

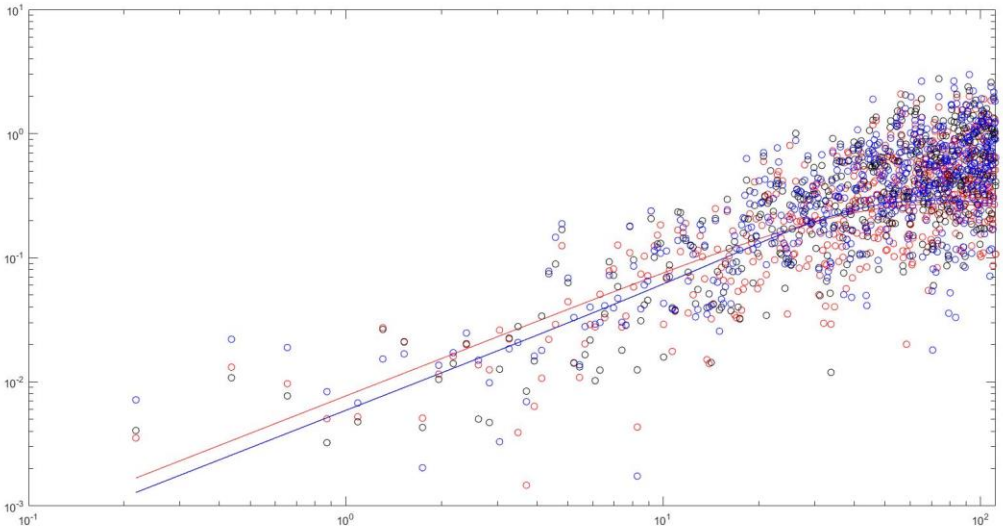

1-2-5-400

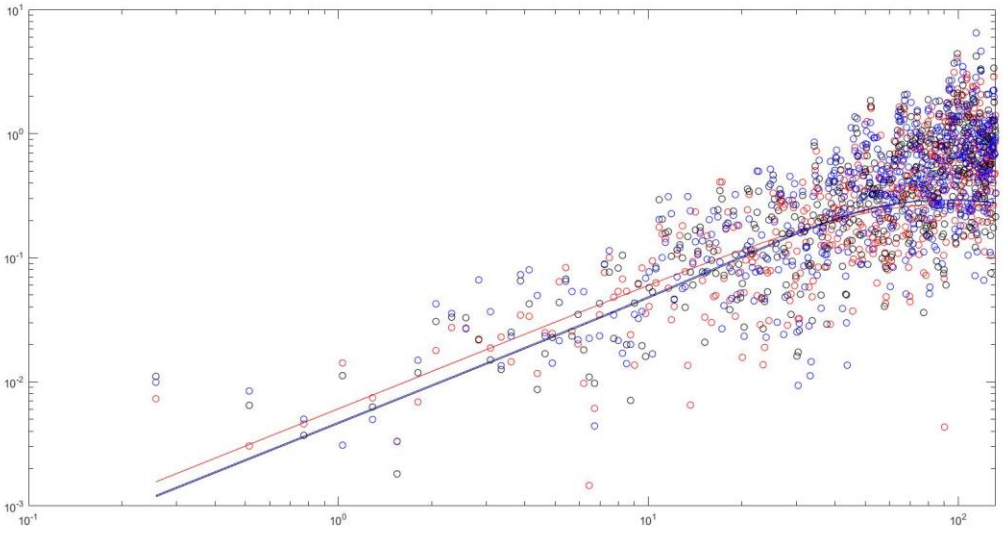

1-2-1-500

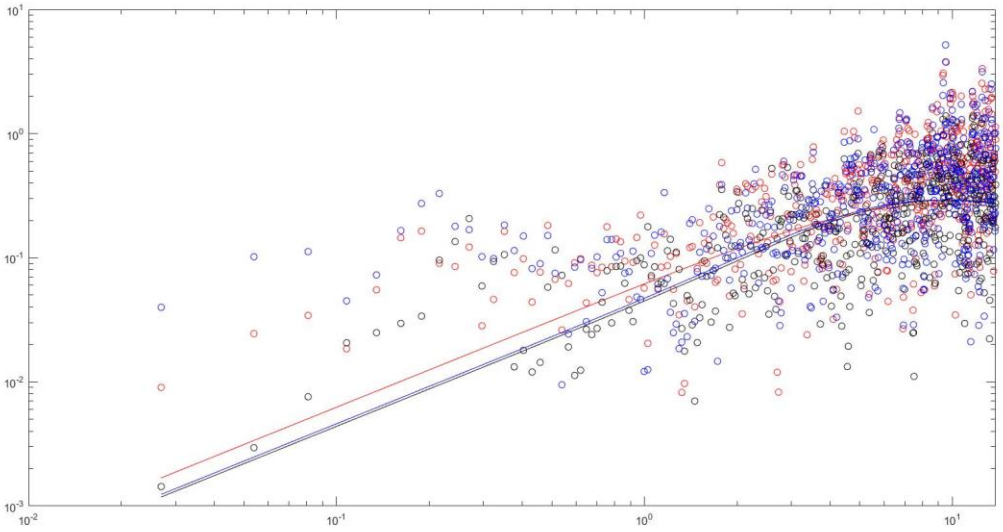

1-2-2-500

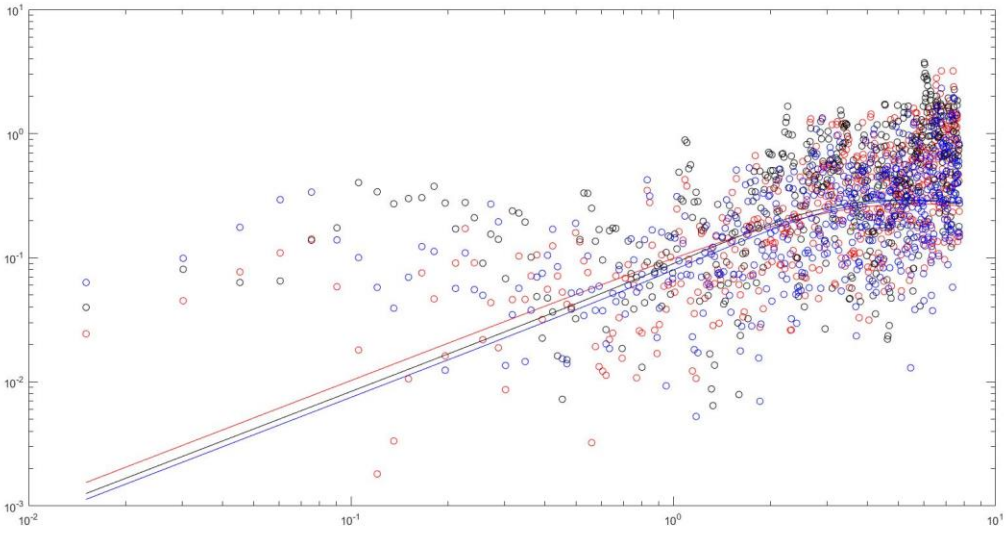

1-2-3-500

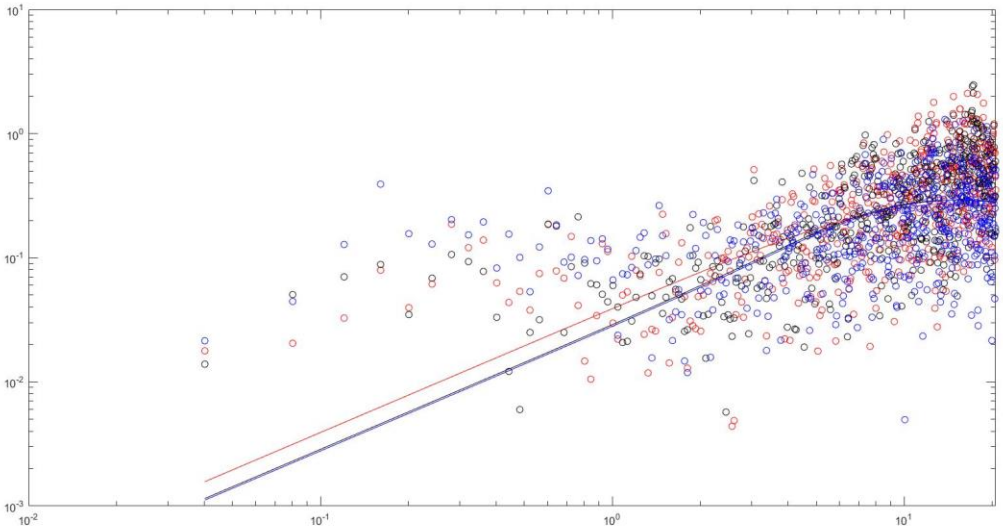

1-2-4-500

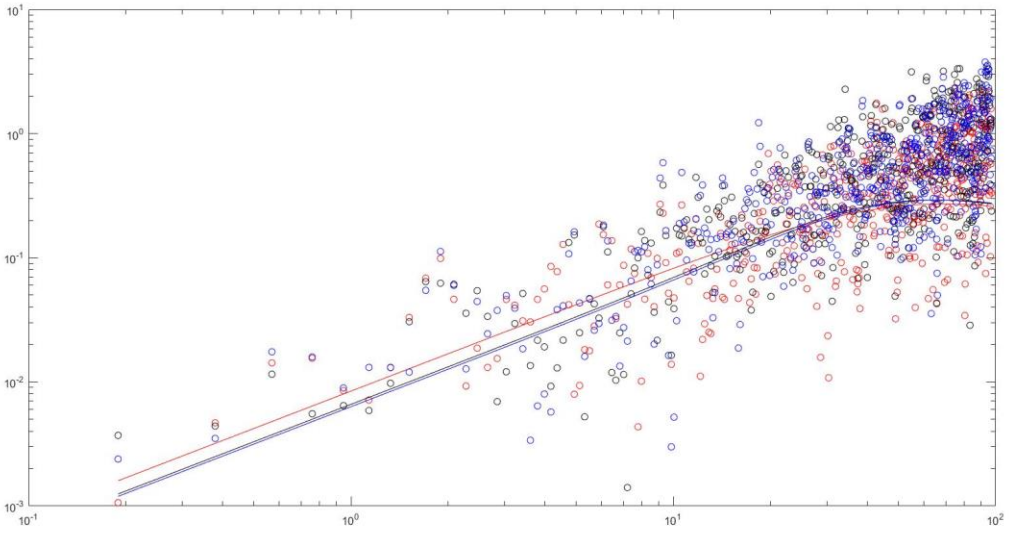

1-2-5-500

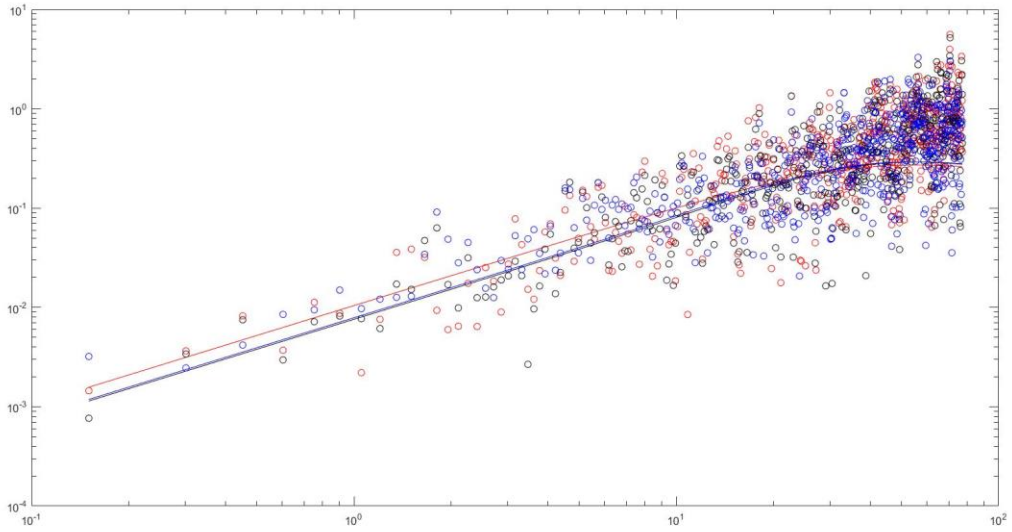

1-2-1-600

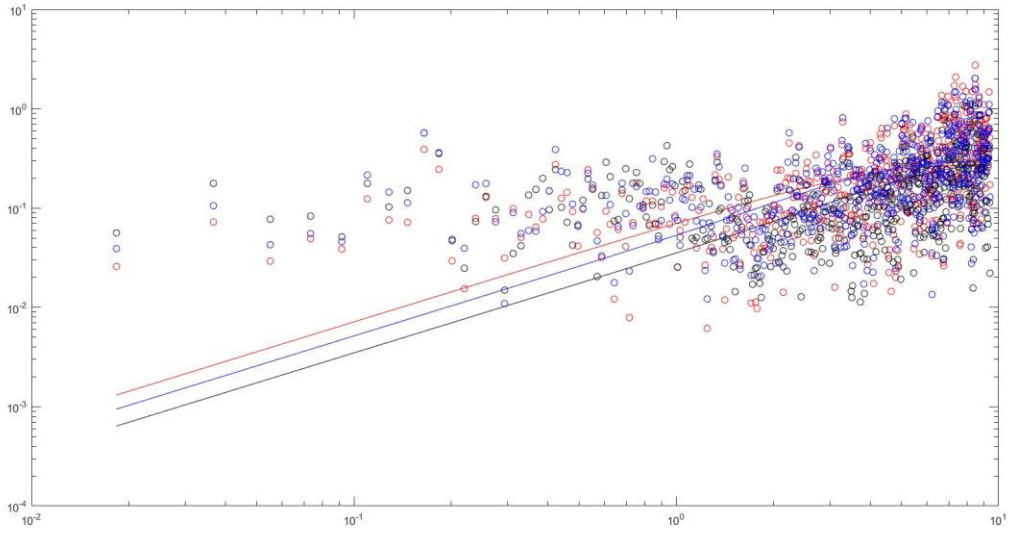

1-2-2-600

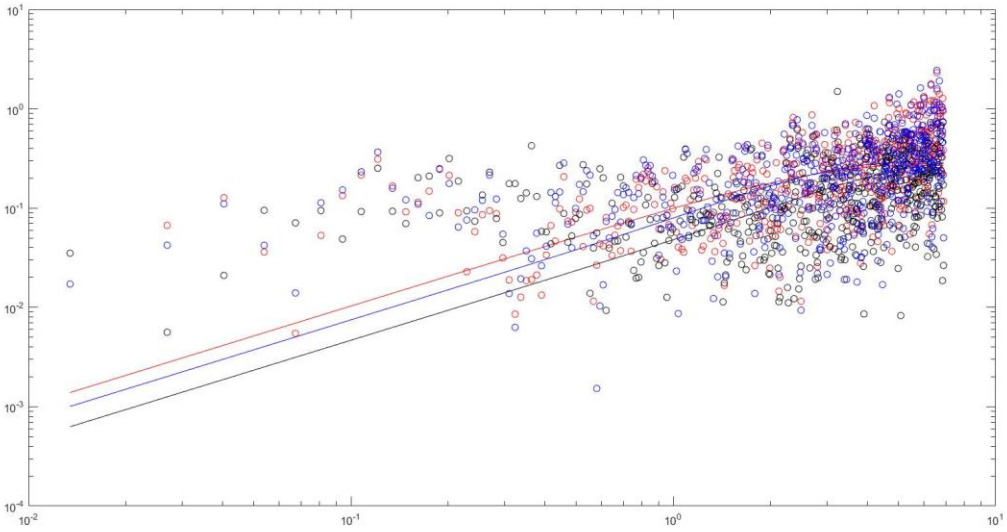

1-2-3-600

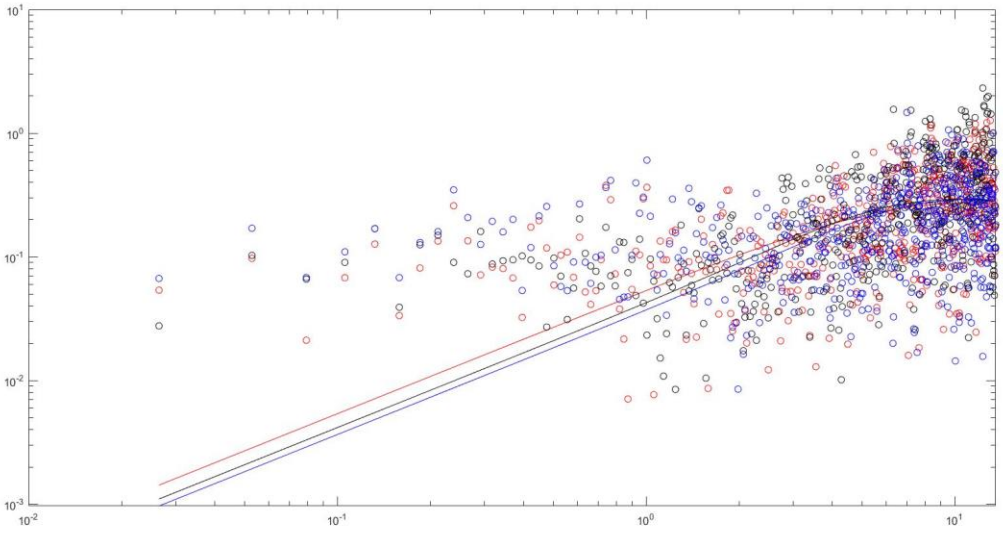

1-2-4-600

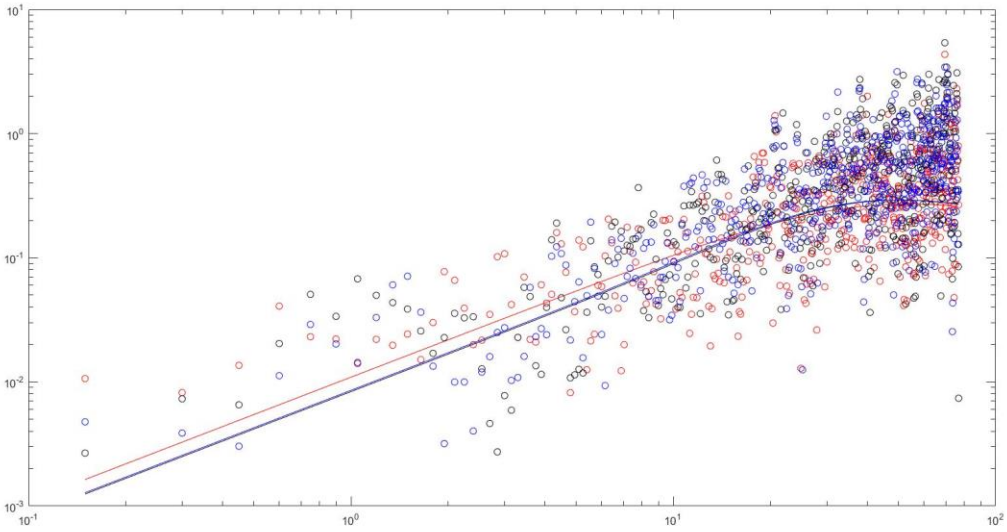

1-2-5-600

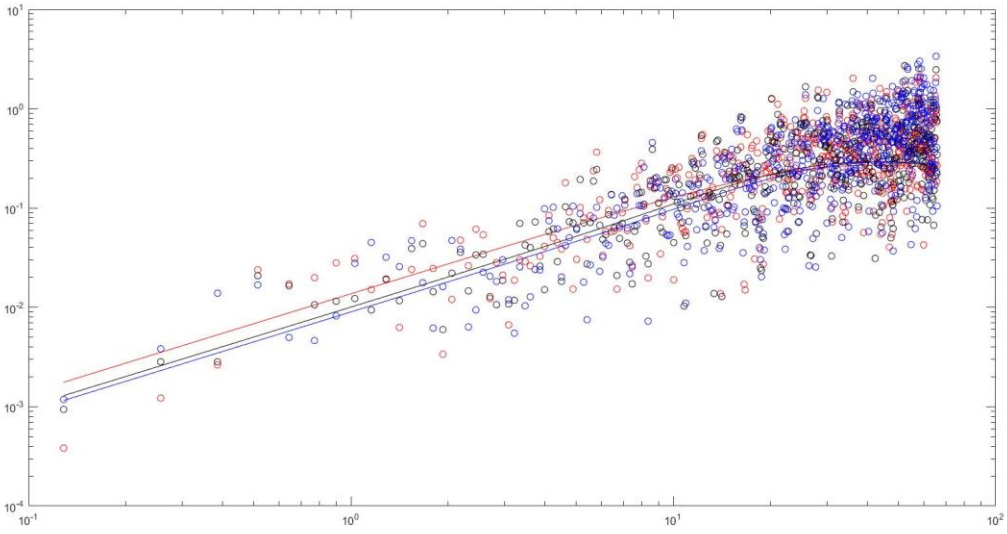

1-2-1-700

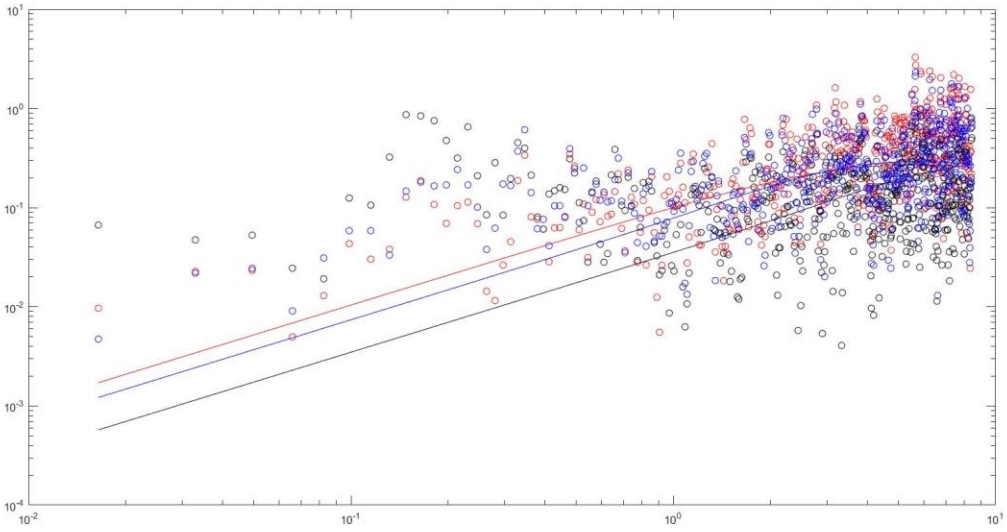

1-2-2-700

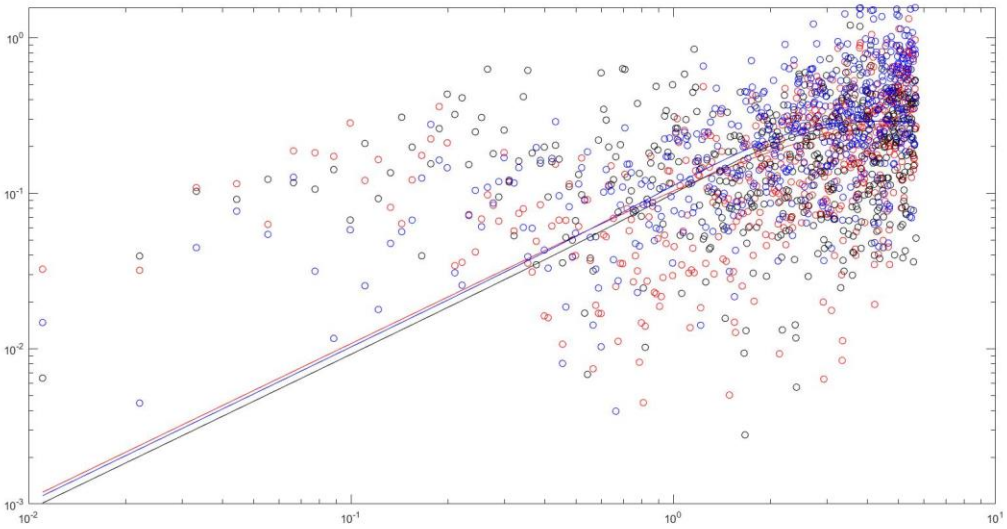

1-2-3-700

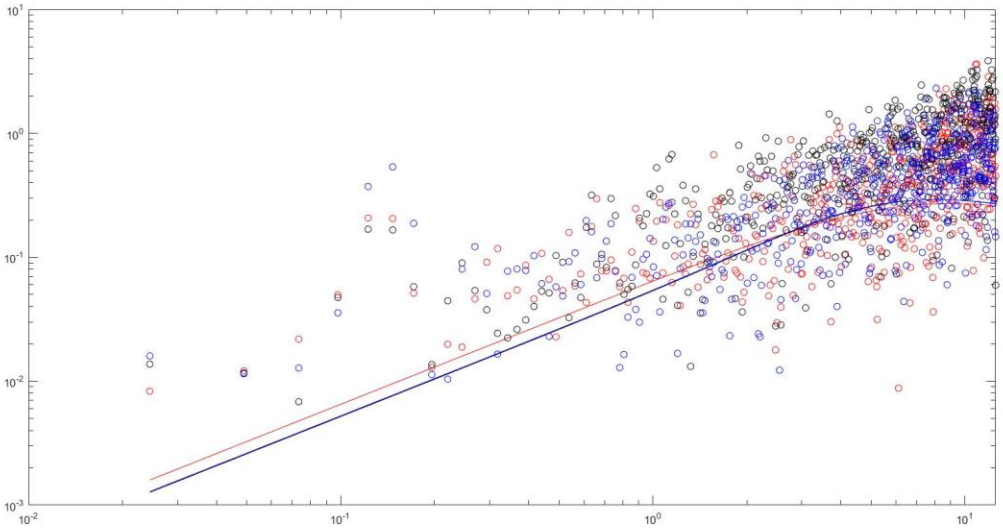

1-2-4-700

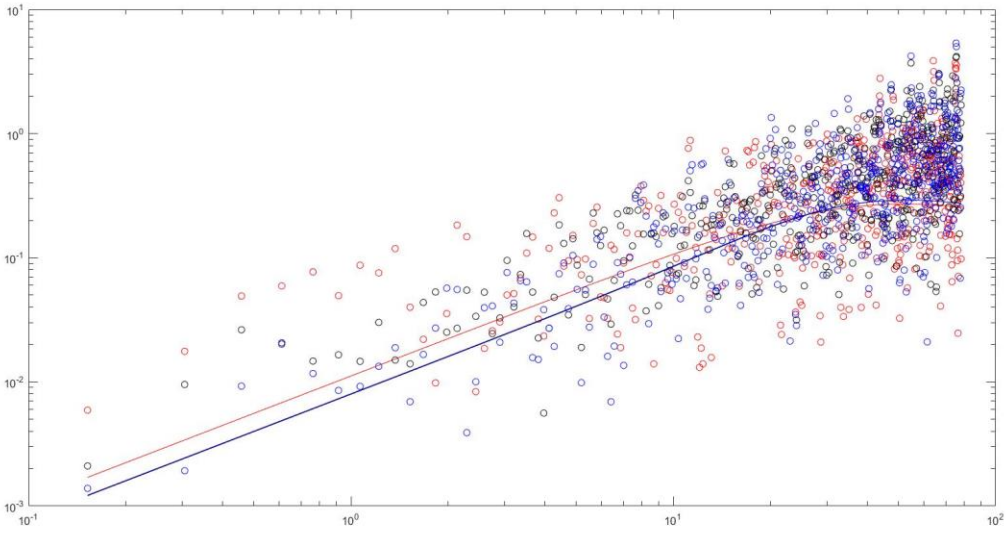

1-2-5-700

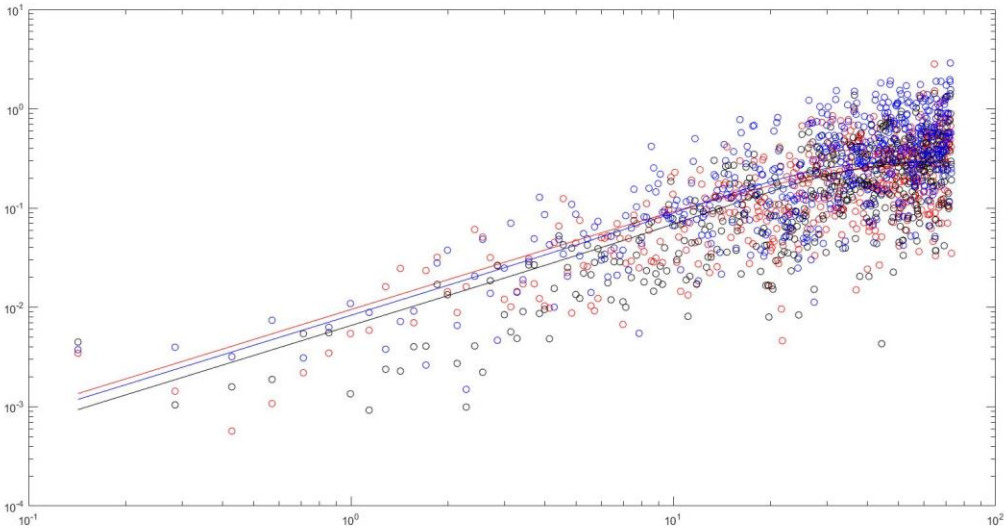

1-2-1-800

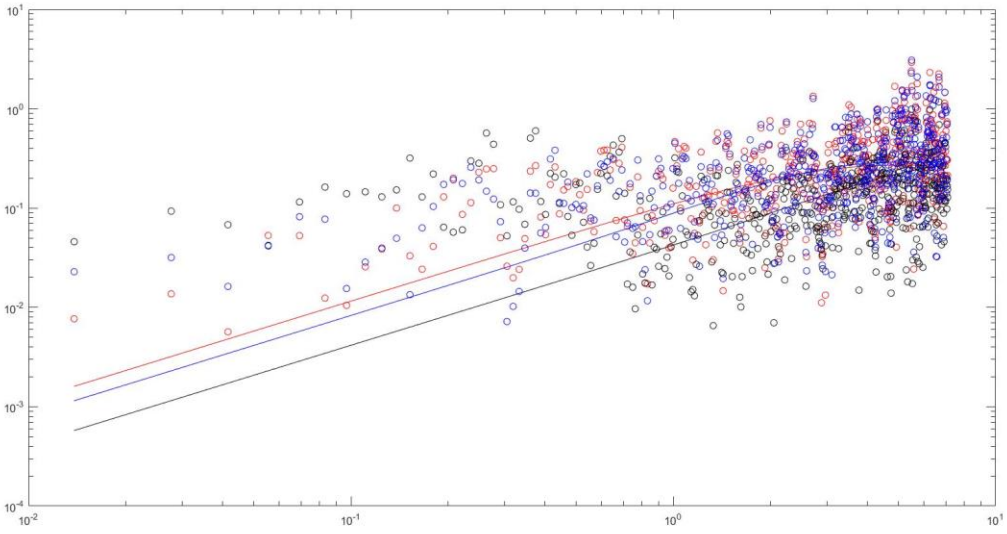

1-2-2-800

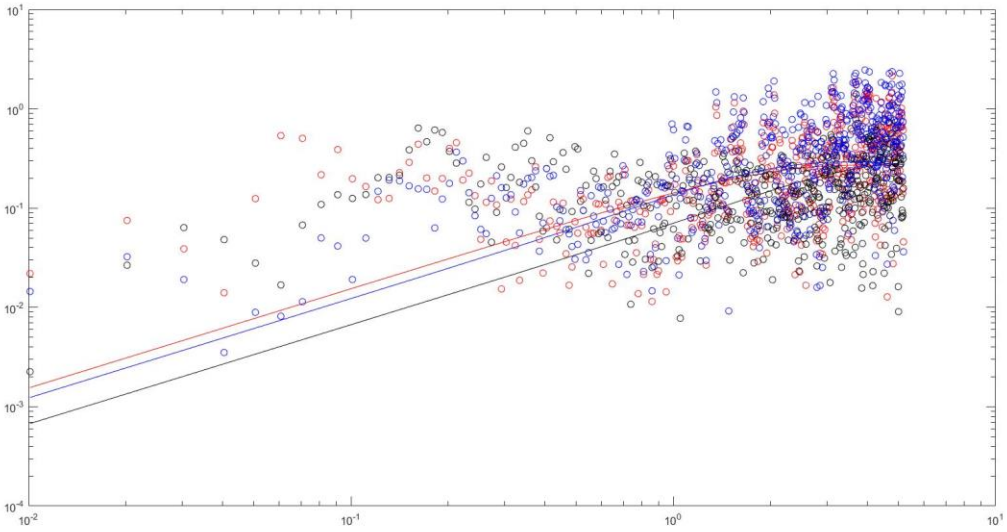

1-2-3-800

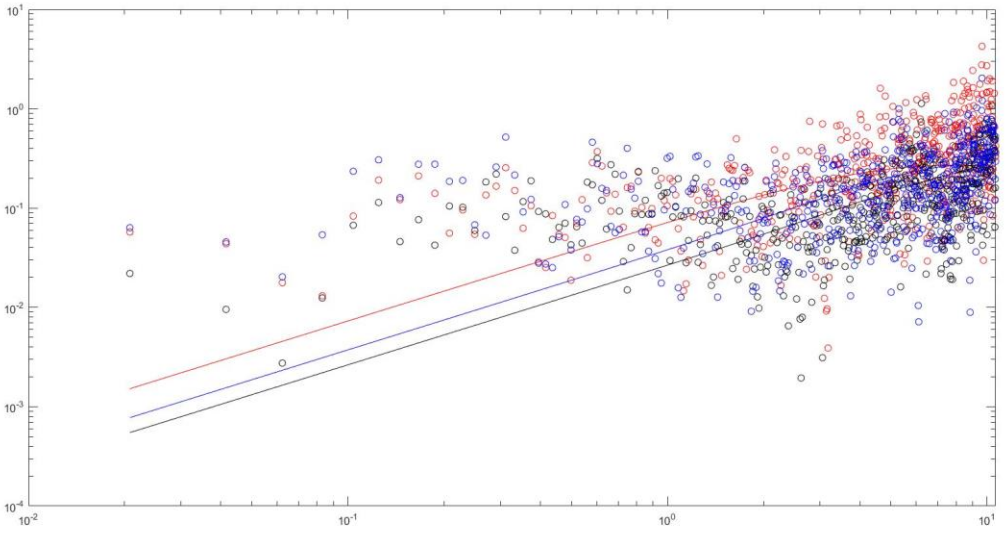

1-2-4-800

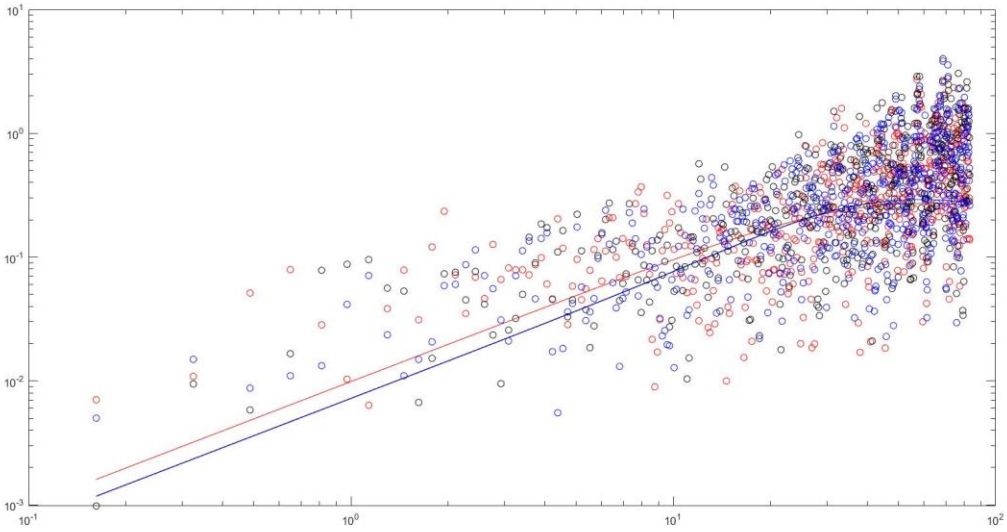

1-2-5-800

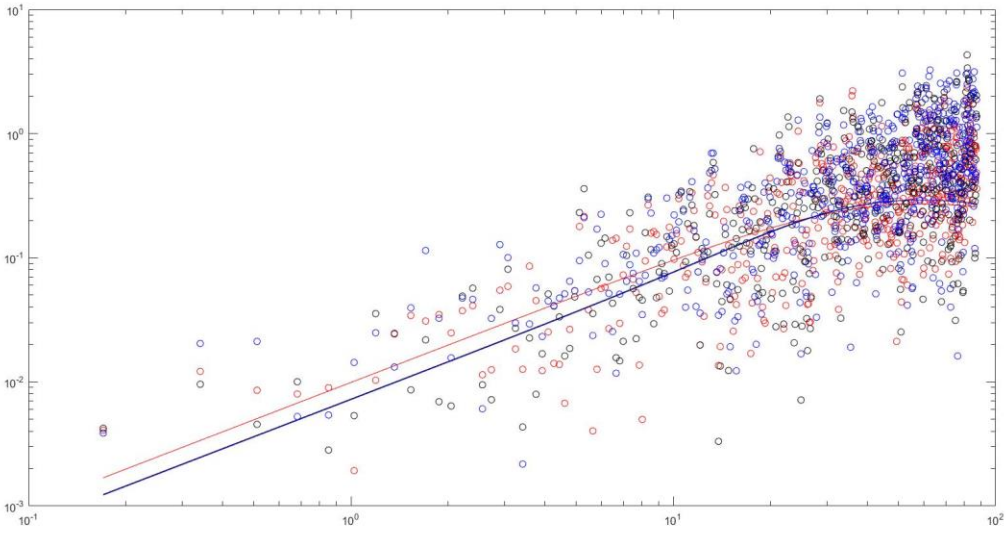

Location 3

1-3-1-400

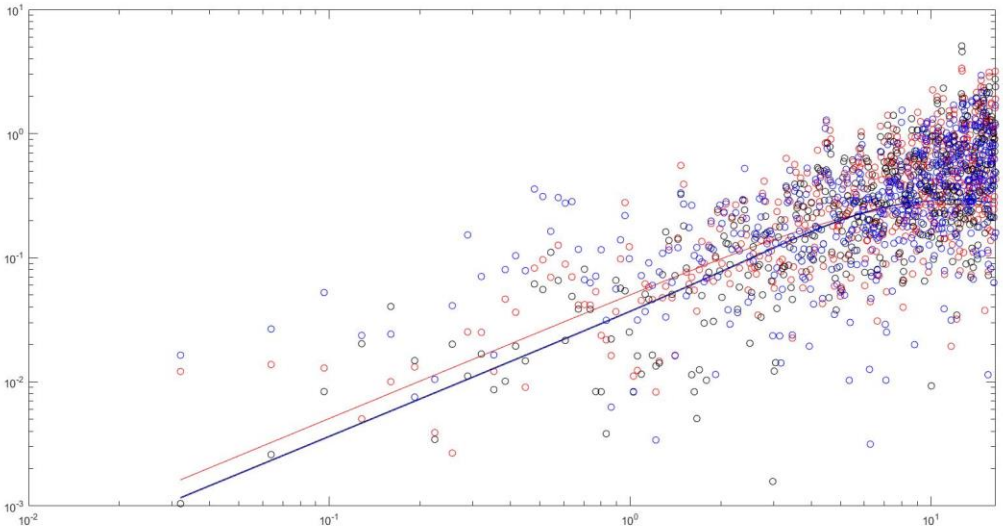

1-3-2-400

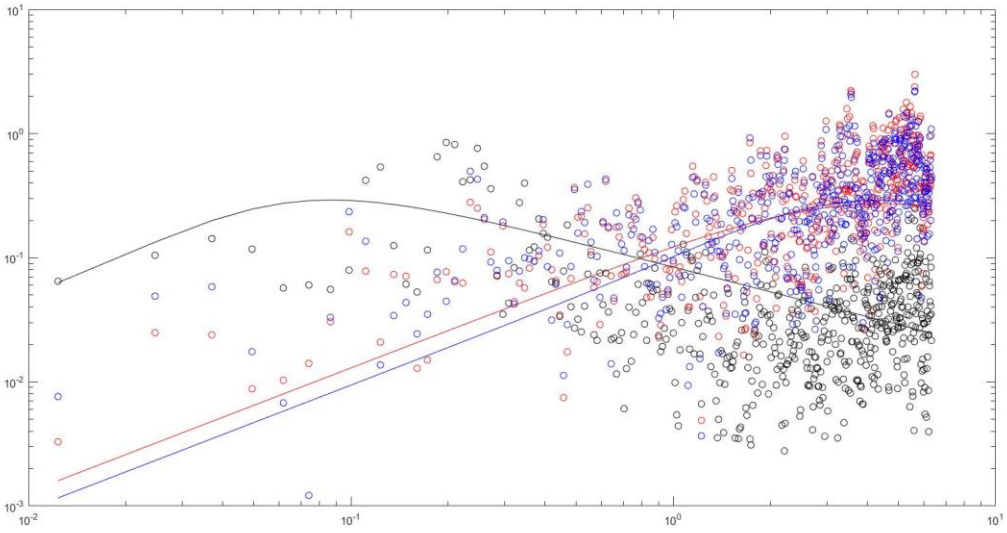

1-3-3-400

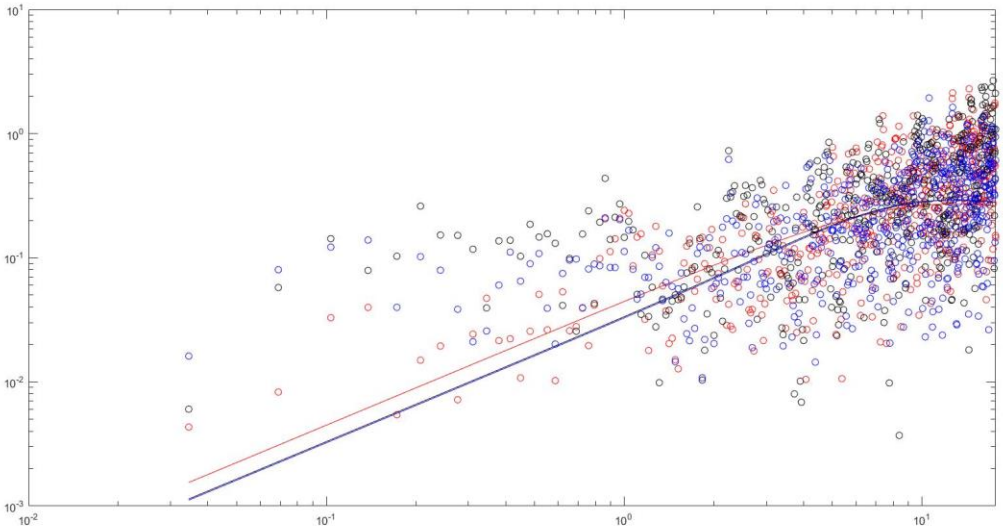

1-3-4-400

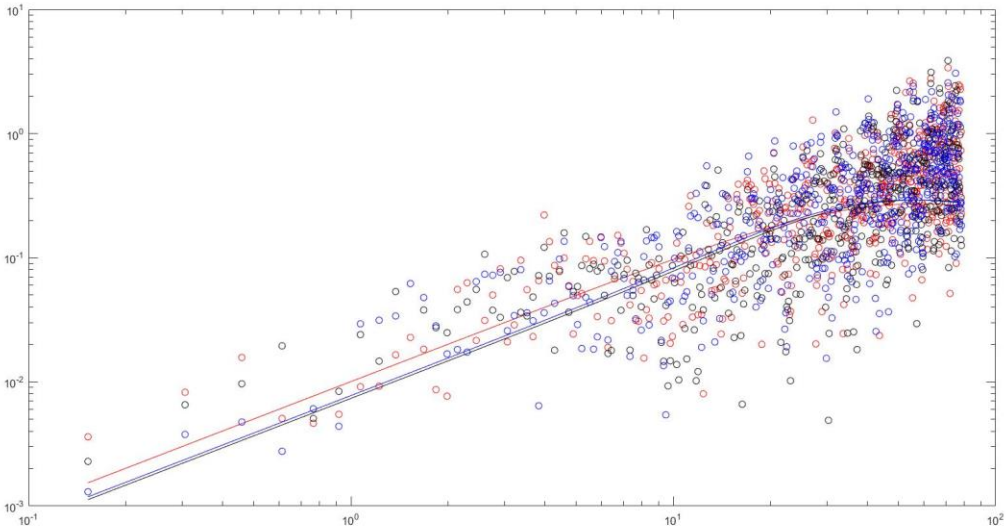

1-3-5-400

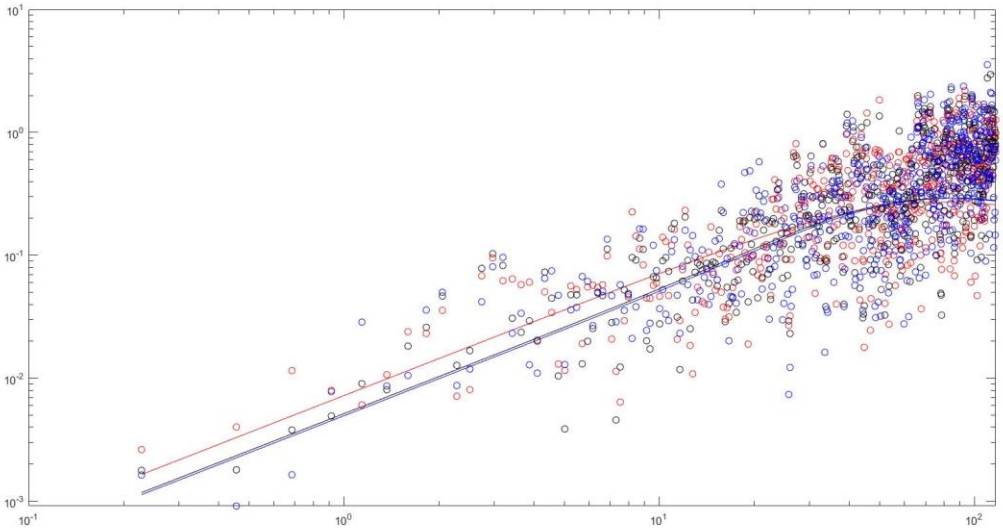

1-3-1-500

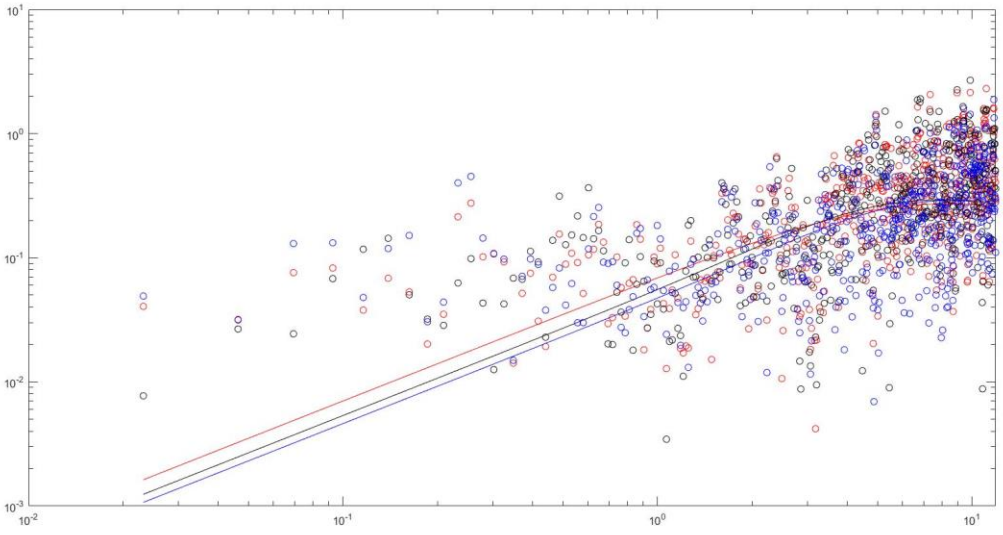

1-3-2-500

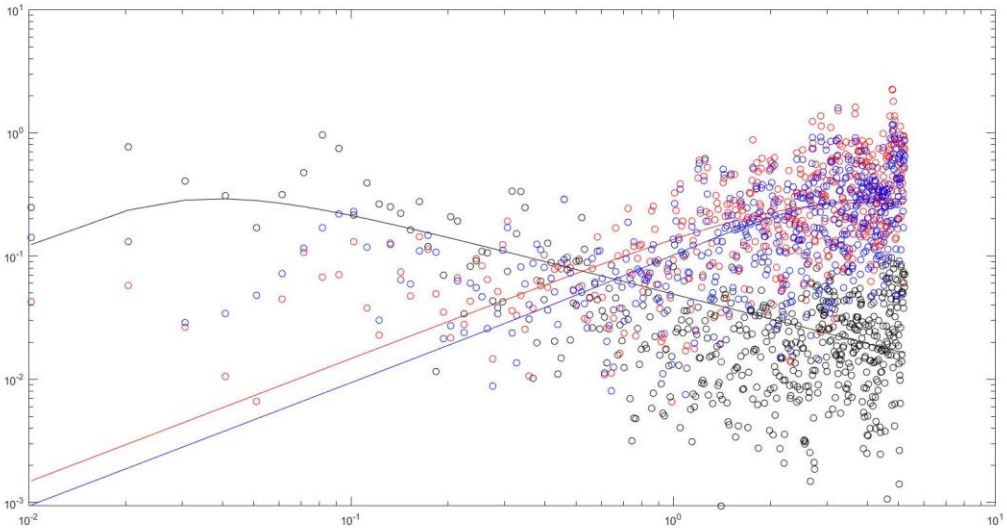

1-3-3-500

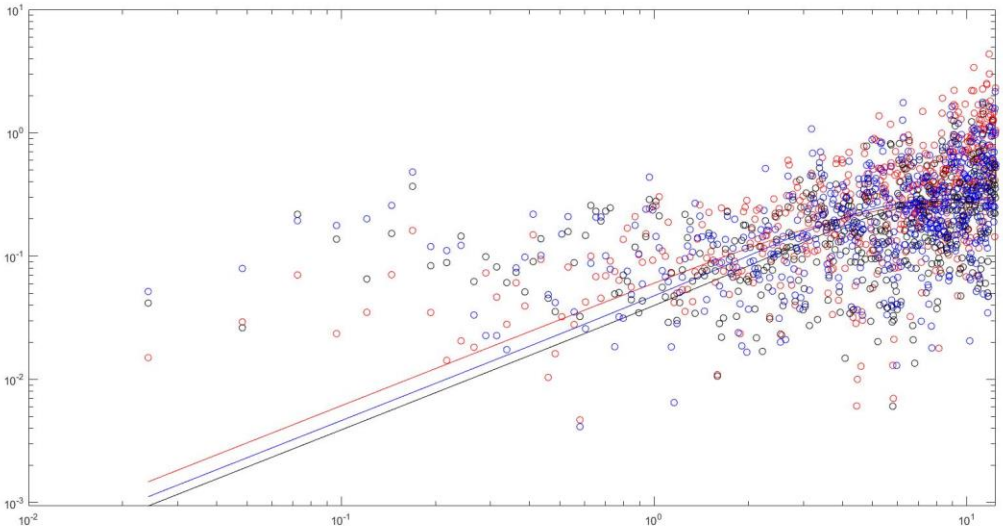

1-3-4-500

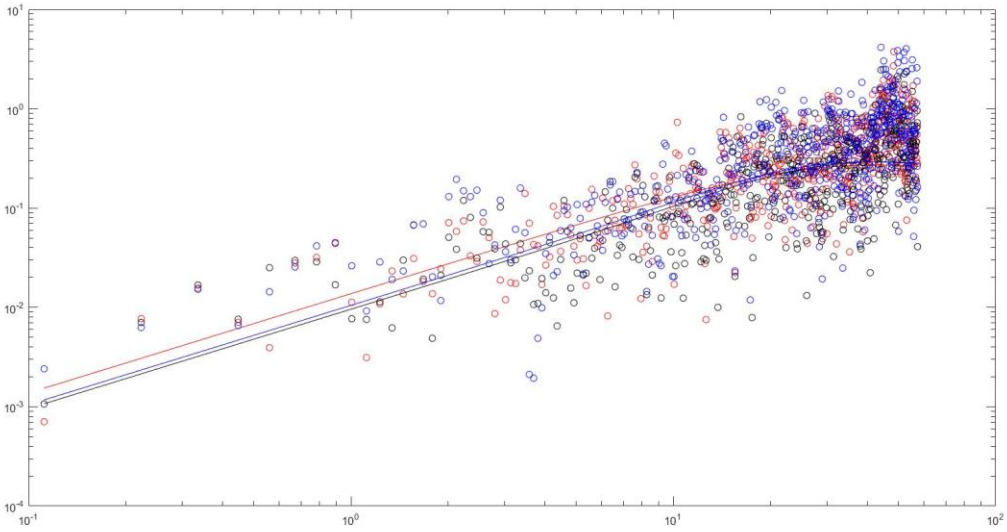

1-3-5-500

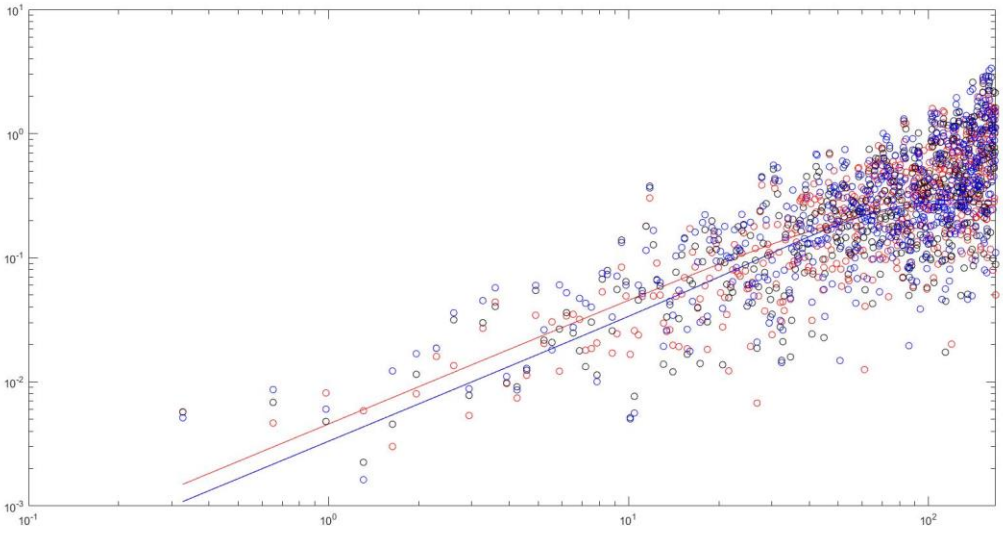

1-3-1-600

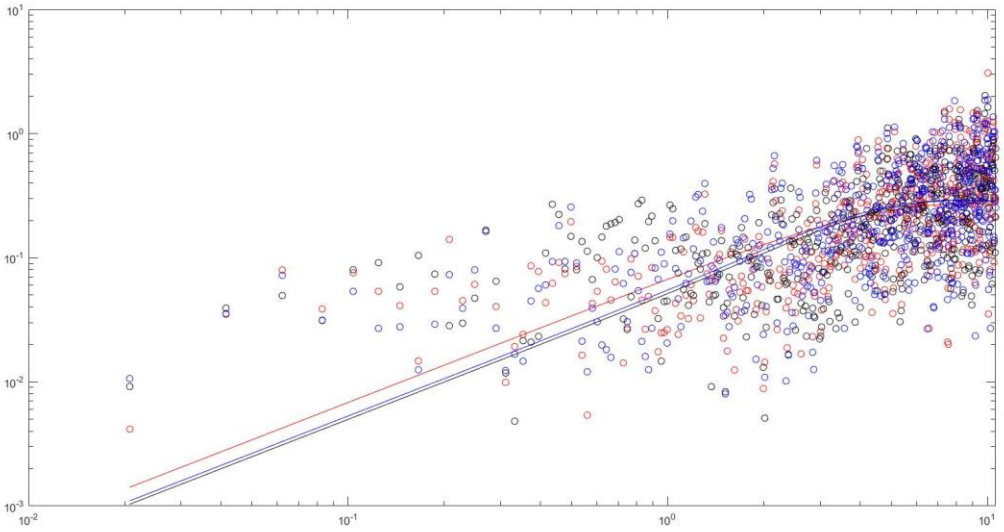

1-3-2-600

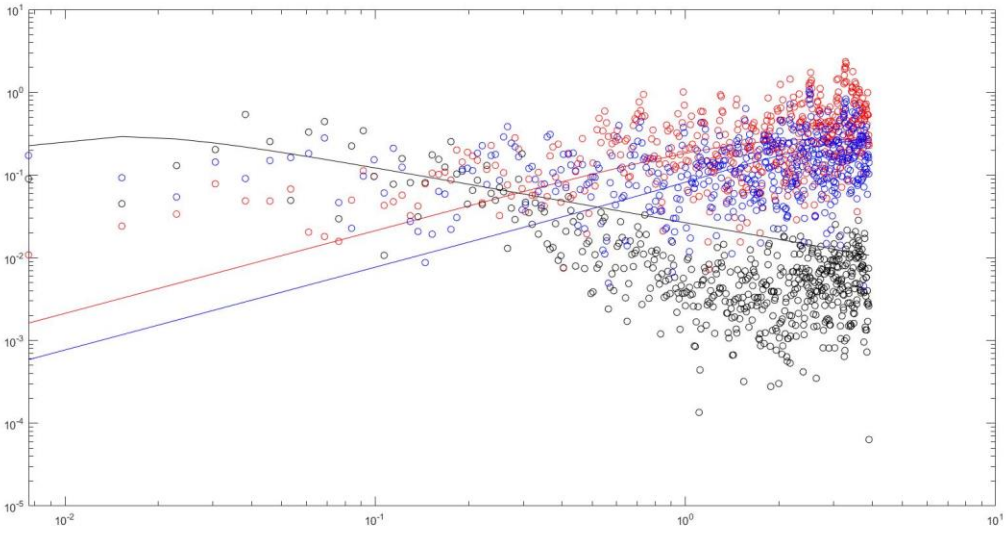

1-3-3-600

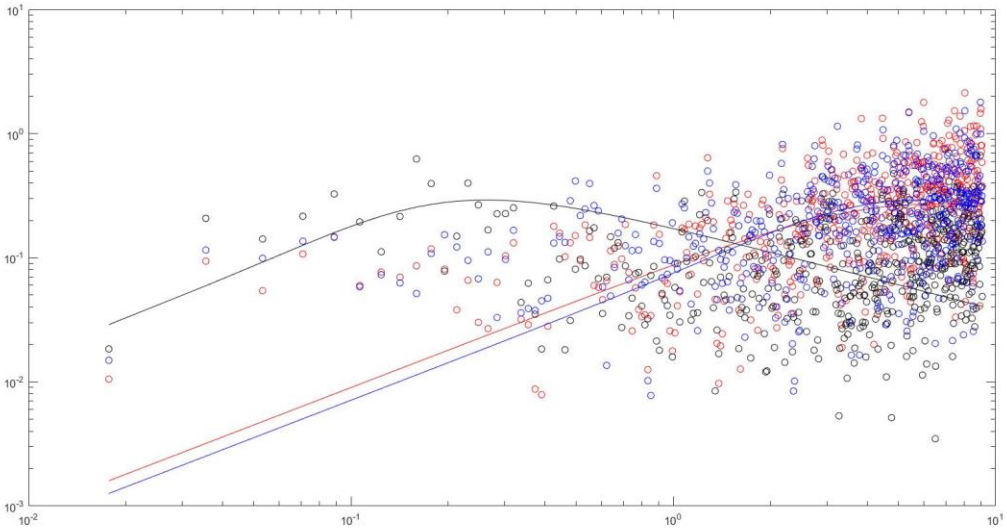

1-3-4-600

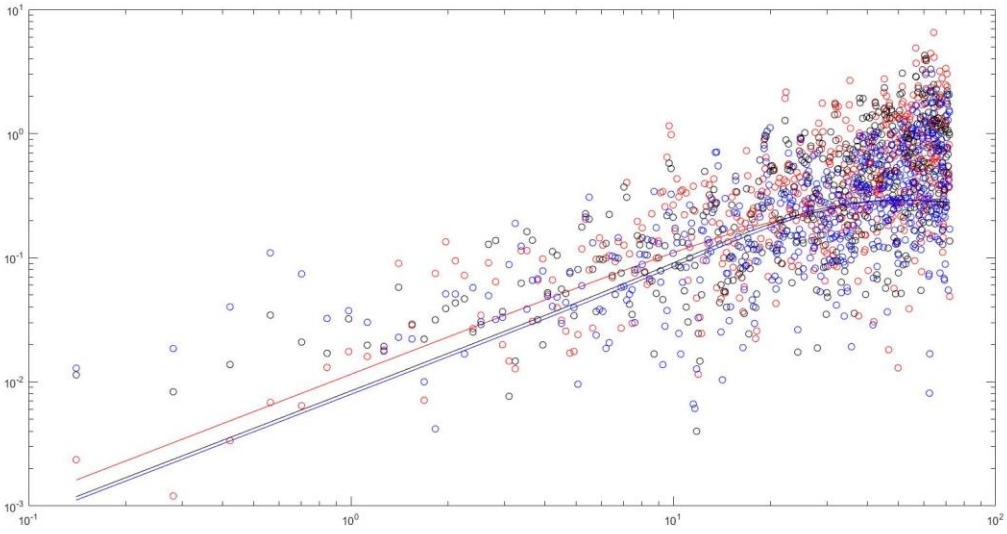

1-3-5-600

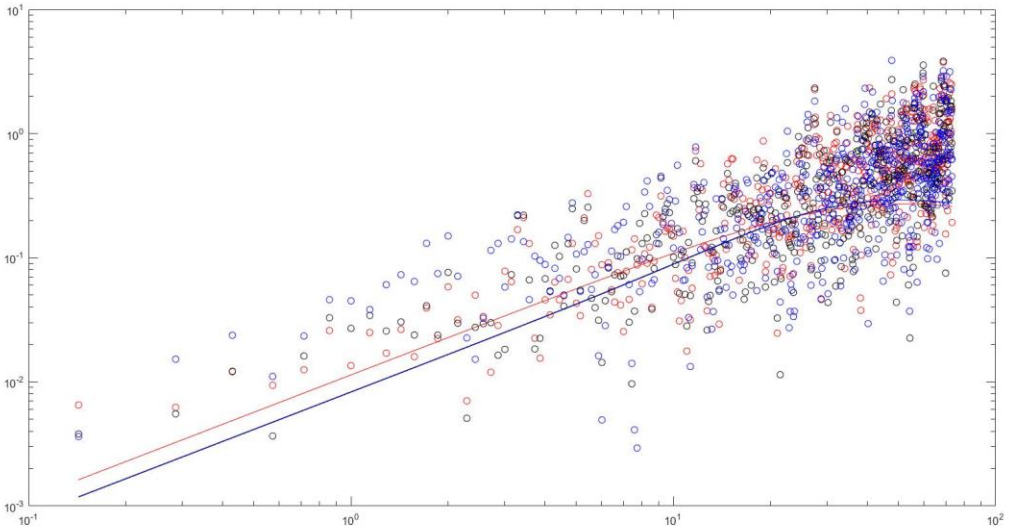

1-2-1-700

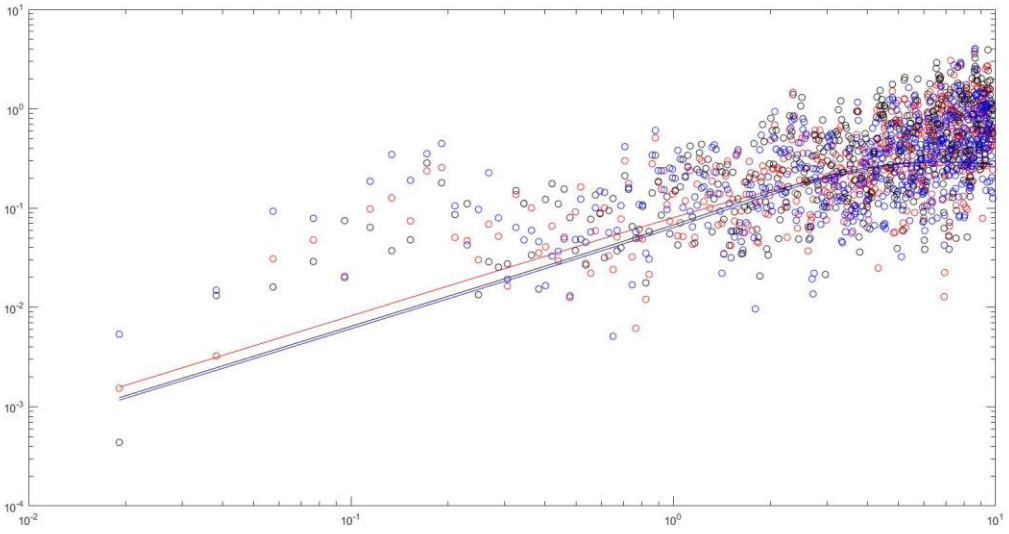

1-3-2-700

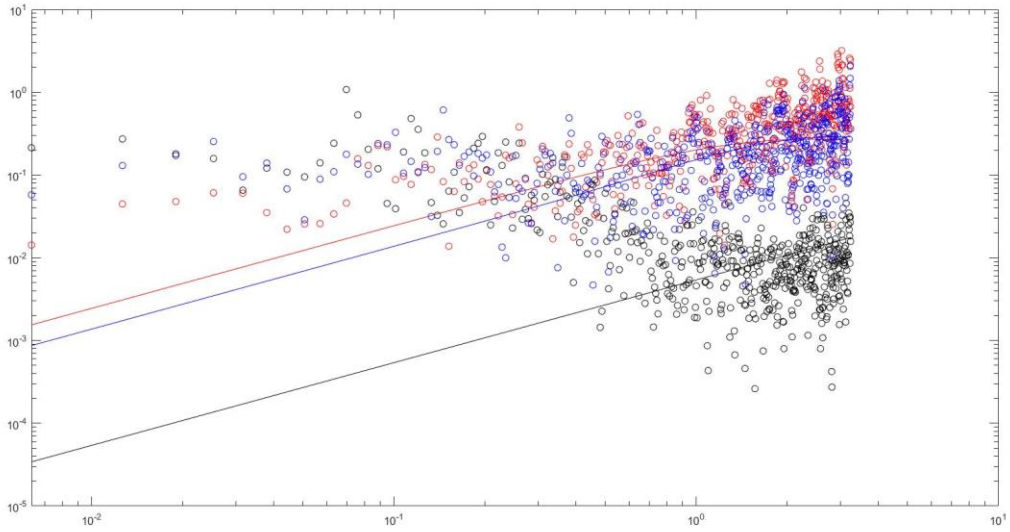

1-3-3-700

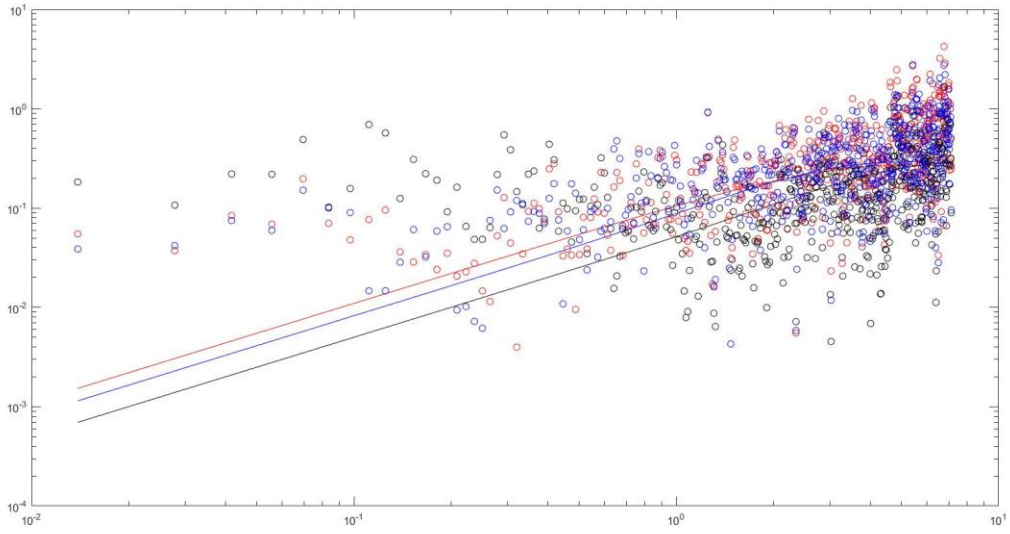

1-3-4-700

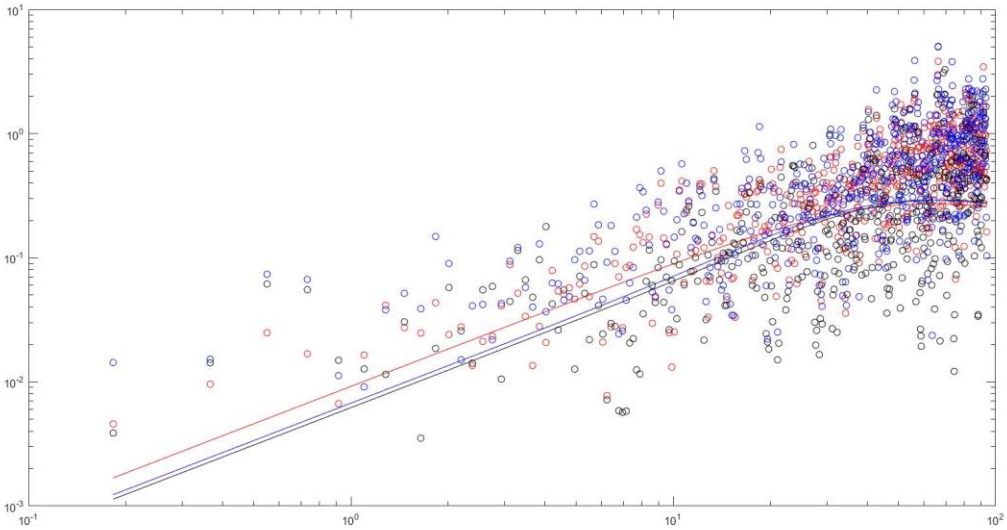

1-3-5-700

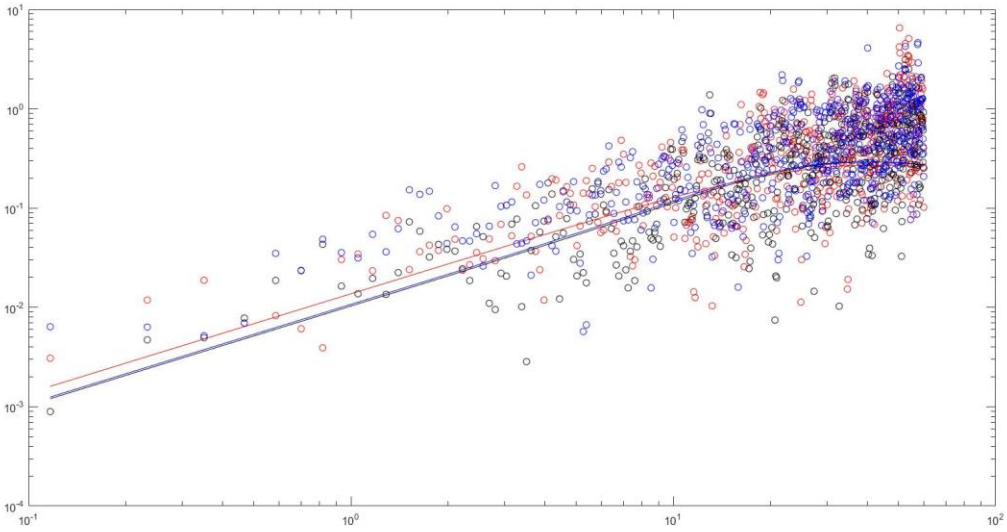

1-3-1-800

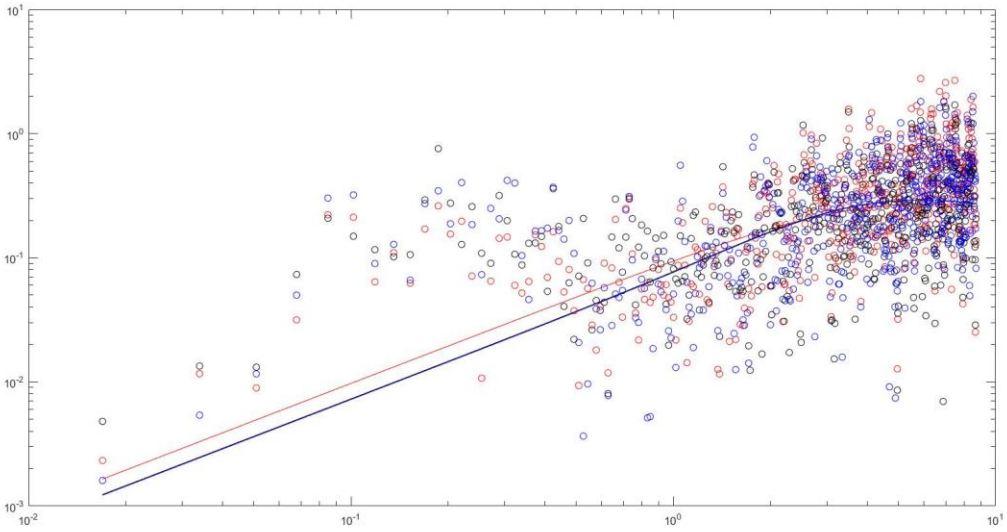

1-3-2-800

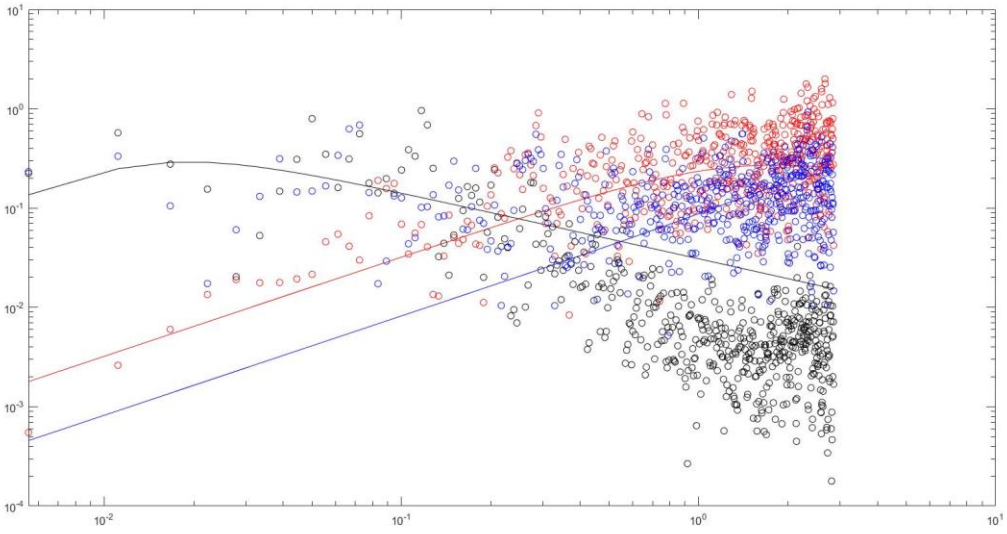

1-3-3-800

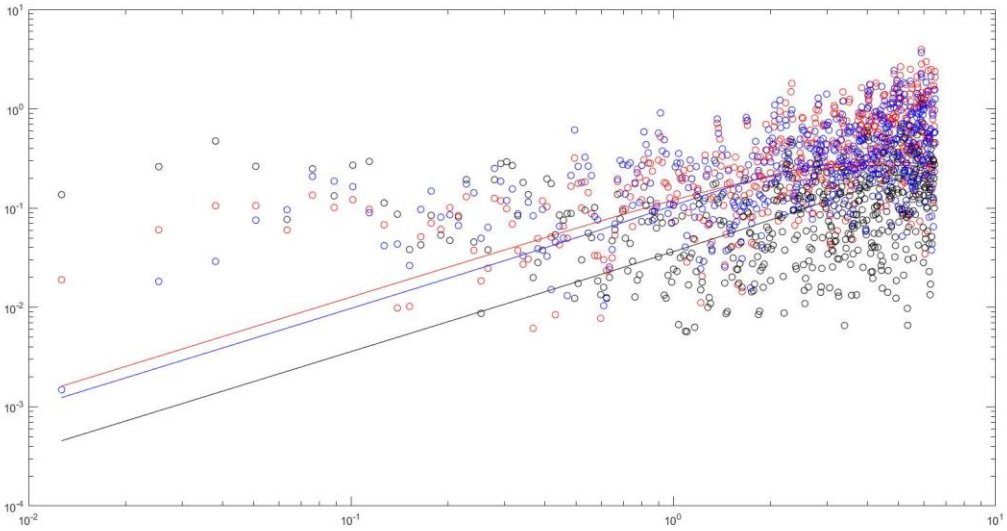

1-3-4-800

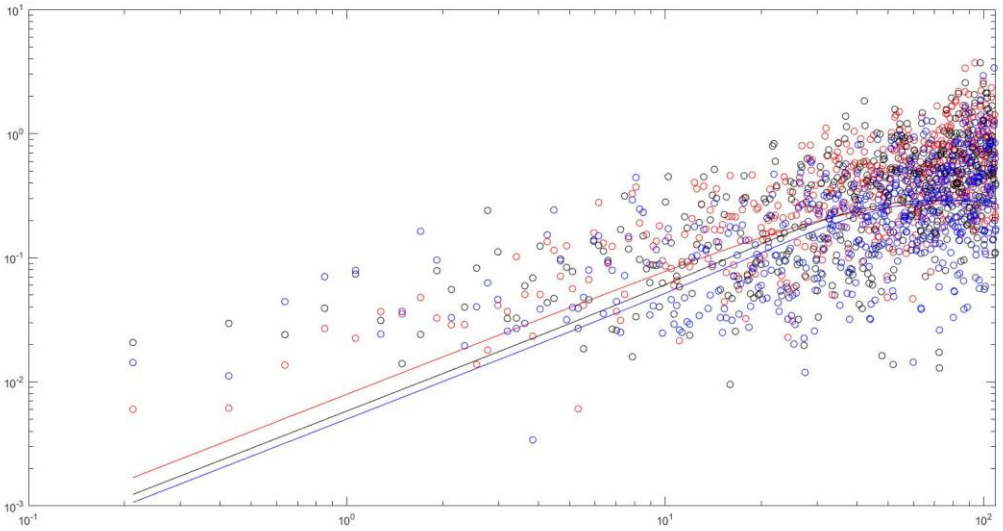

1-3-5-800

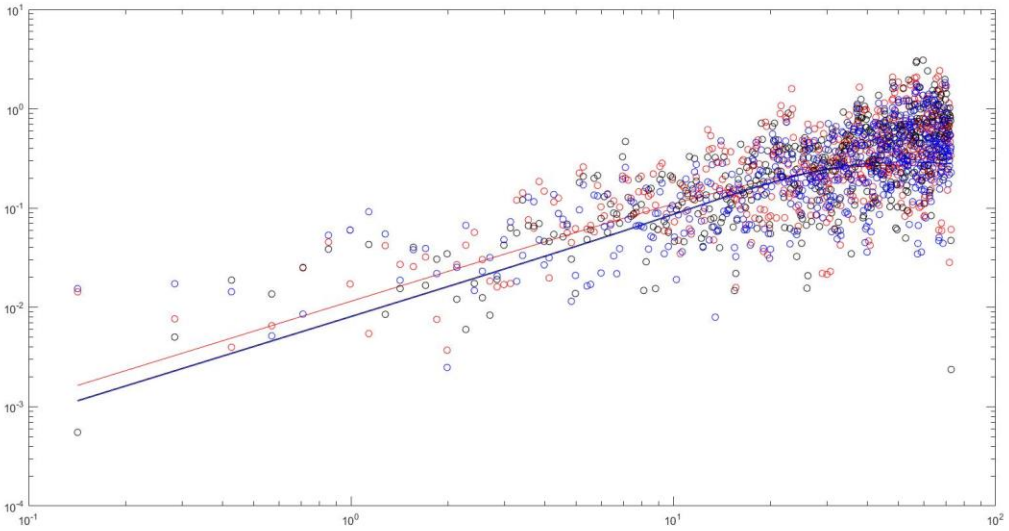

Location 4

1-4-1-400

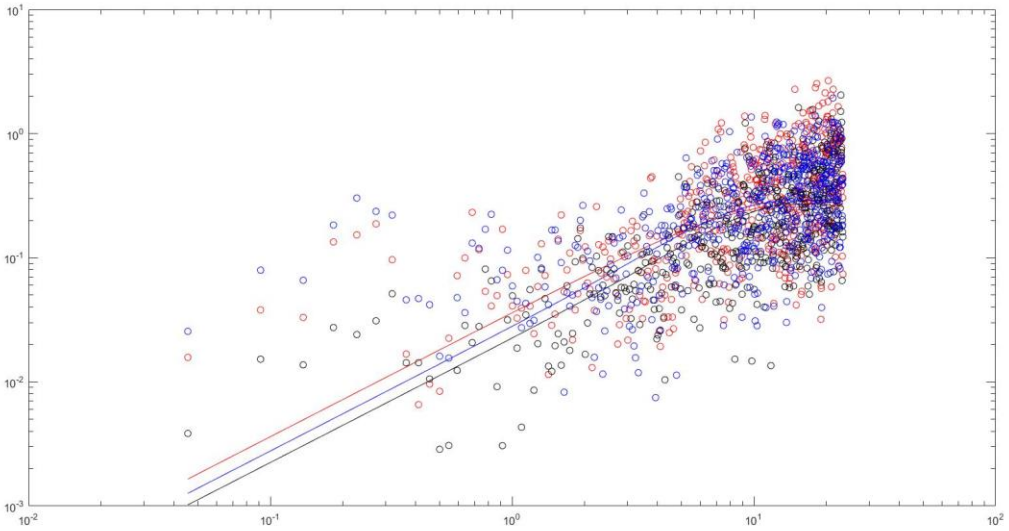

1-4-2-400

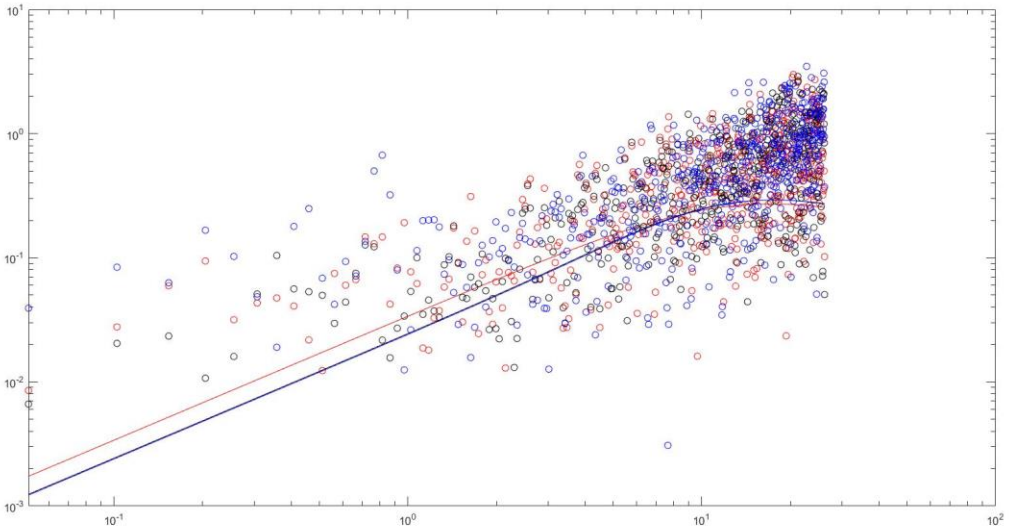

1-4-3-400

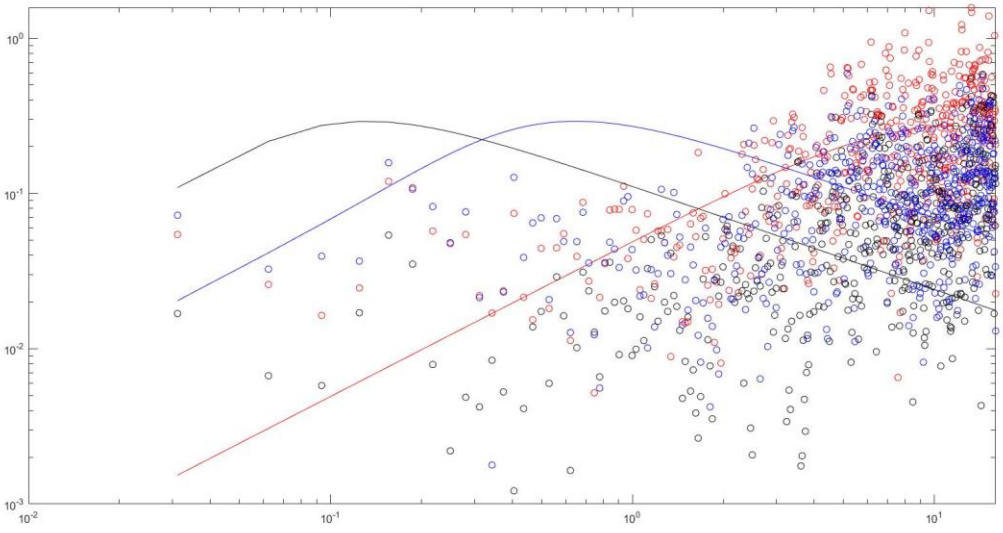

1-4-4-400

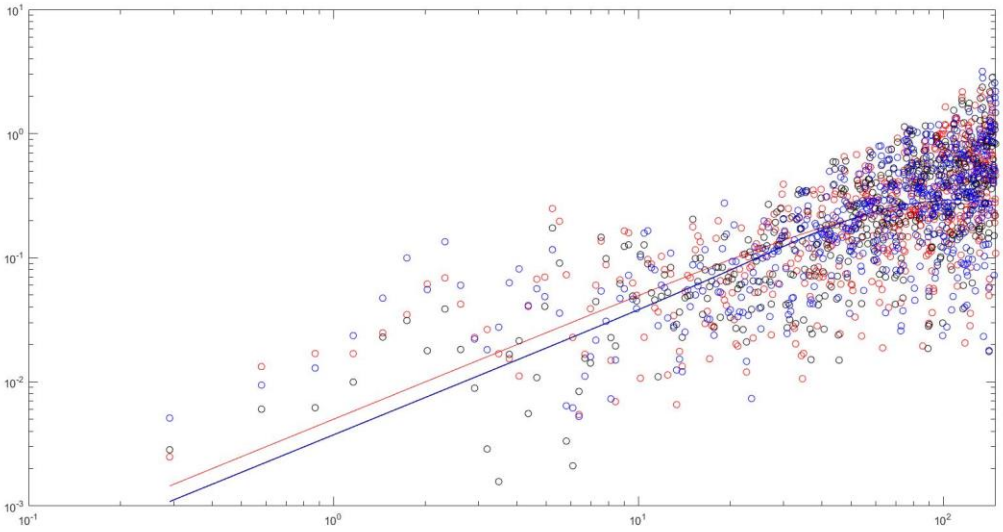

1-4-5-400

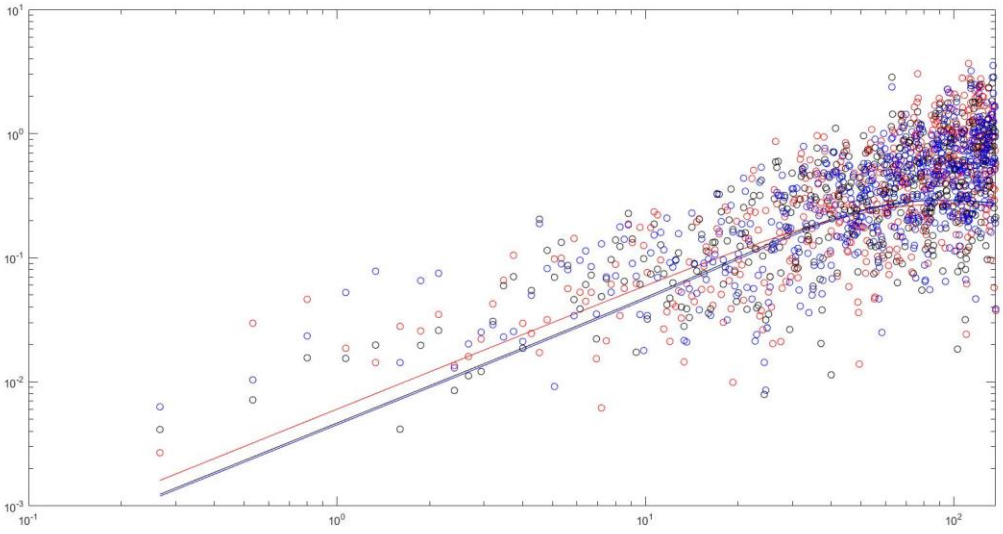

1-4-1-500

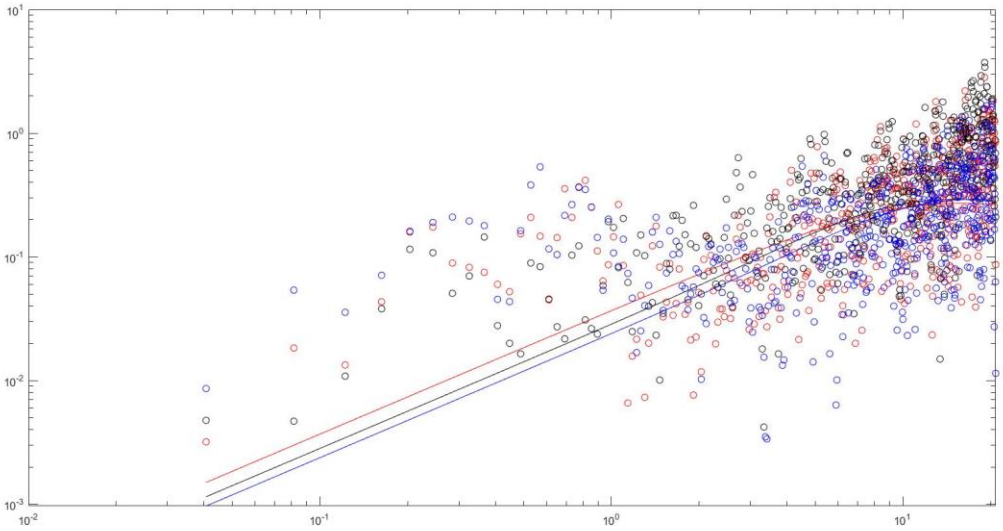

1-4-2-500

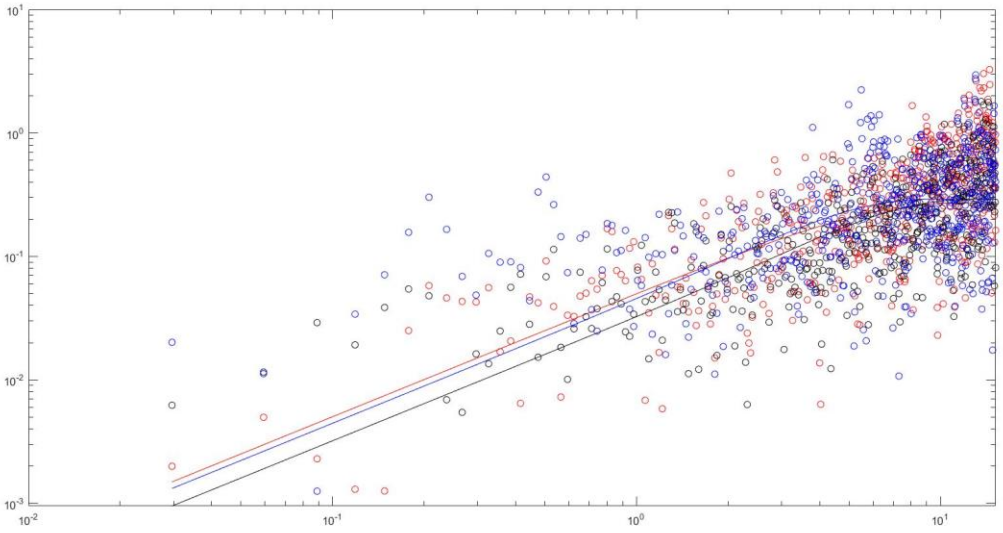

1-4-3-500

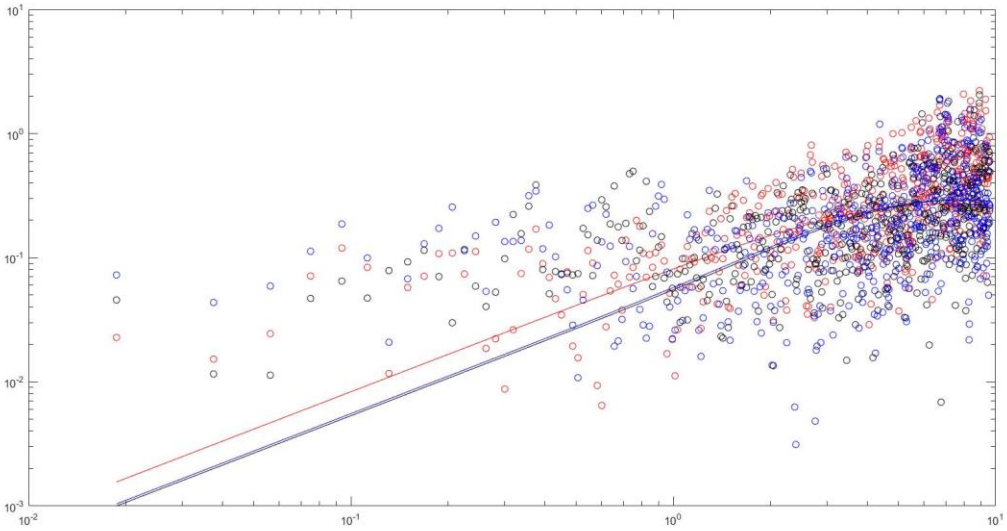

1-4-4-500

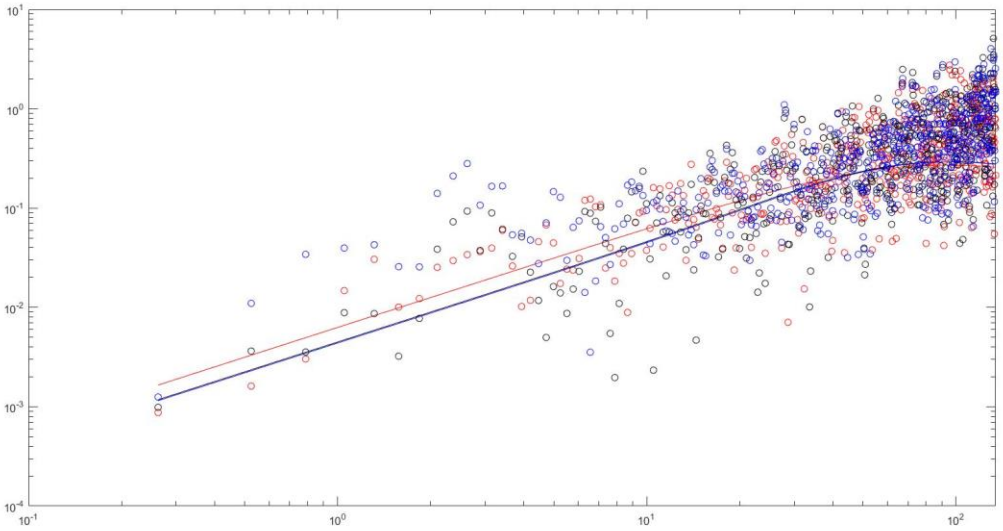

1-4-5-500

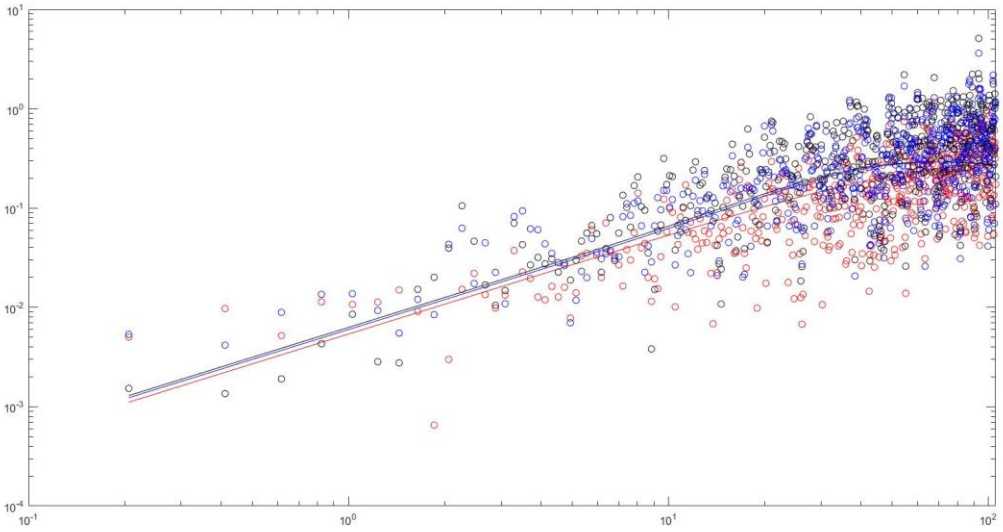

1-4-1-600

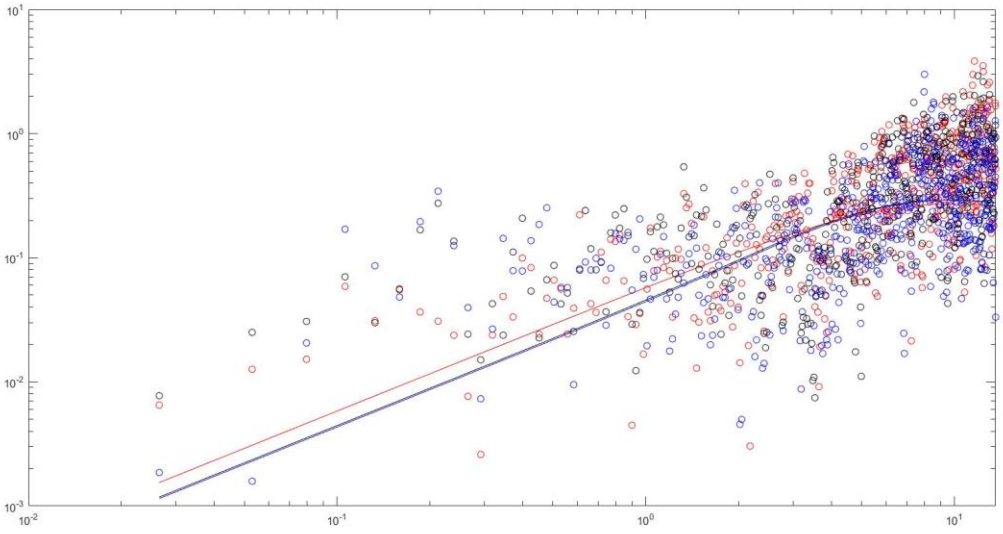

1-4-2-600

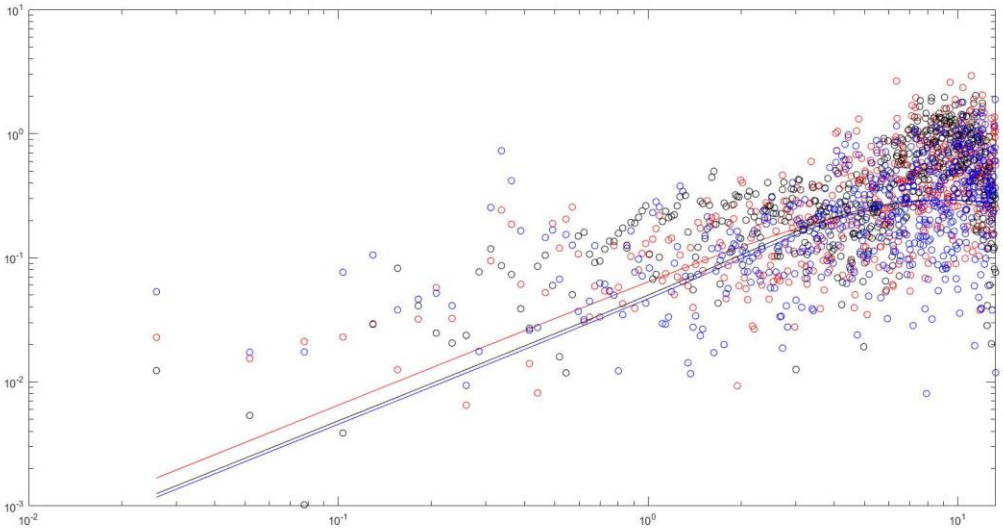

1-4-3-600

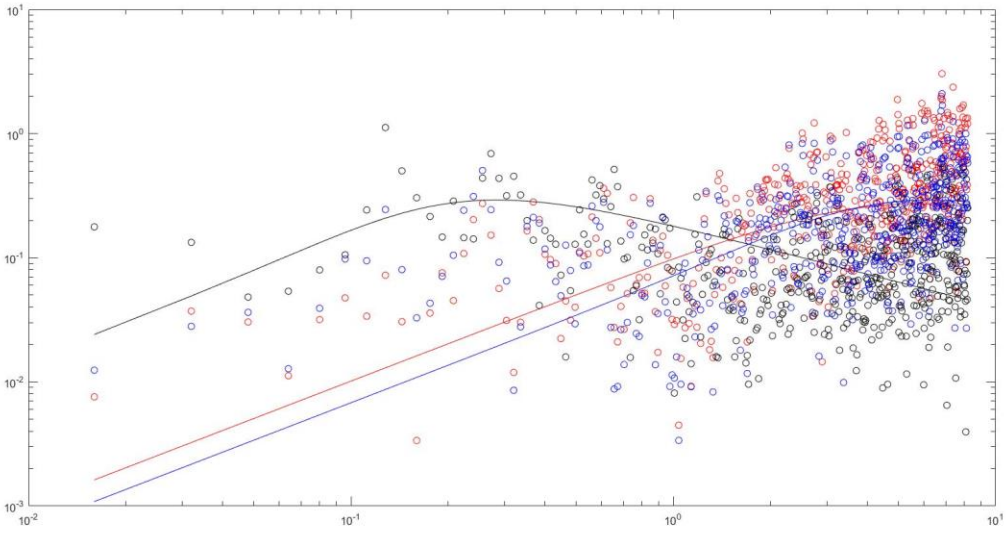

1-4-4-600

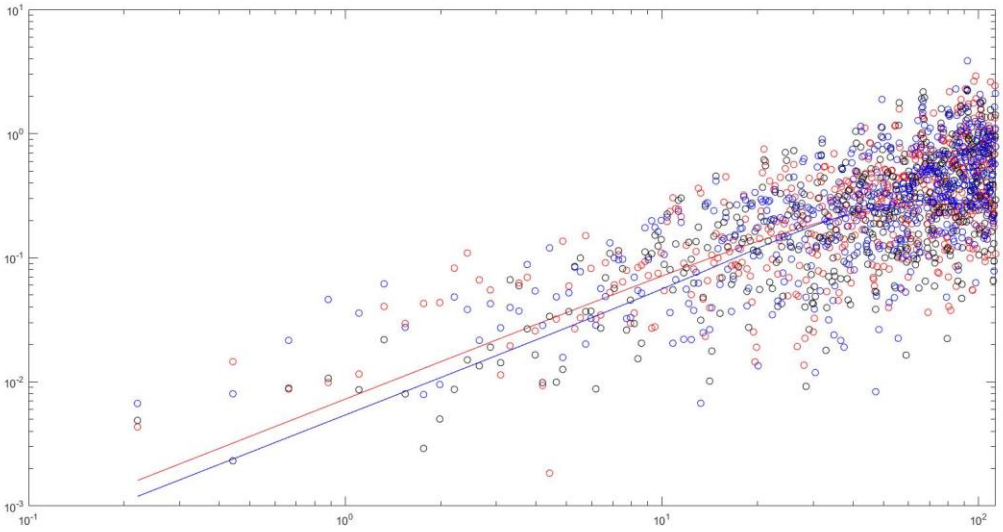

1-4-5-600

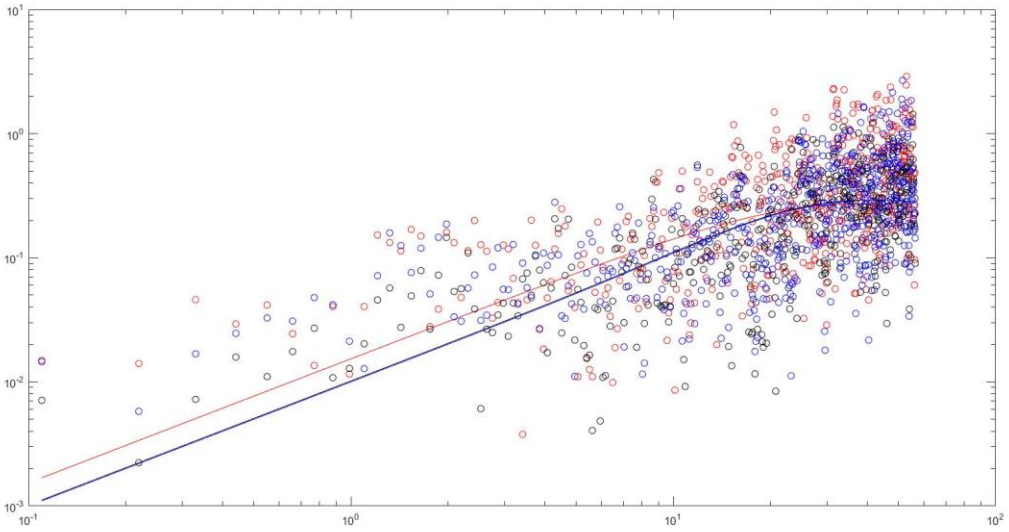

1-4-1-700

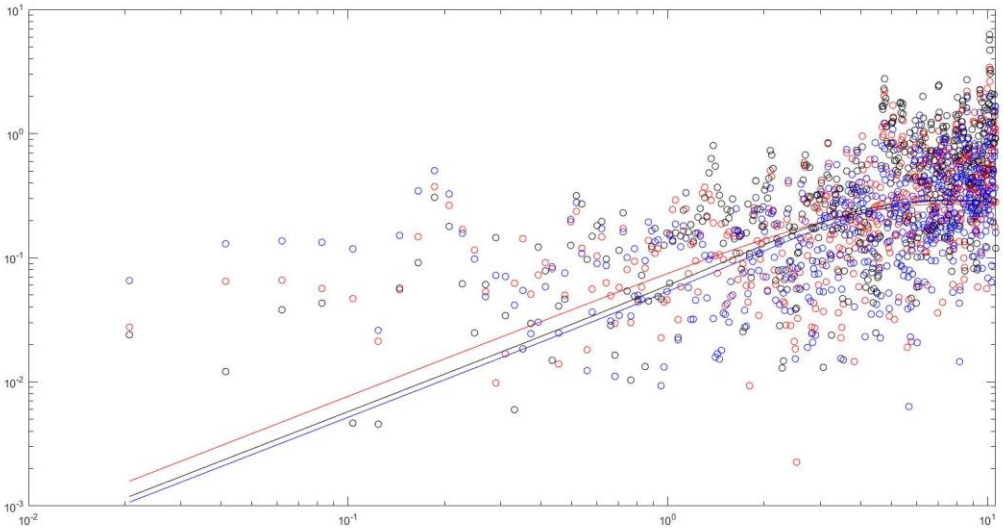

1-4-2-700

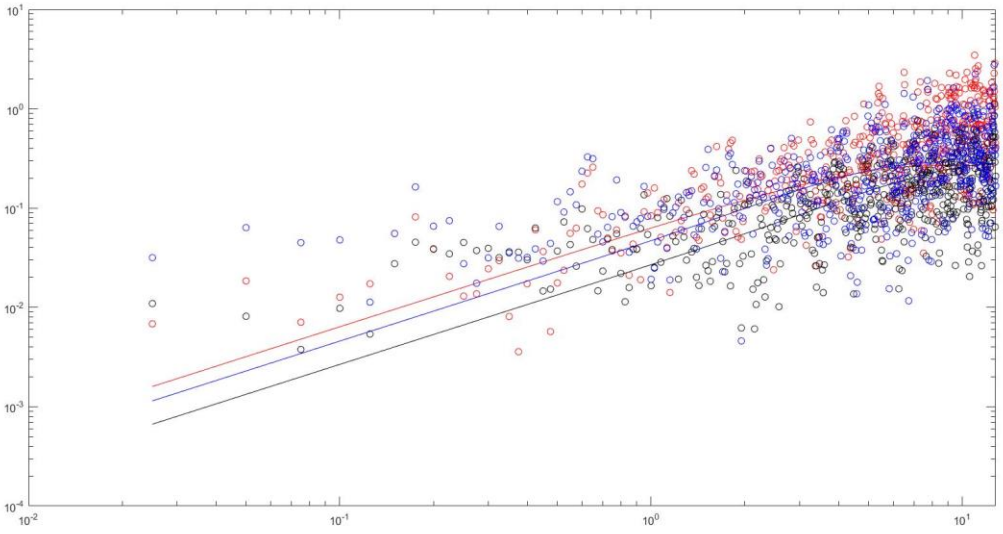

1-4-3-700

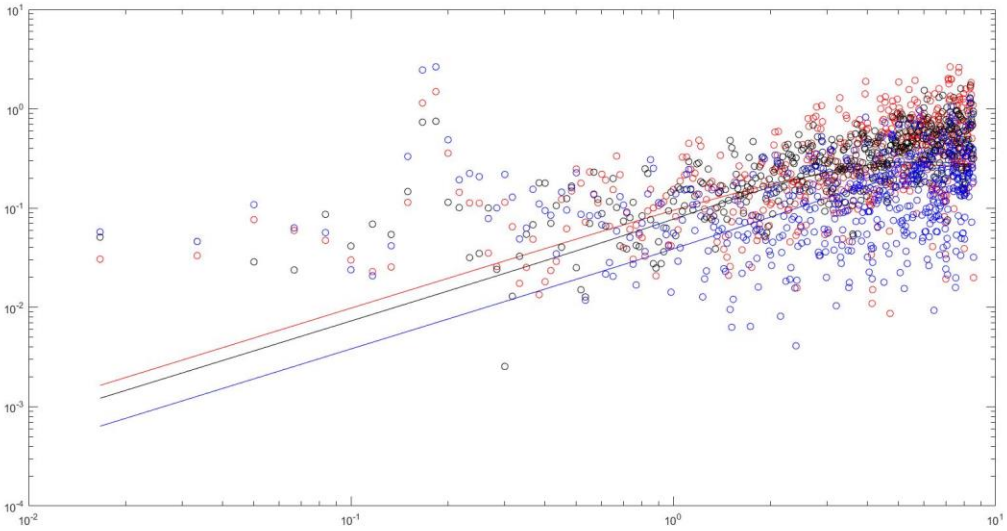

1-4-4-700

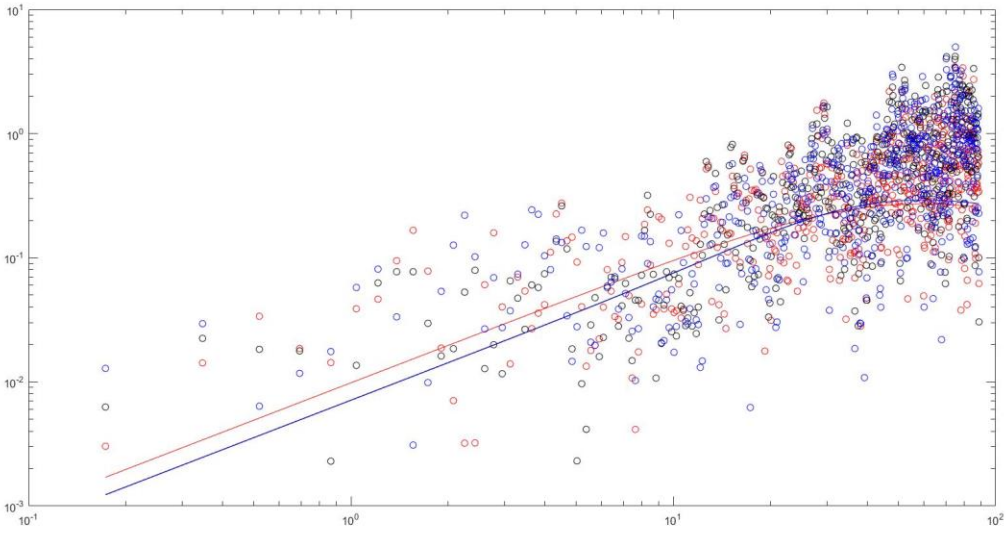

1-4-5-700

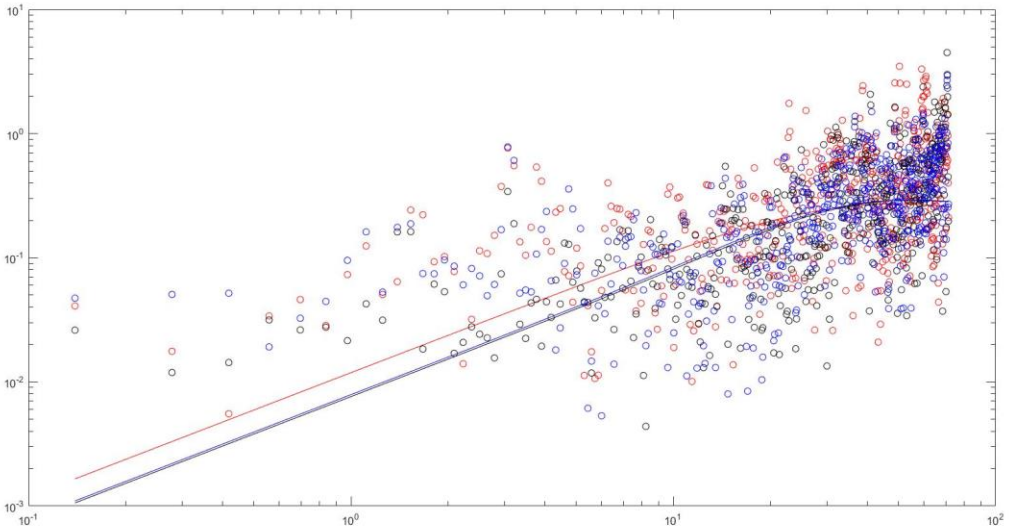

1-4-1-800

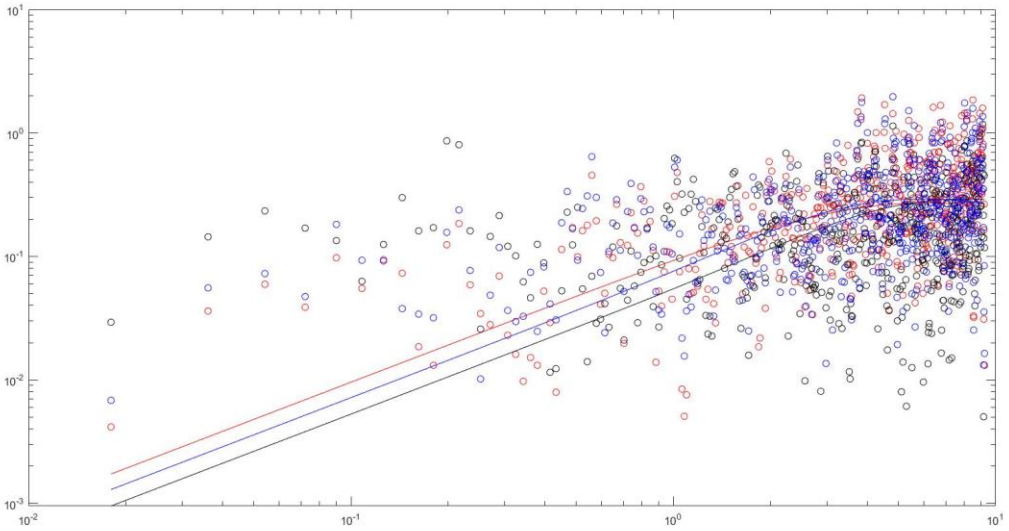

1-4-2-800

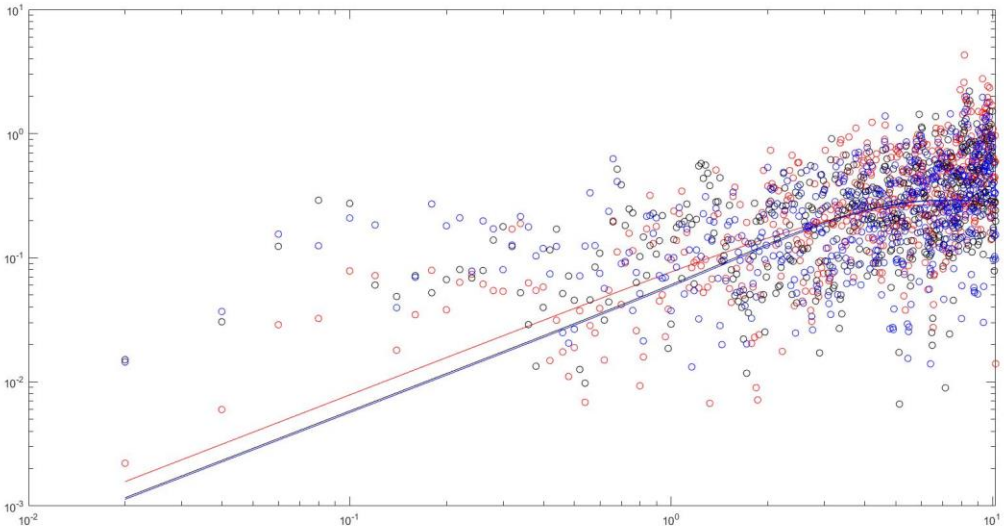

1-4-3-800

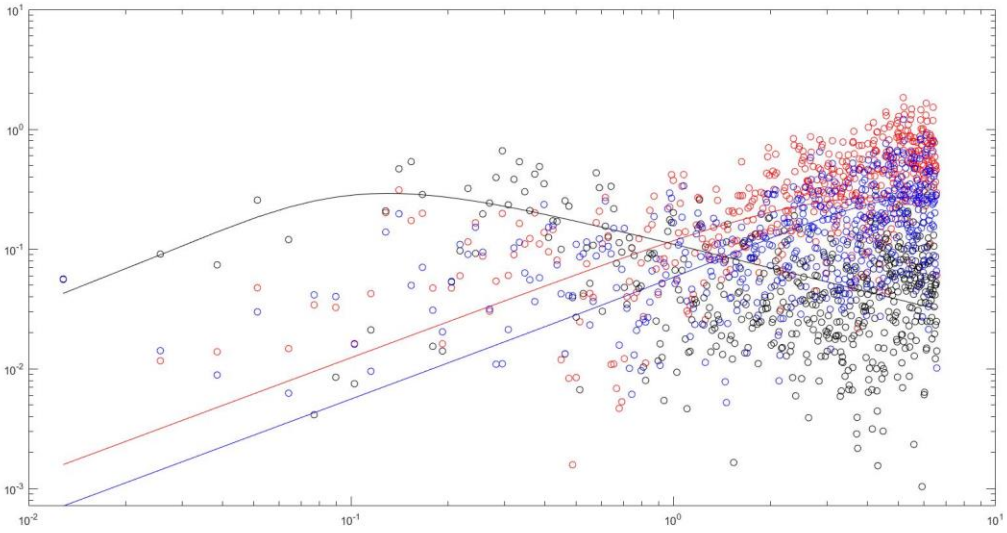

1-4-4-800

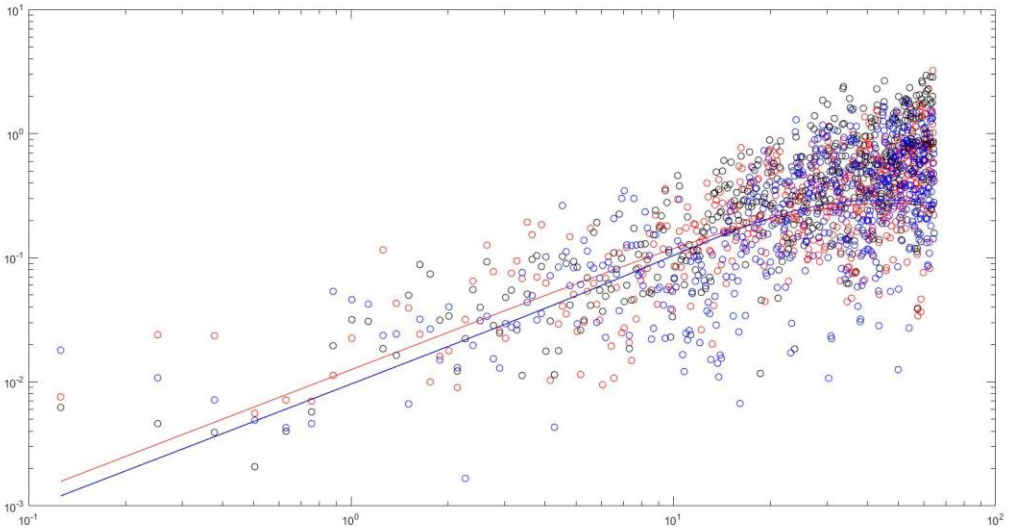

1-4-5-800

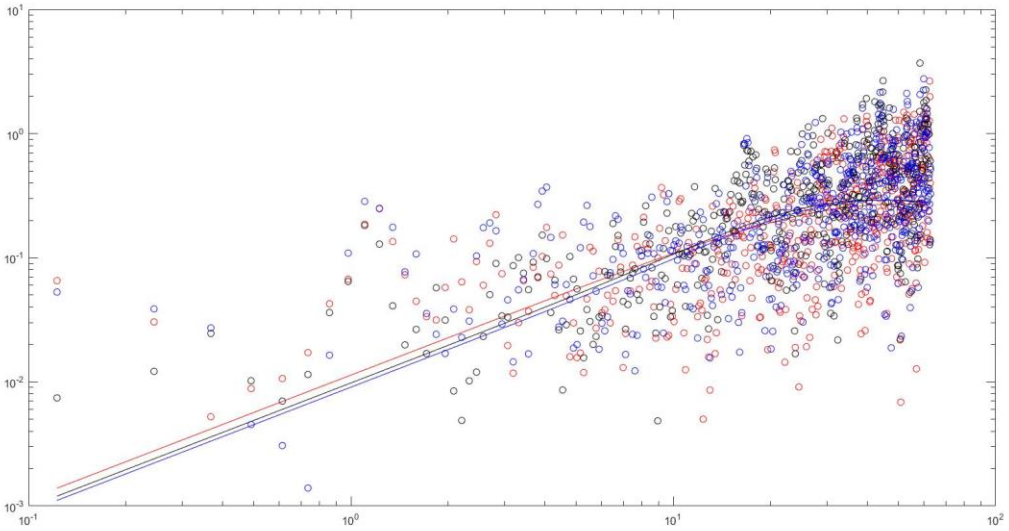

Spectra

Case 2

a-b-c-d

a=case number, b=location, c=height, d=RPM

Location 1

2-1-1-400

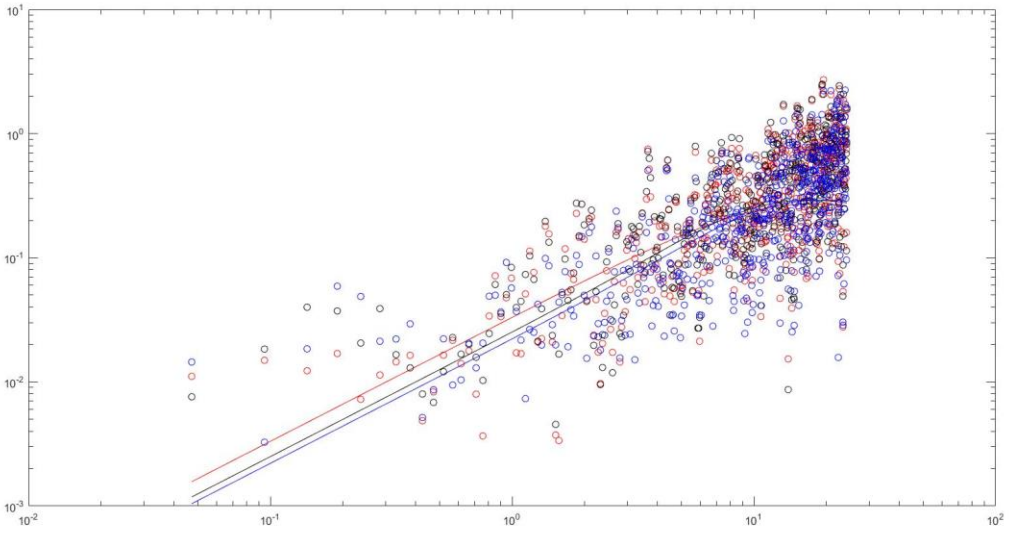

2-1-2-400

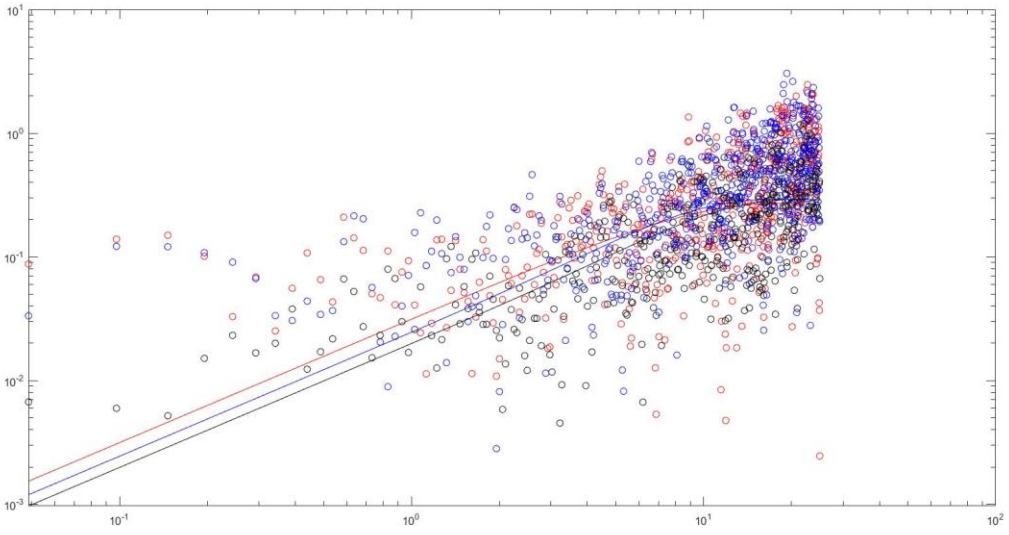

2-1-3-400

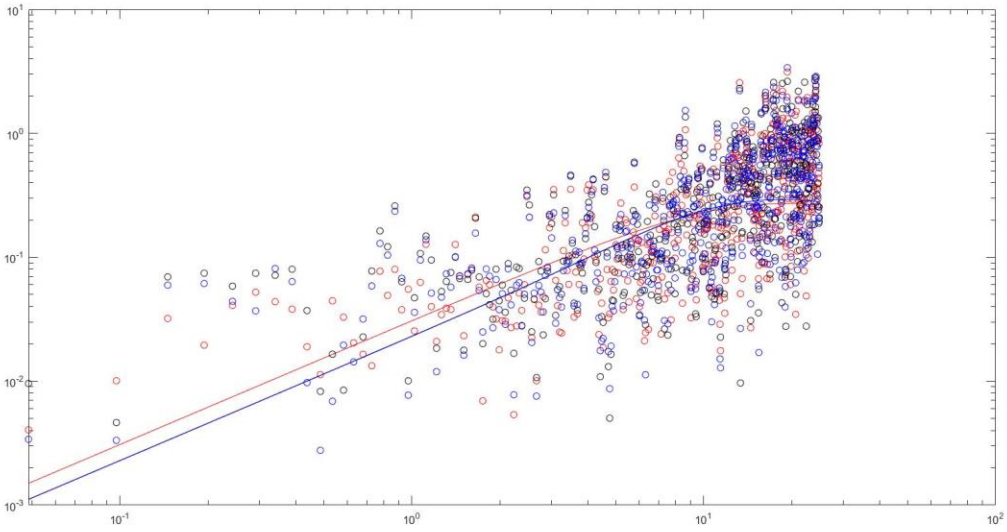

2-1-4-400

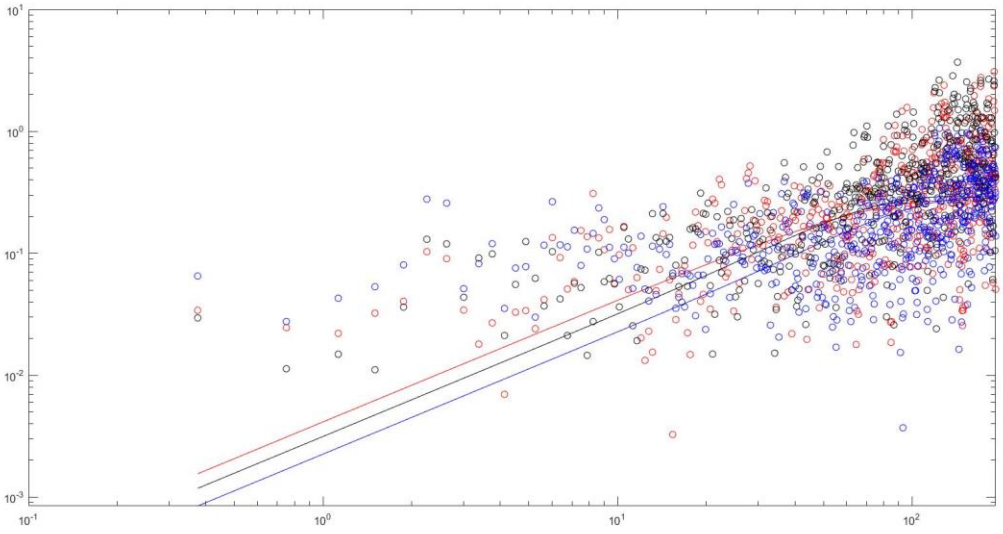

2-1-5-400

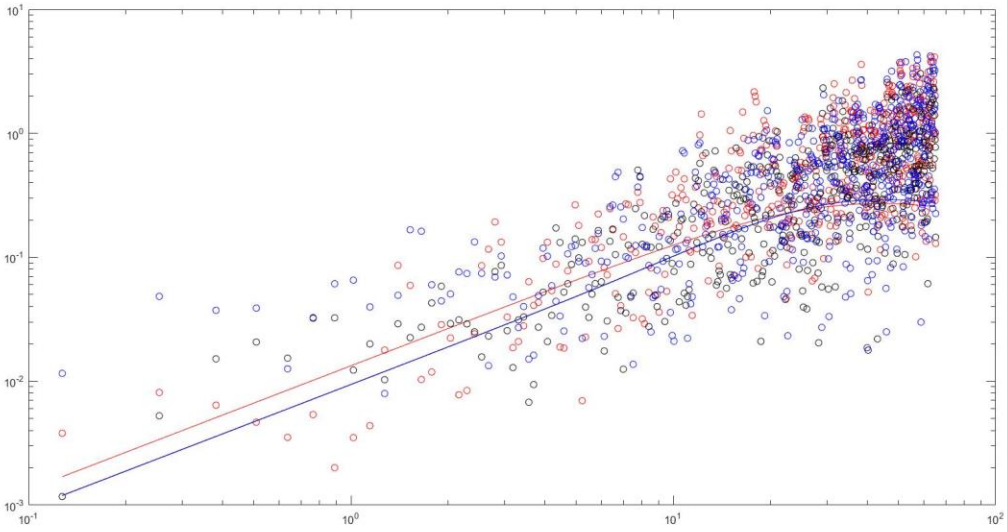

2-1-1-500

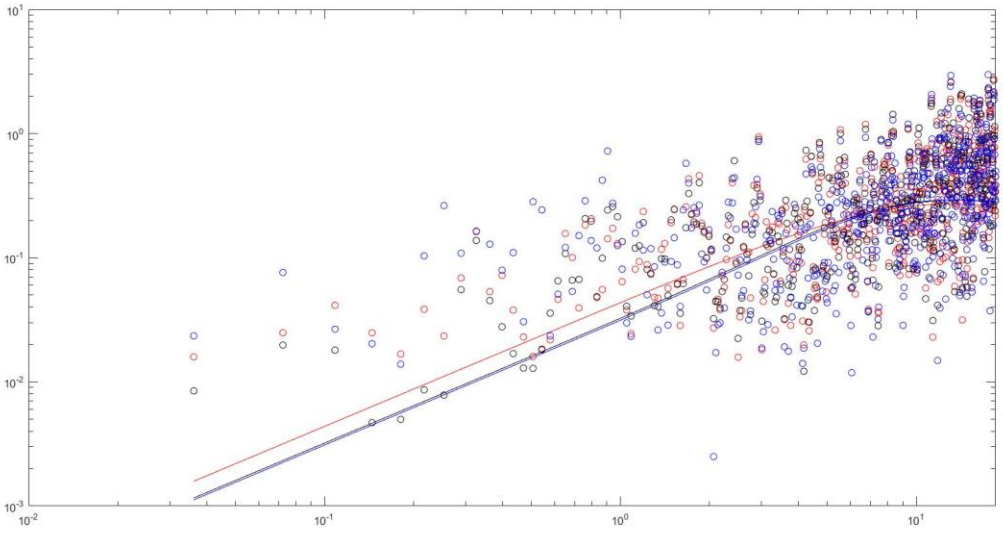

2-1-2-500

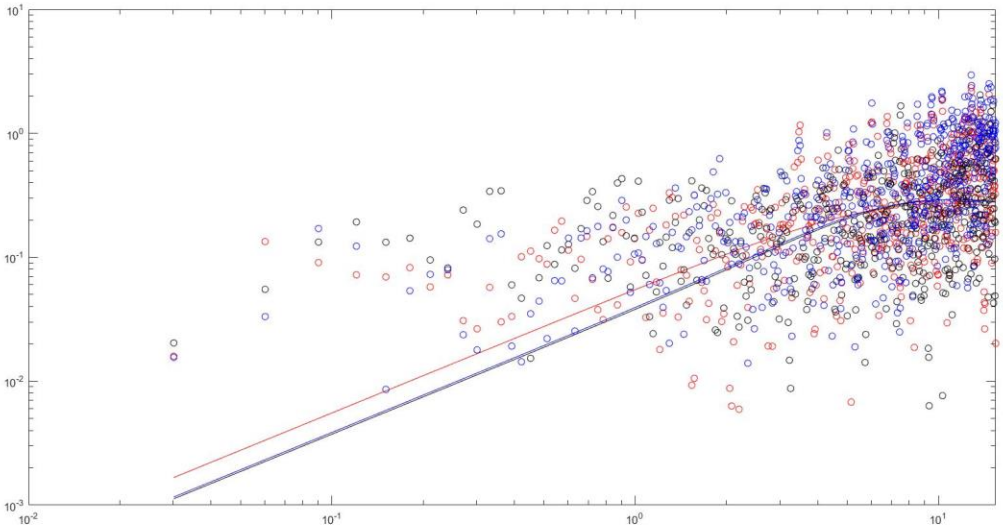

2-1-3-500

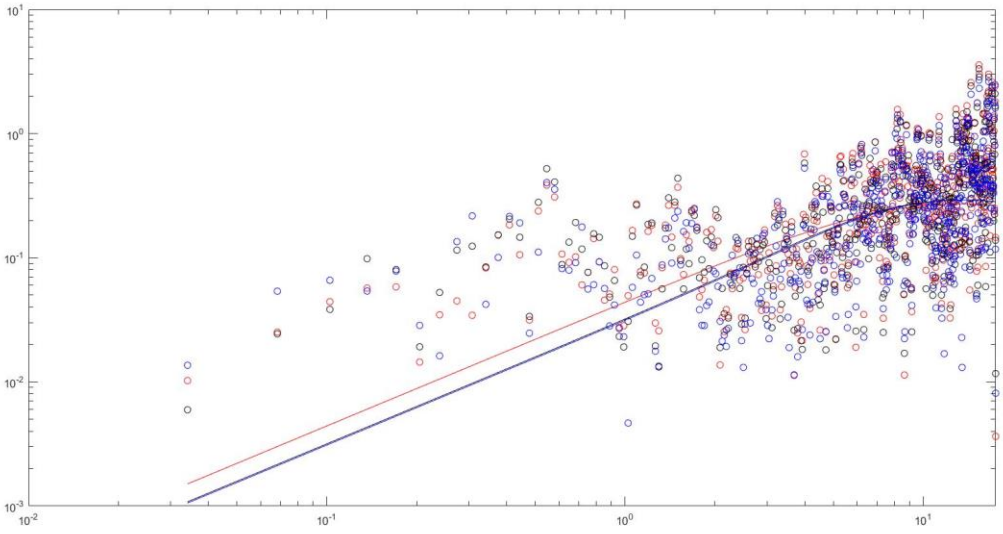

2-1-4-500

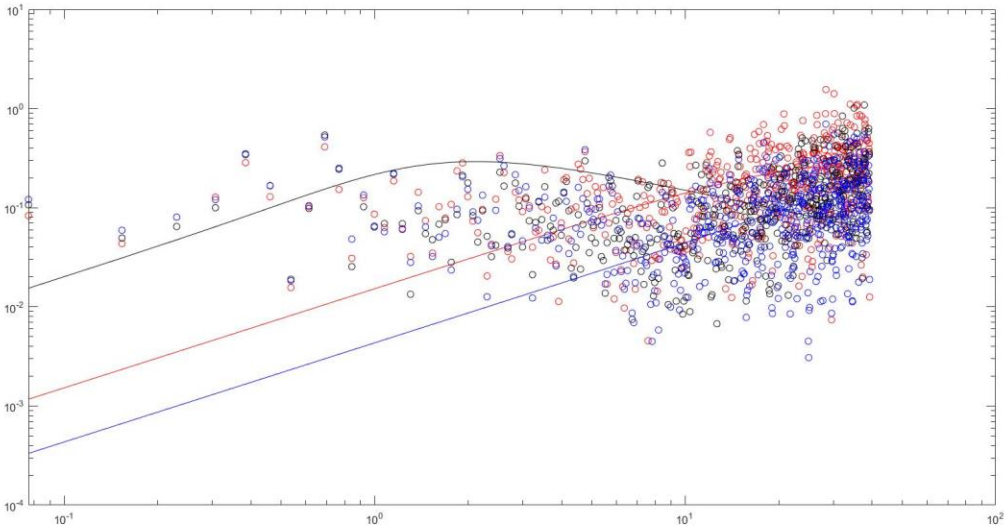

2-1-5-500

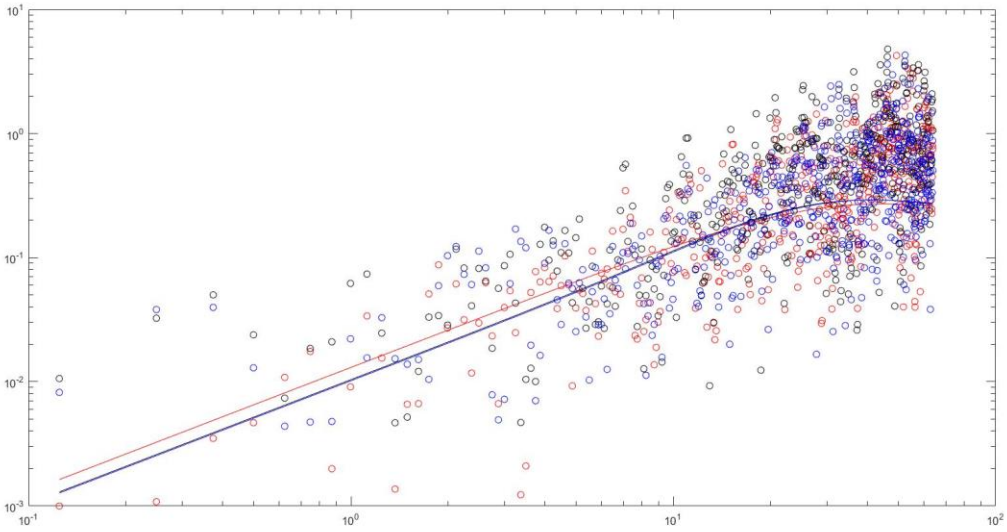

2-1-1-600

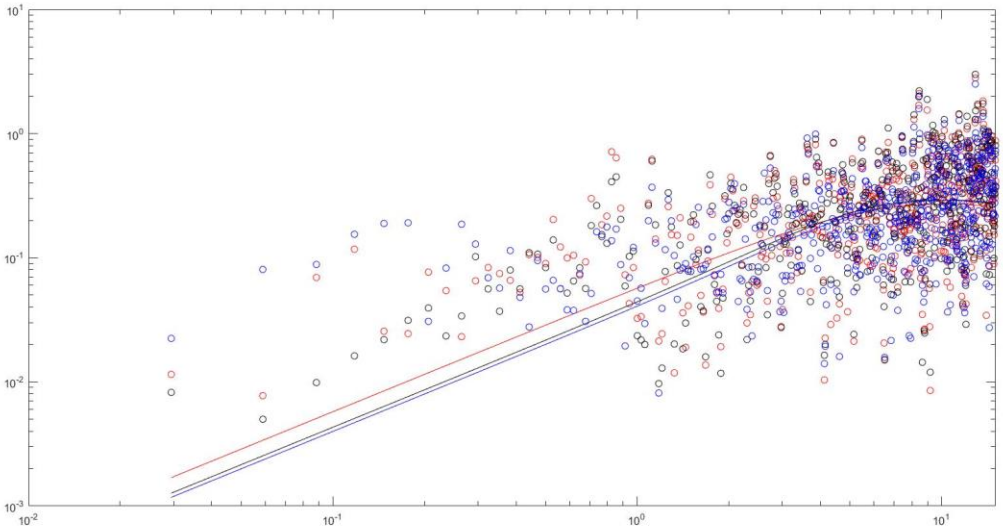

2-1-2-600

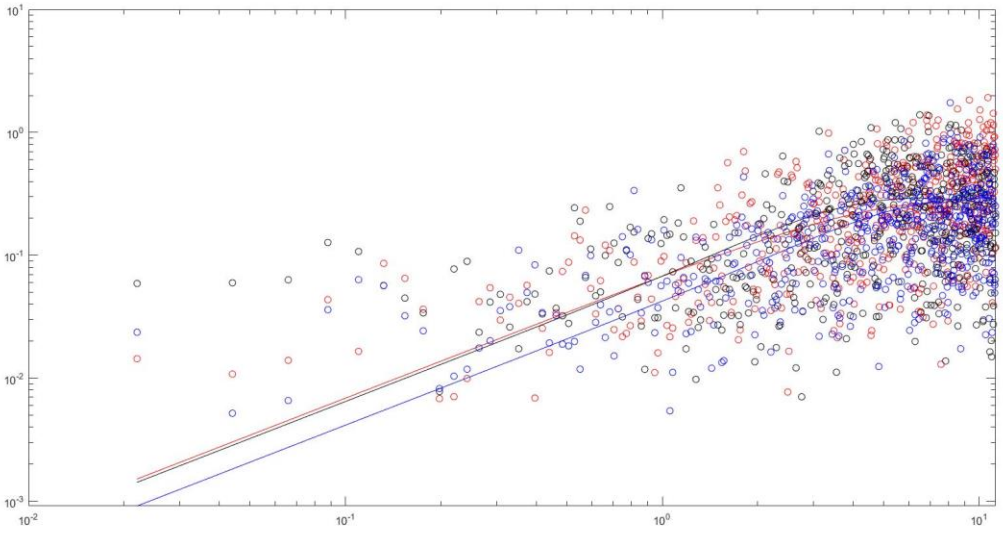

2-1-3-600

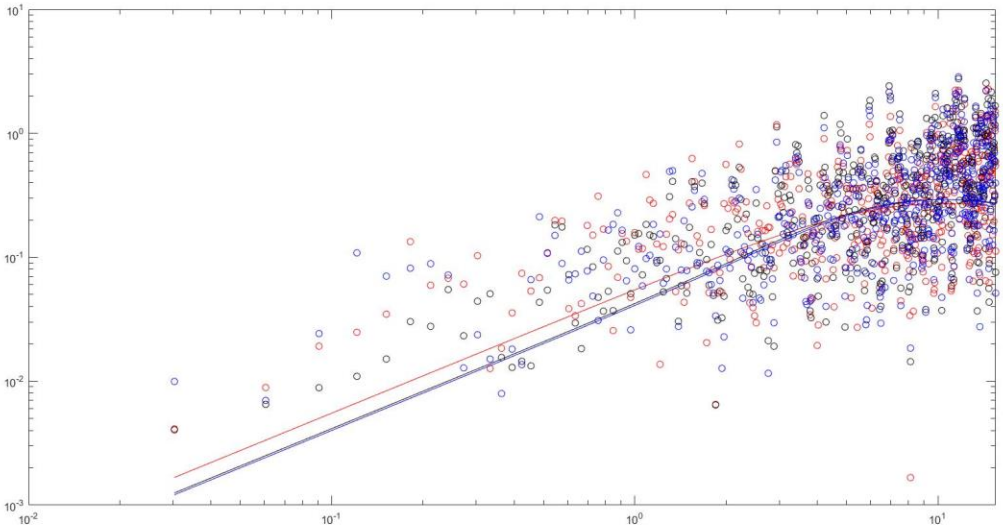

2-1-4-600

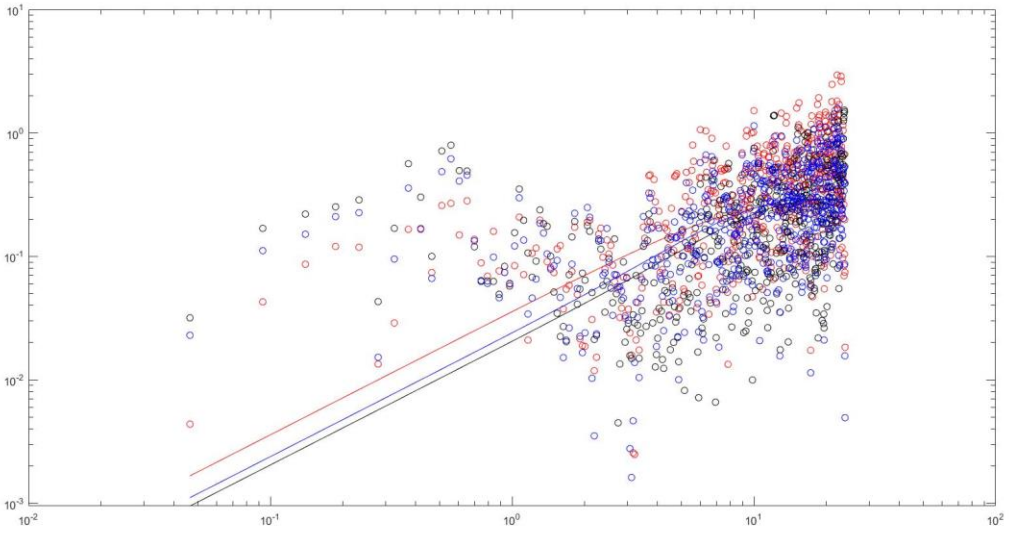

2-1-5-600

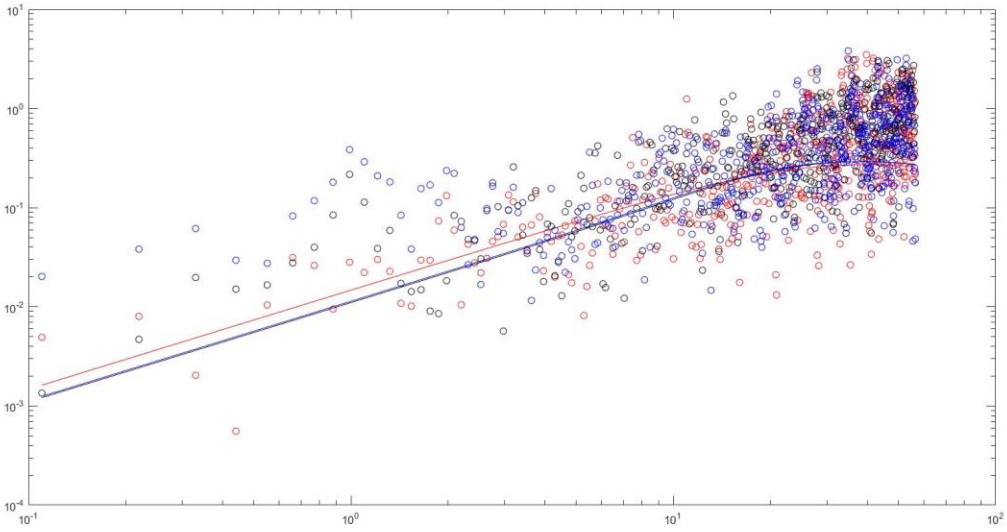

2-1-1-700

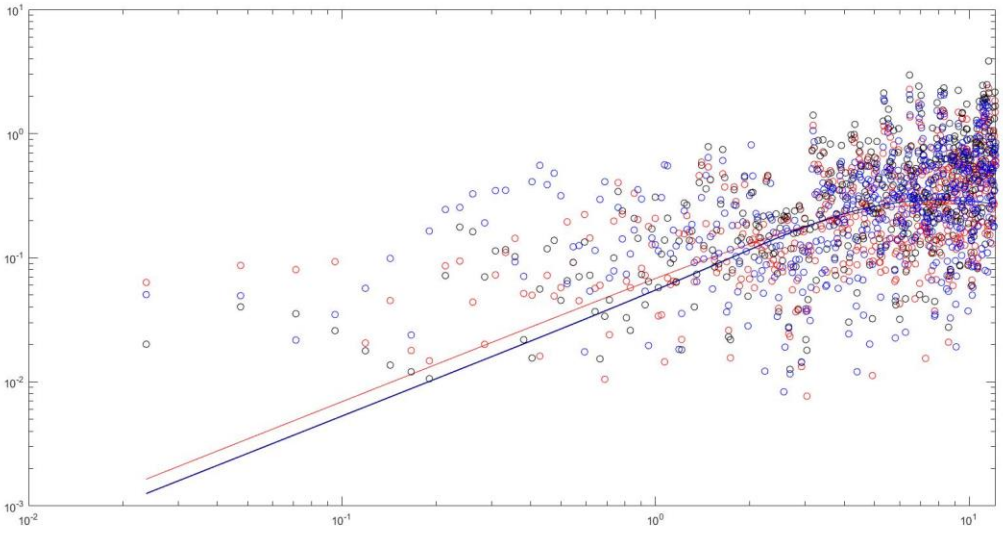

2-1-2-700

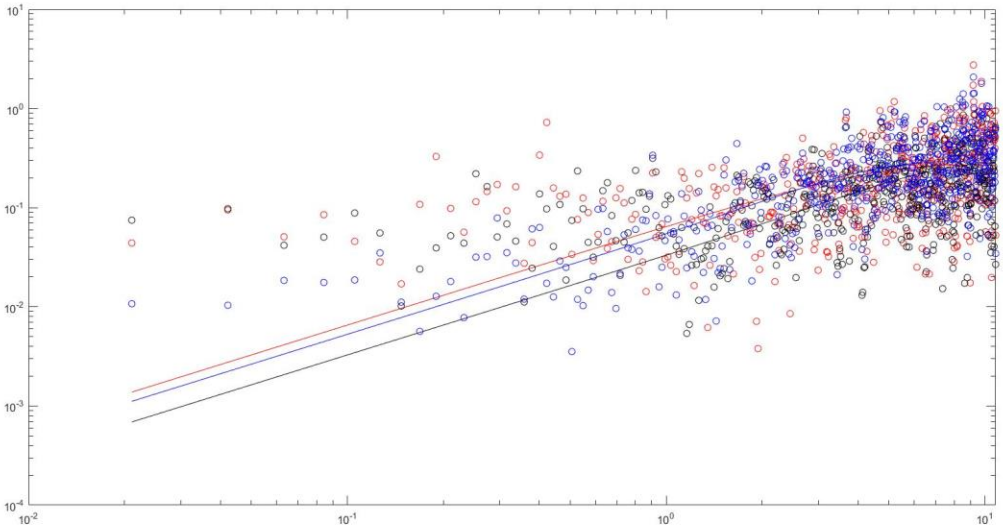

2-1-3-700

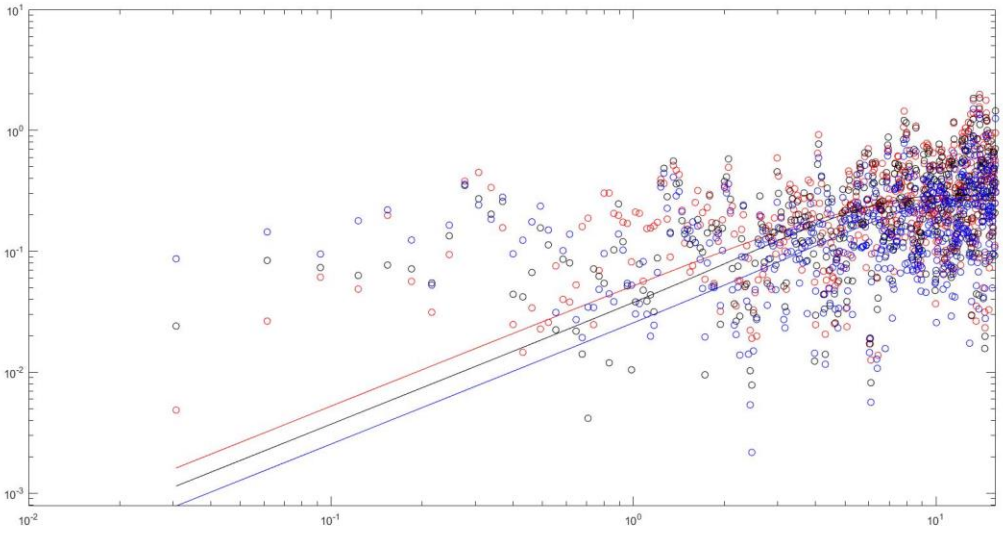

2-1-4-700

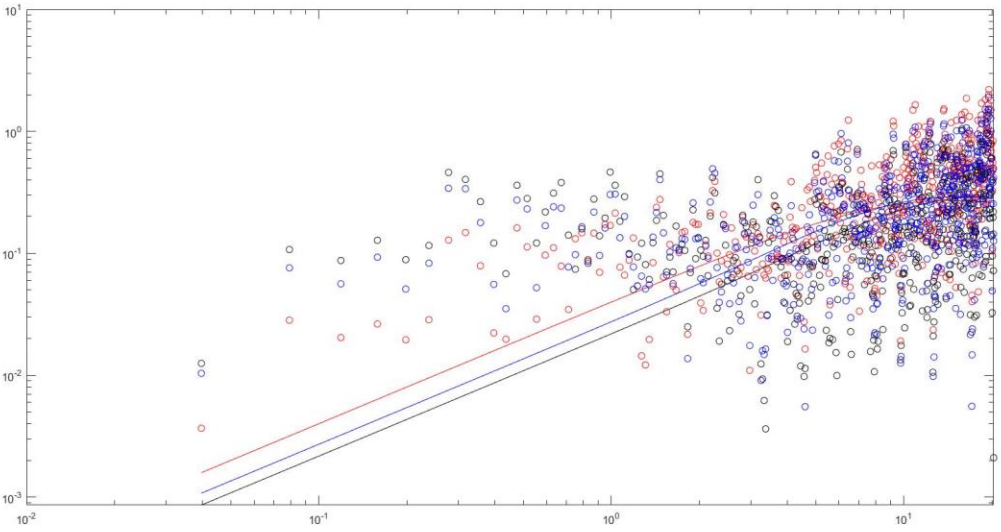

2-1-5-700

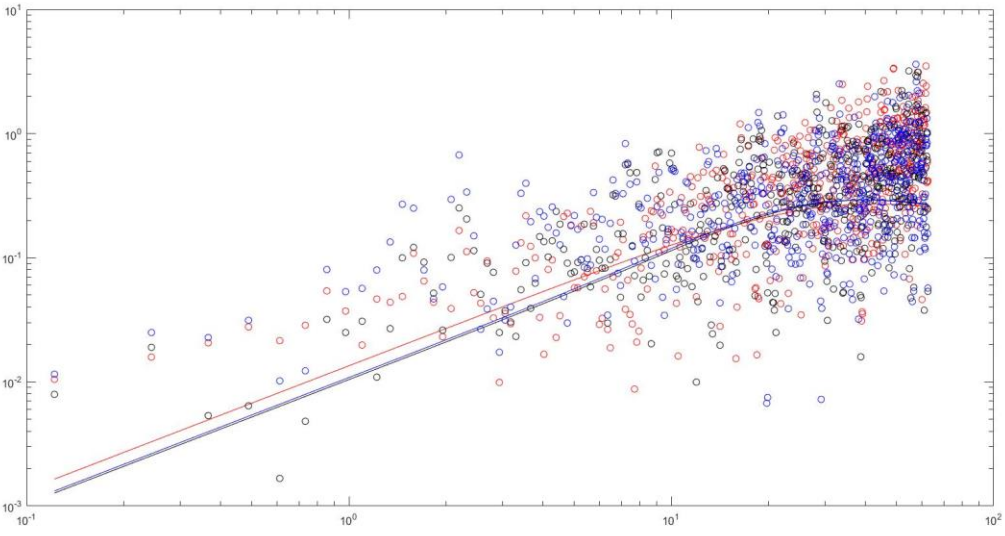

2-1-1-800

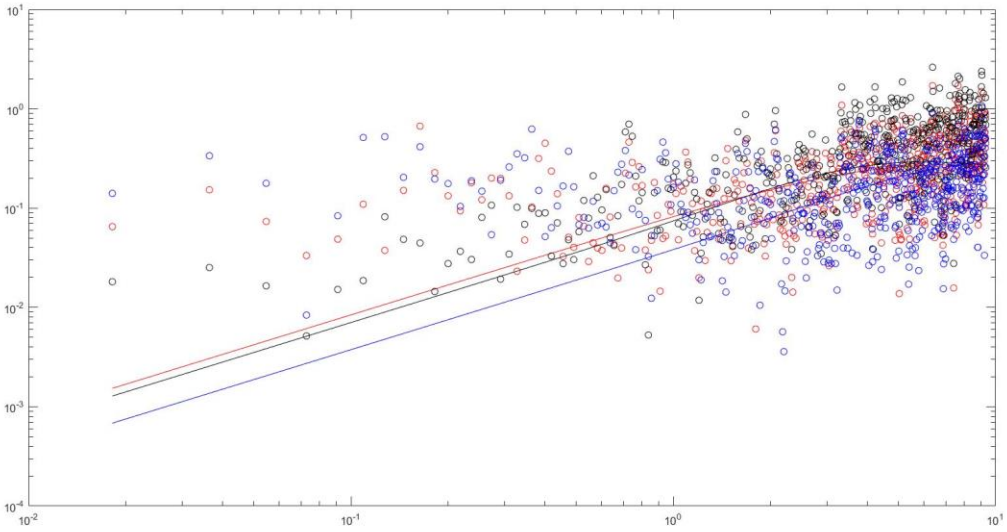

2-1-2-800

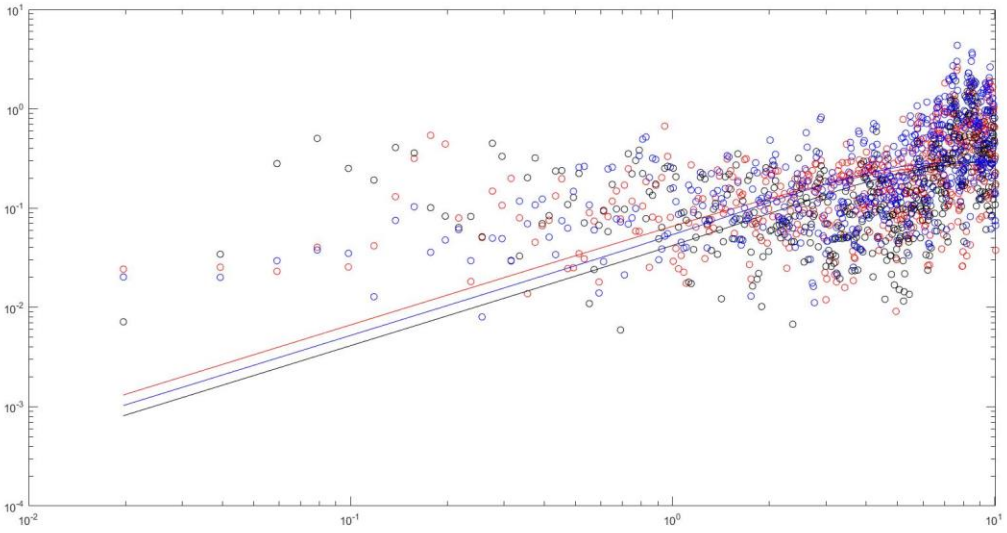

2-1-3-800

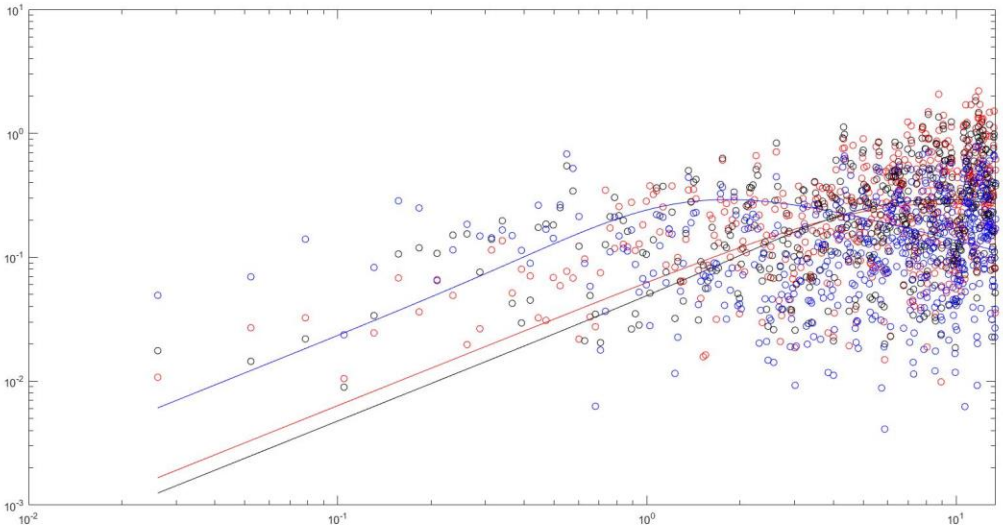

2-1-4-800

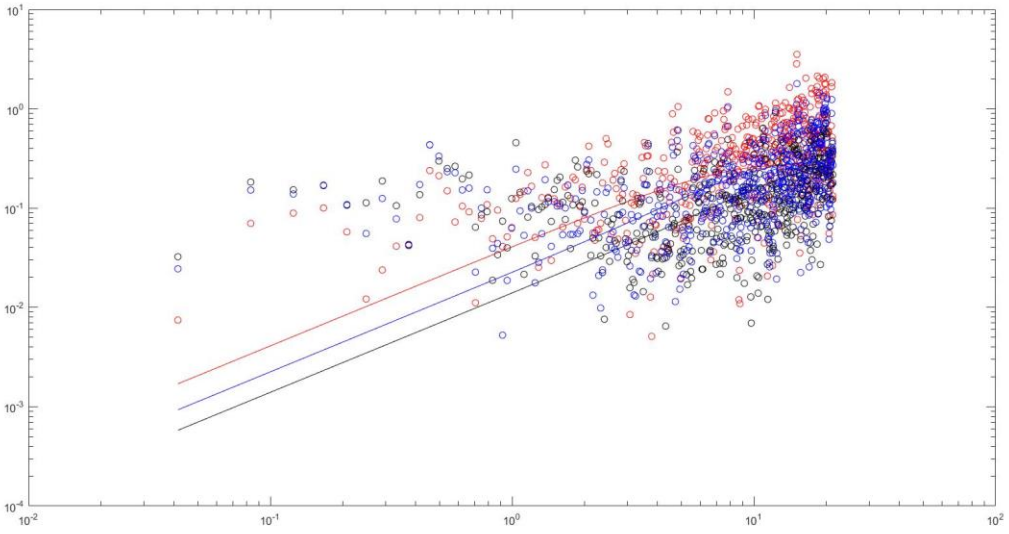

2-1-5-800

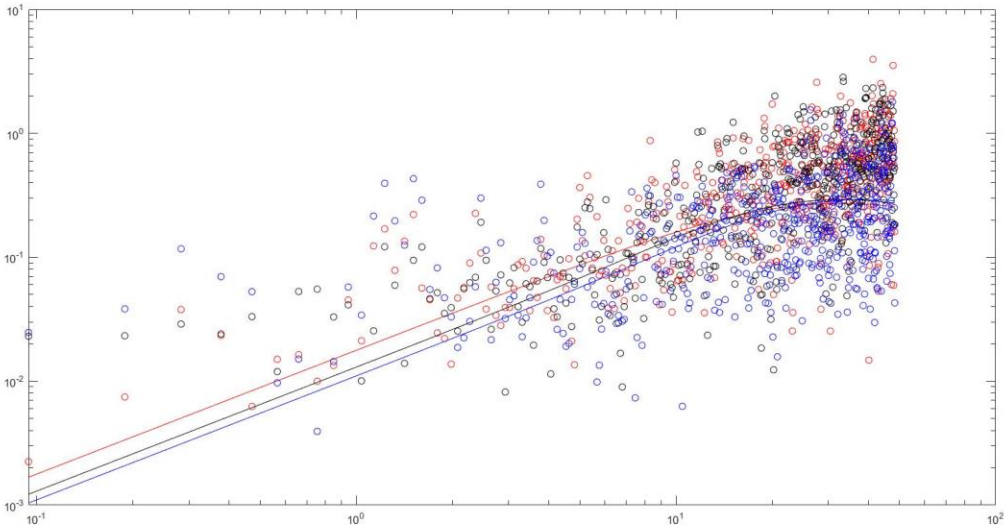

Location 2

2-2-1-400

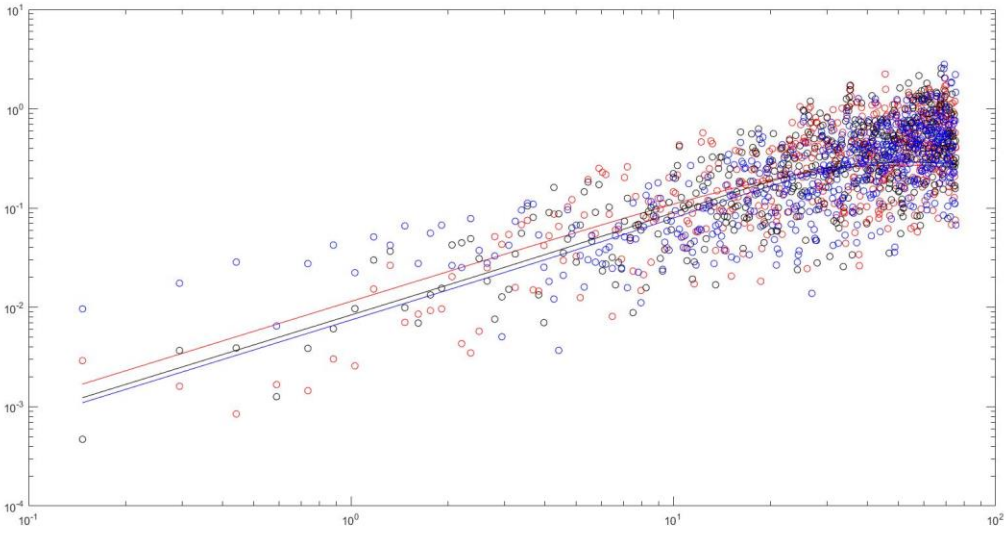

2-2-2-400

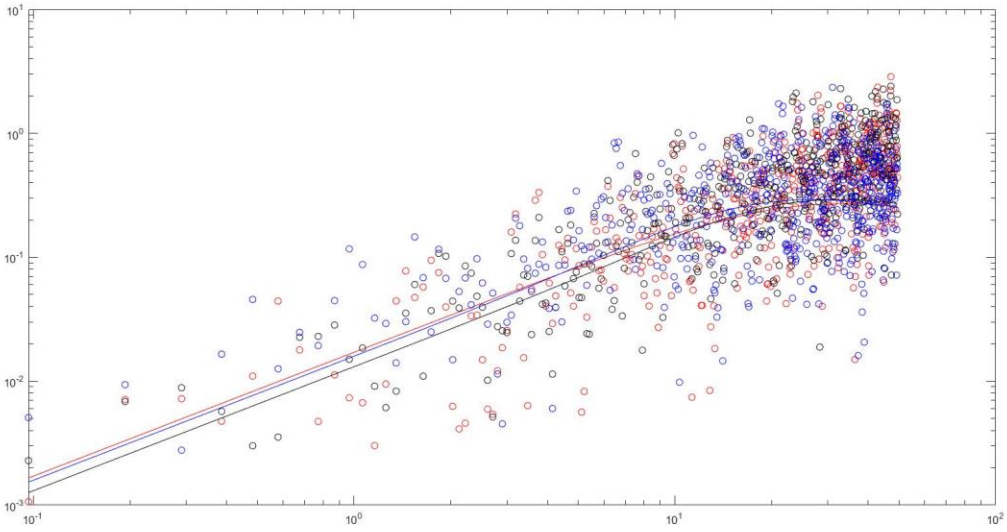

2-2-3-400

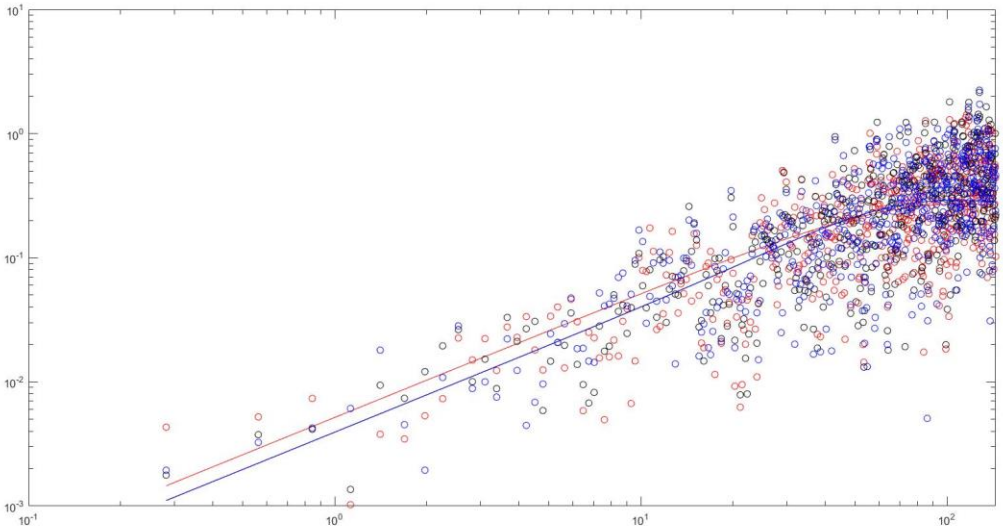

2-2-4-400

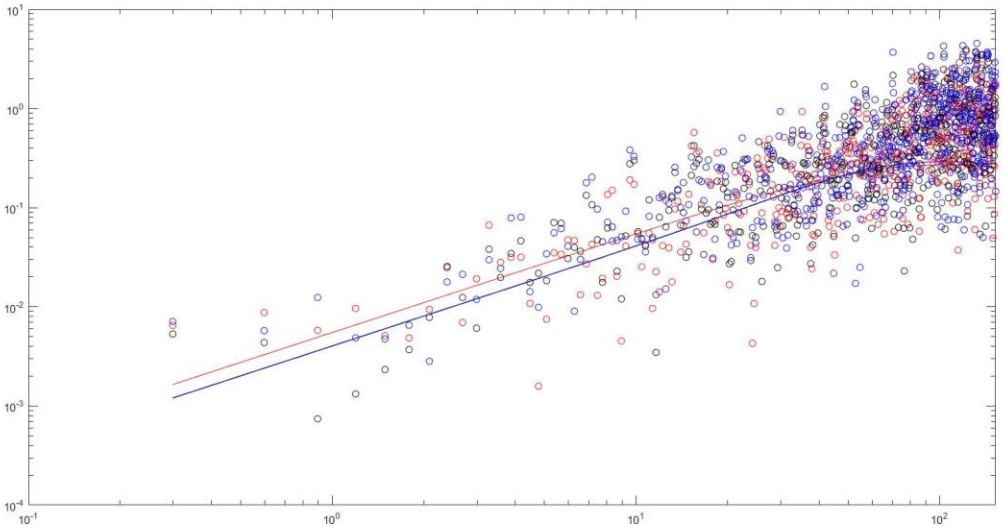

2-2-5-400

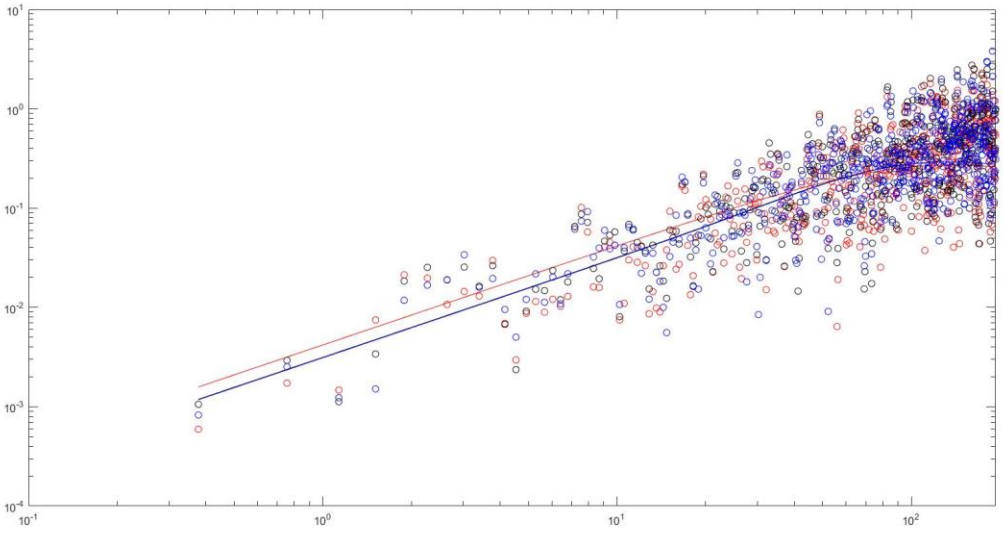

2-2-1-500

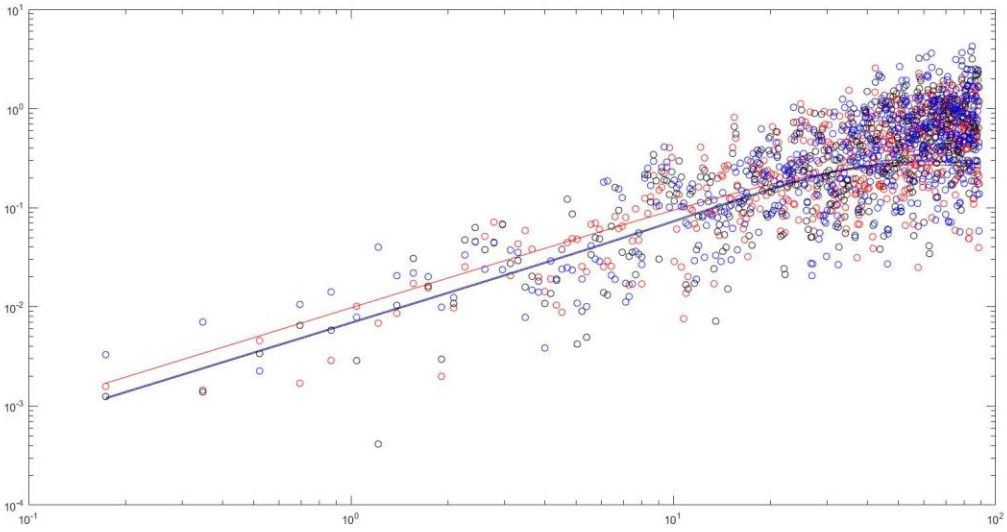

2-2-2-500

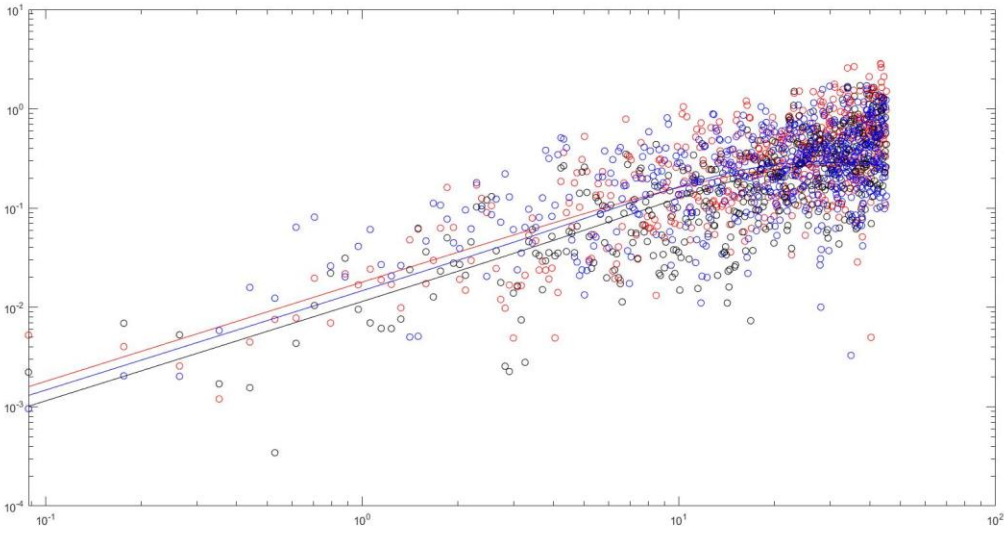

2-2-3-500

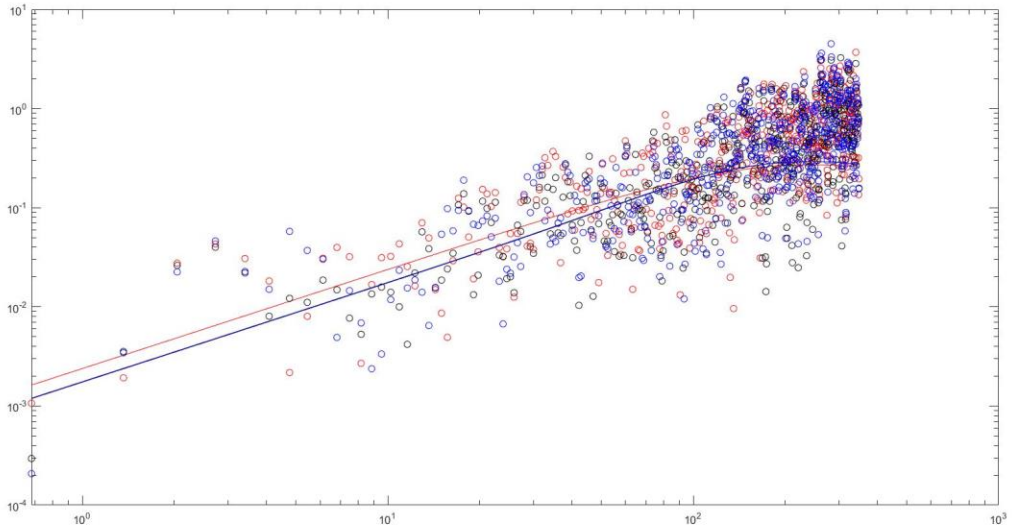

2-2-4-500

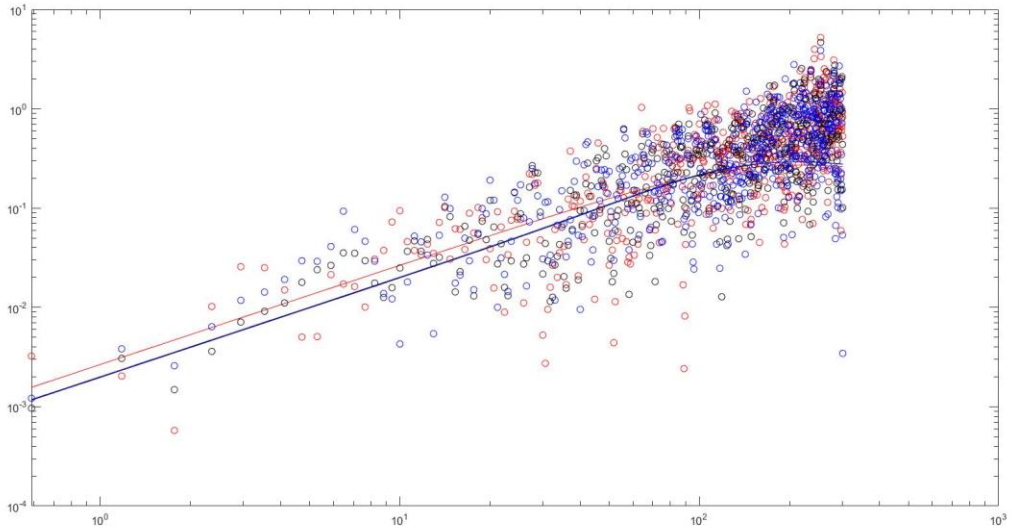

2-2-4-500

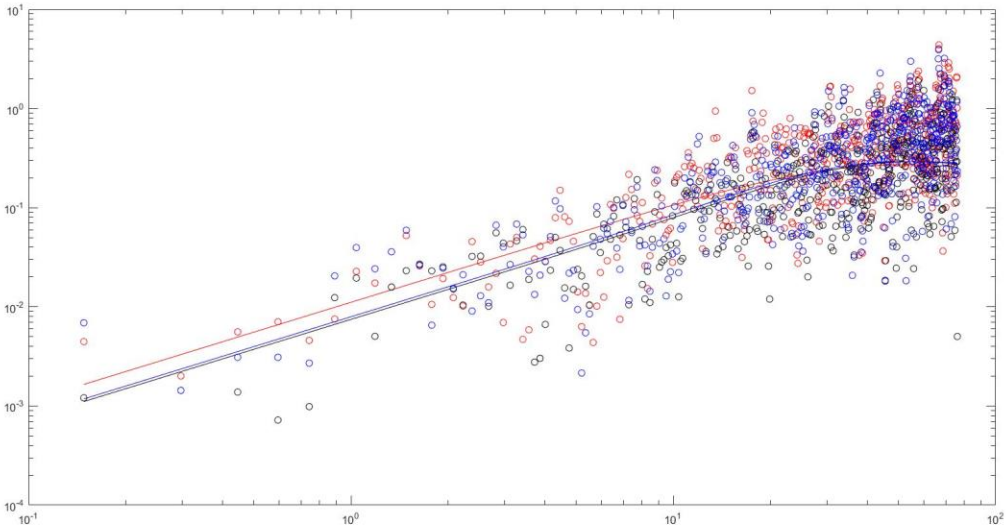

2-2-5-500

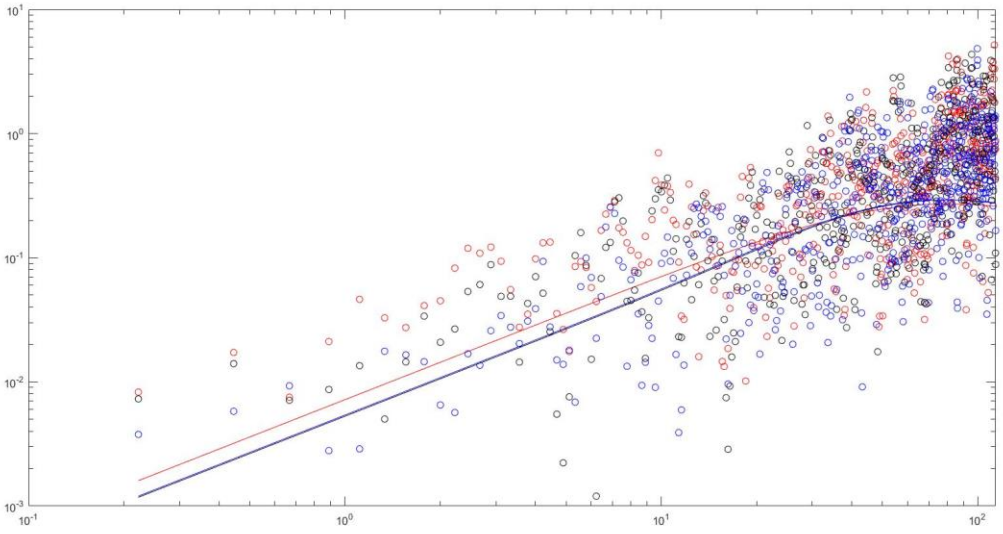

2-2-1-600

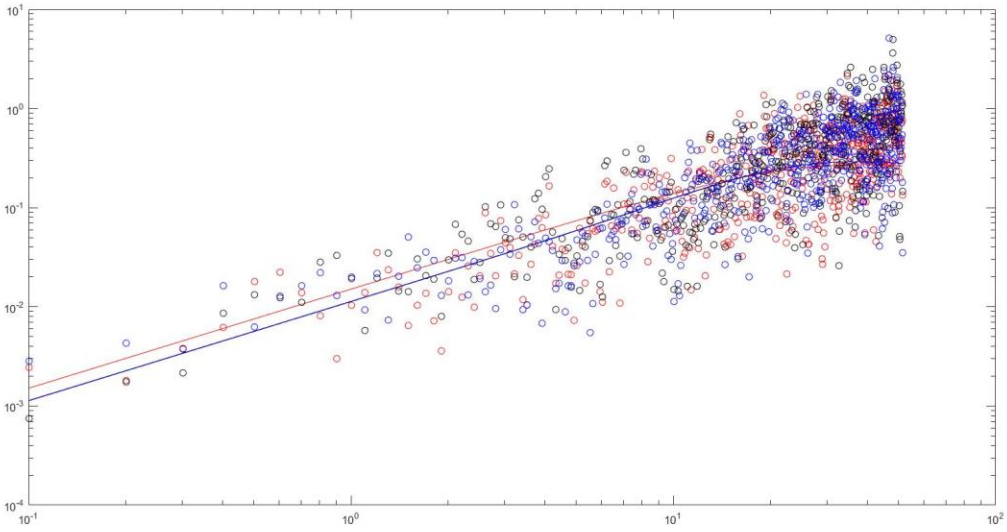

2-2-2-600

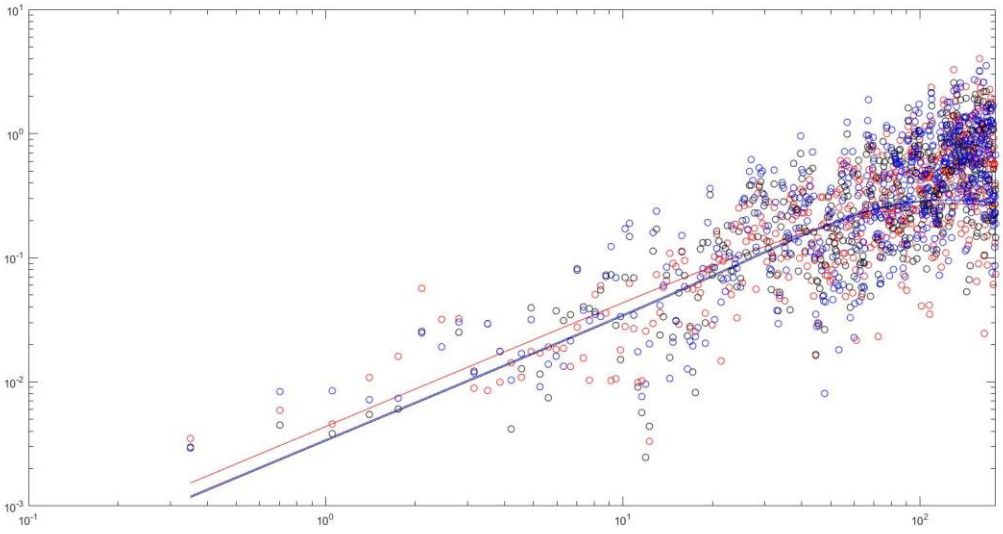

2-2-3-600

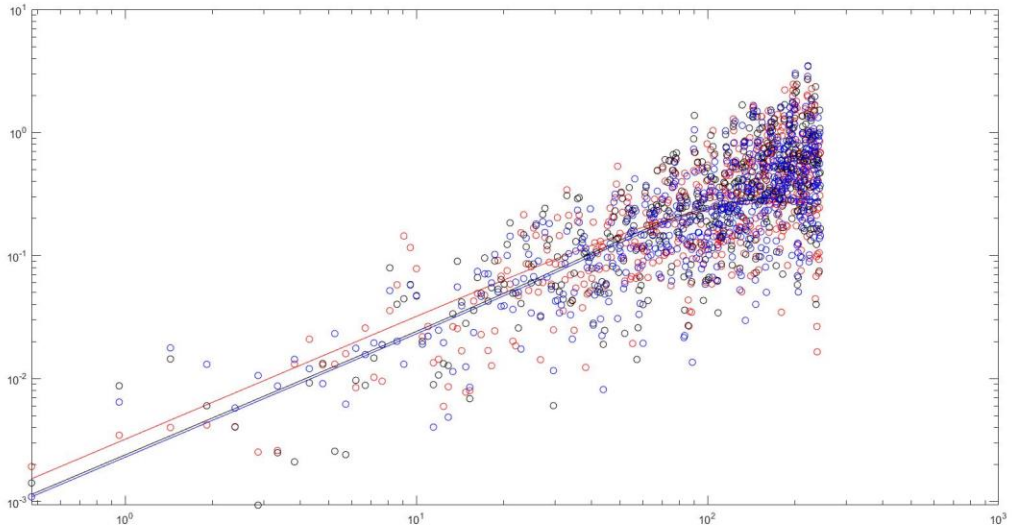

2-2-4-600

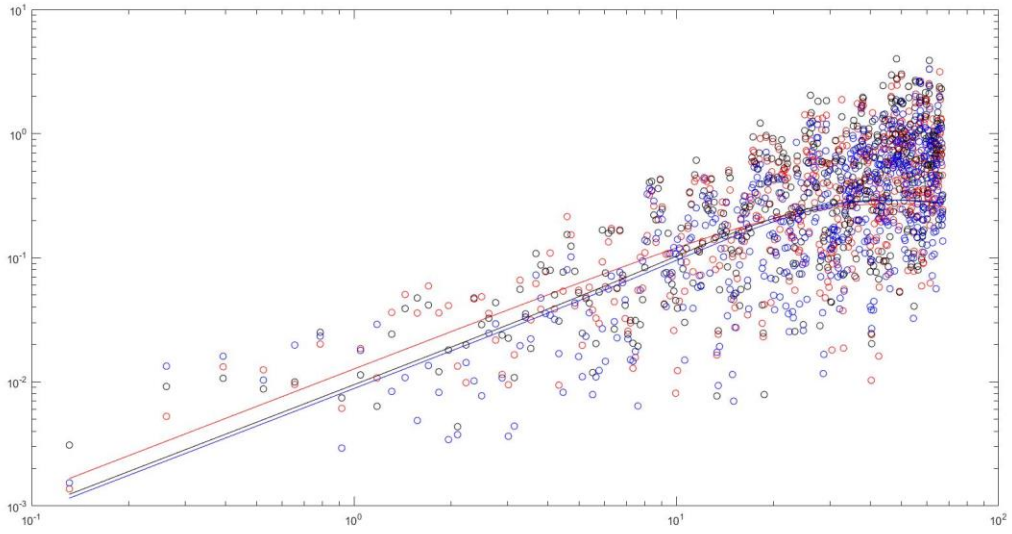

2-2-5-600

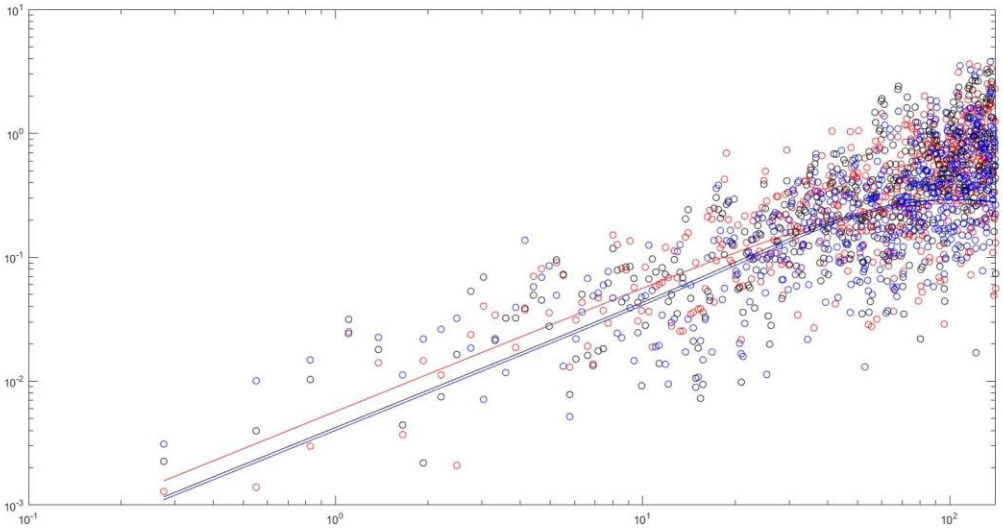

2-2-1-700

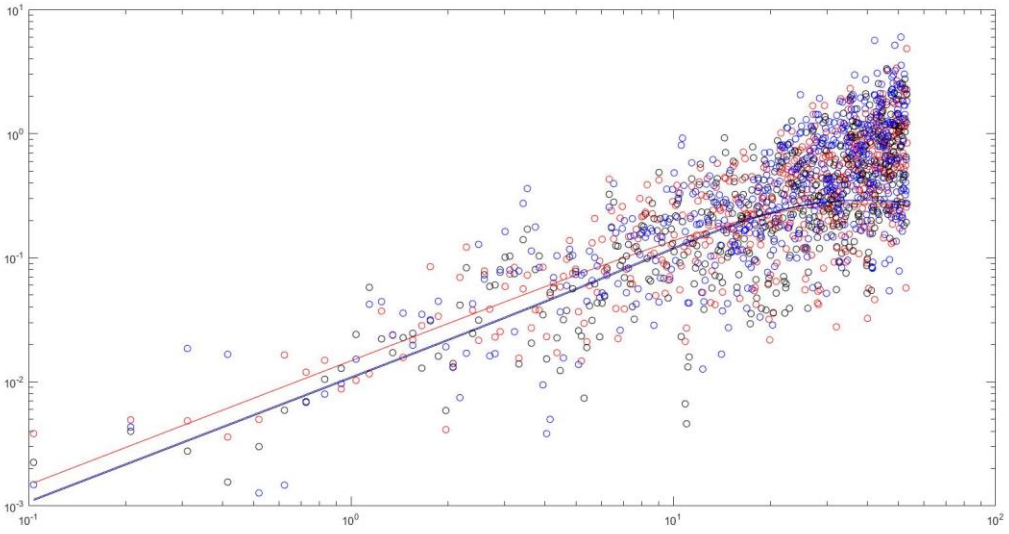

2-2-2-700

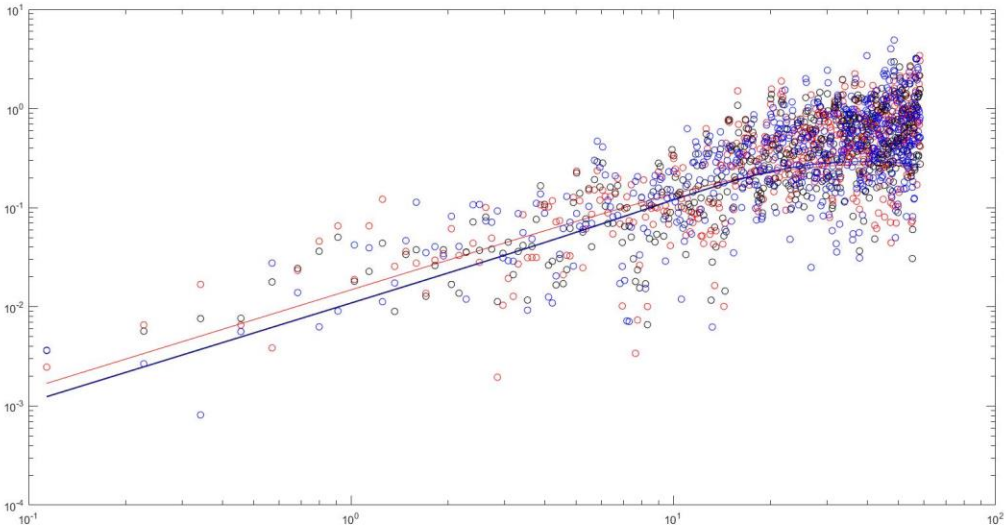

2-2-3-700

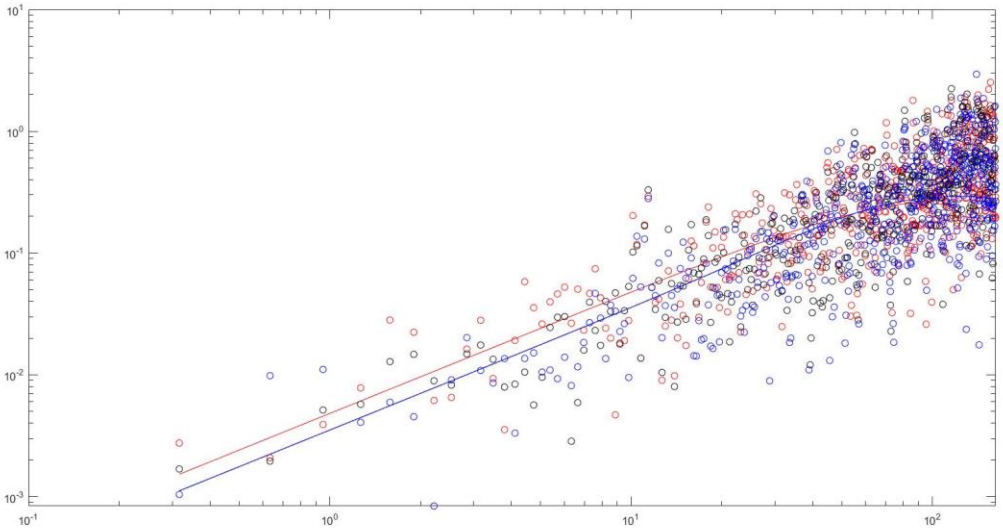

2-2-4-700

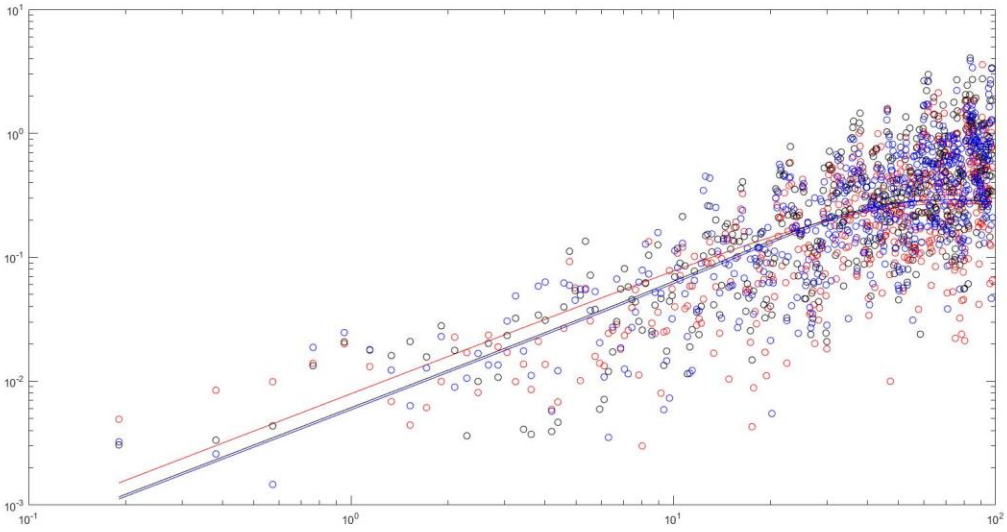

2-2-5-700

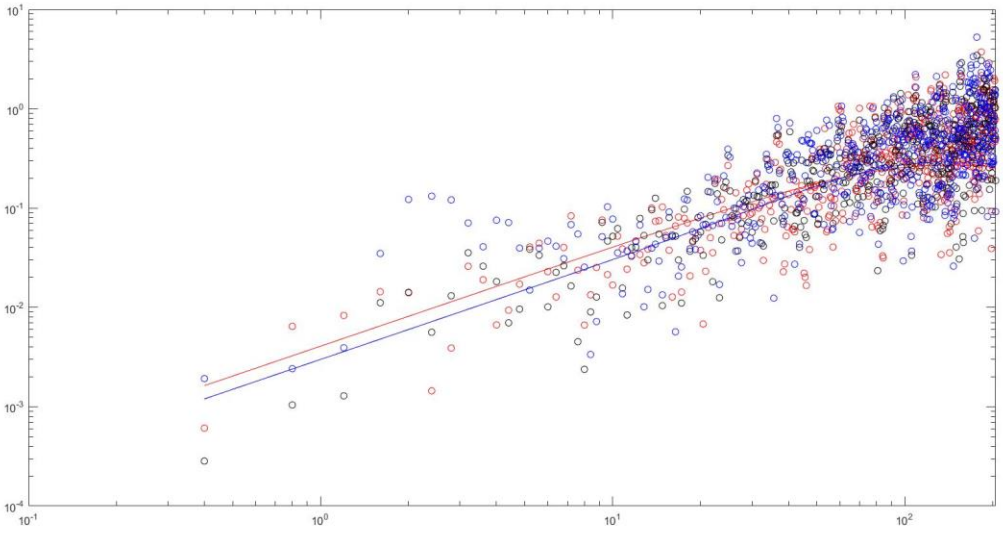

2-2-1-800

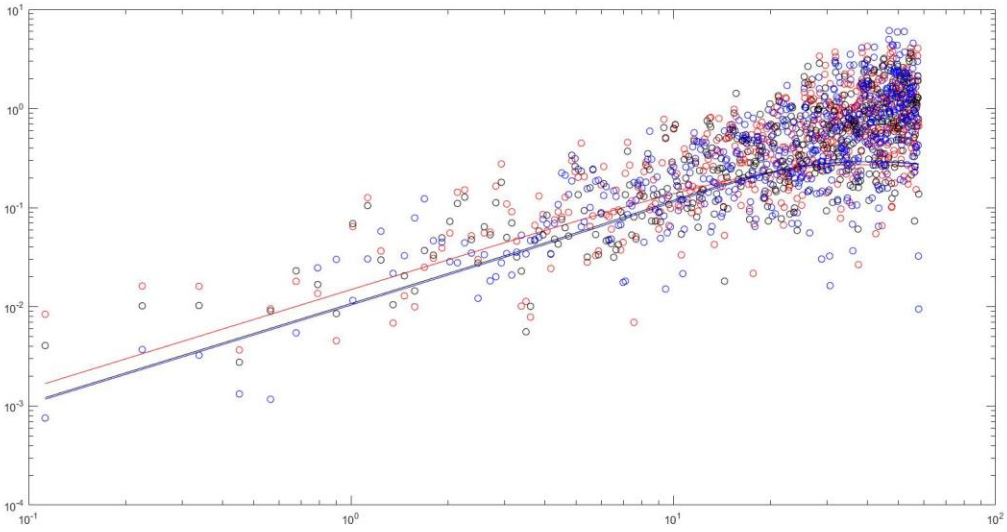

2-2-2-800

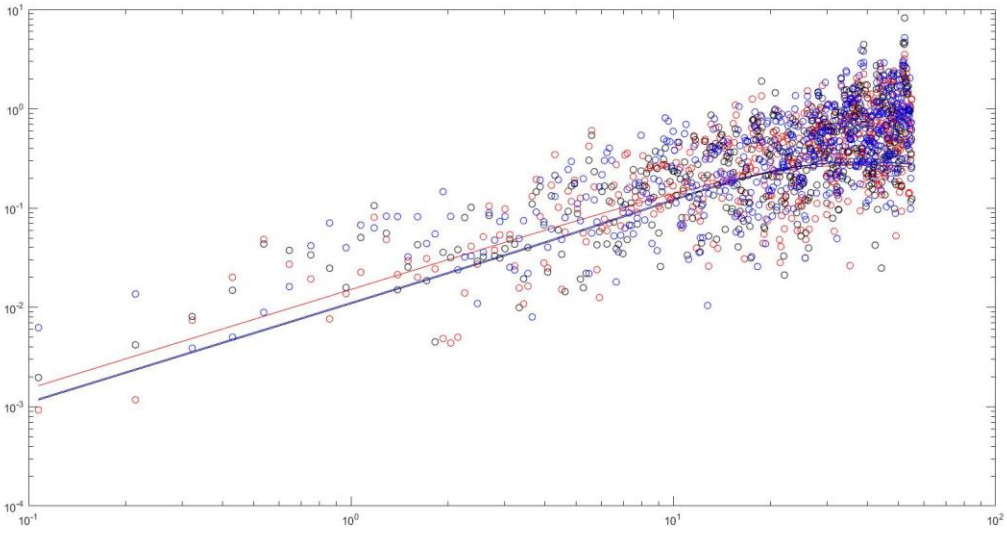

2-2-3-800

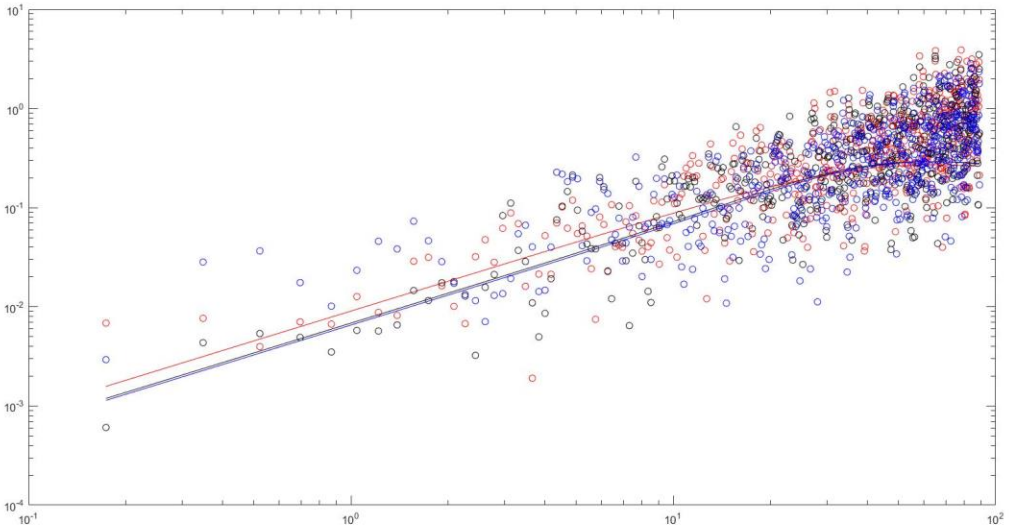

2-2-4-800

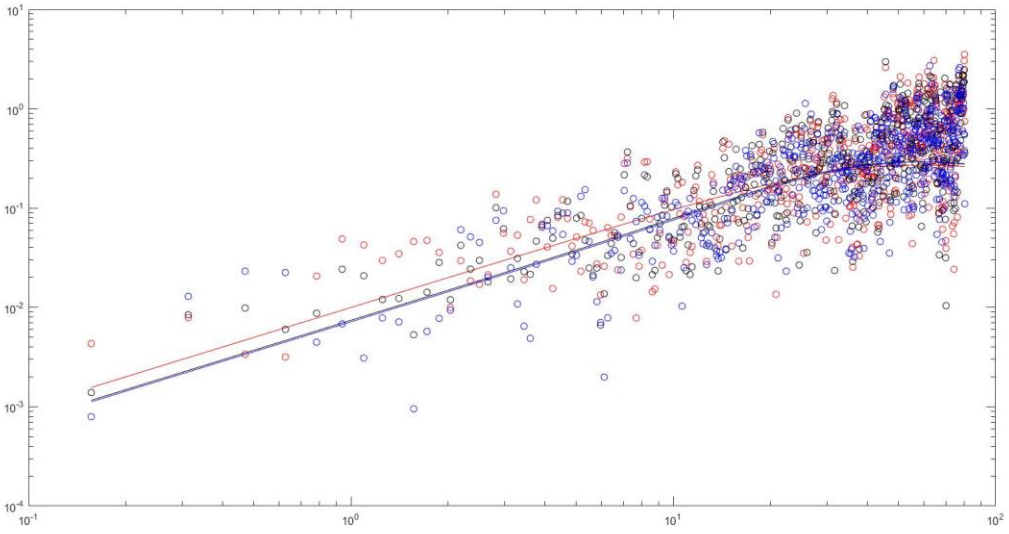

Location 3

2-3-1-400

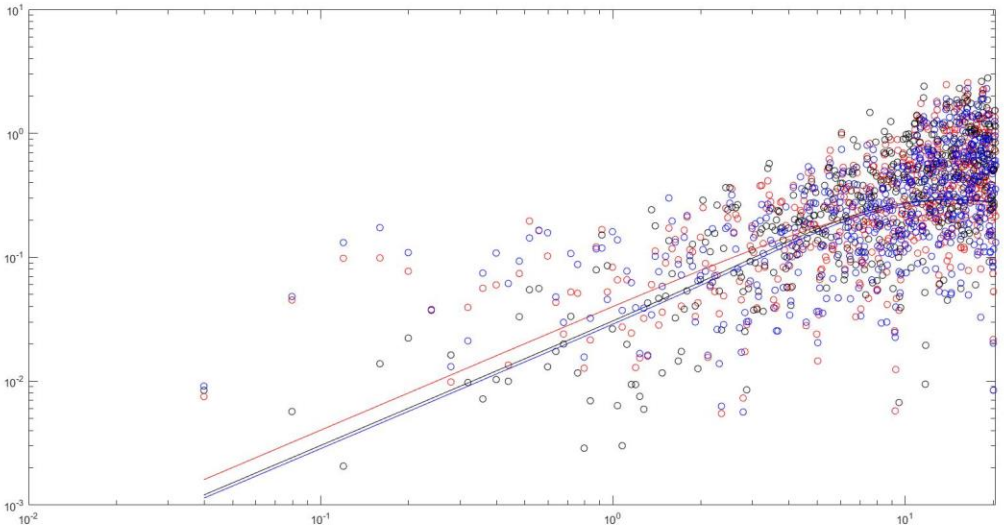

2-3-2-400

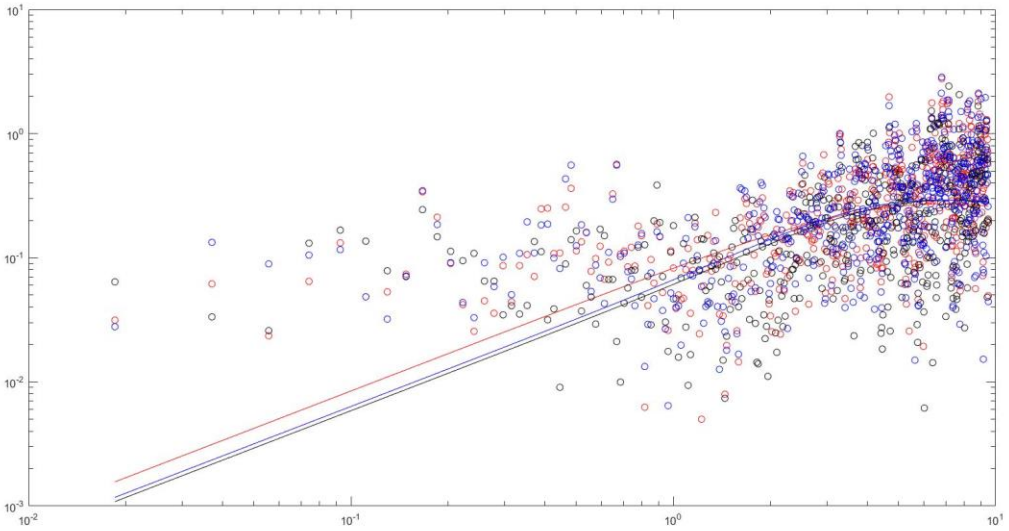

2-3-3-400

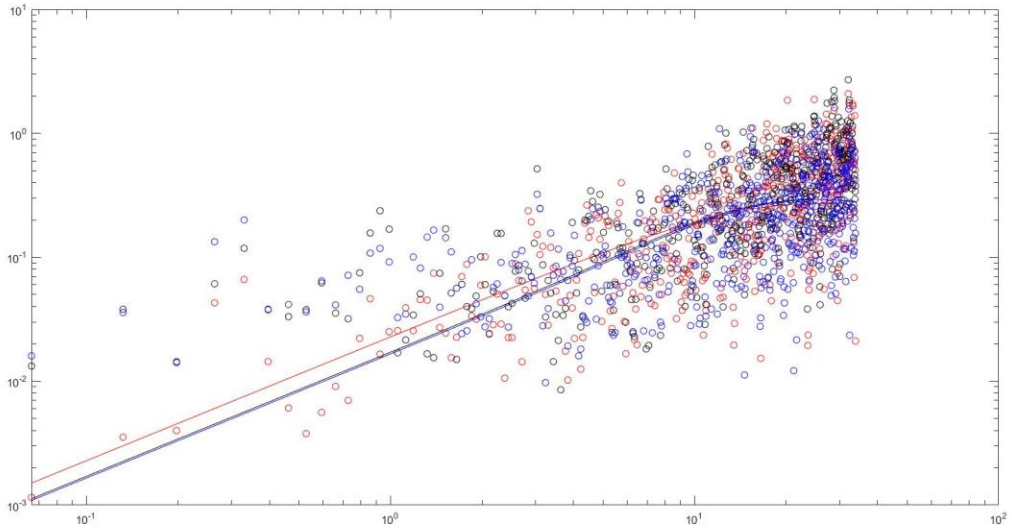

2-3-4-400

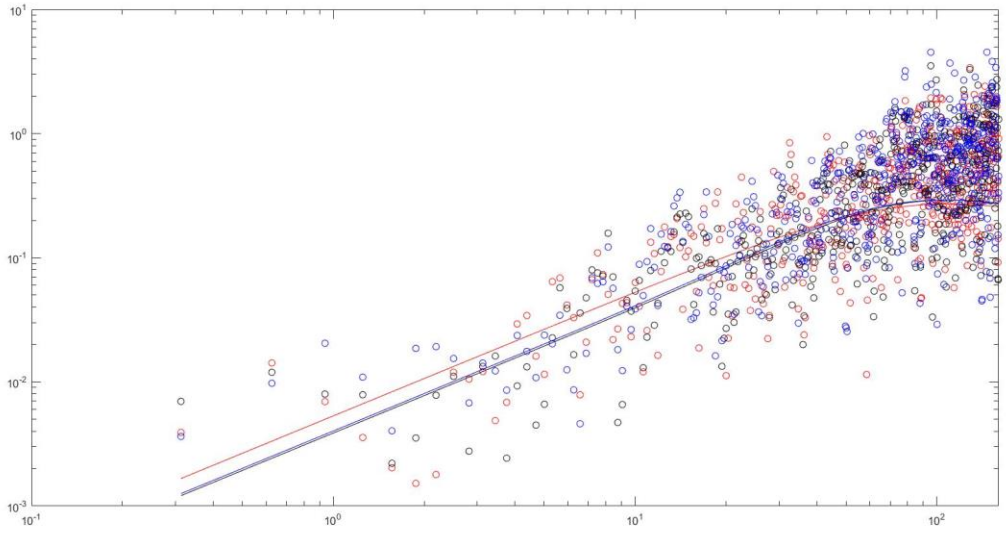

2-3-5-400

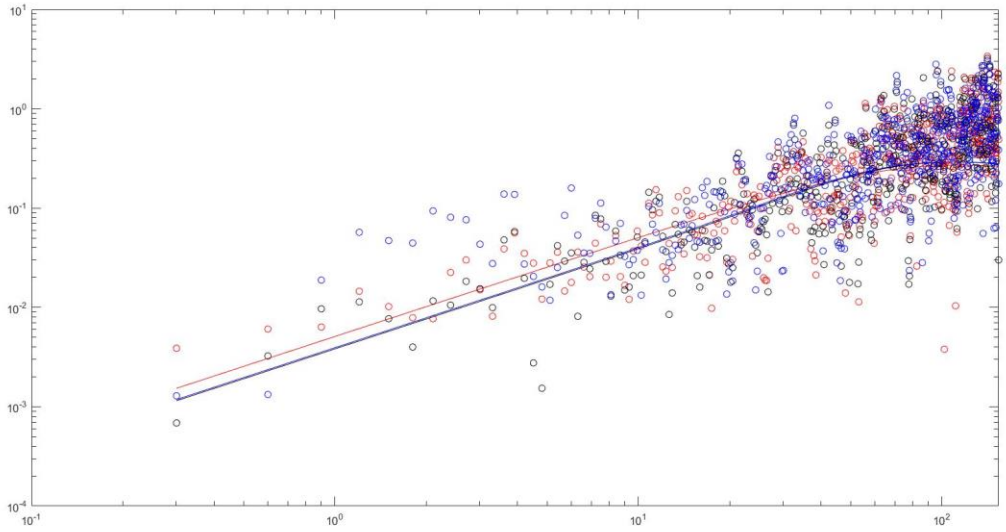

2-3-1-500

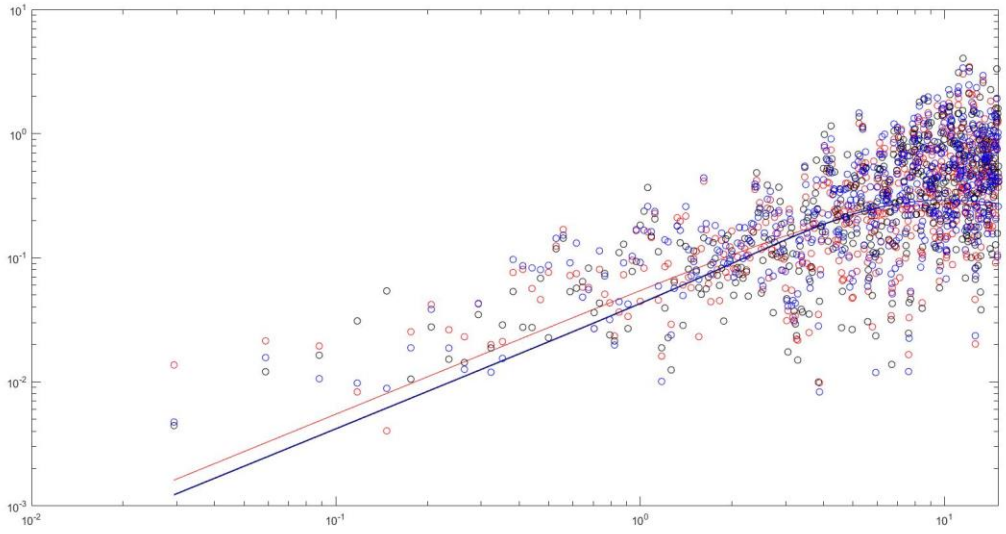

2-3-2-500

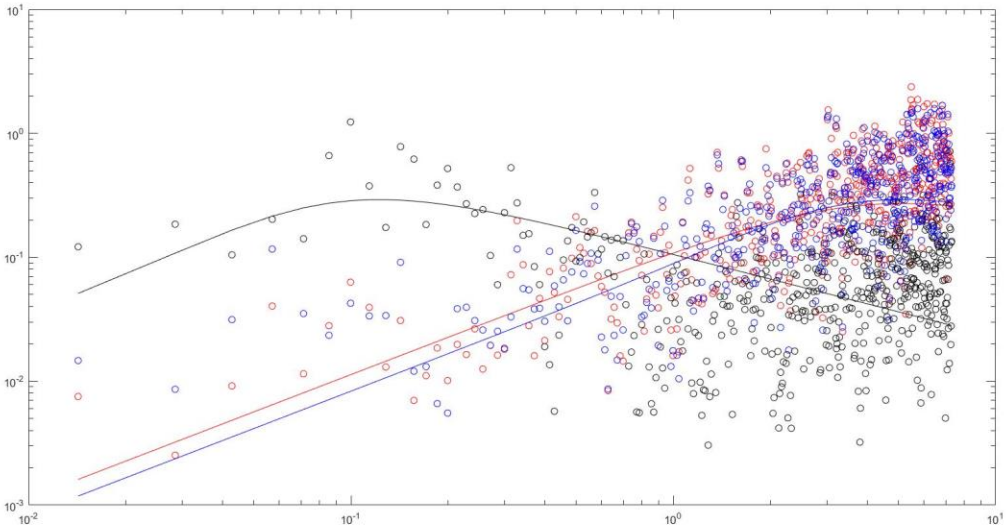

2-3-3-500

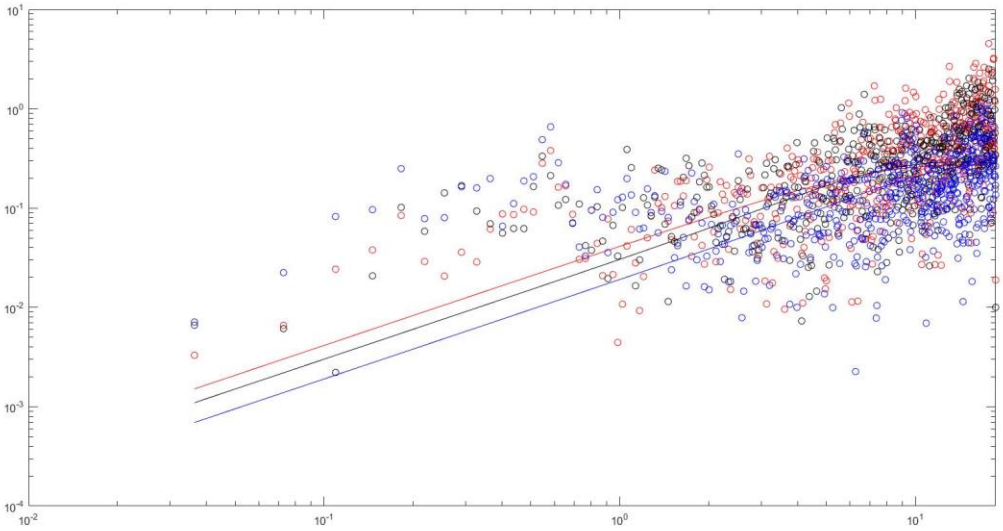

2-3-4-500

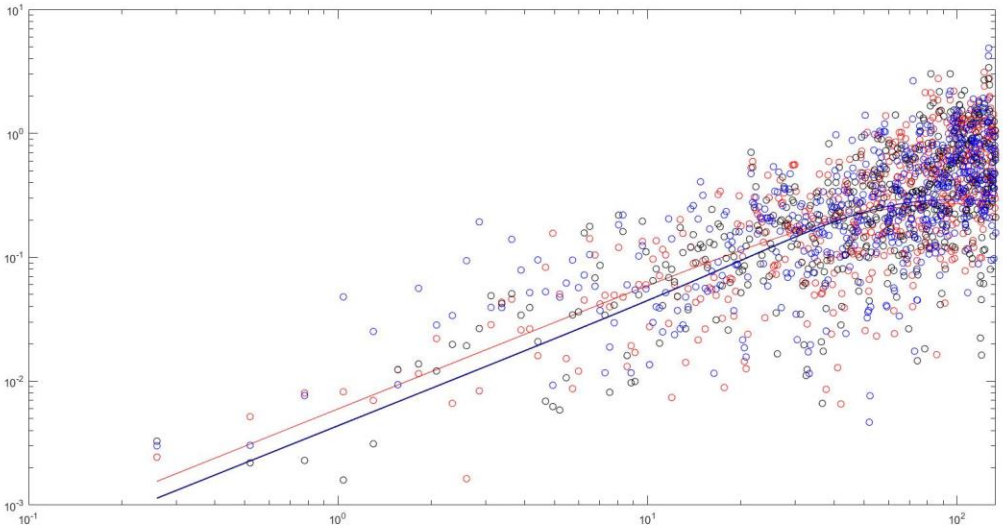

2-3-5-500

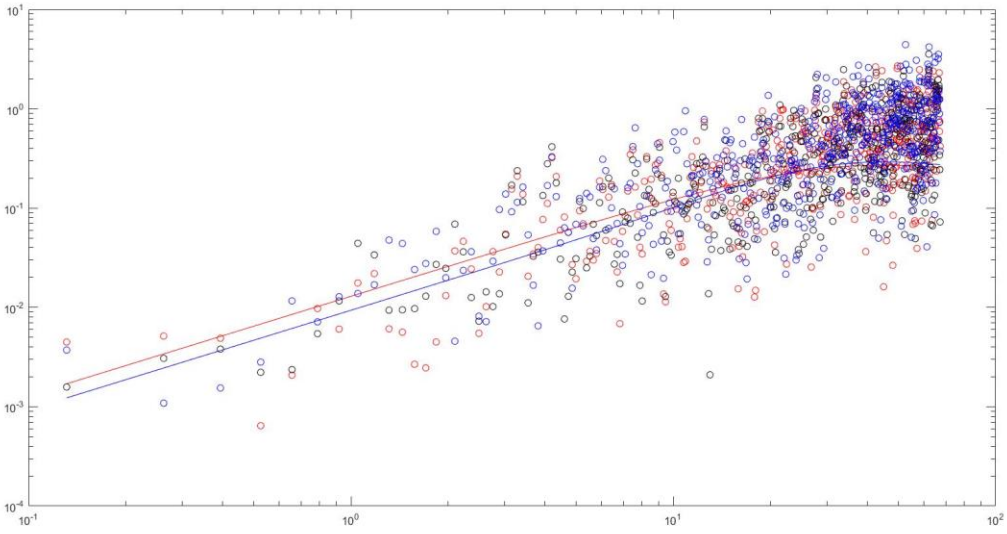

2-3-1-600

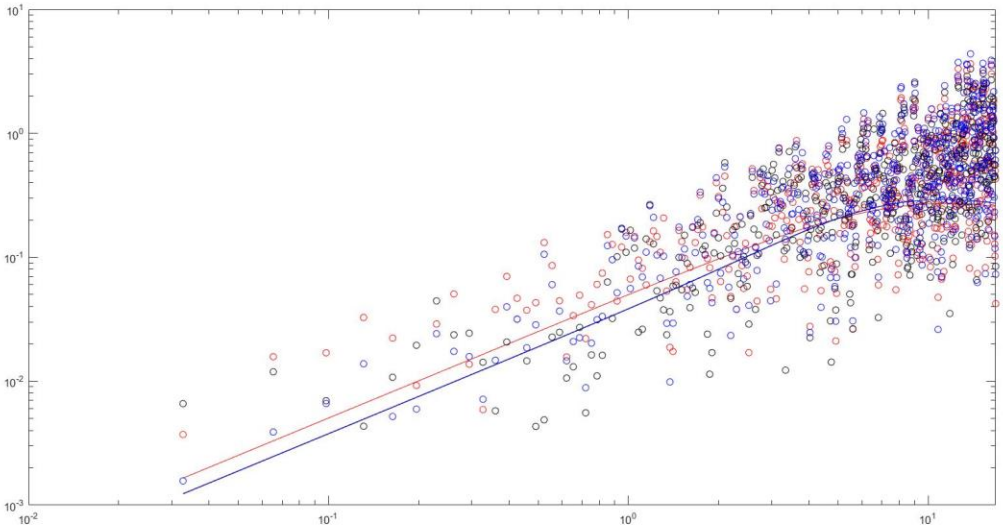

2-3-2-600

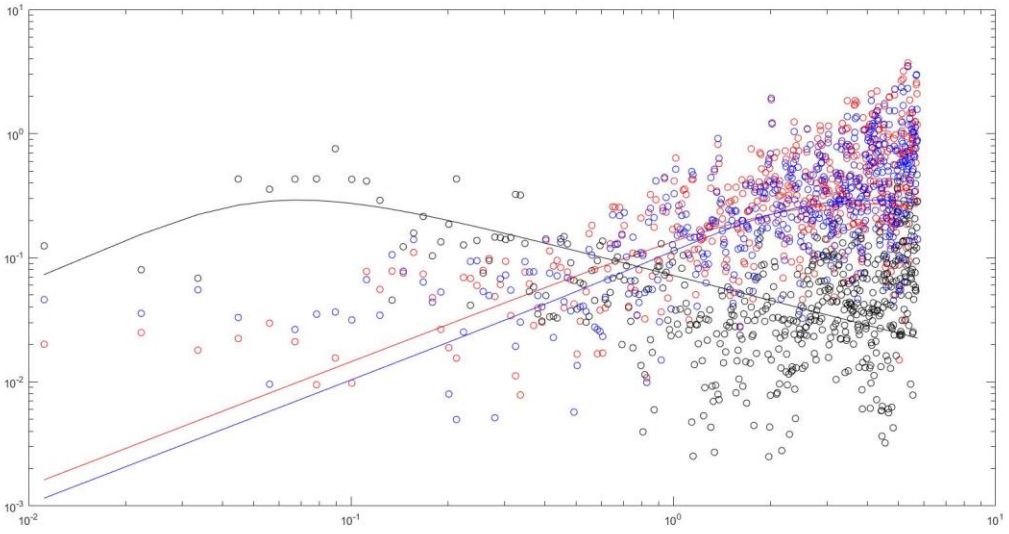

2-3-3-600

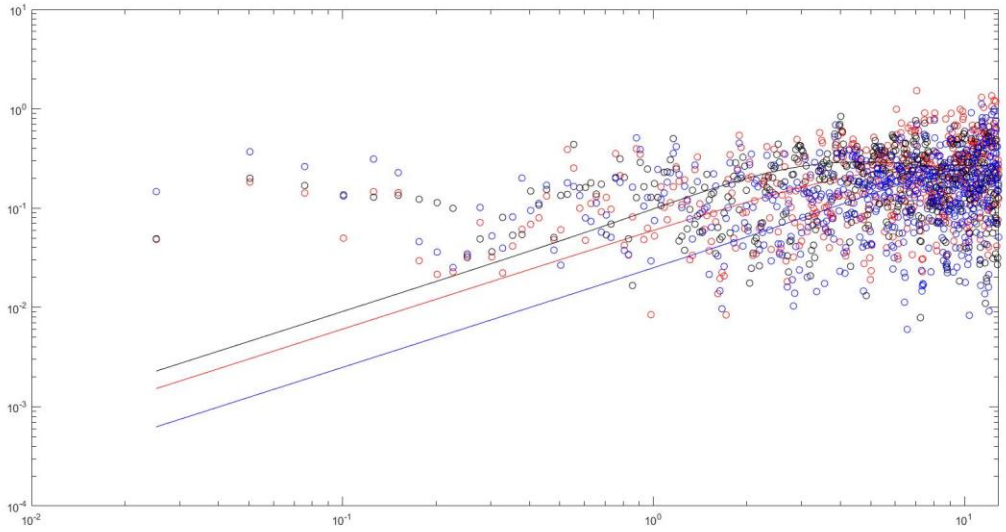

2-3-4-600

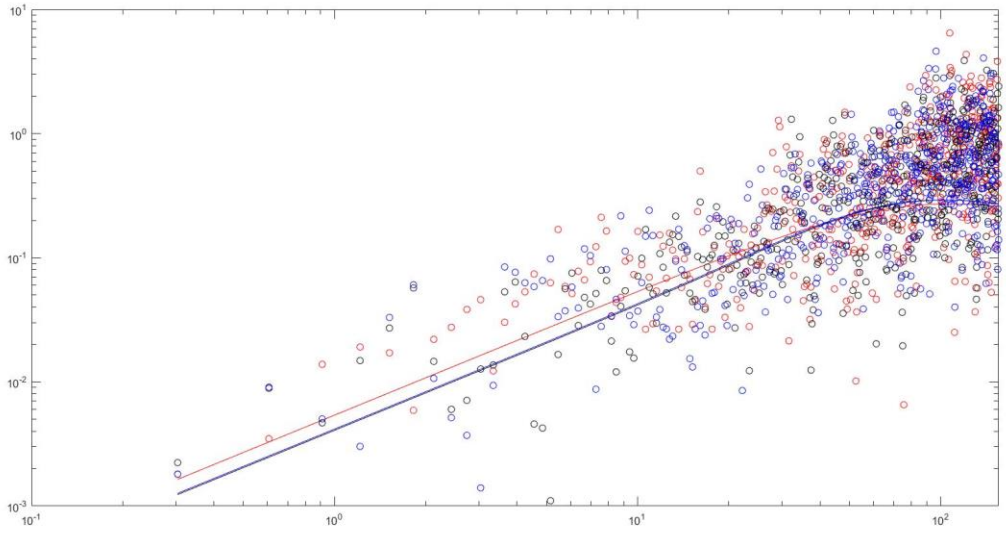

2-3-5-600

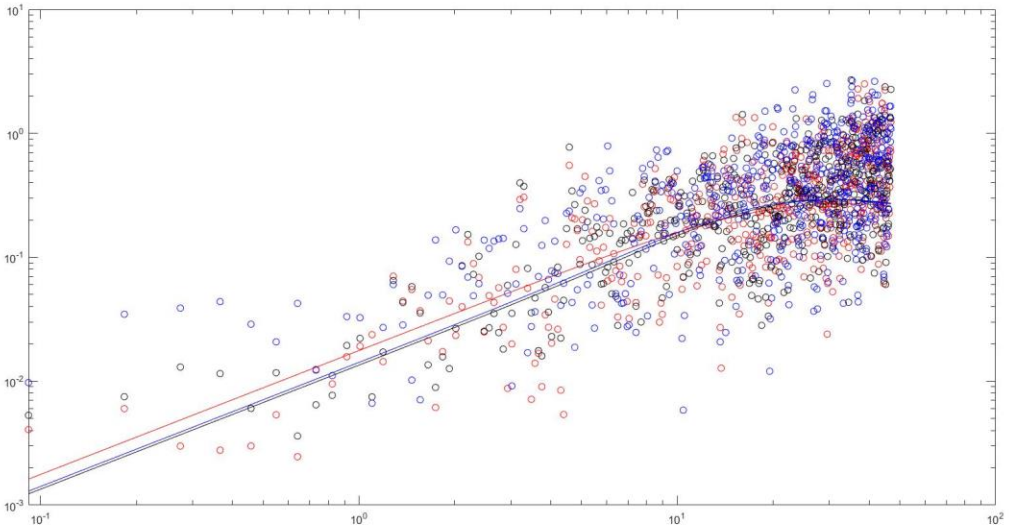

2-3-1-700

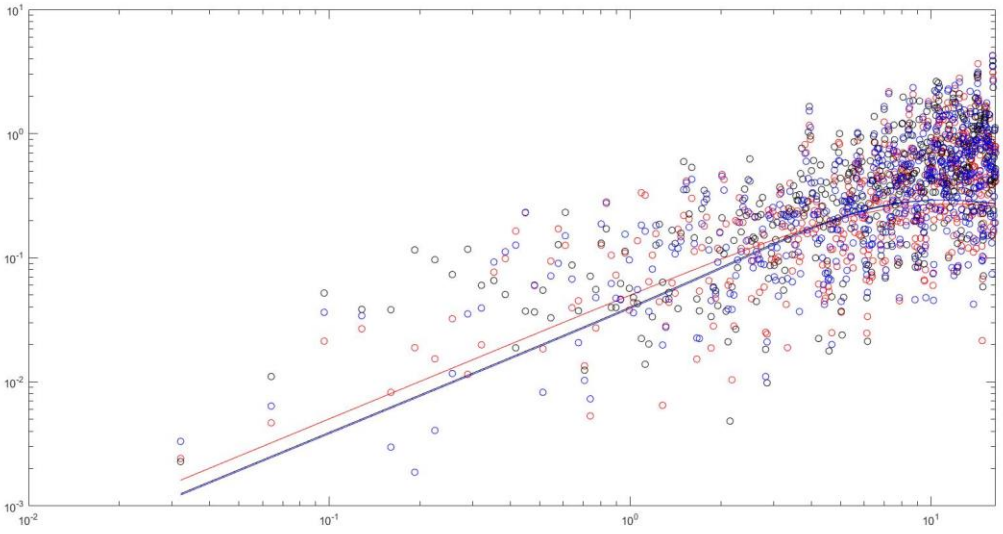

2-3-2-700

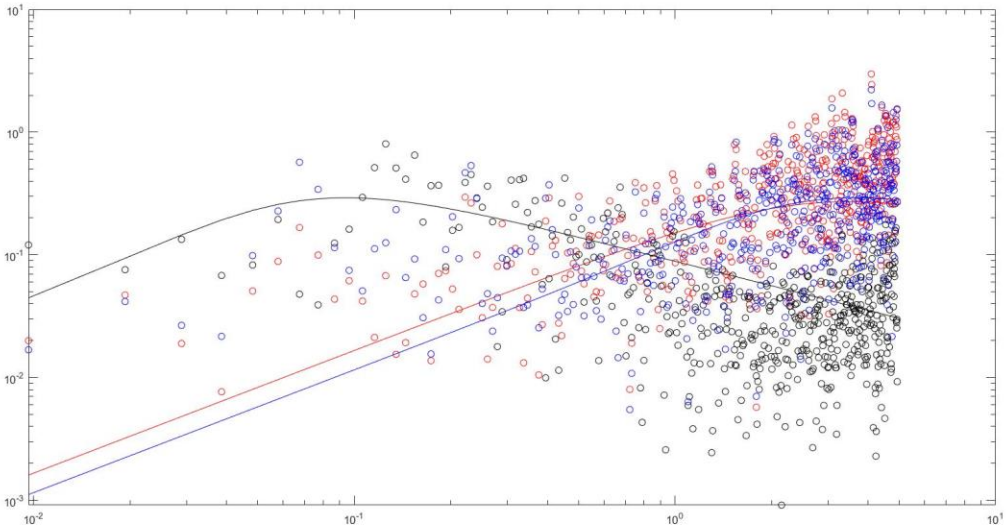

2-3-3-700

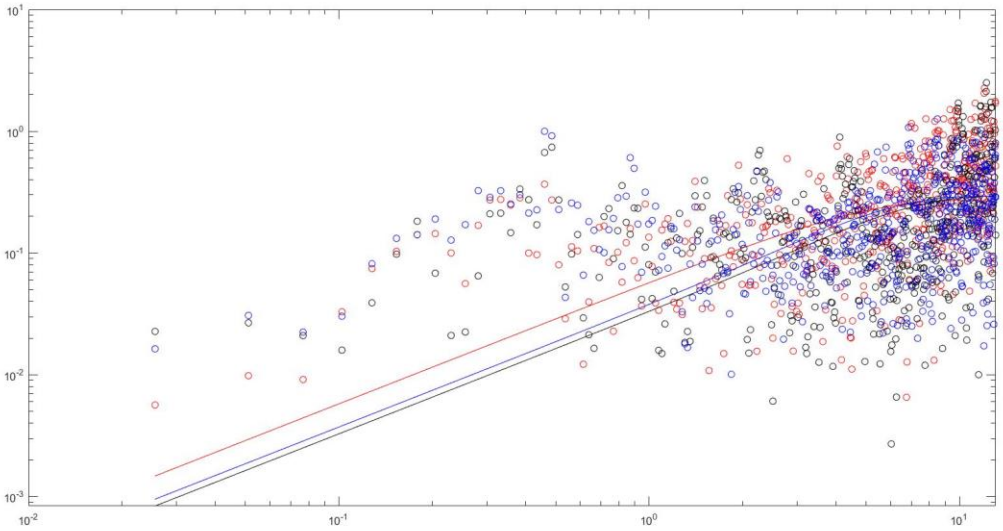

2-3-4-700

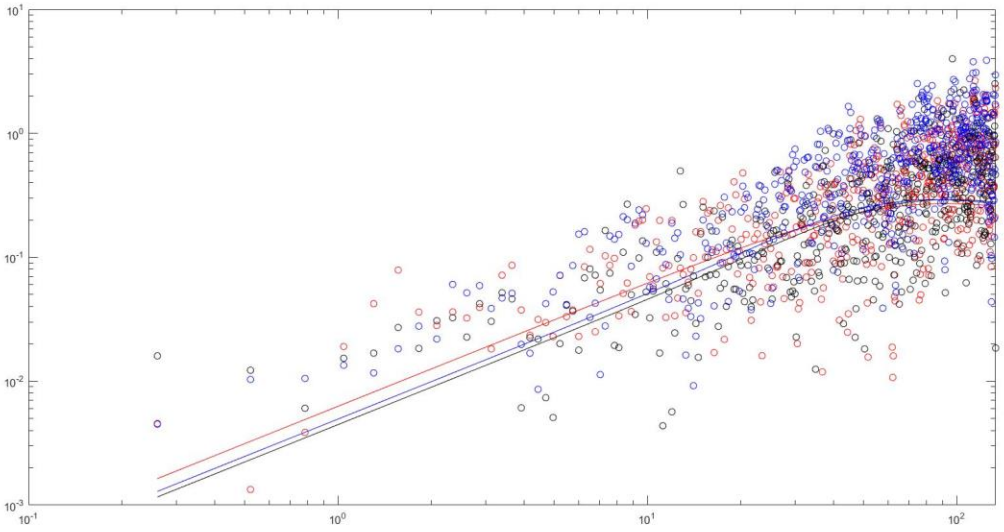

2-3-5-700

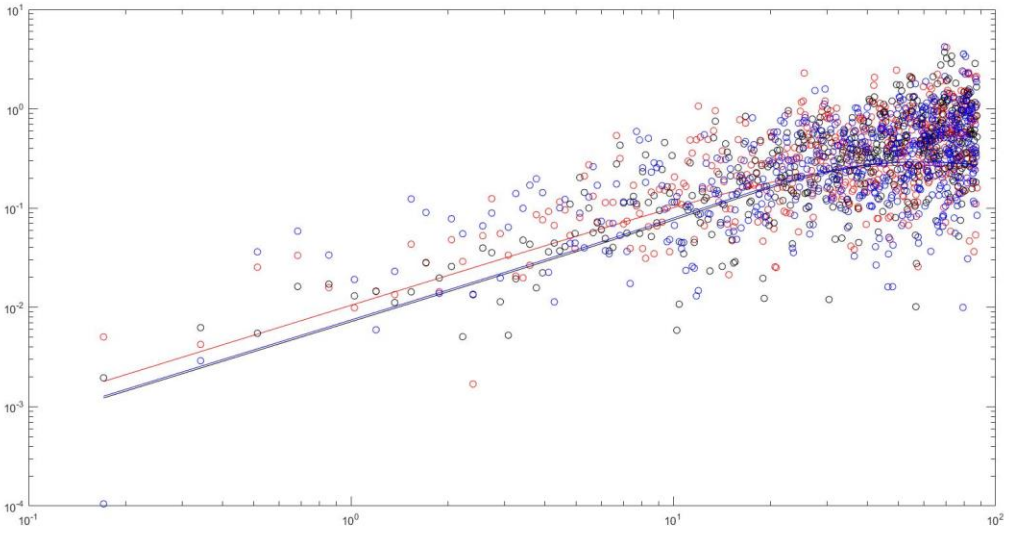

2-3-1-800

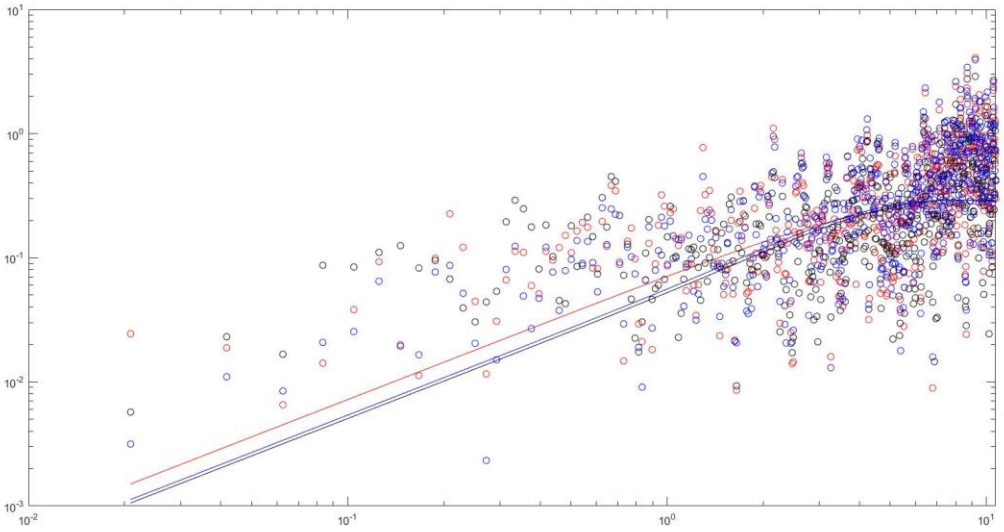

2-3-2-800

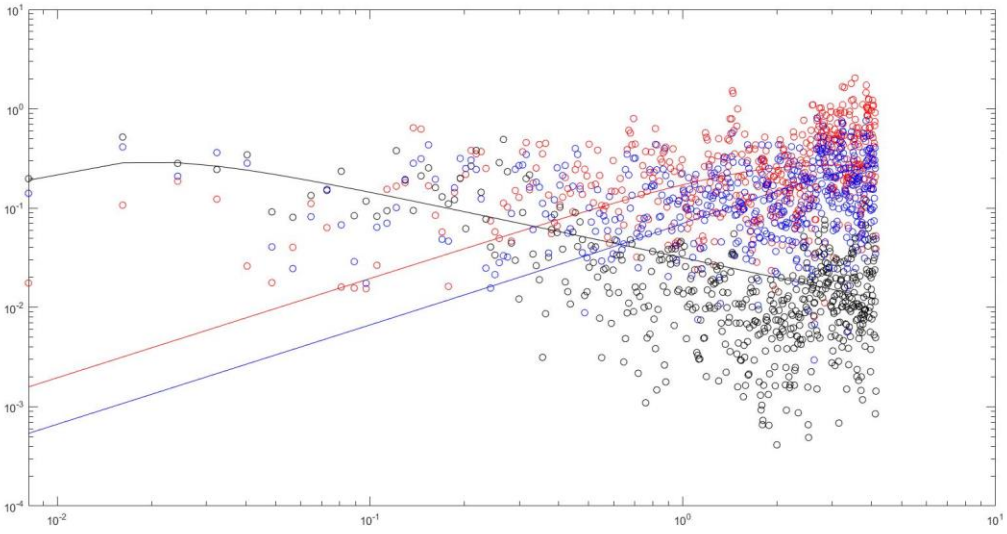

2-3-3-800

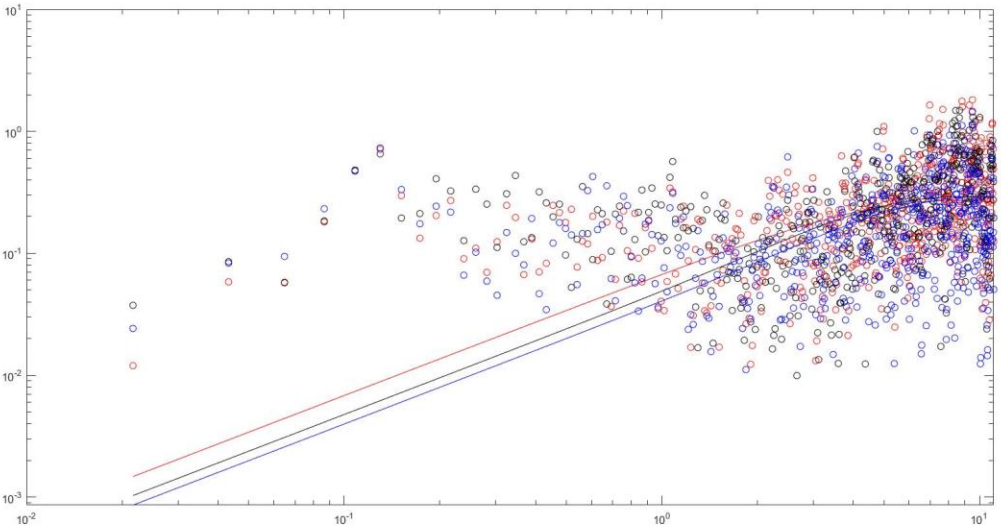

2-3-4-800

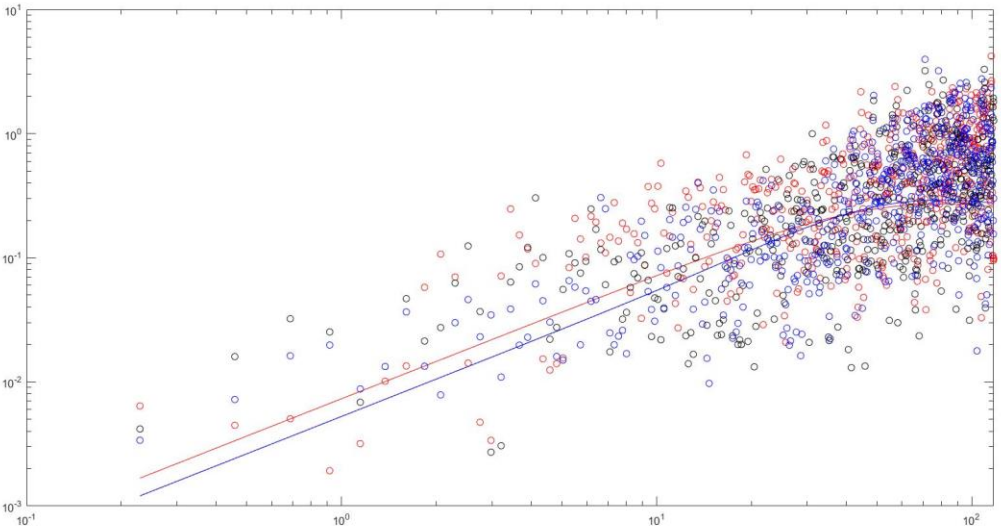

2-3-5-800

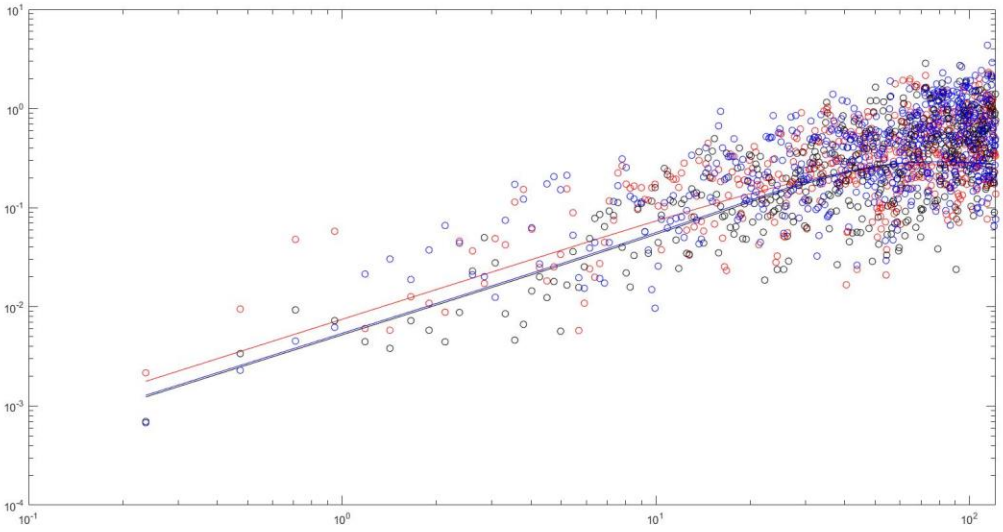

Location 4

2-4-1-400

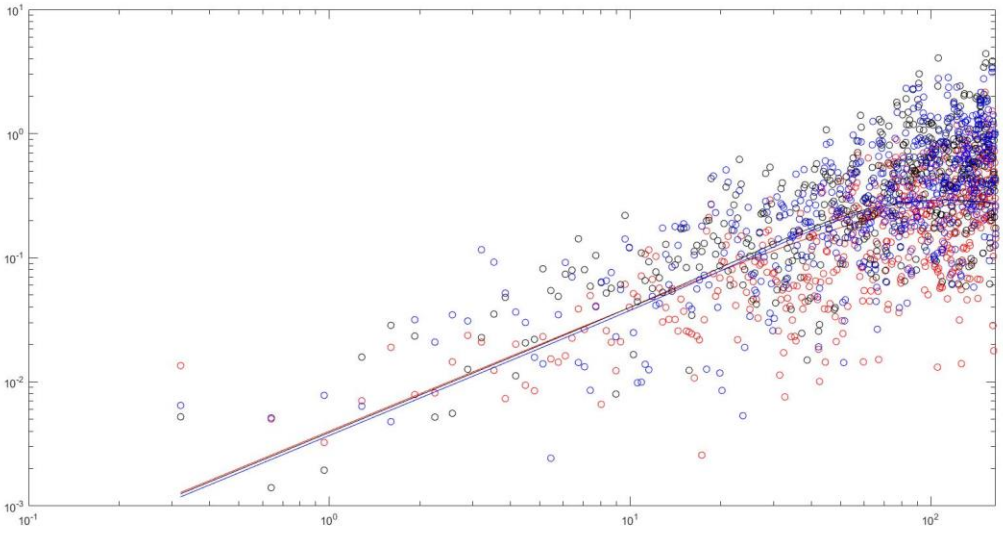

2-4-2-400

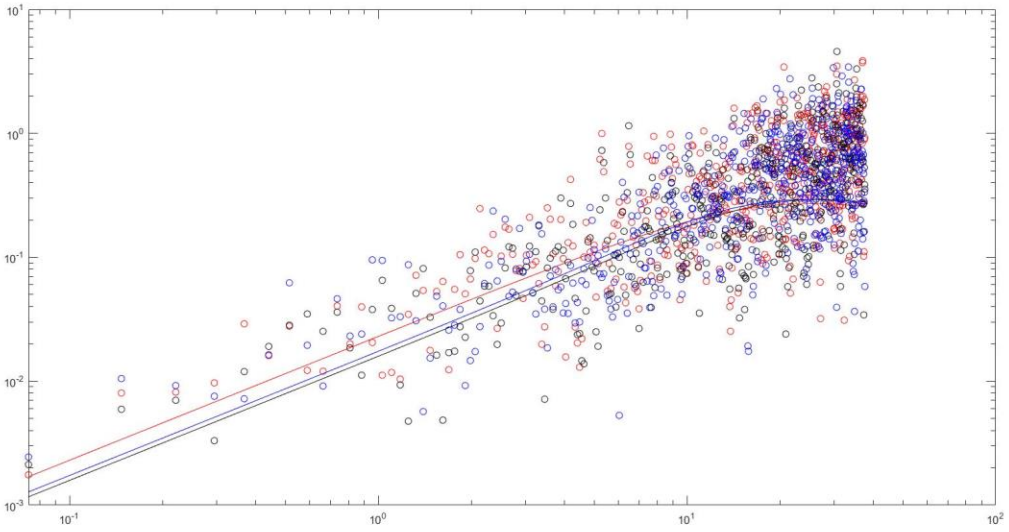

2-4-3-400

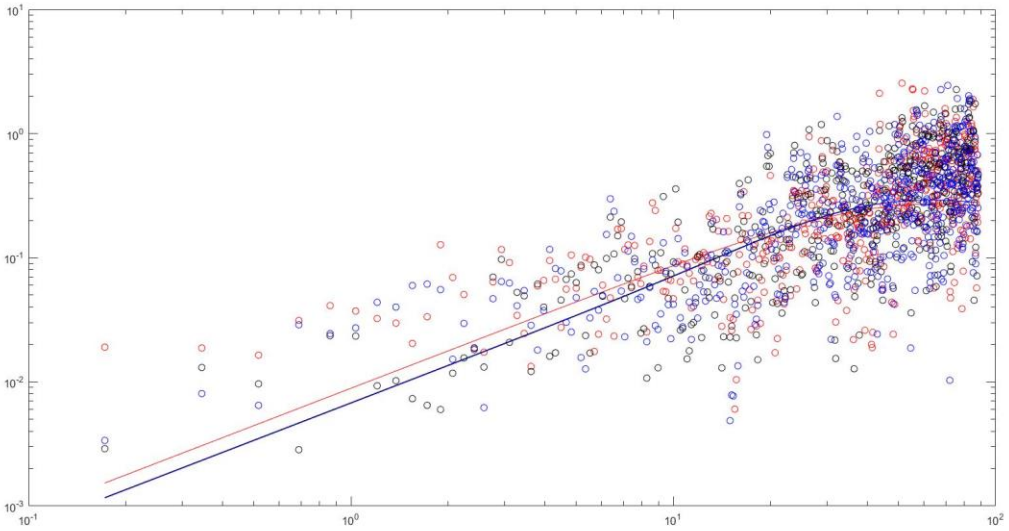

2-4-4-400

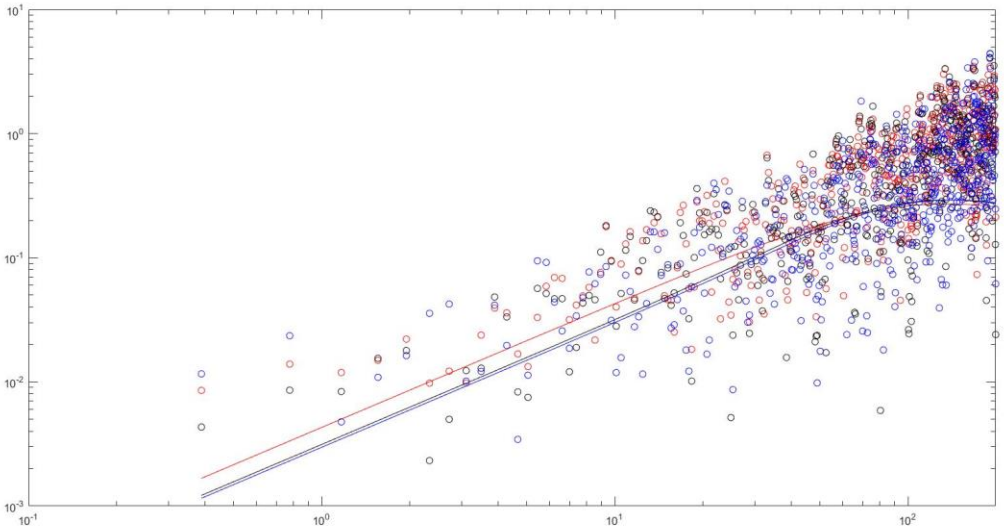

2-4-5-400

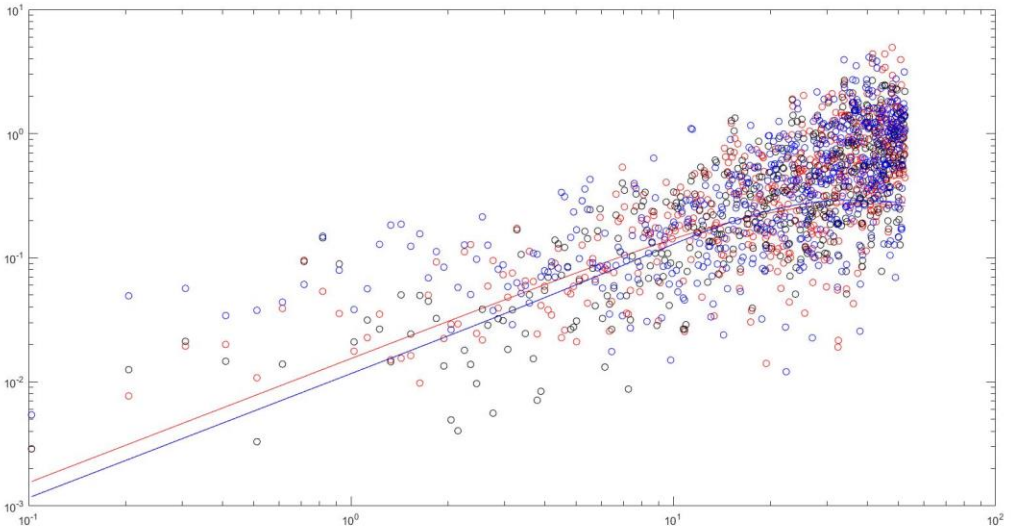

2-4-1-500

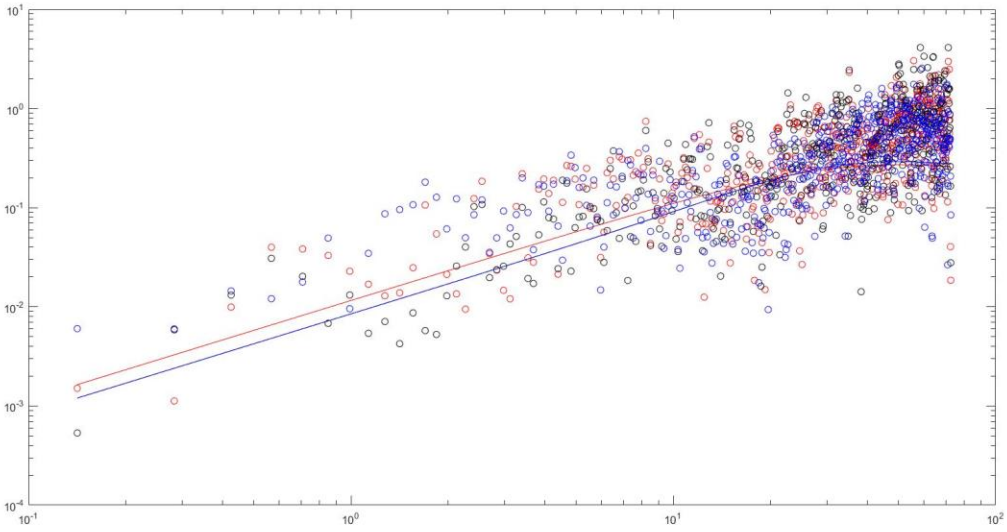

2-4-2-500

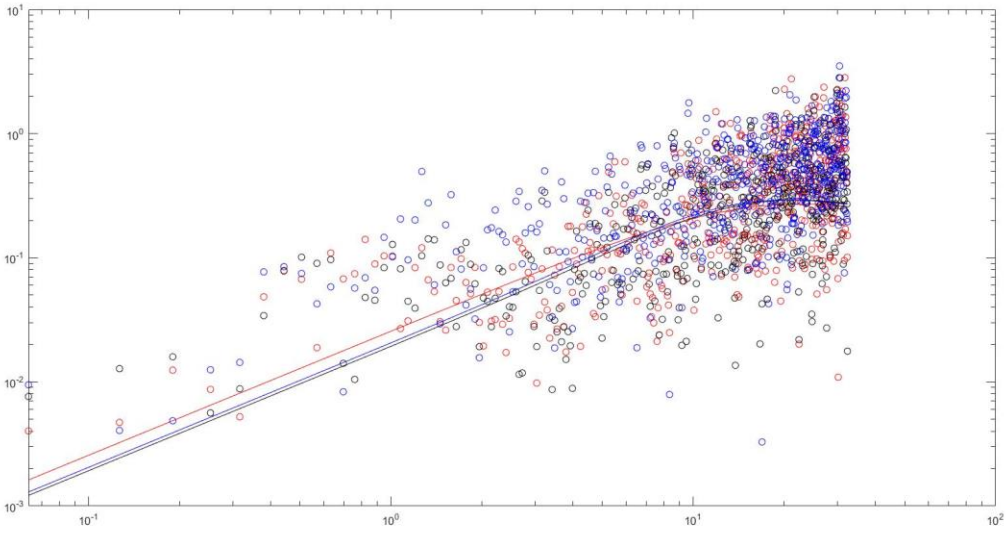

2-4-3-500

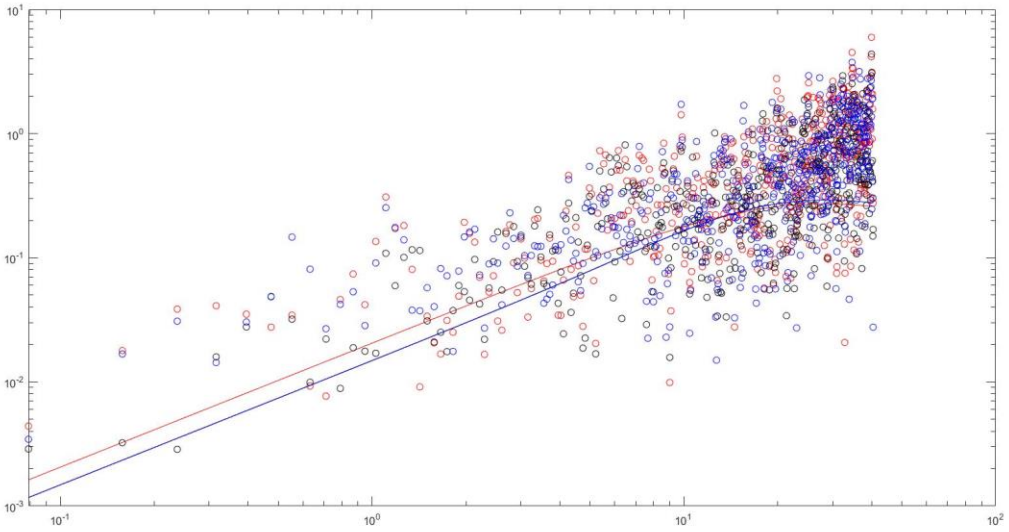

2-4-4-500

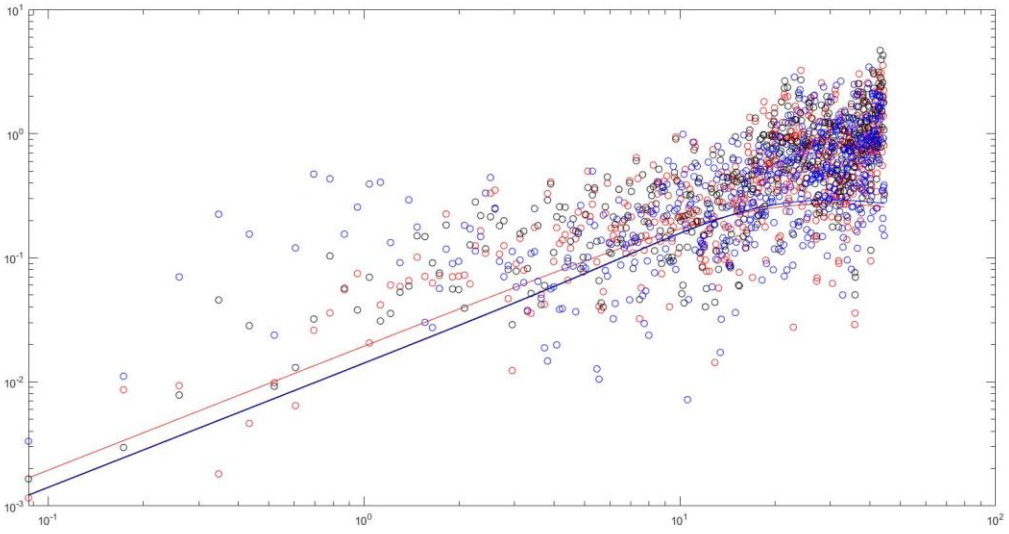

2-4-5-500

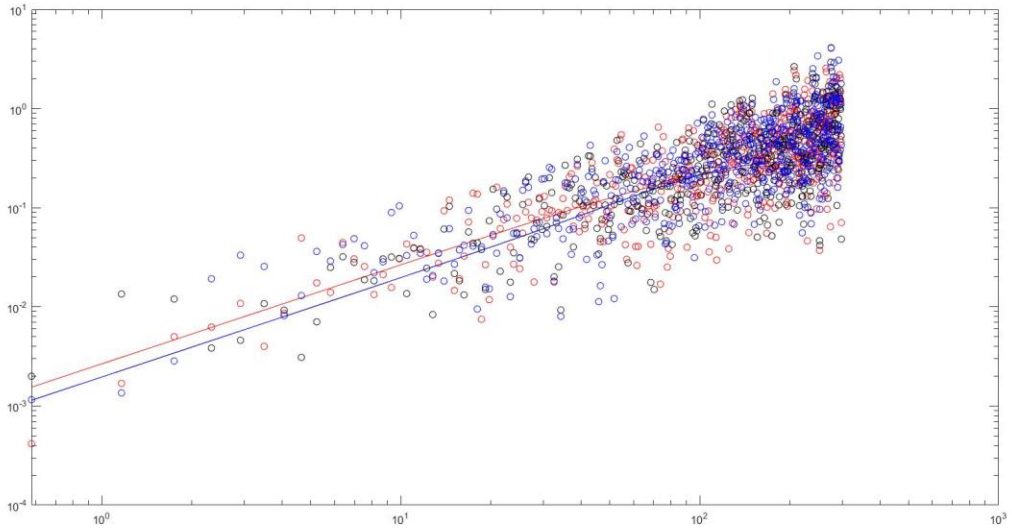

2-4-1-600

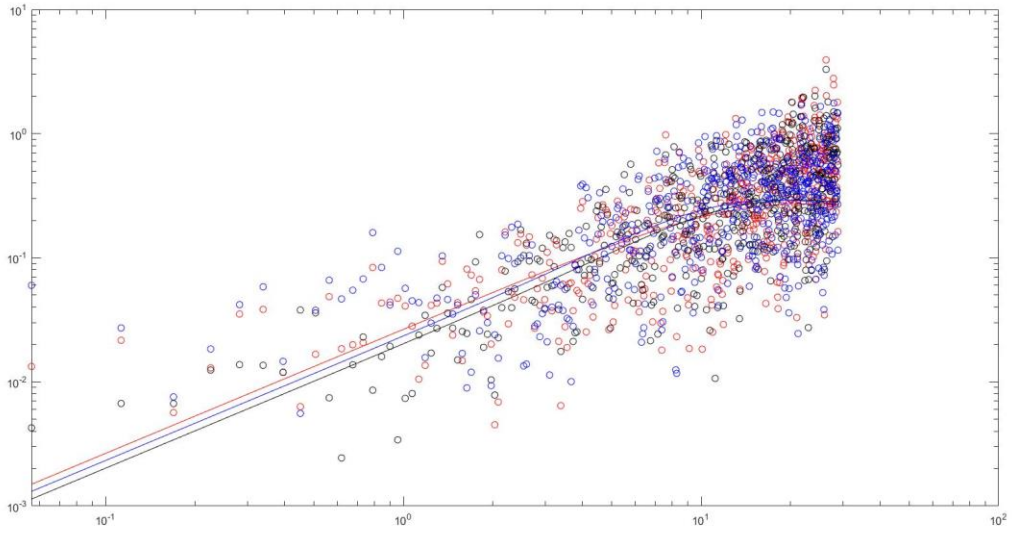

2-4-2-600

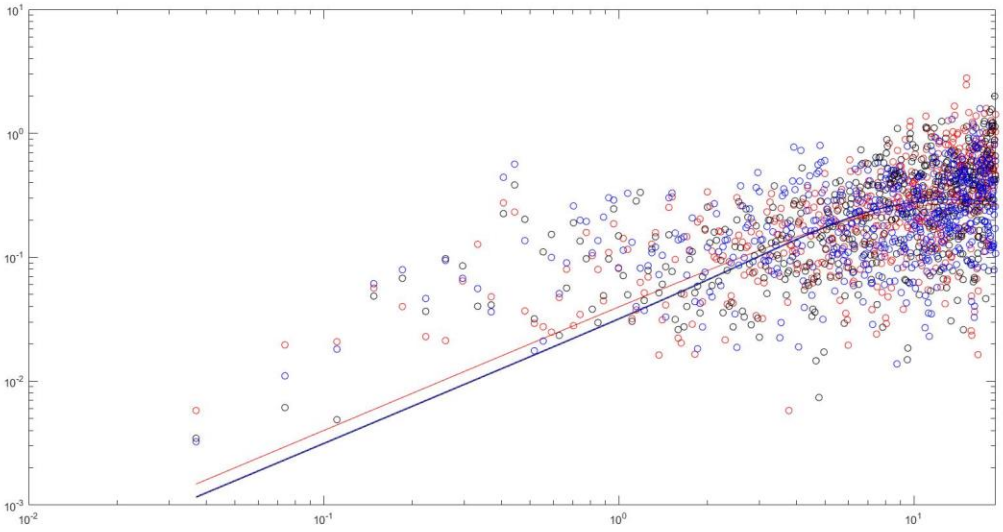

2-4-3-600

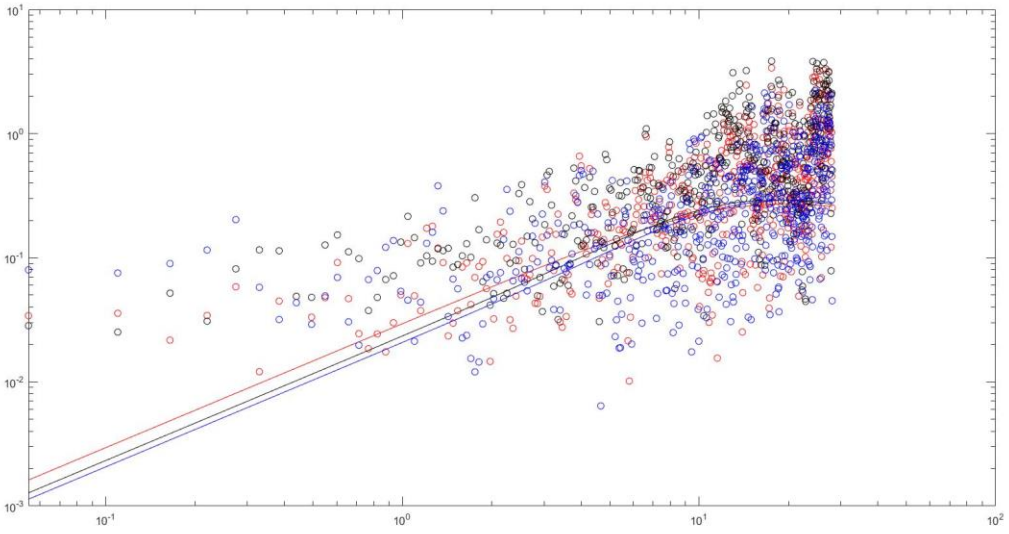

2-4-4-600

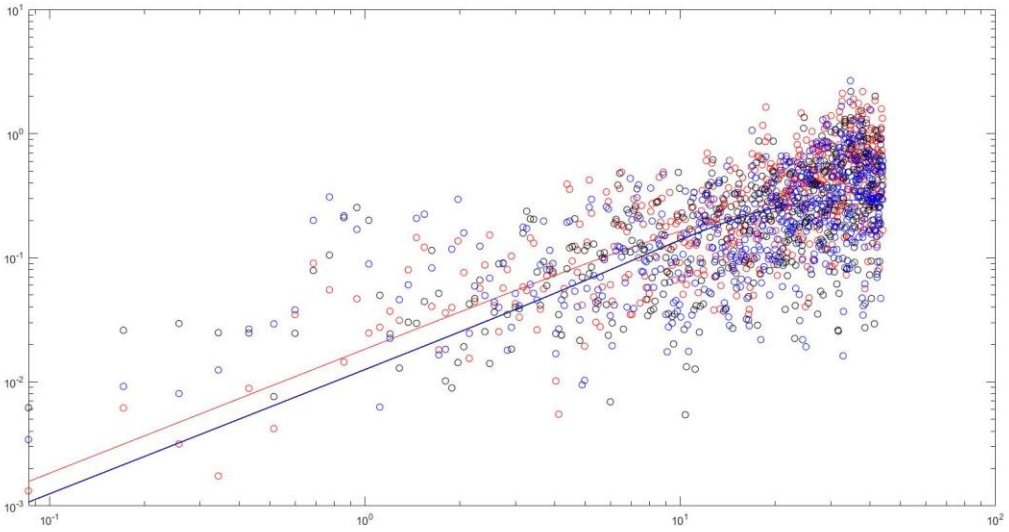

2-4-5-600

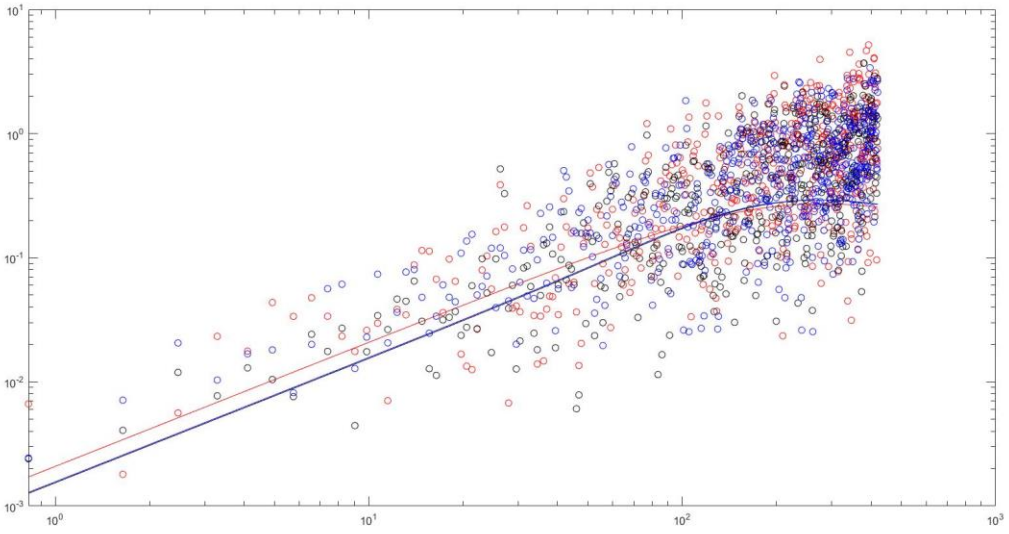

2-4-1-700

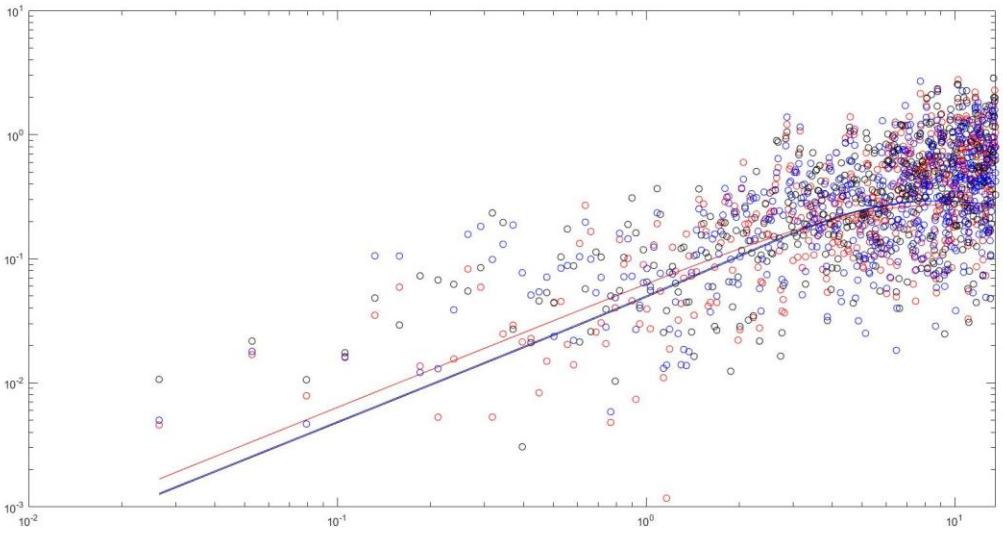

2-4-2-700

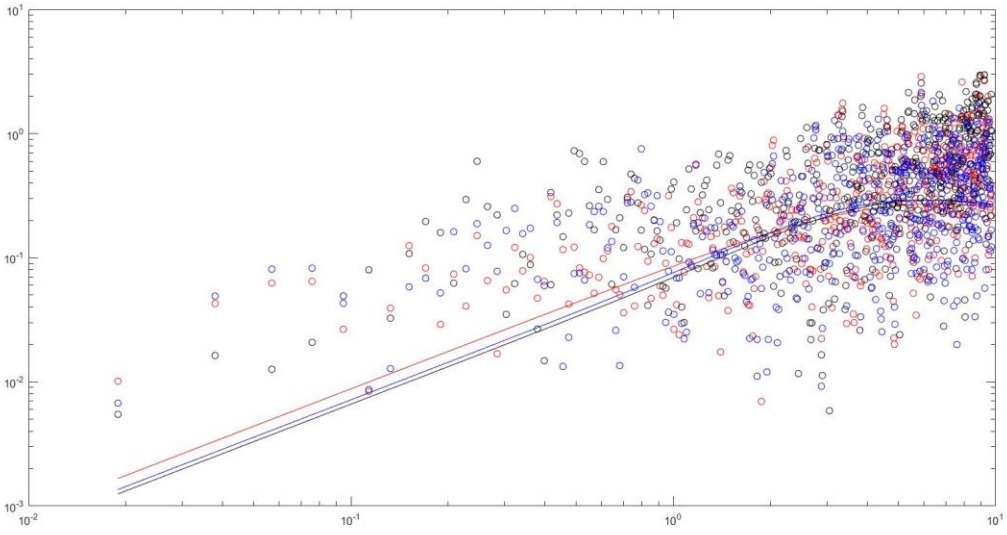

2-4-3-700

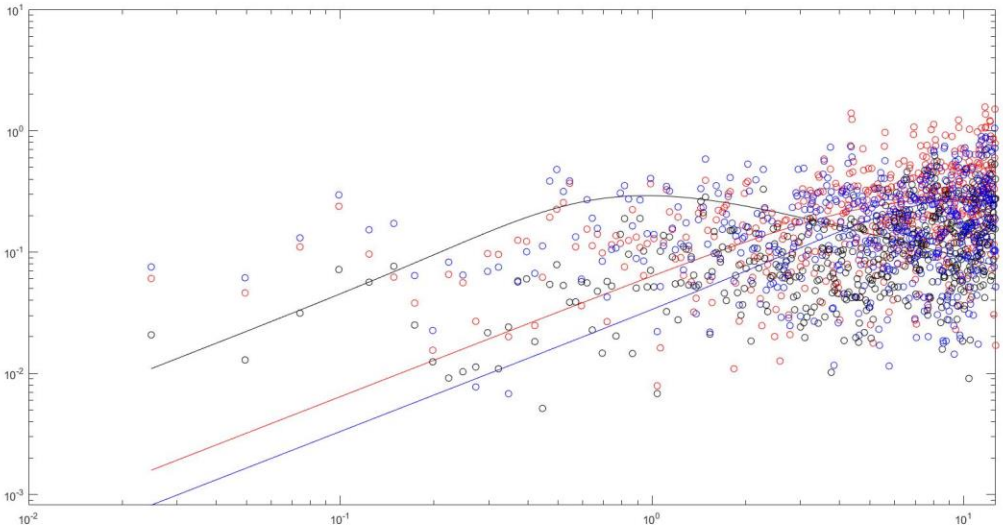

2-4-4-700

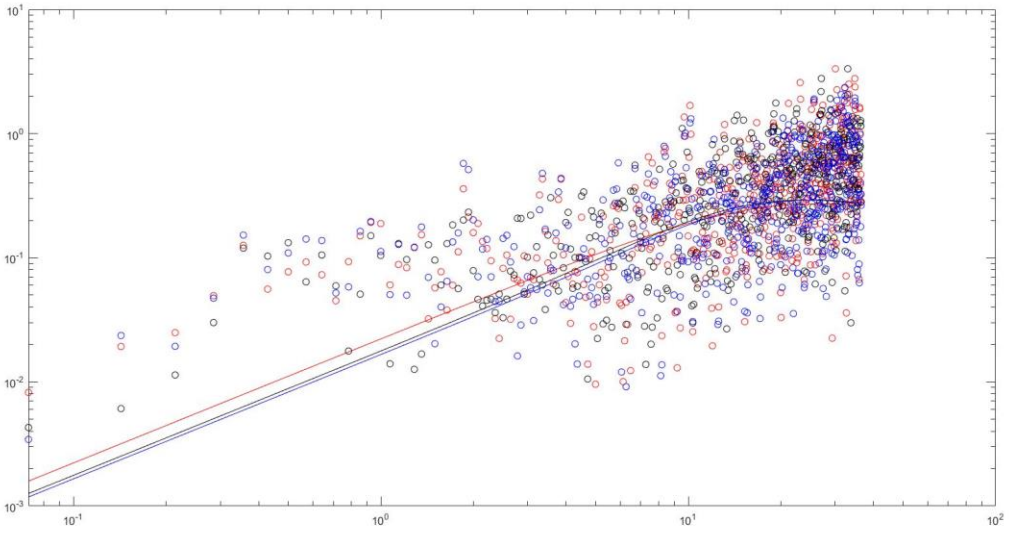

2-4-5-700

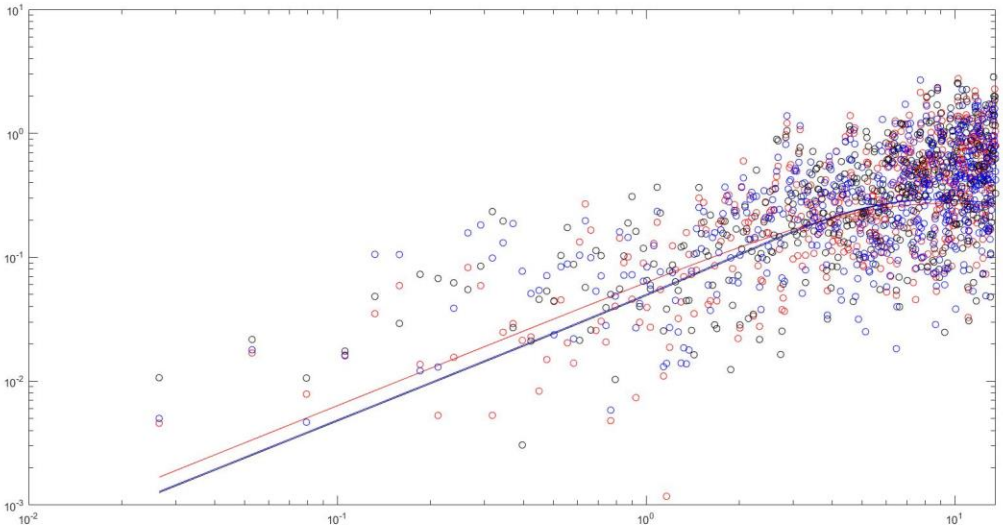

2-4-1-800

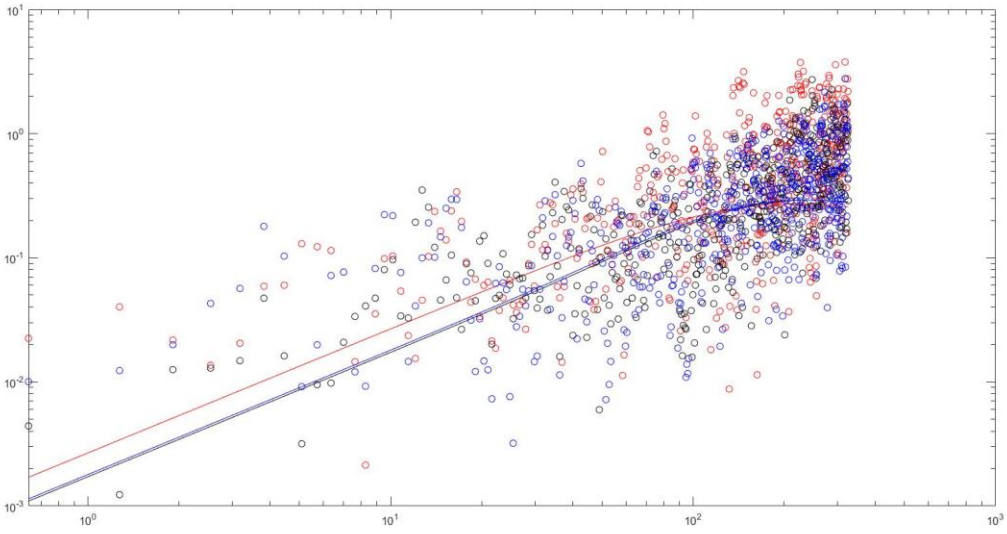

2-4-2-800

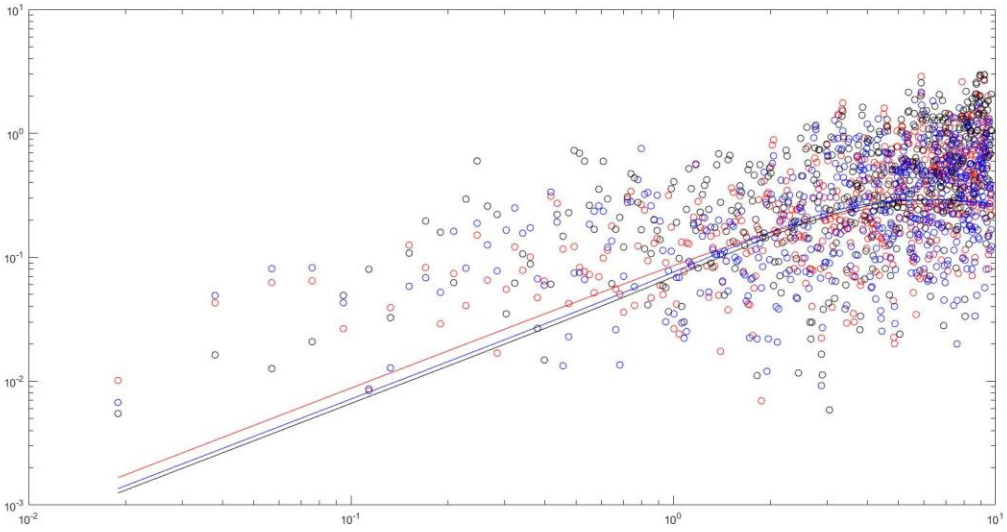

2-4-3-800

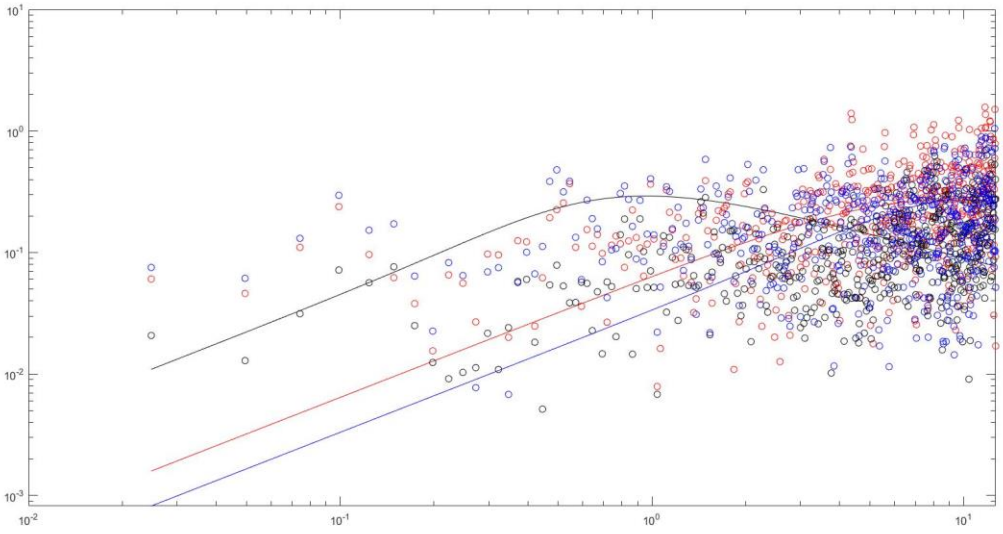

2-4-4-800

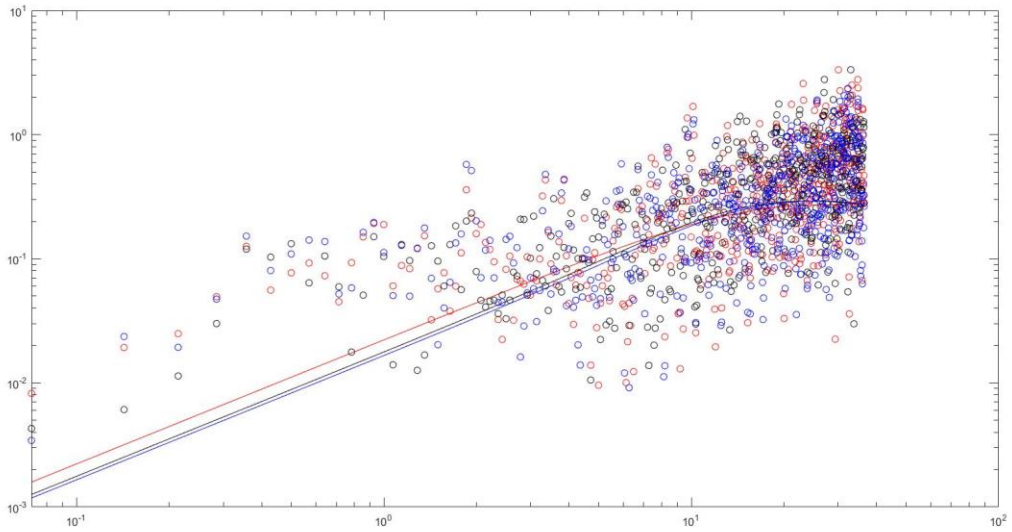

2-4-5-800

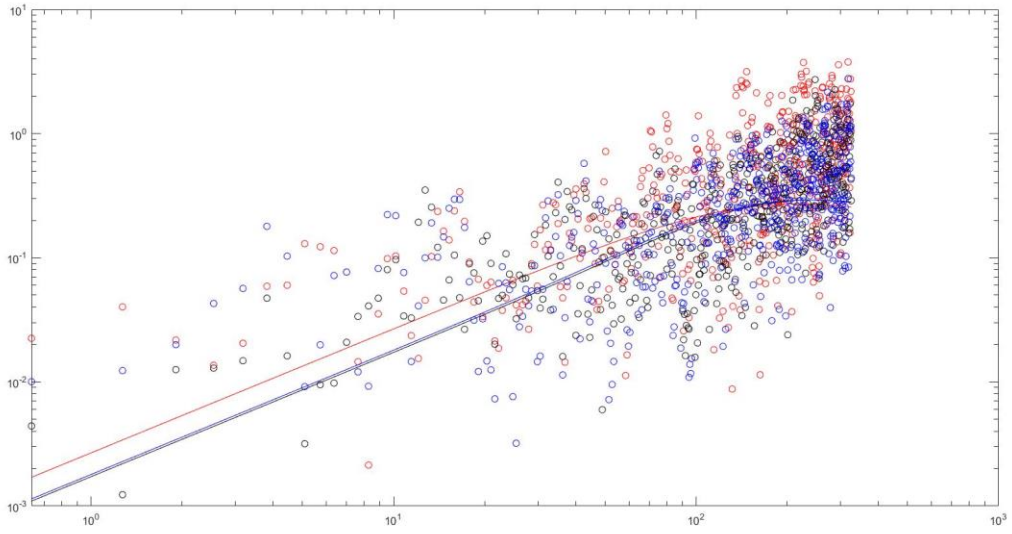

Spectra

Case 2

a-b-c-d

a=case number, b=location, c=height, d=RPM

Location 1

3-1-1-400

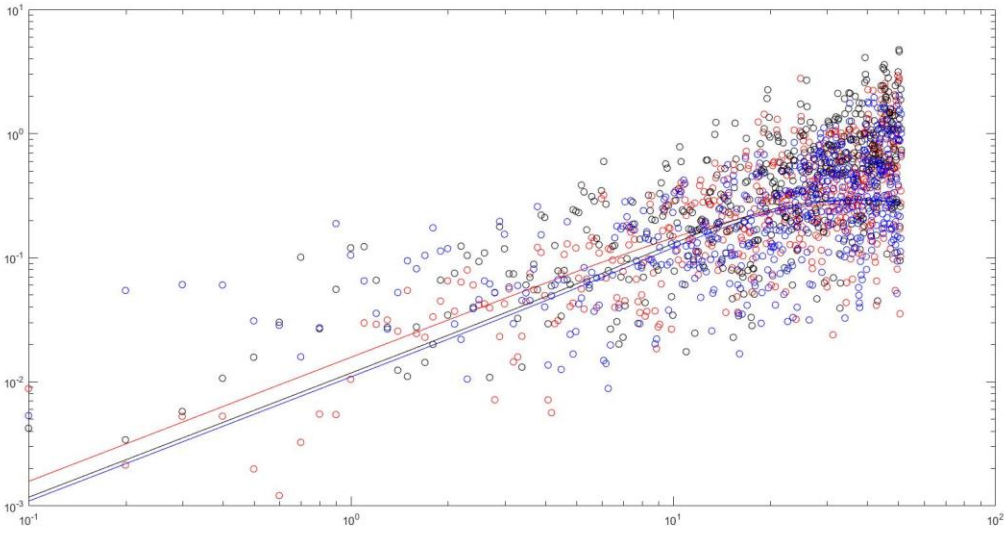

3-1-2-400

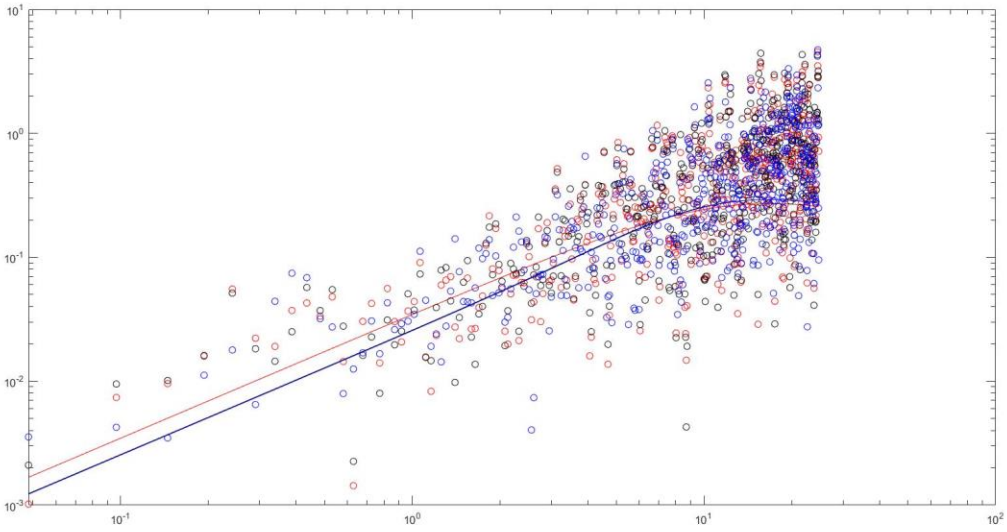

3-1-3-400

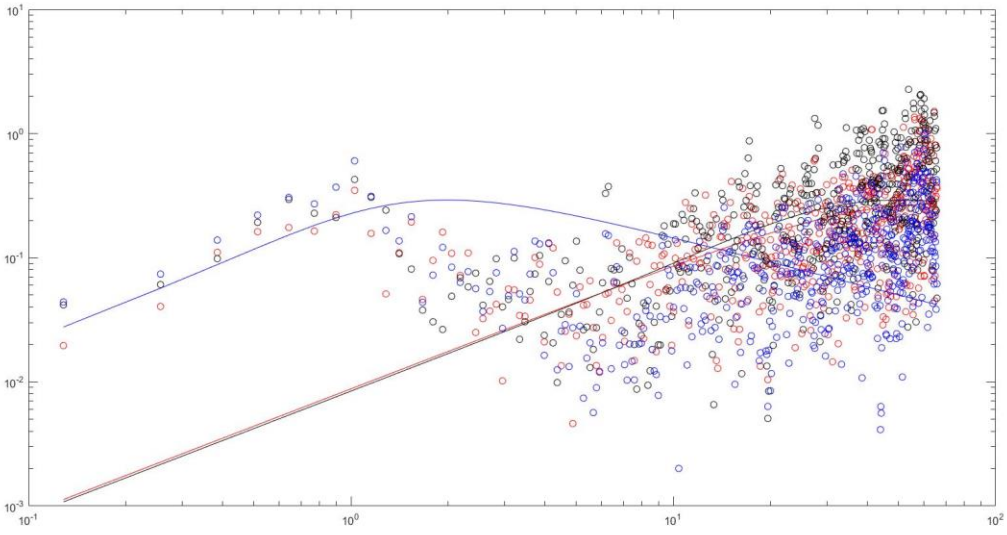

3-1-4-400

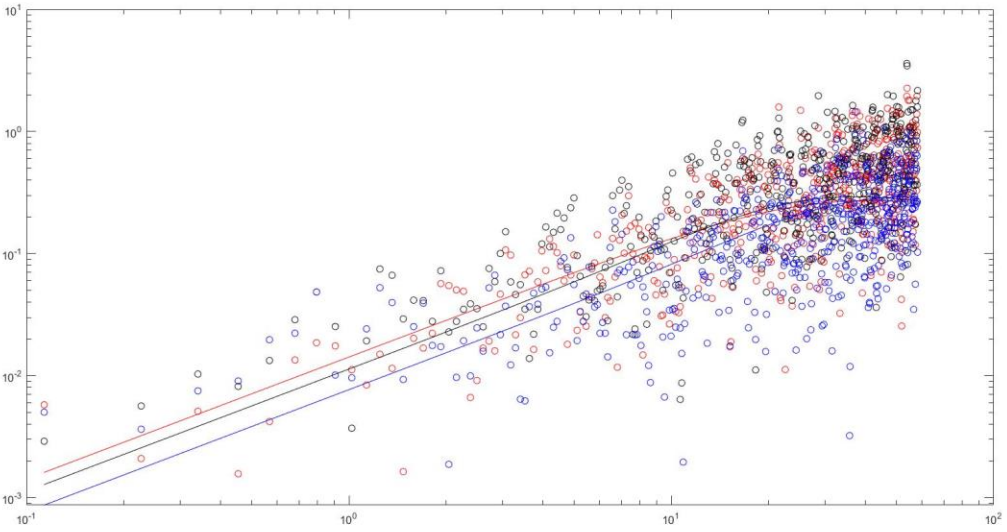

3-1-5-400

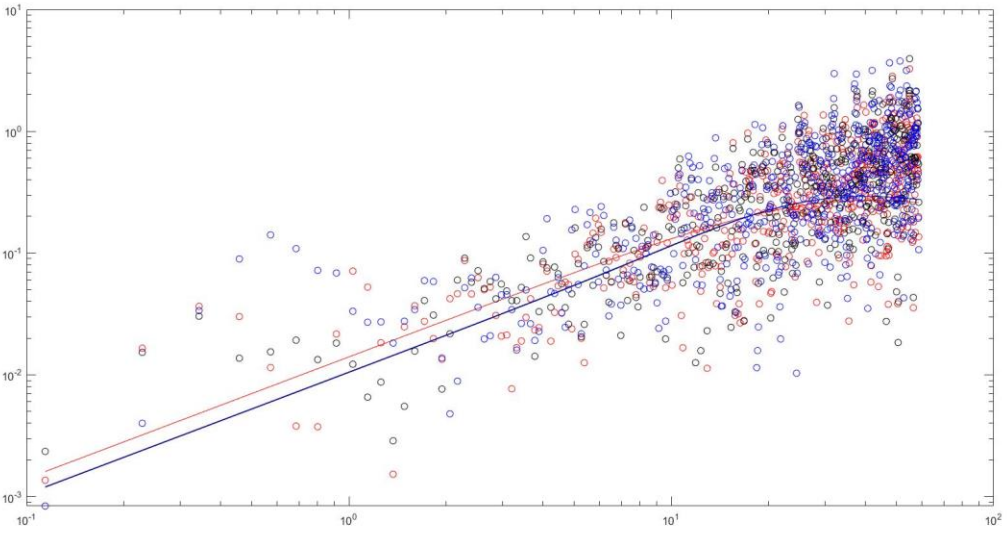

3-1-1-500

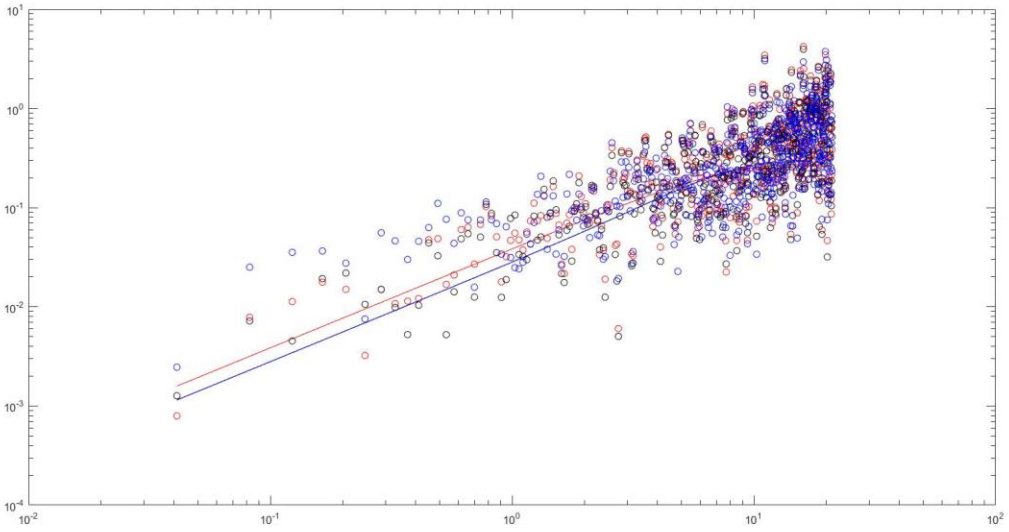

3-1-2-500

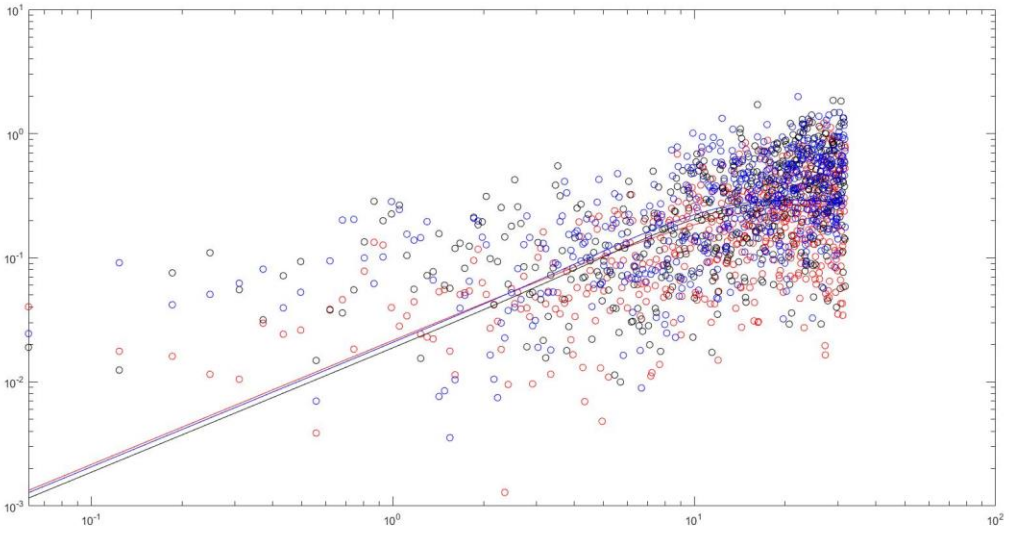

3-1-3-500

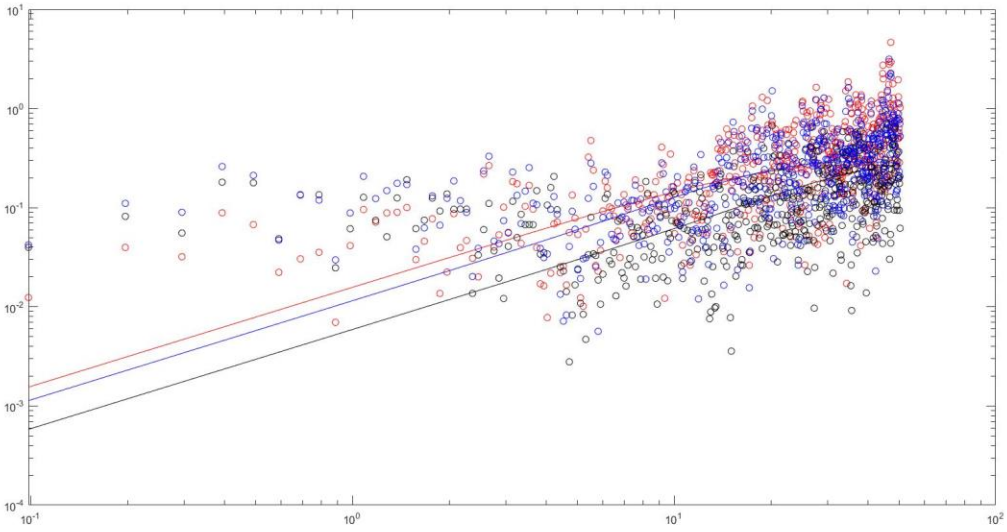

3-1-4-500

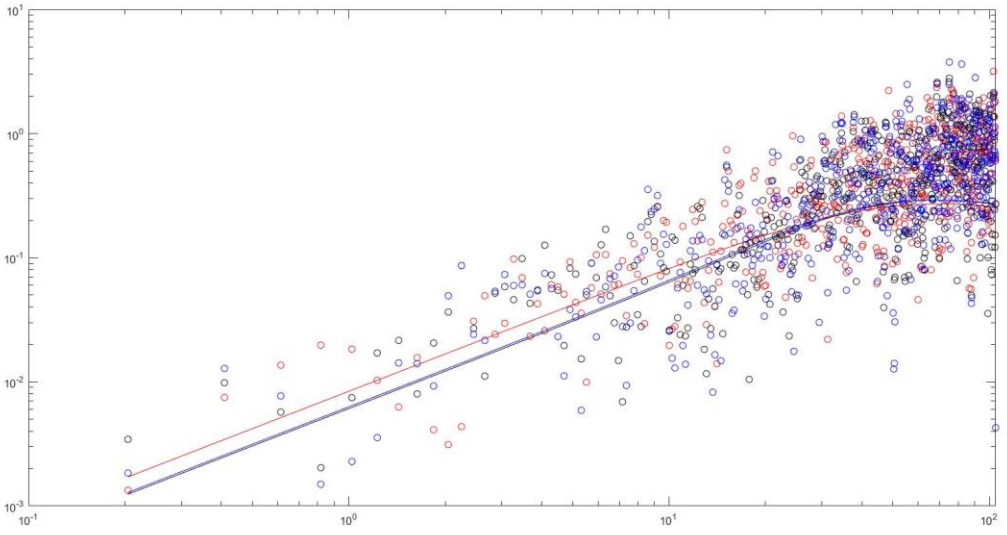

3-1-5-500

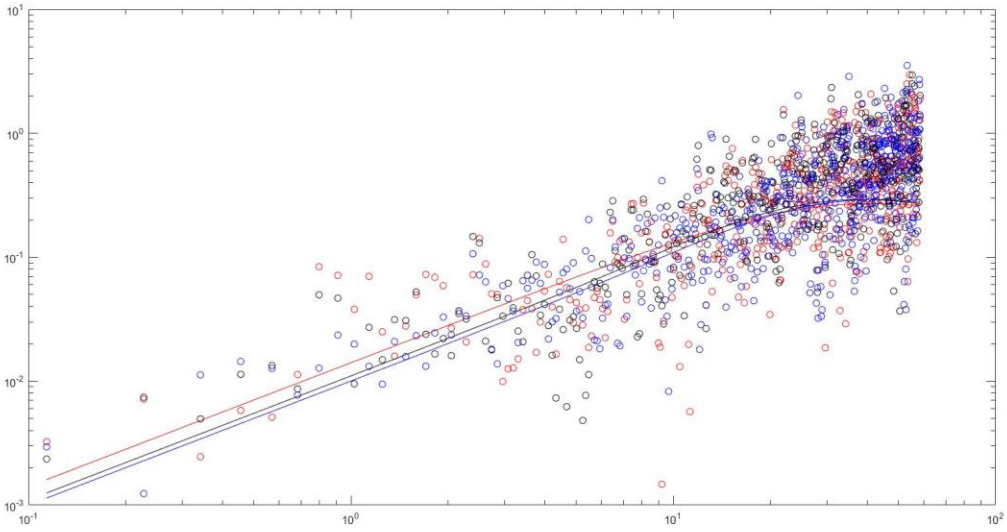

3-1-1-600

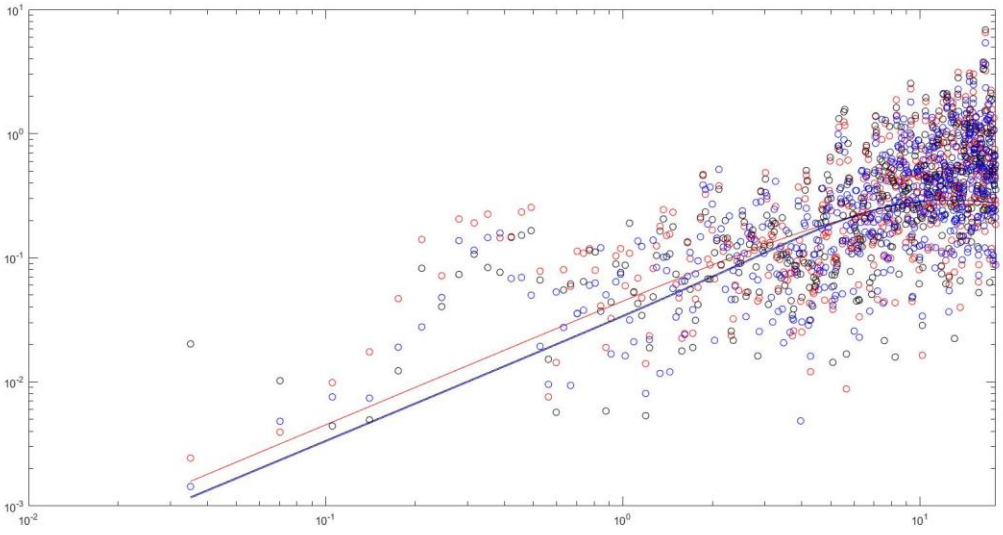

3-1-2-600

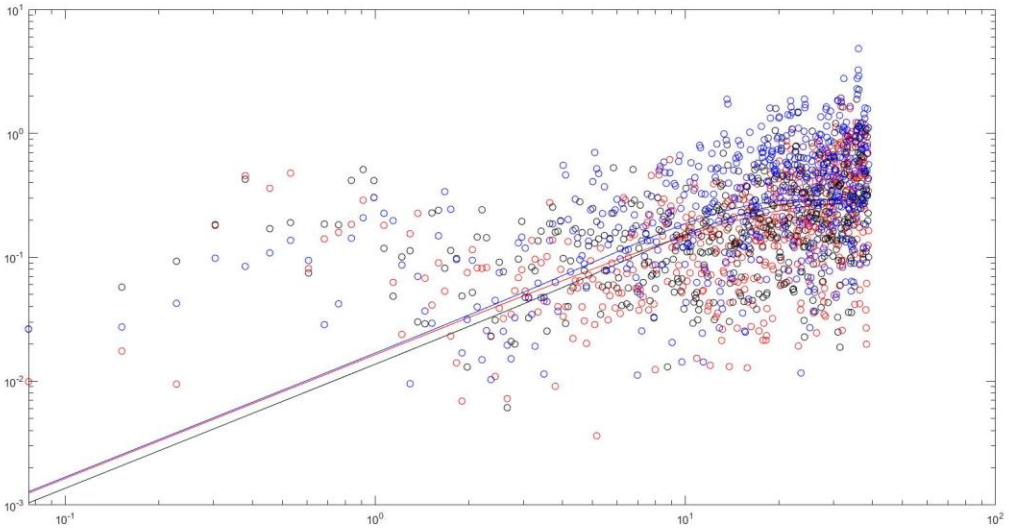

3-1-3-600

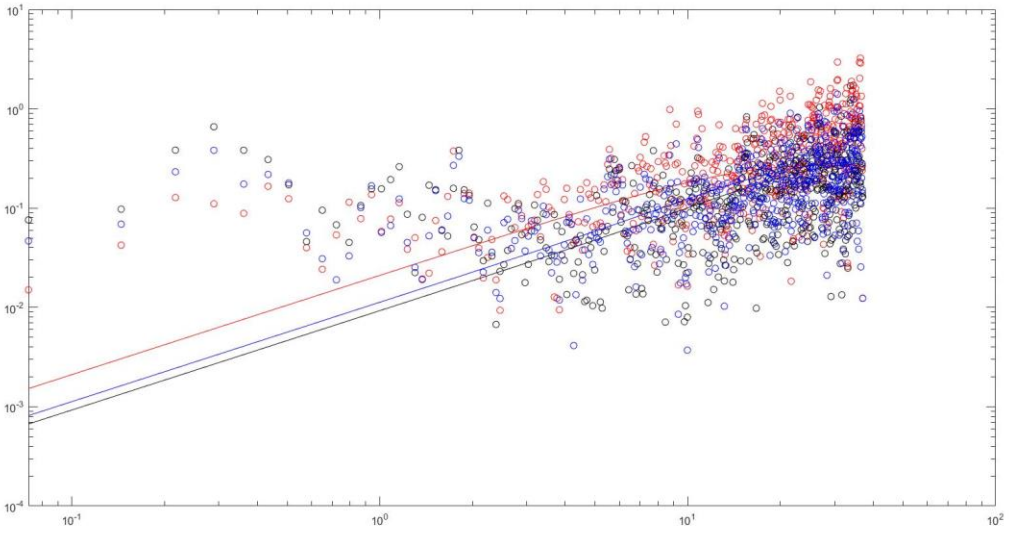

3-1-4-600

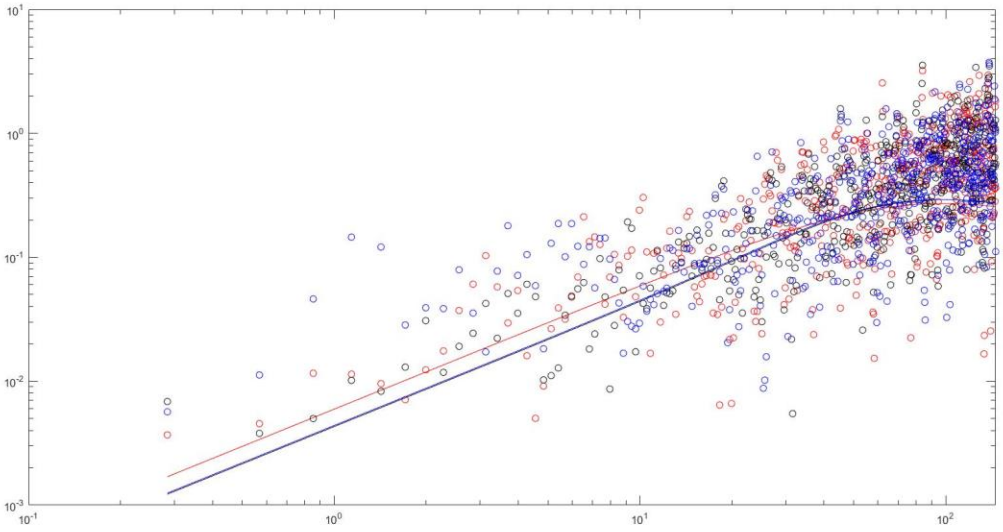

3-1-5-600

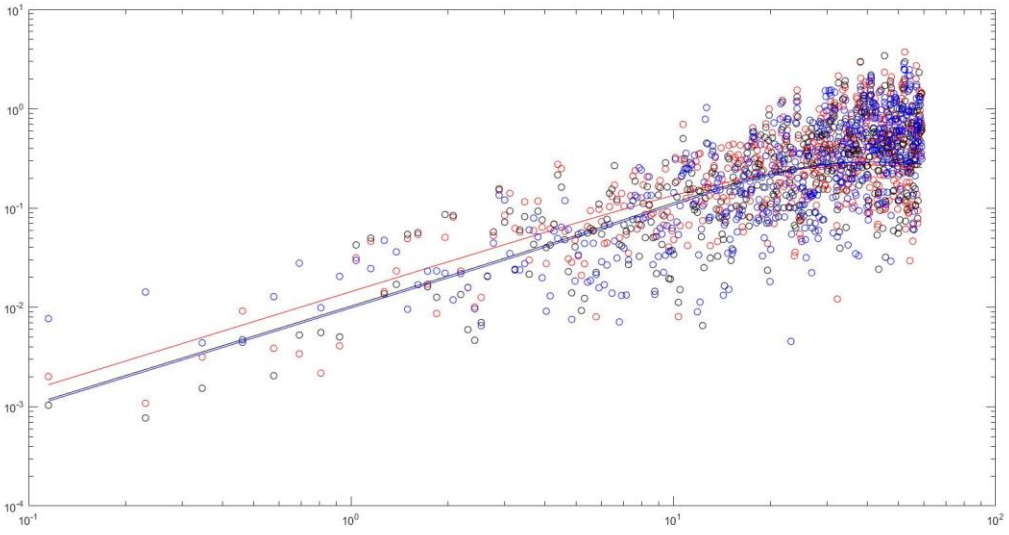

3-1-1-700

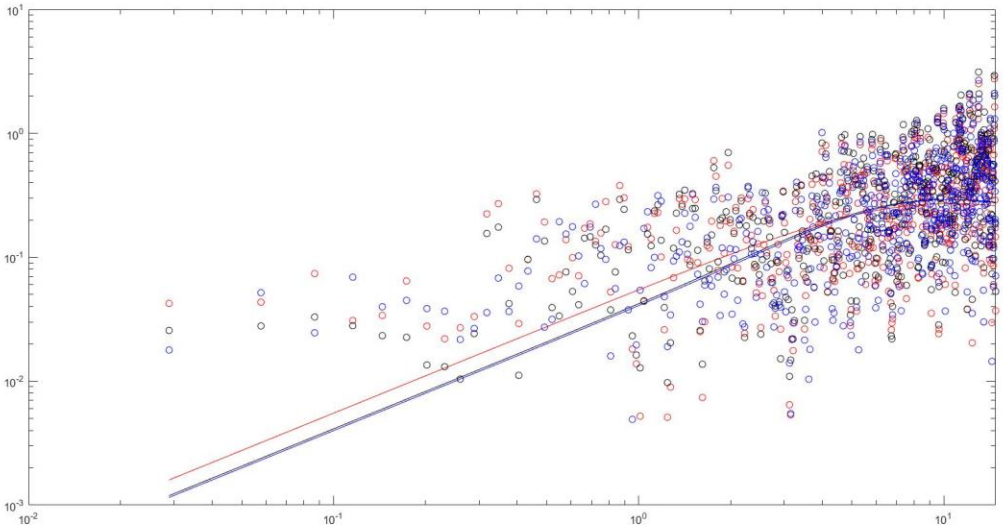

3-1-2-700

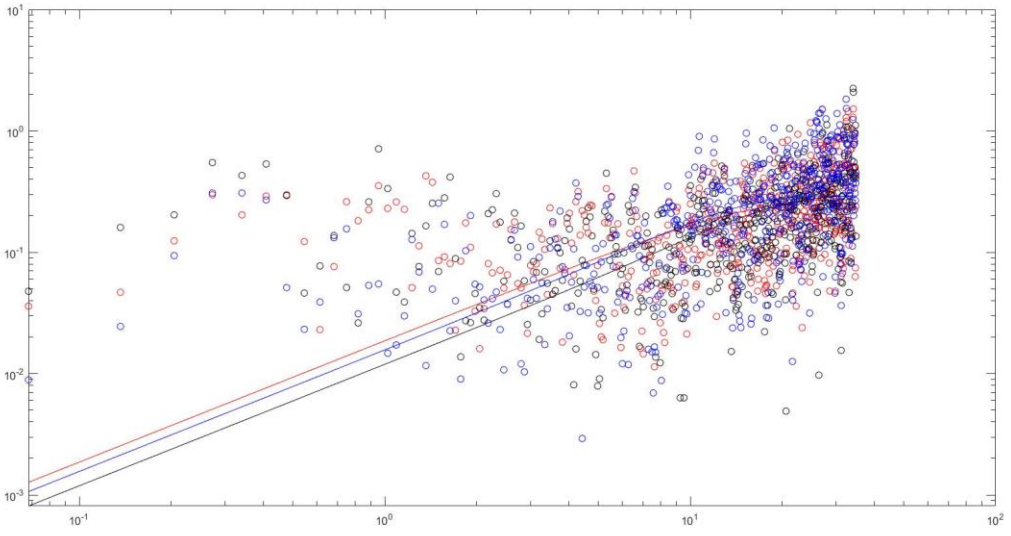

3-1-3-700

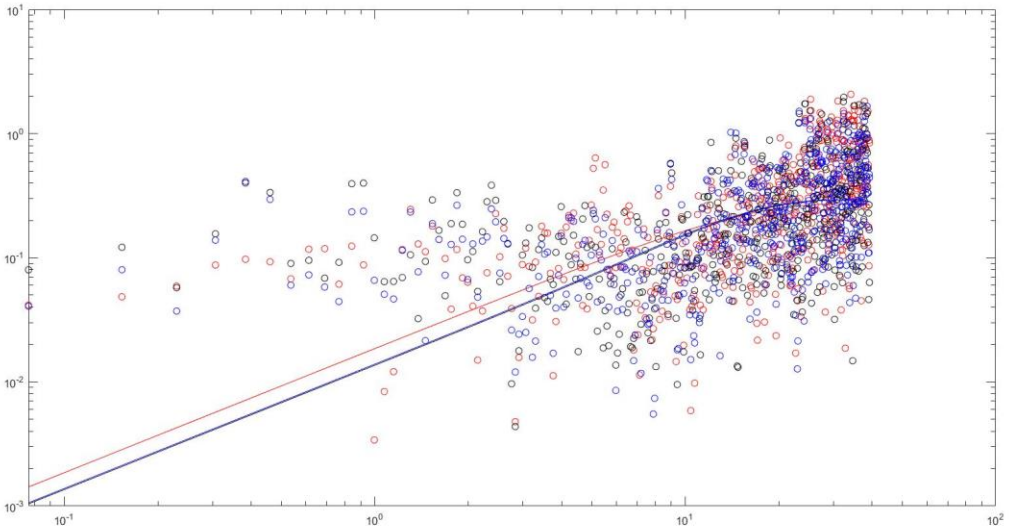

3-1-4-700

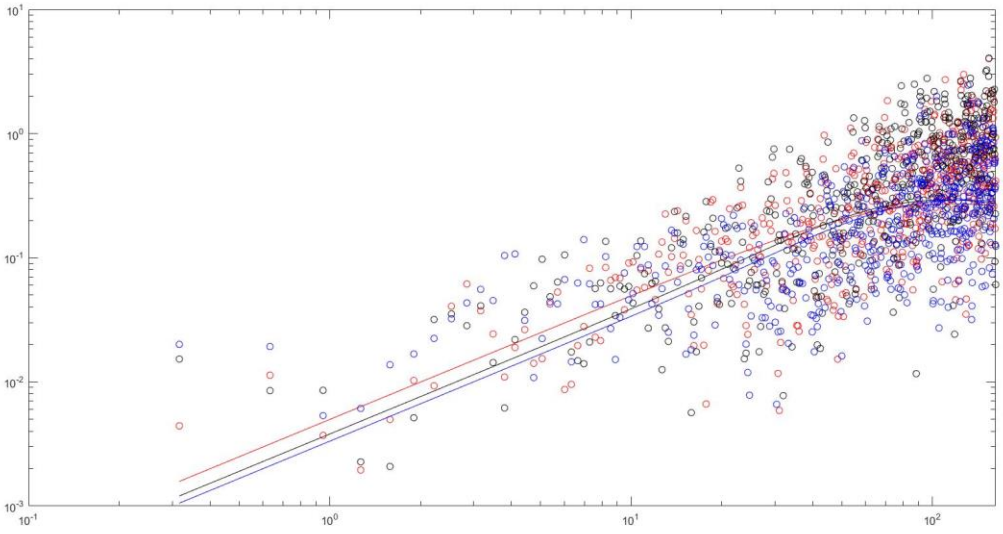

3-1-5-700

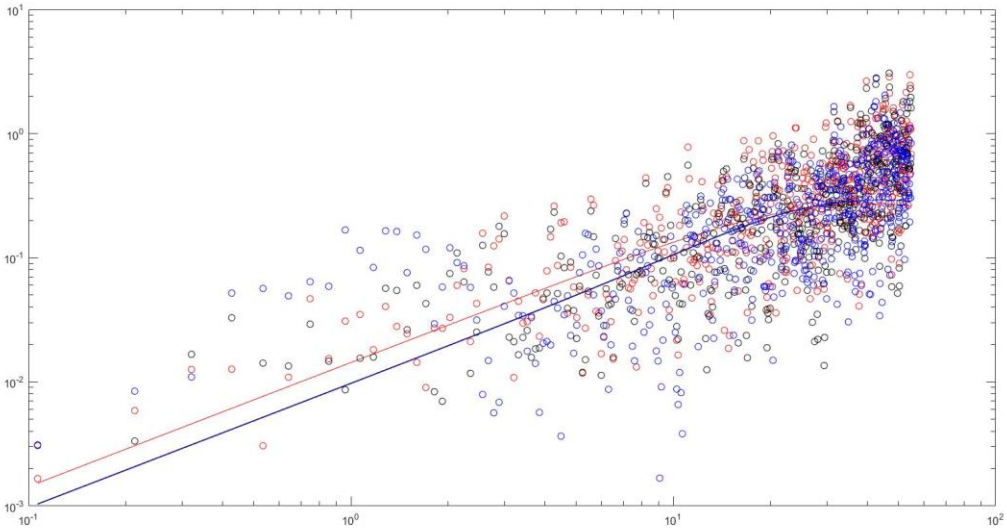

3-1-1-800

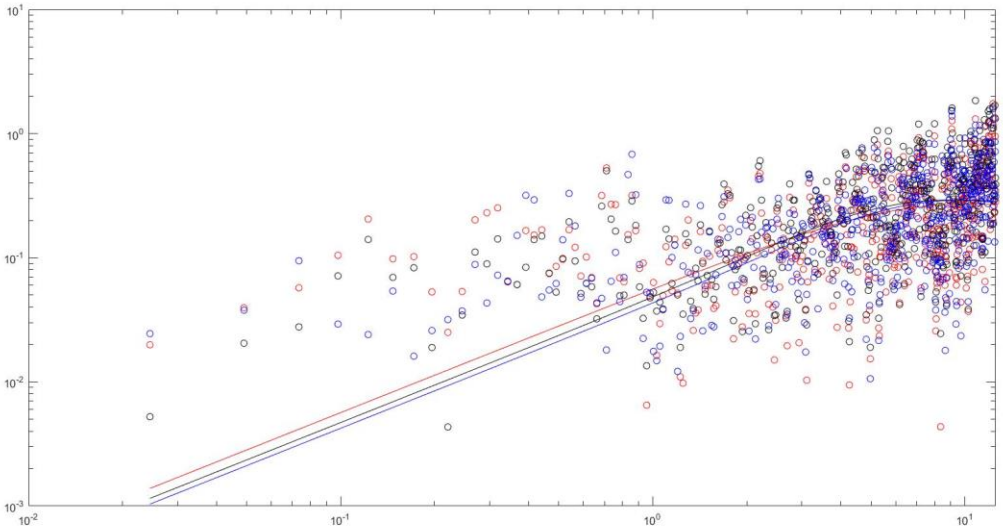

3-1-2-800

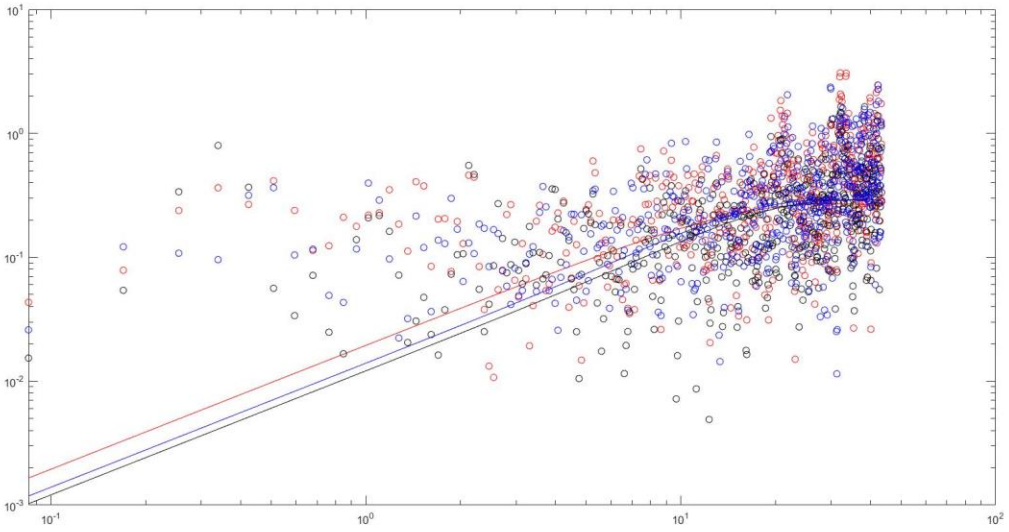

3-1-3-800

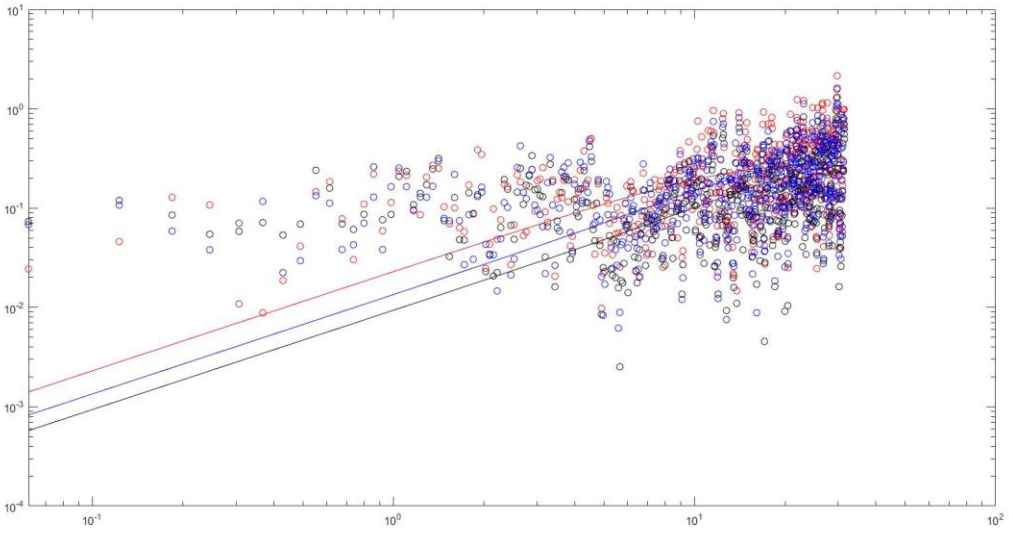

3-1-4-800

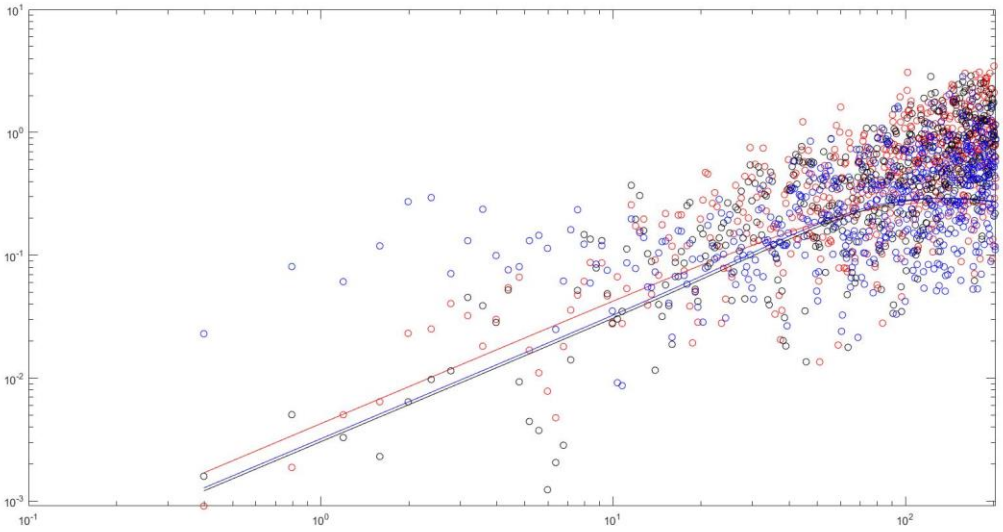


3-1-5-800

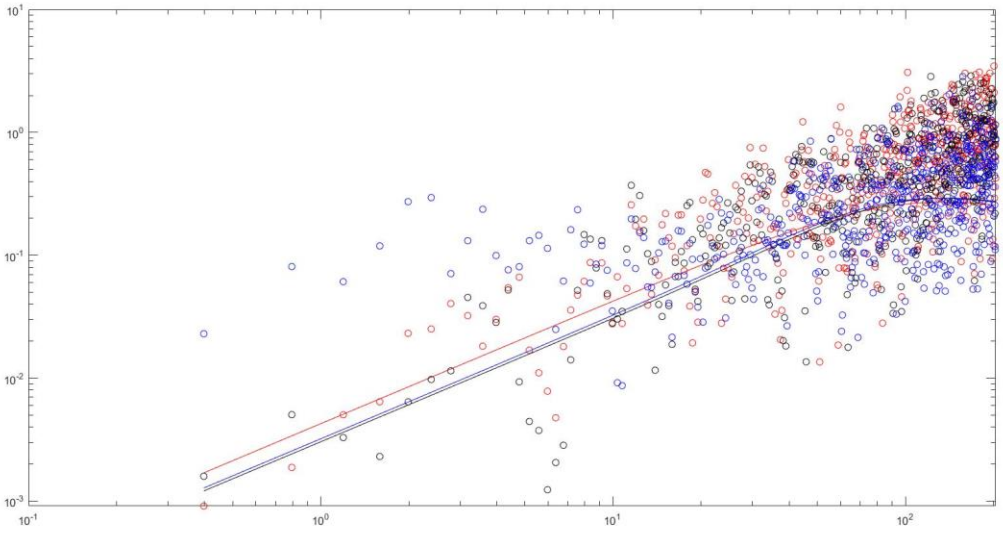


Location 2

3-2-1-400

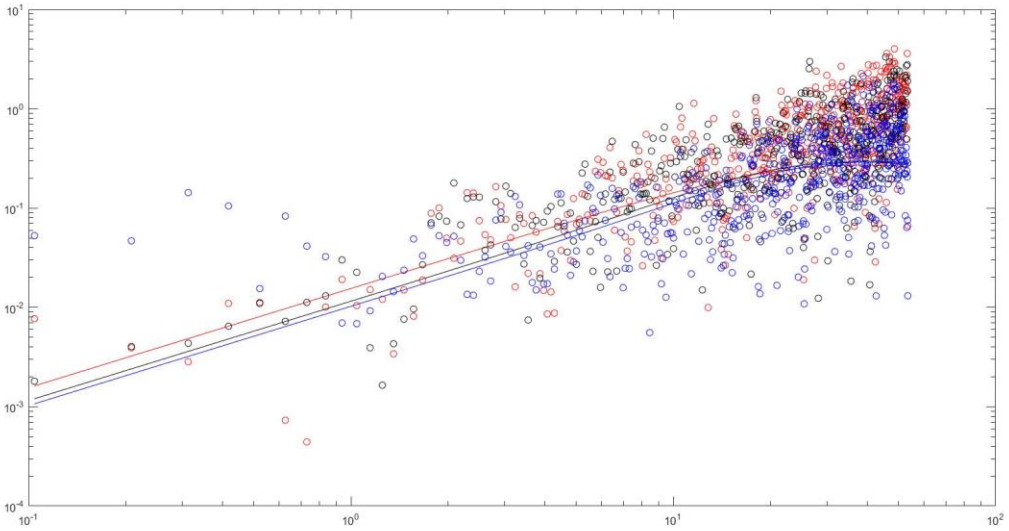

3-2-3-400

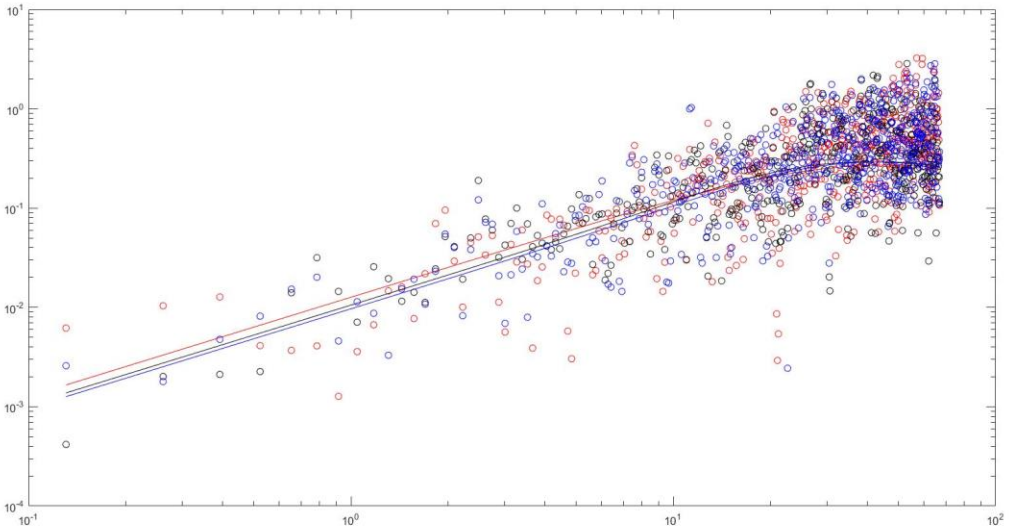

3-2-4-400

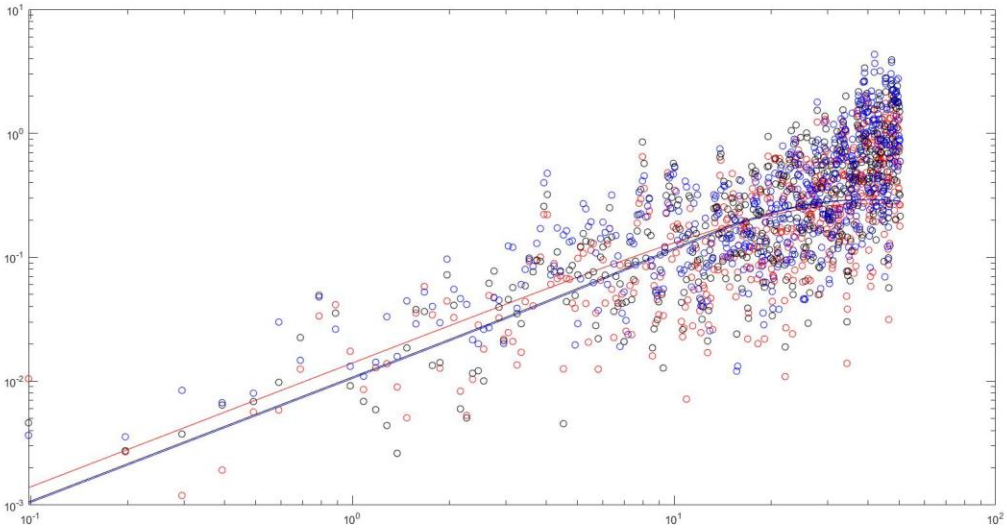

3-2-5-400

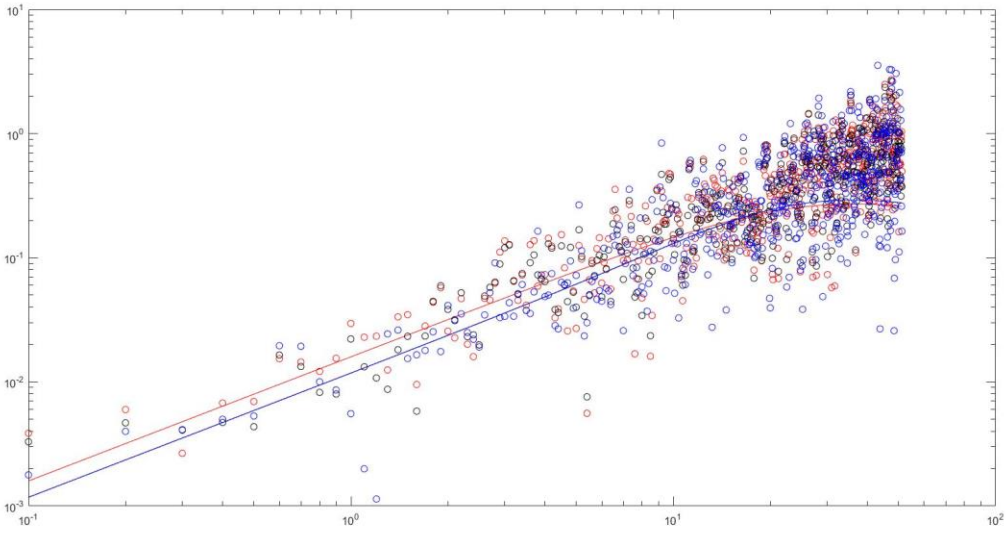

3-2-1-500

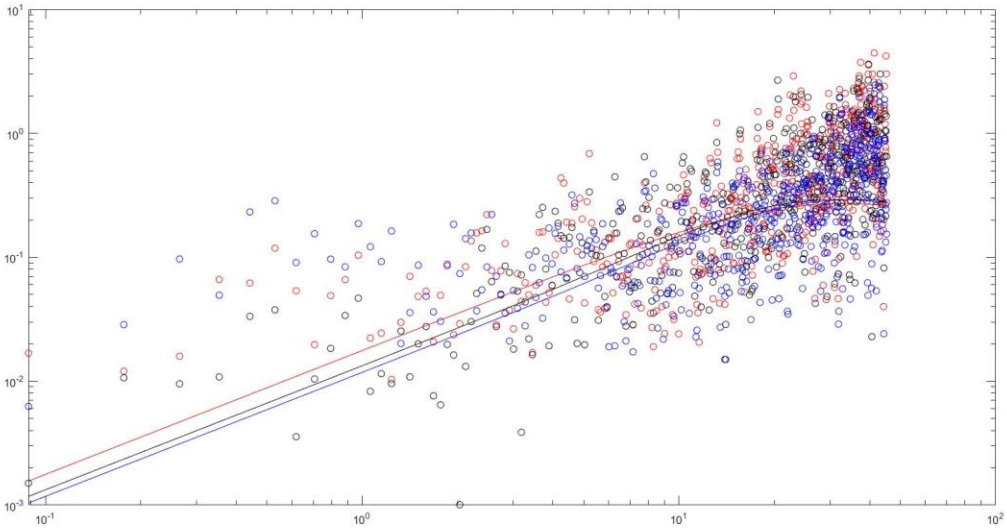

3-2-2-500

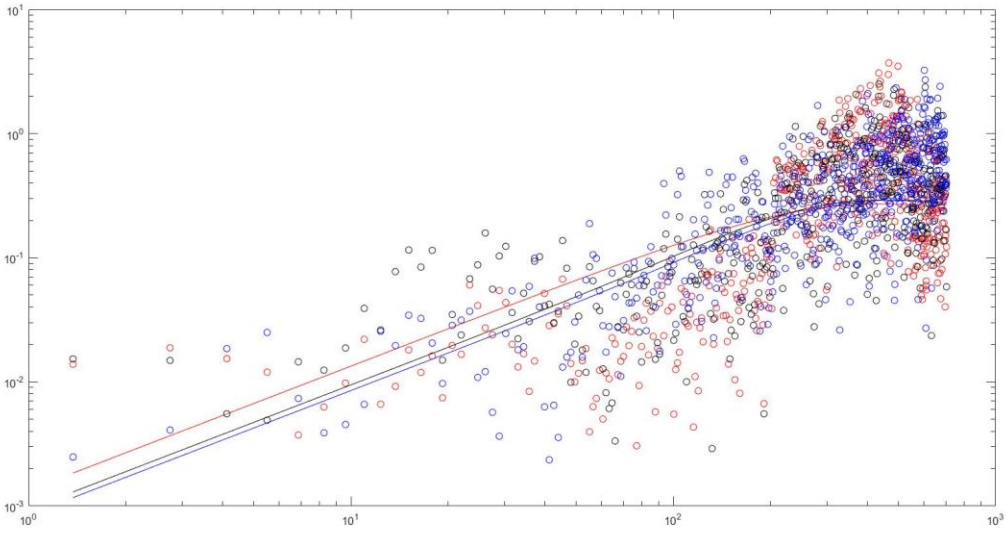

3-2-3-500

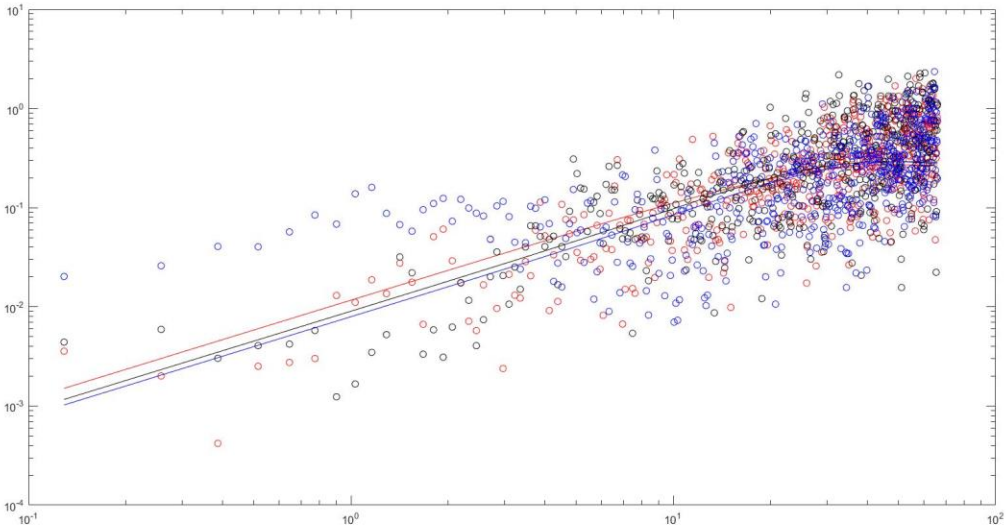

3-2-4-500

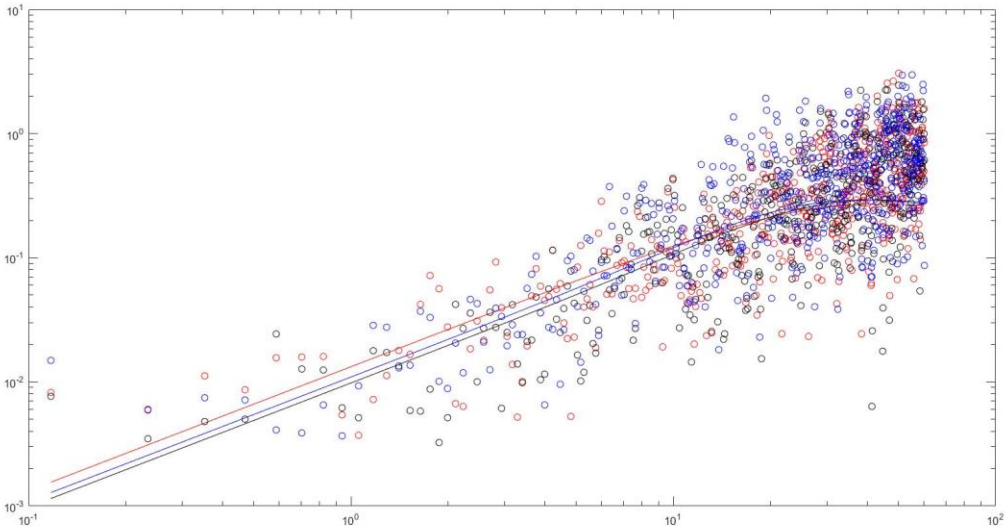

3-2-5-500

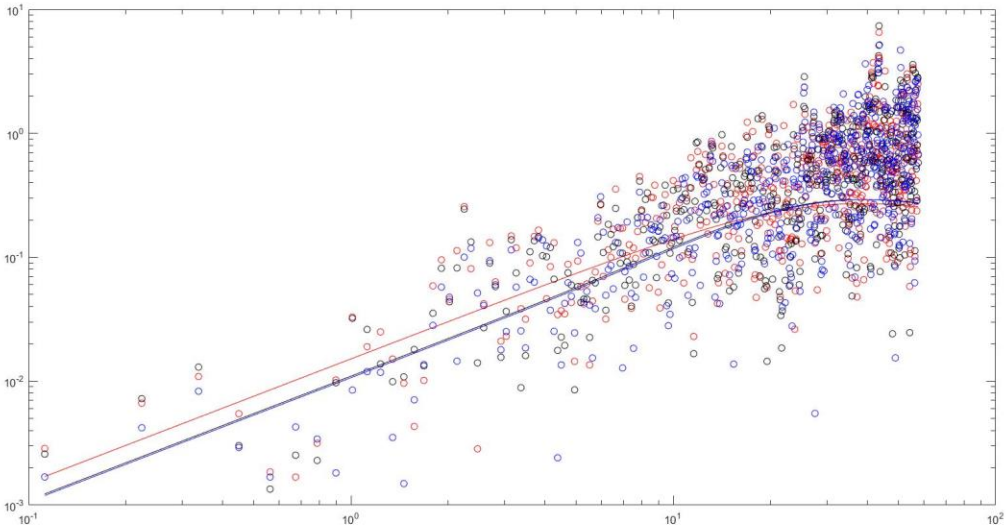

3-2-1-600

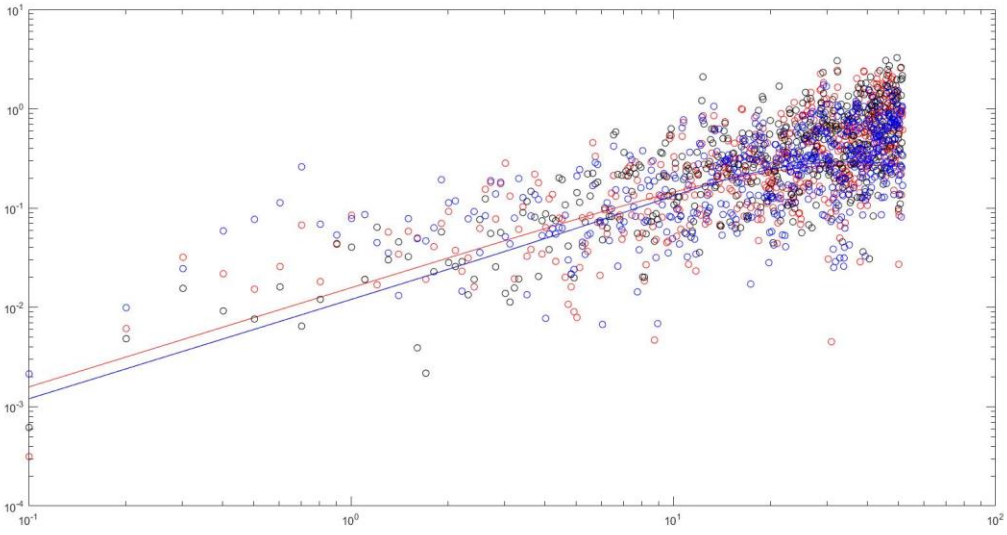

3-2-3-600

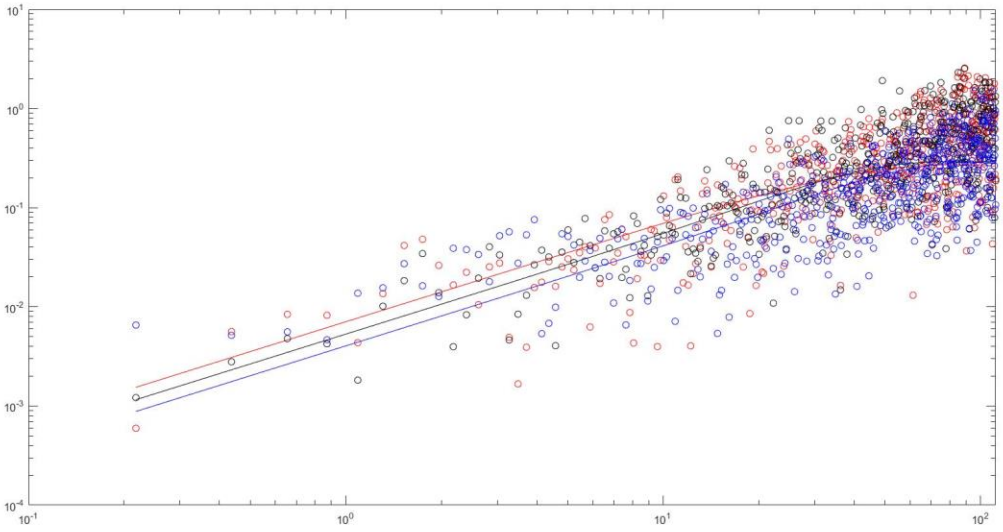

3-2-4-600

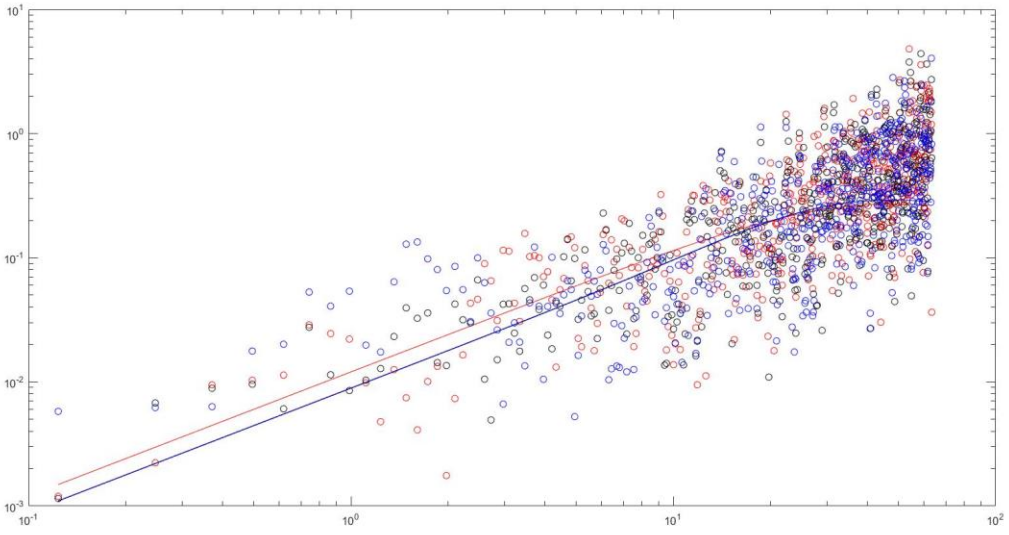

3-2-5-600

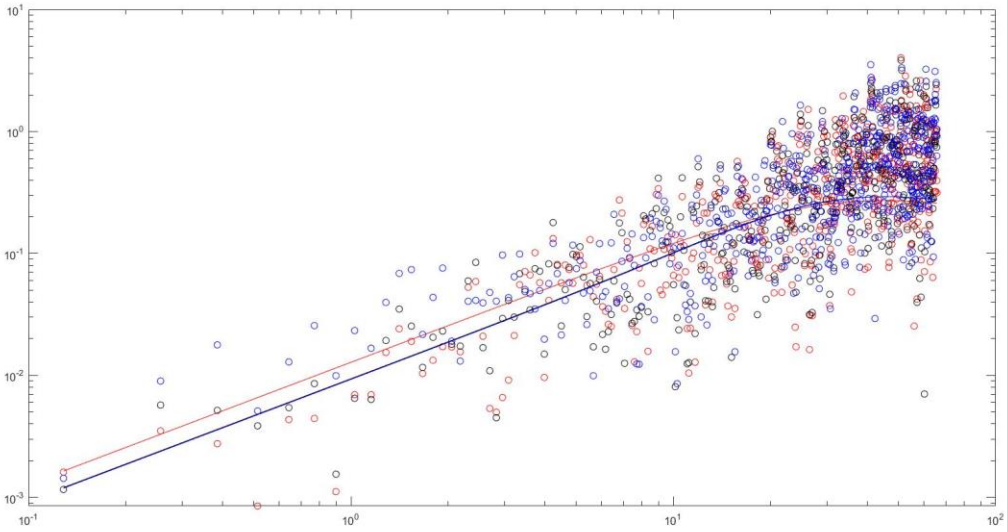

3-2-1-700

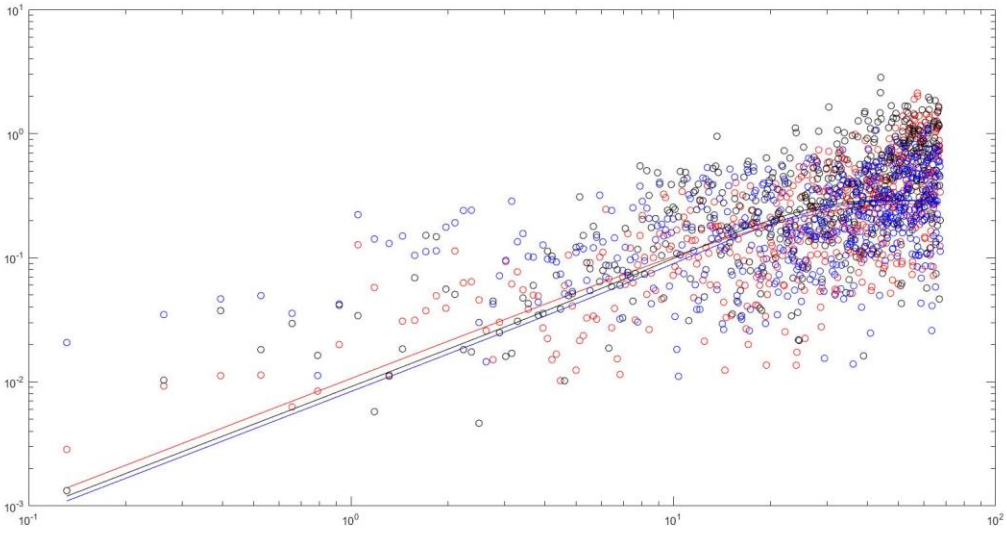

3-2-3-700

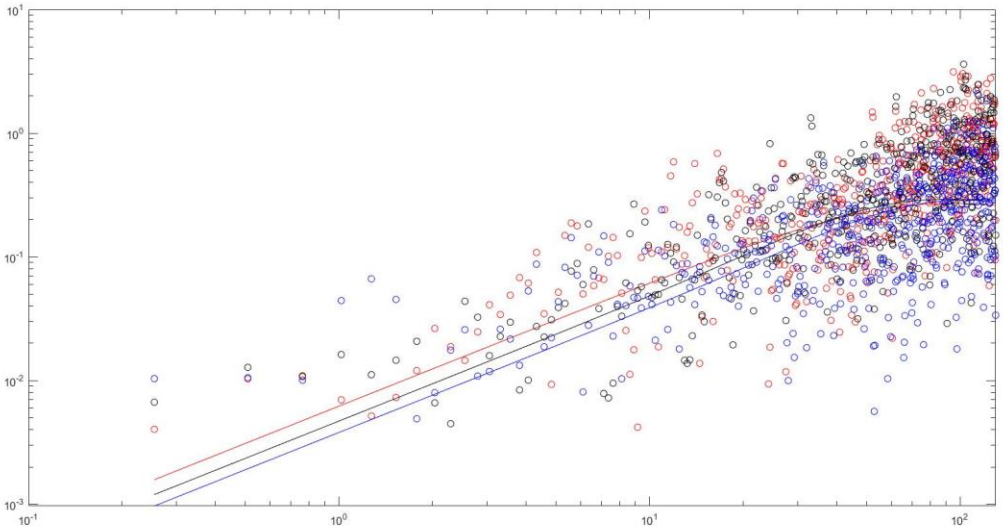

3-2-4-700

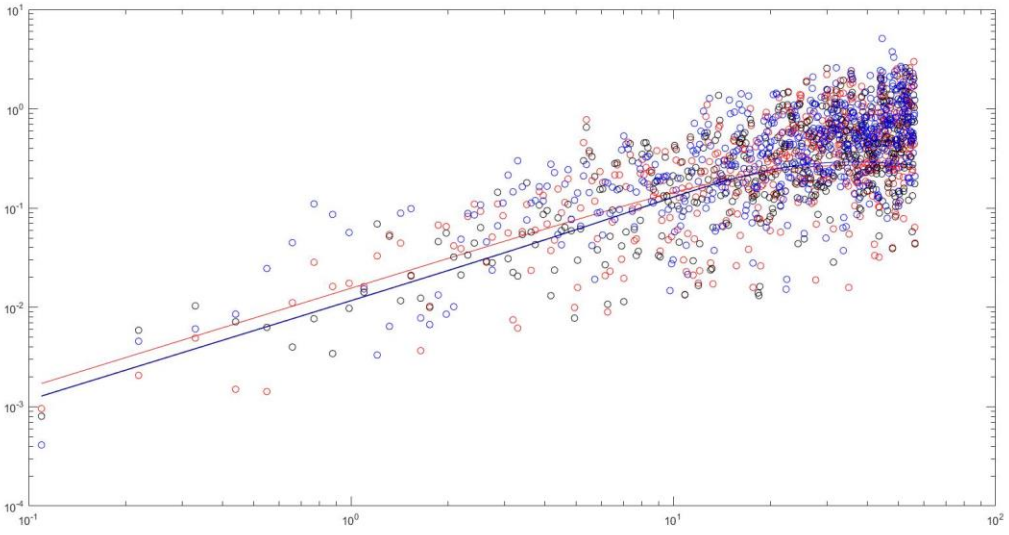

3-2-5-700

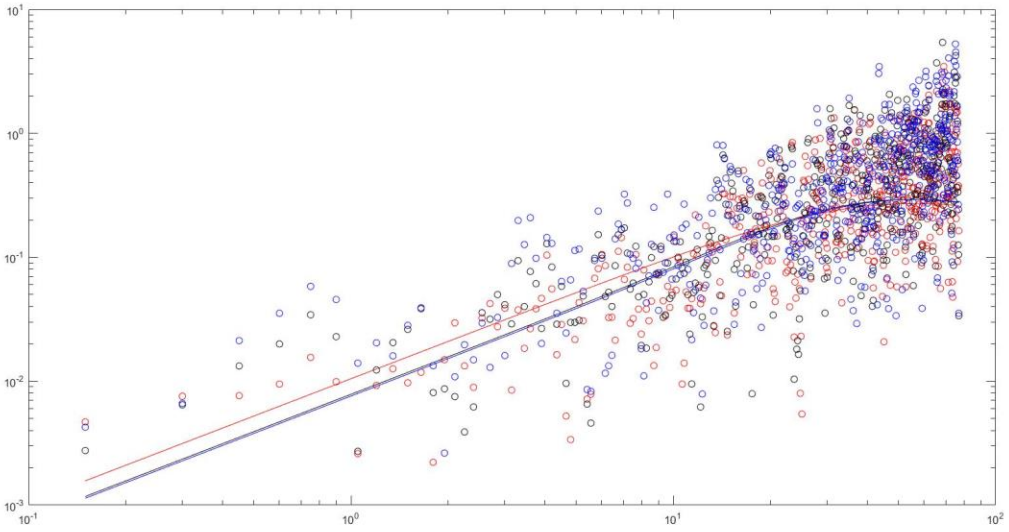

3-2-1-800

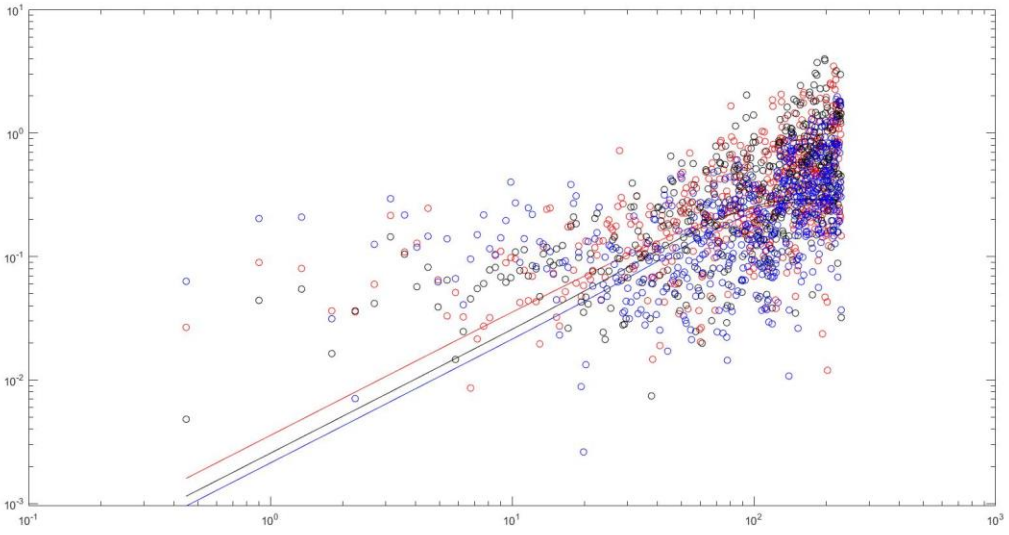

3-2-3-800

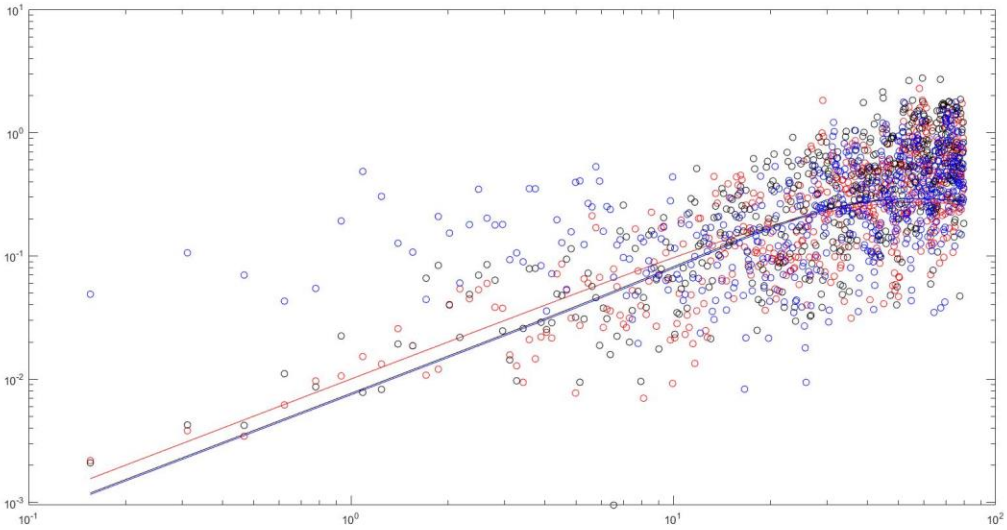

3-2-4-800

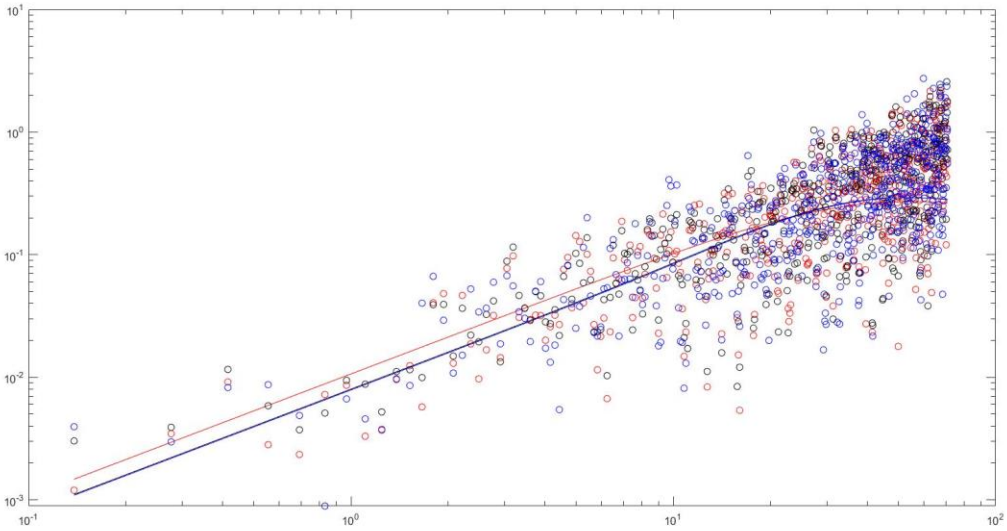

3-2-5-800

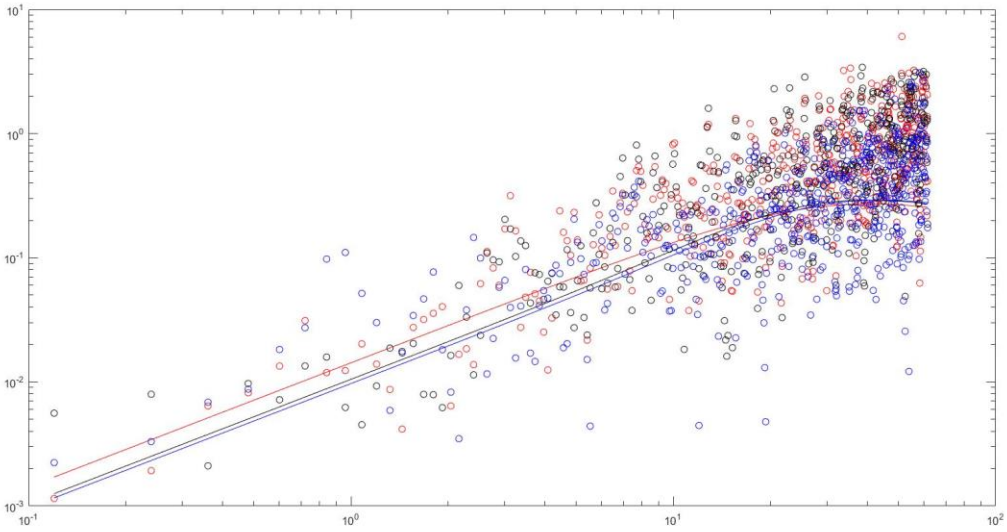

Location 3

3-3-1-400

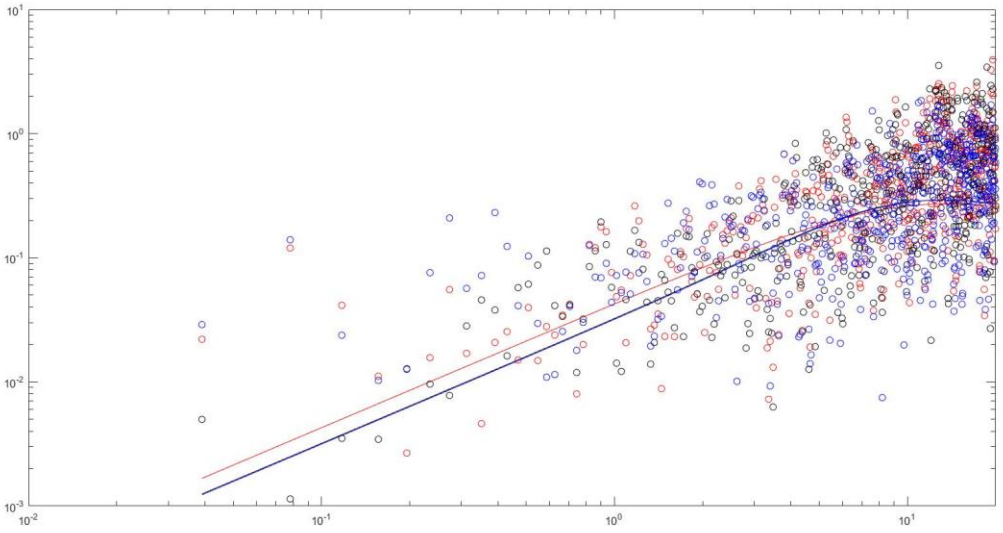

3-3-2-400

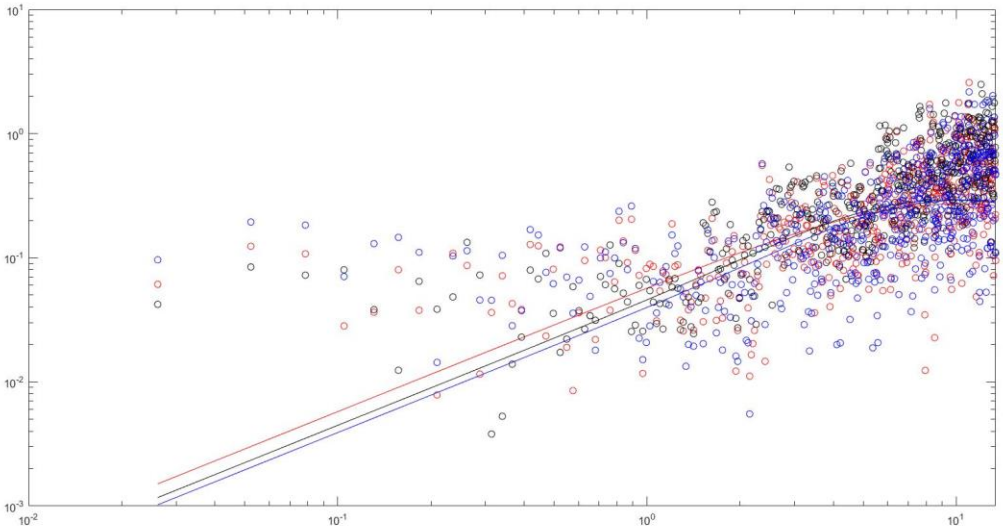

3-3-3-400

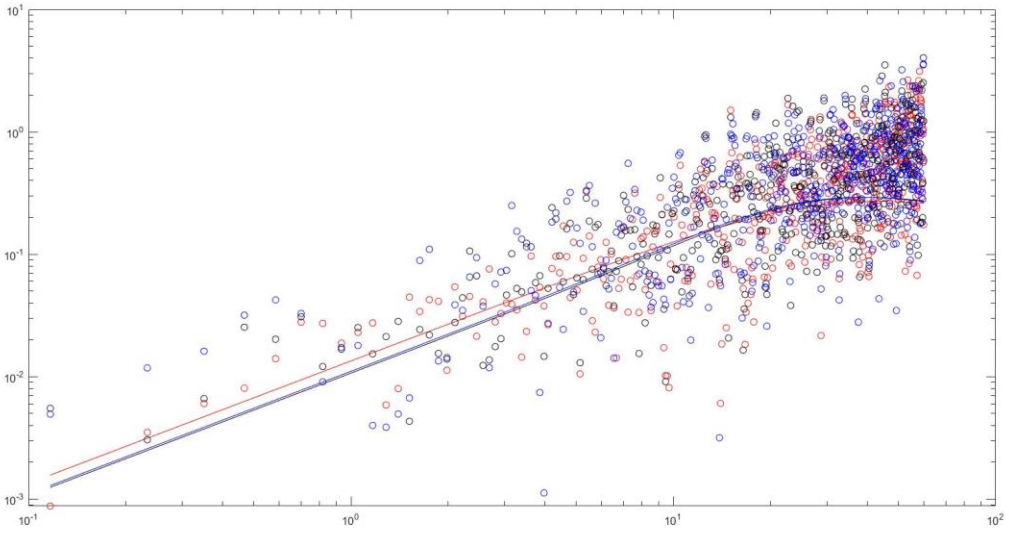

3-3-4-400

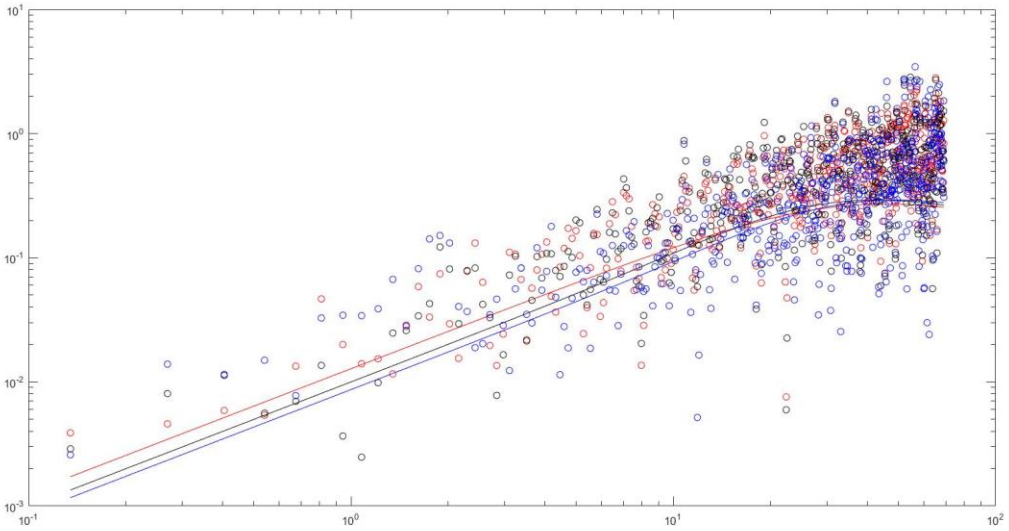

3-3-5-400

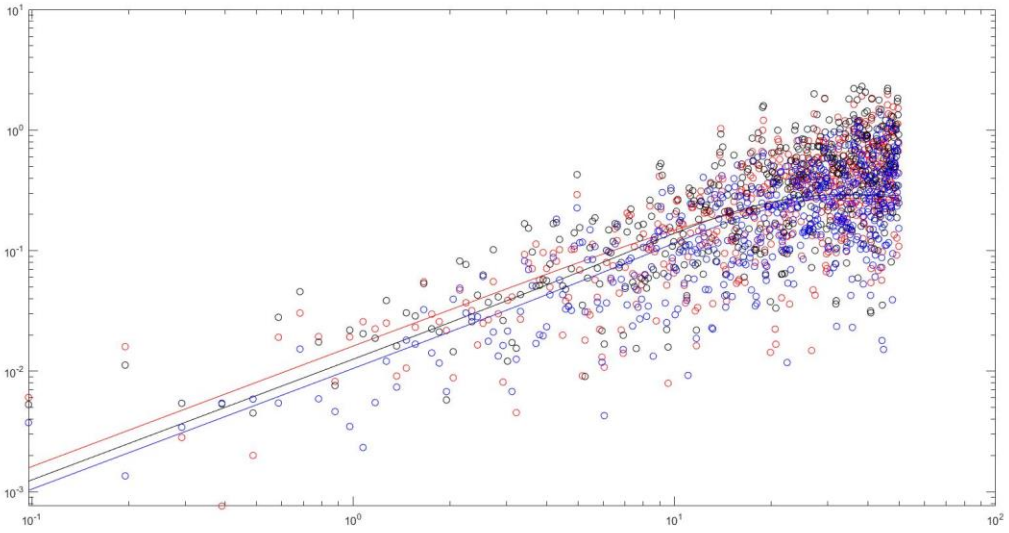

3-3-1-500

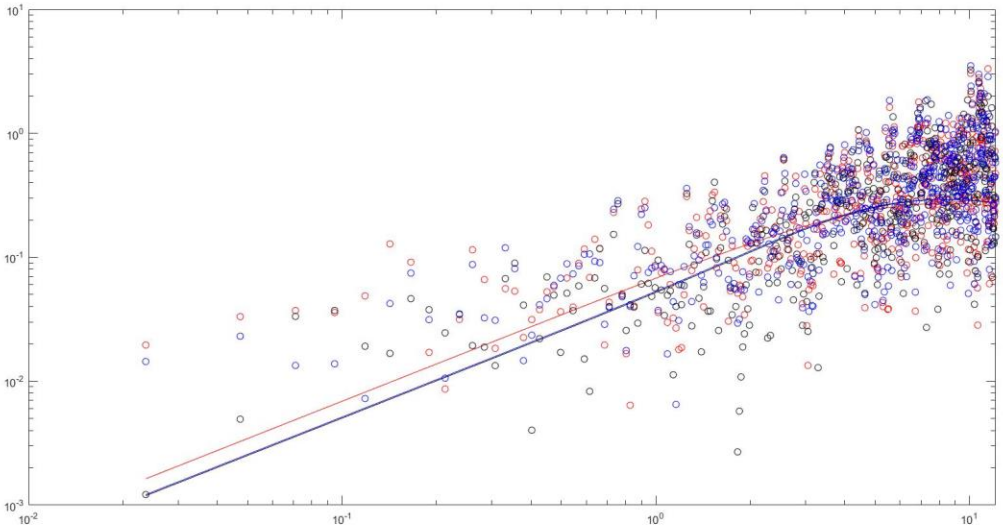

3-3-2-500

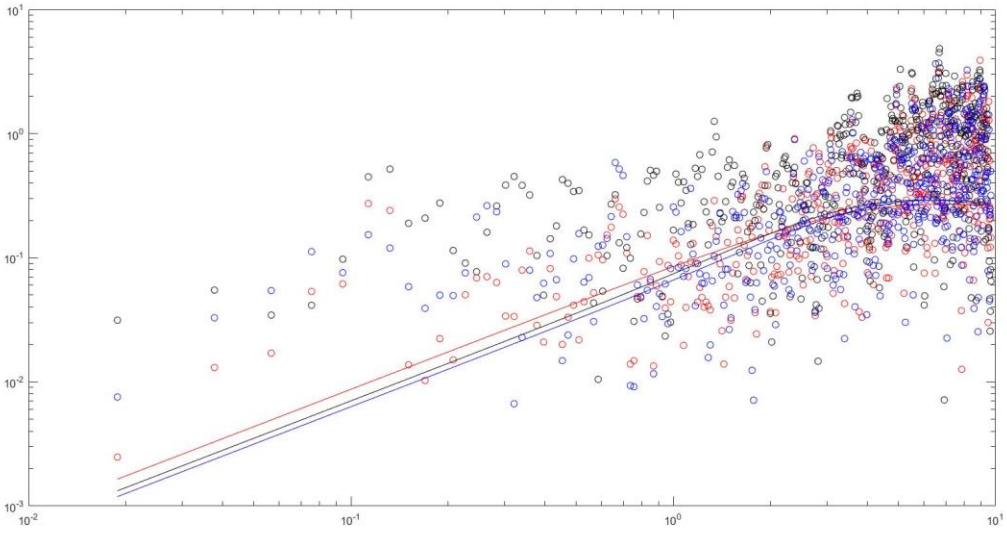

3-3-3-500

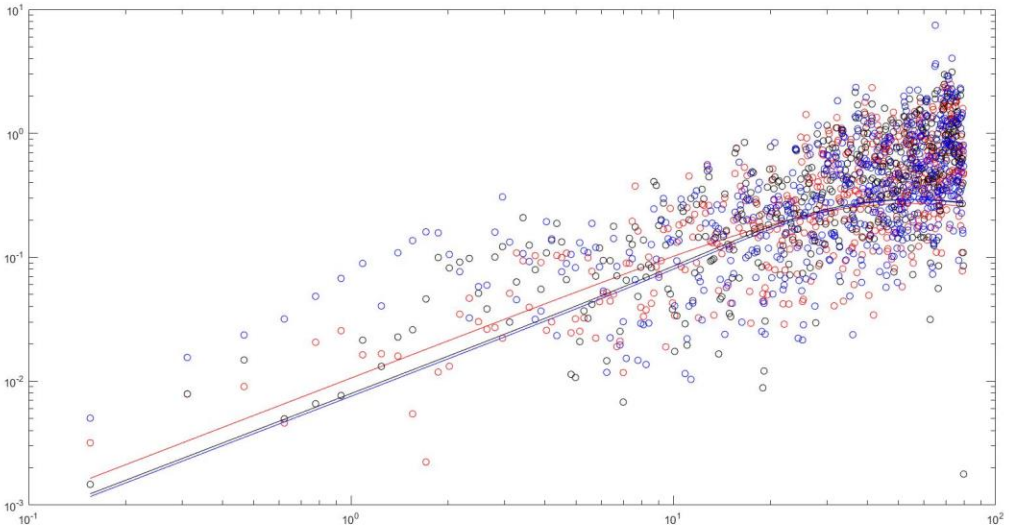

3-3-4-500

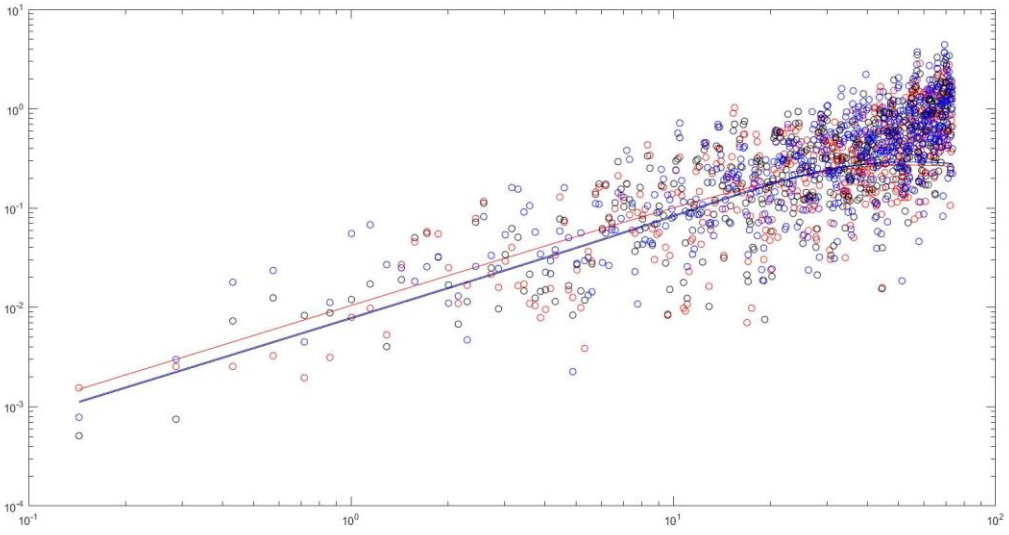

3-3-5-500

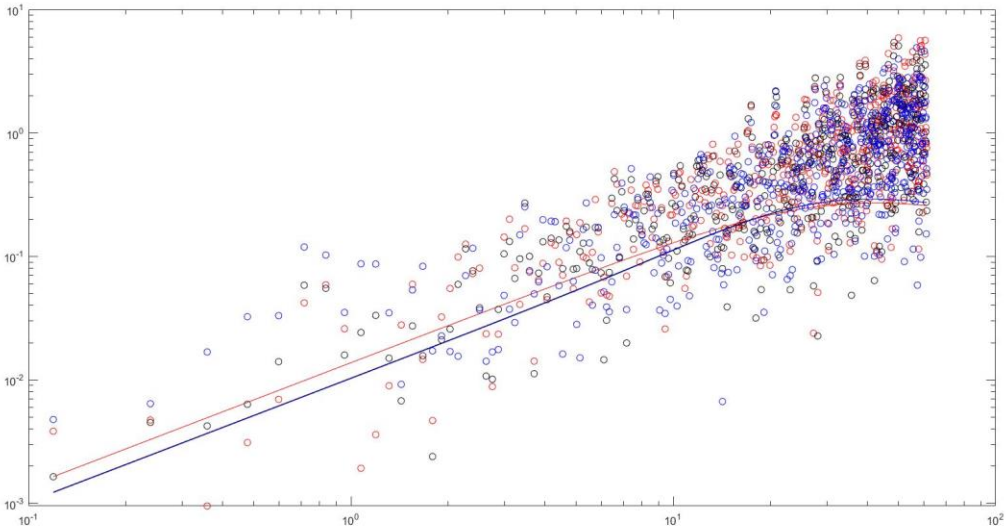

3-3-1-600

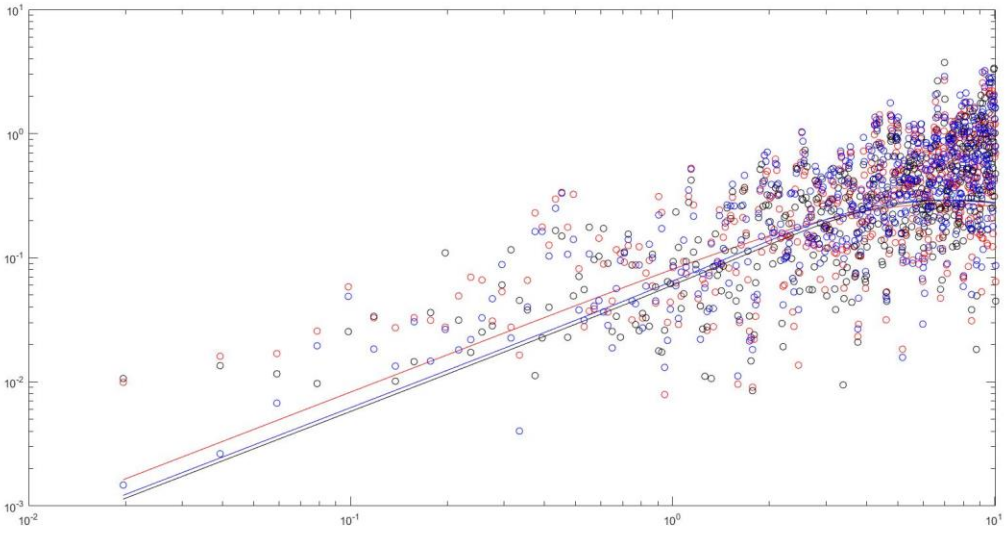

3-3-2-600

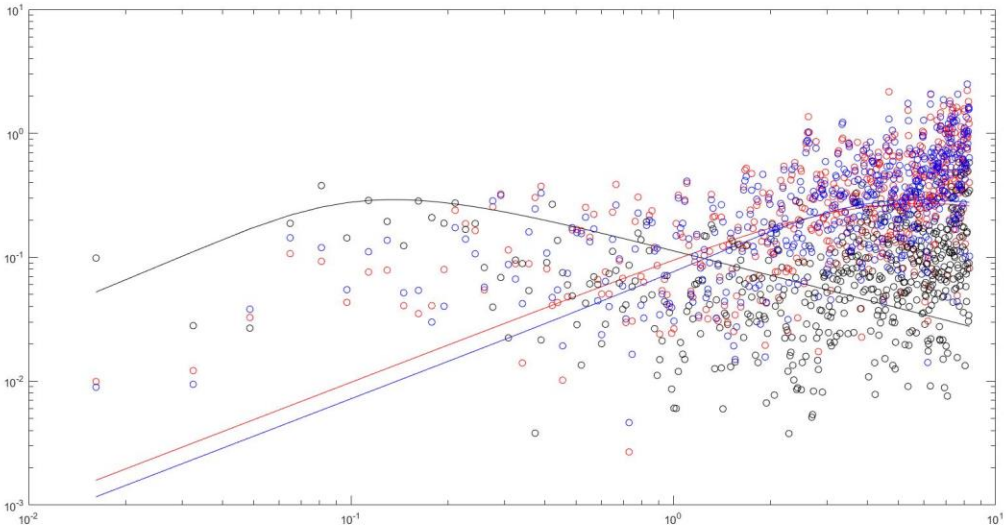

3-3-3-600

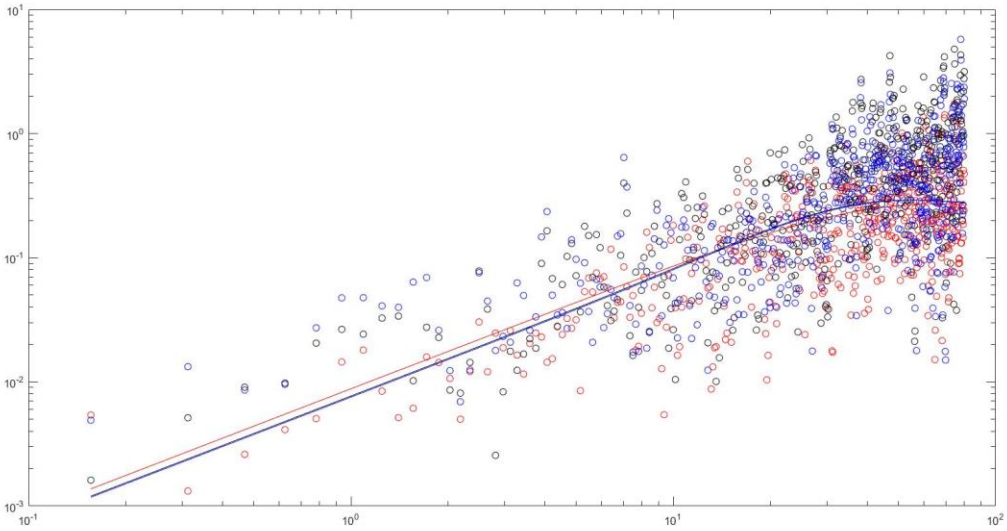

3-3-4-600

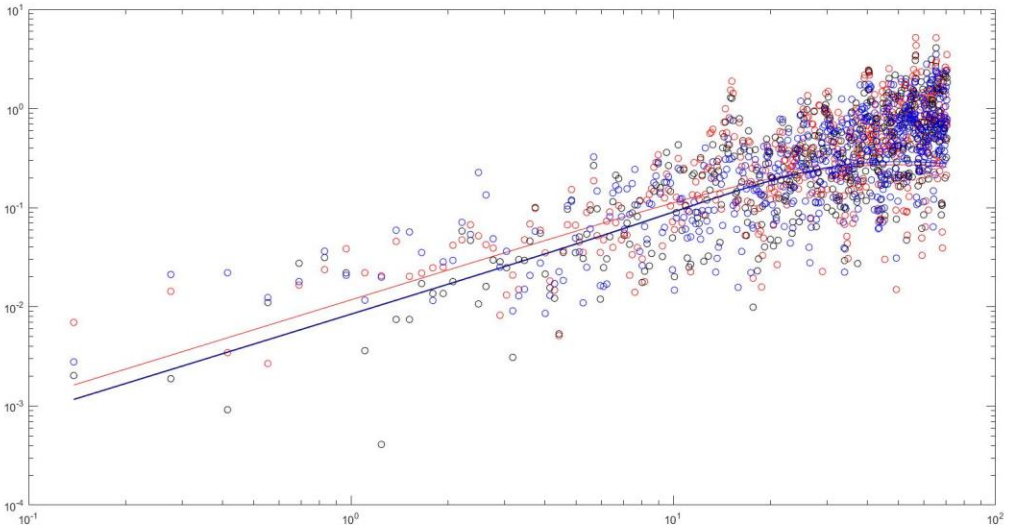

3-3-5-600

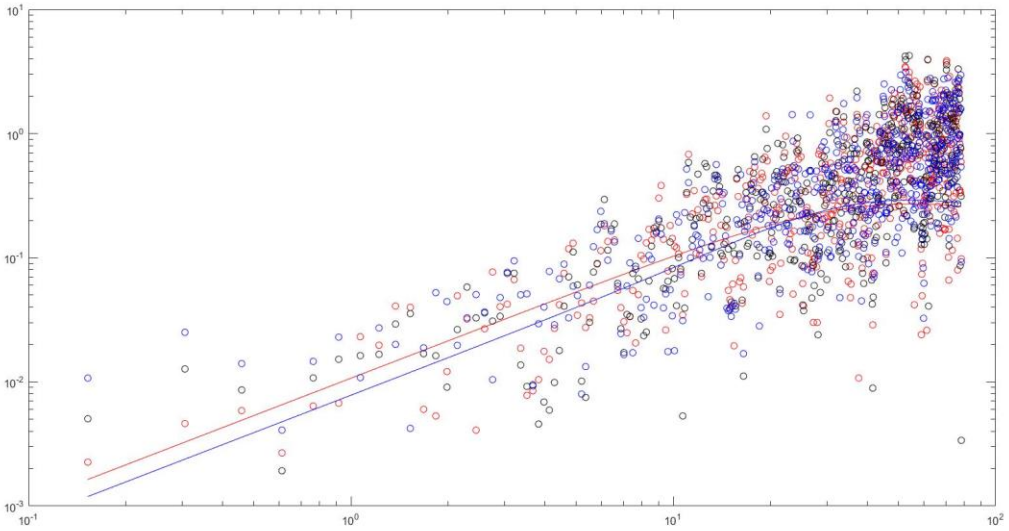

3-3-1-700

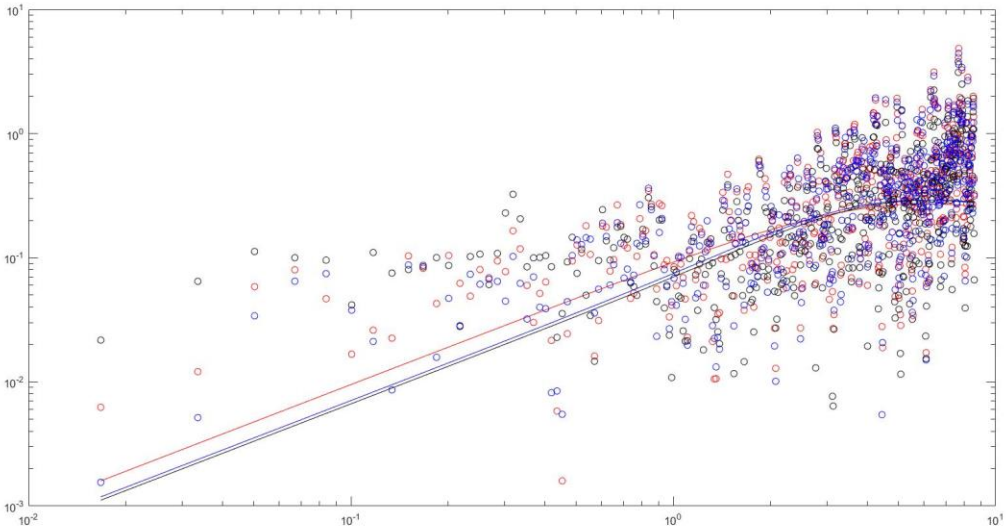

3-3-2-700

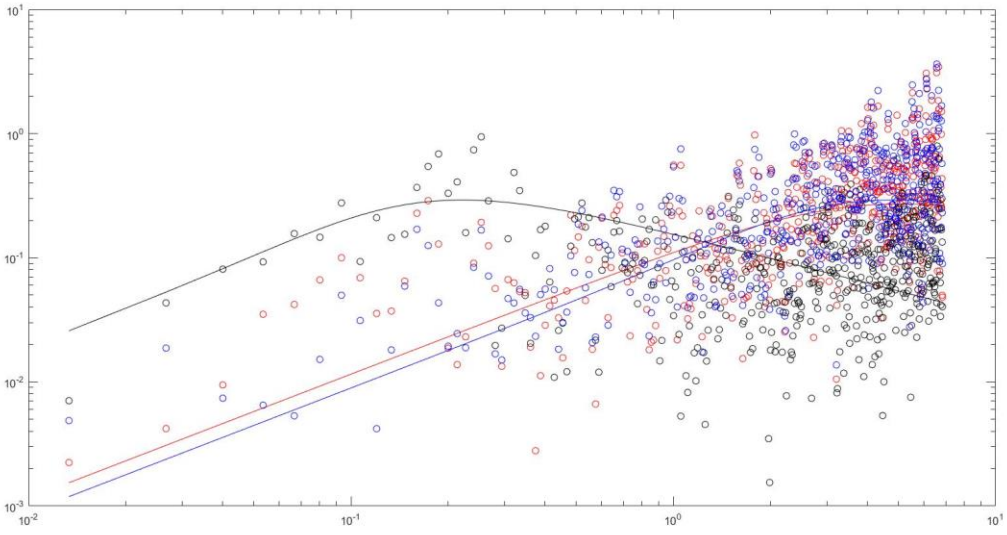

3-3-3-700

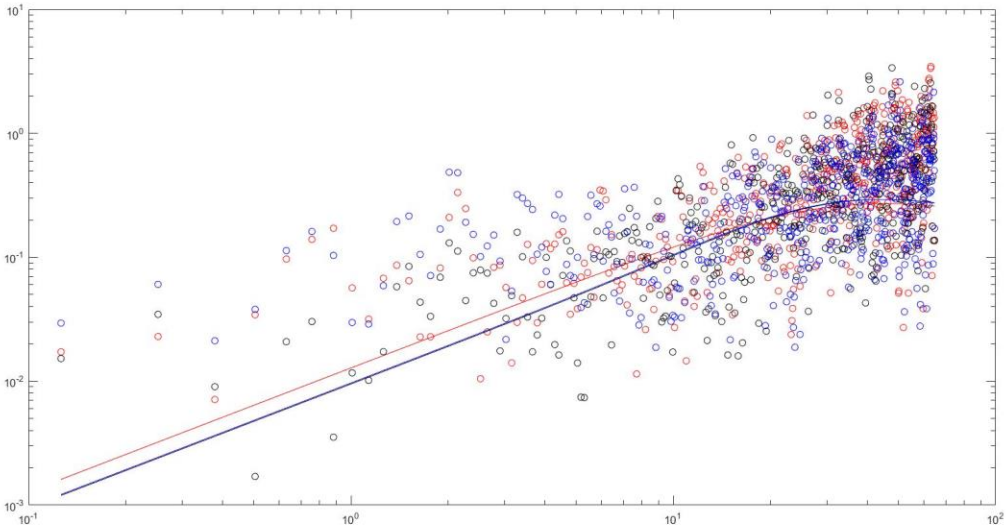

3-3-4-700

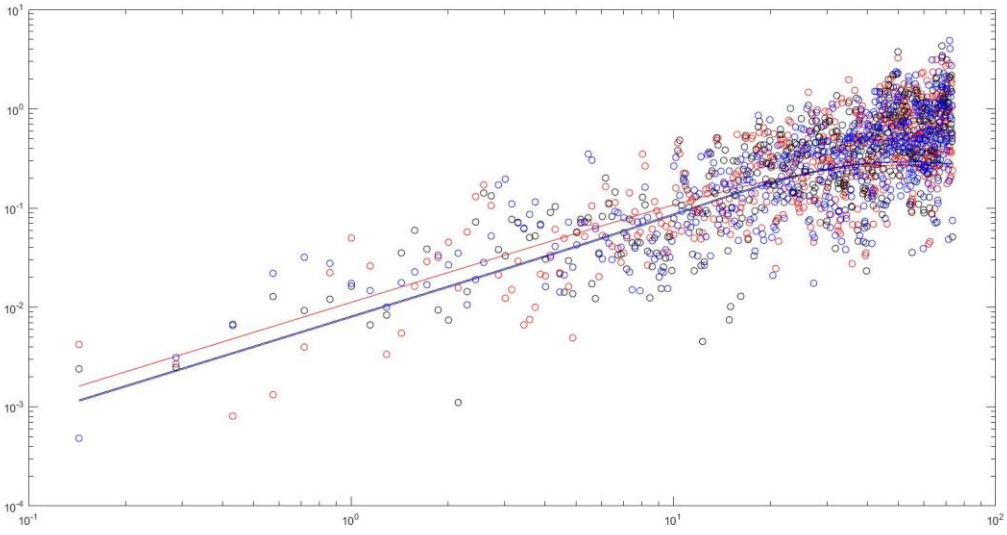

3-3-5-700

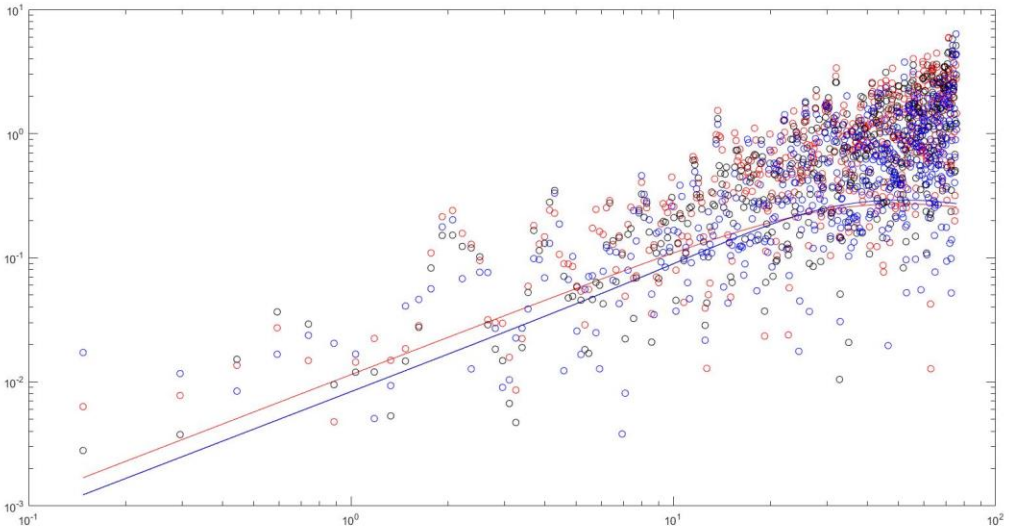

3-3-1-800

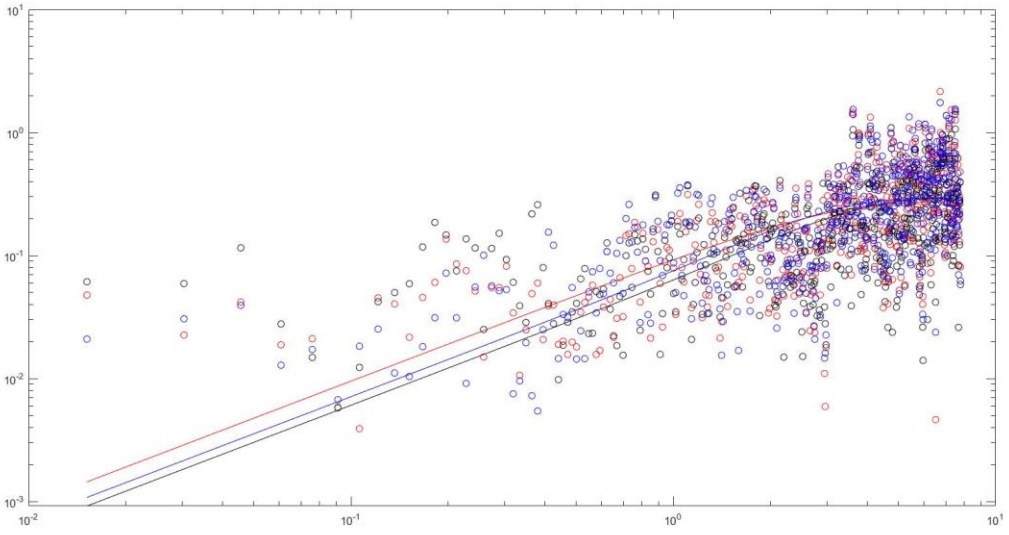

3-3-2-800

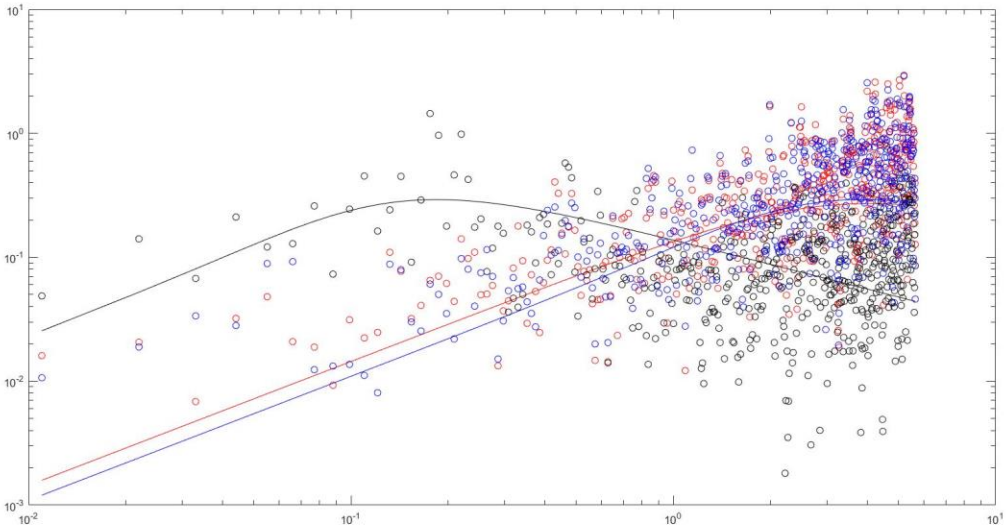

3-3-3-800

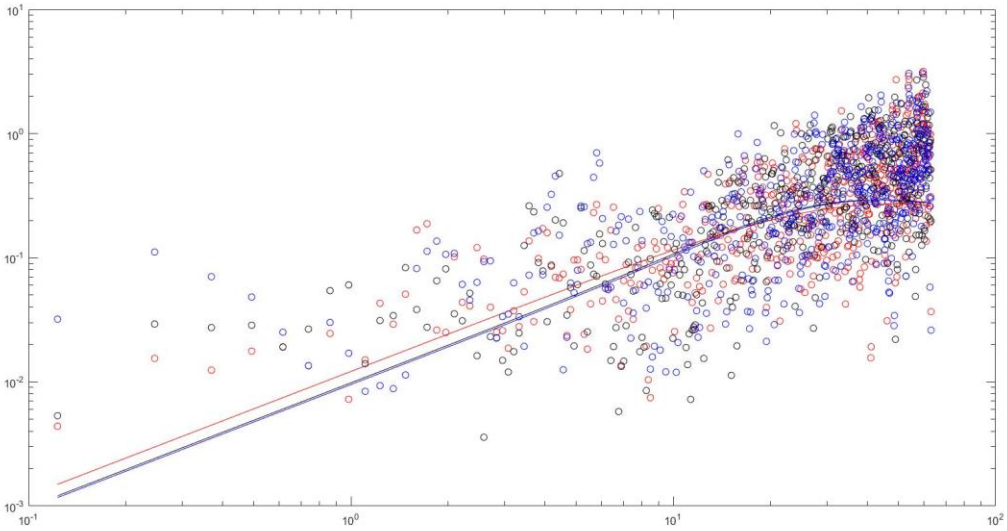

3-3-4-800

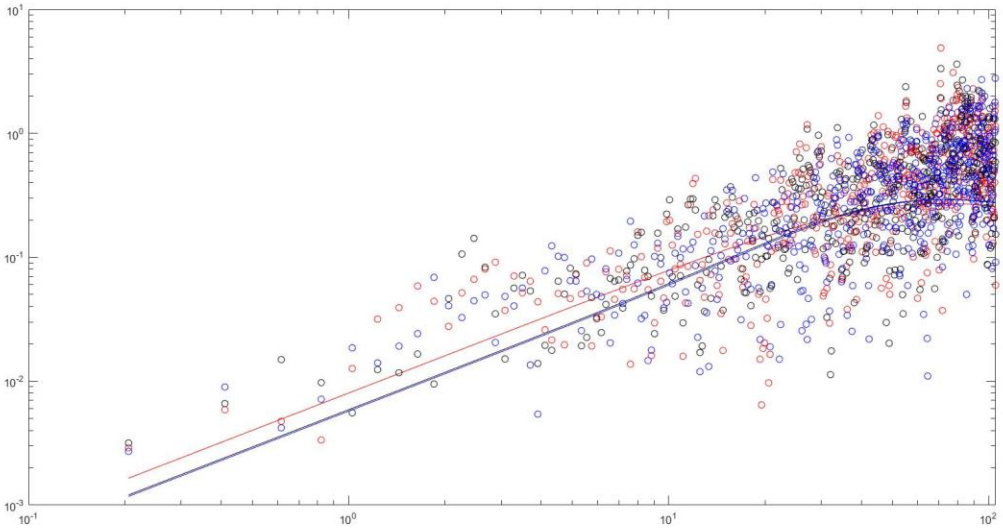

3-3-5-800

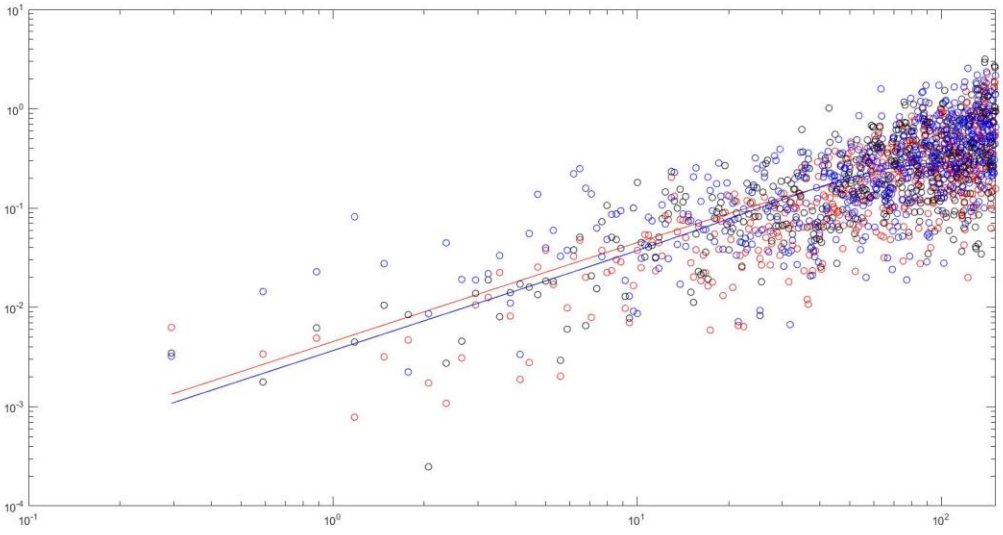

Location 4

3-4-1-400

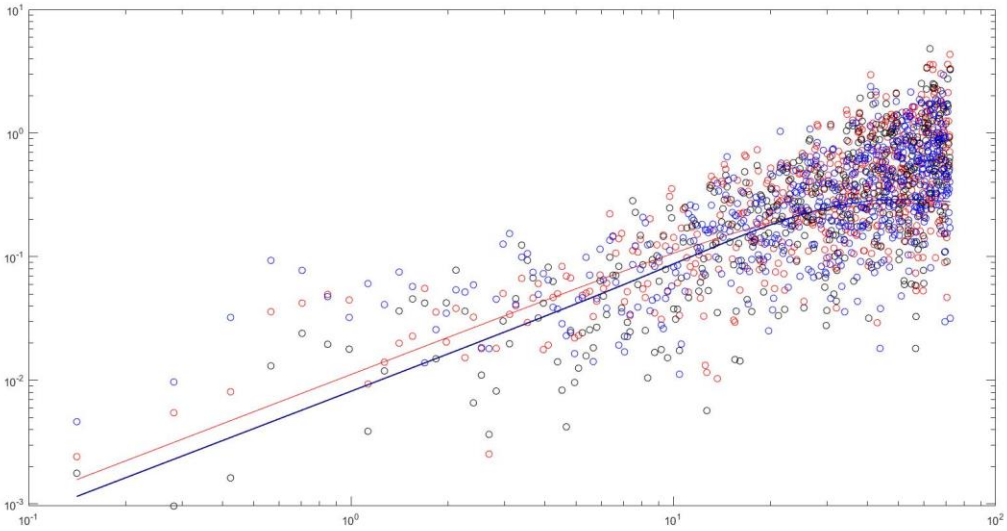

3-4-2-400

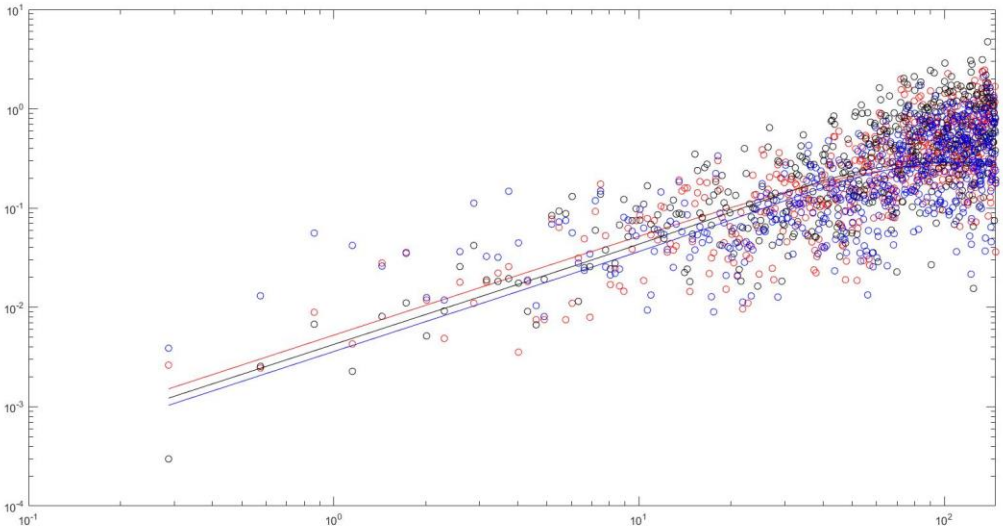

3-4-3-400

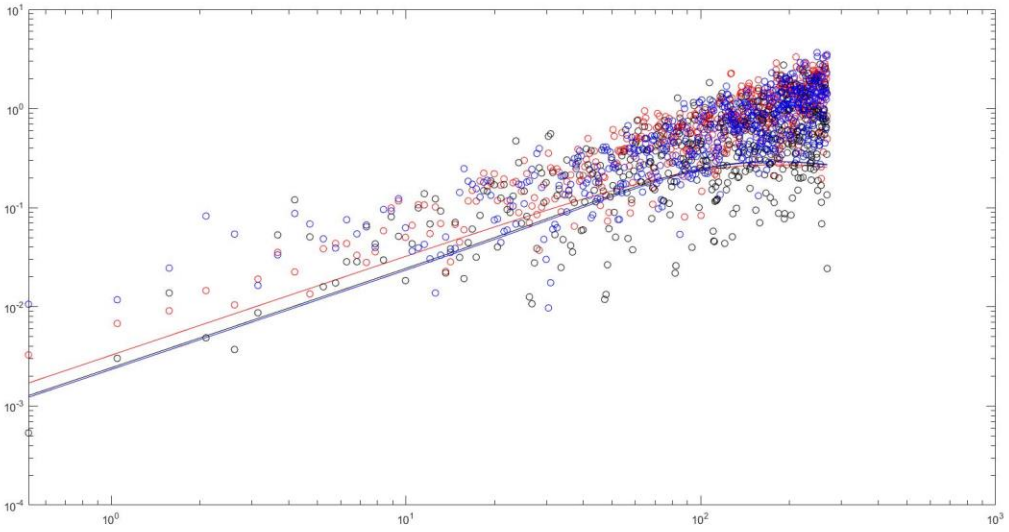

3-4-4-400

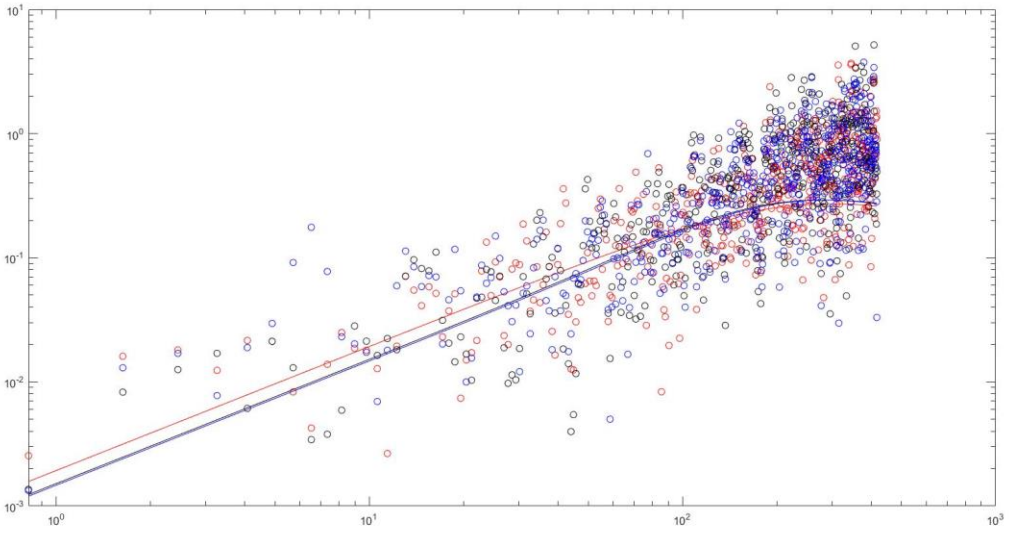

3-4-5-400

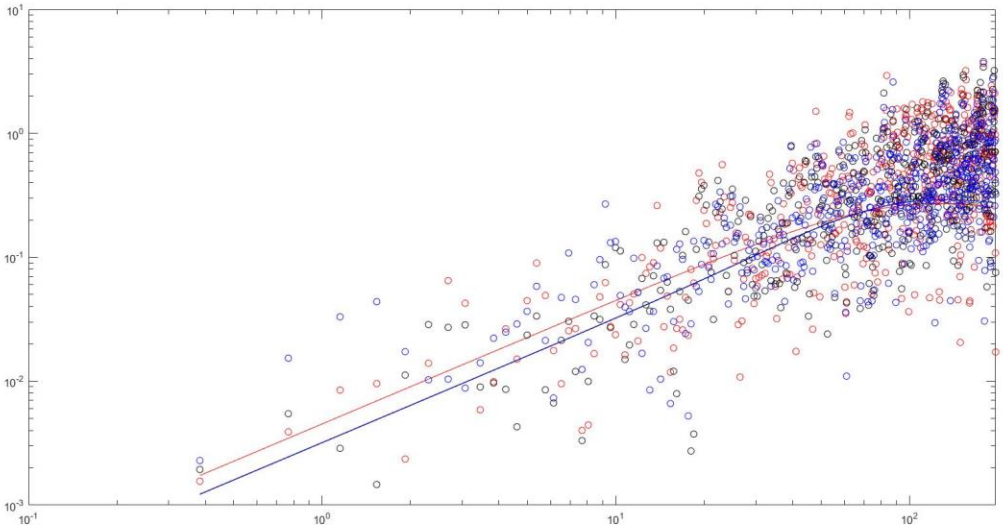

3-4-1-500

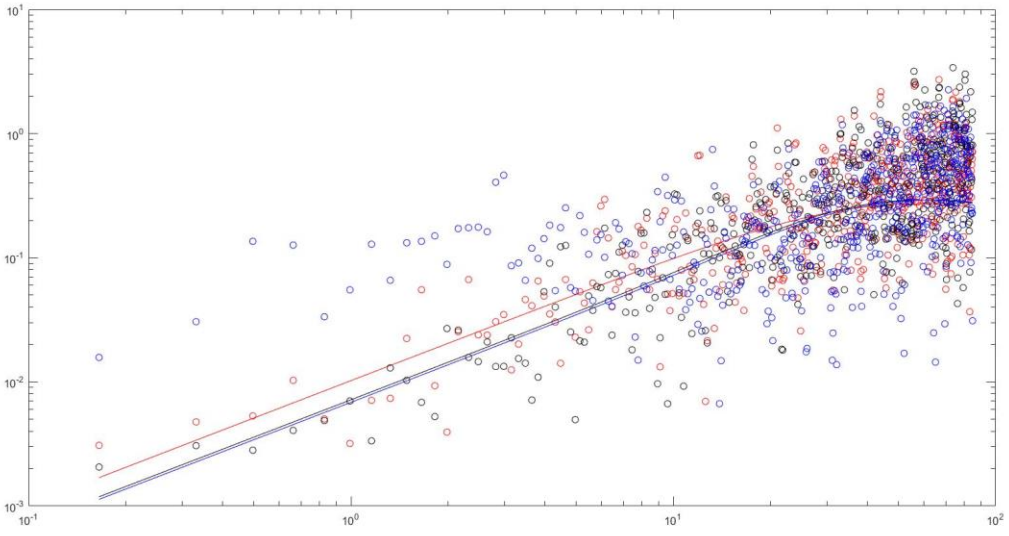

3-4-2-500

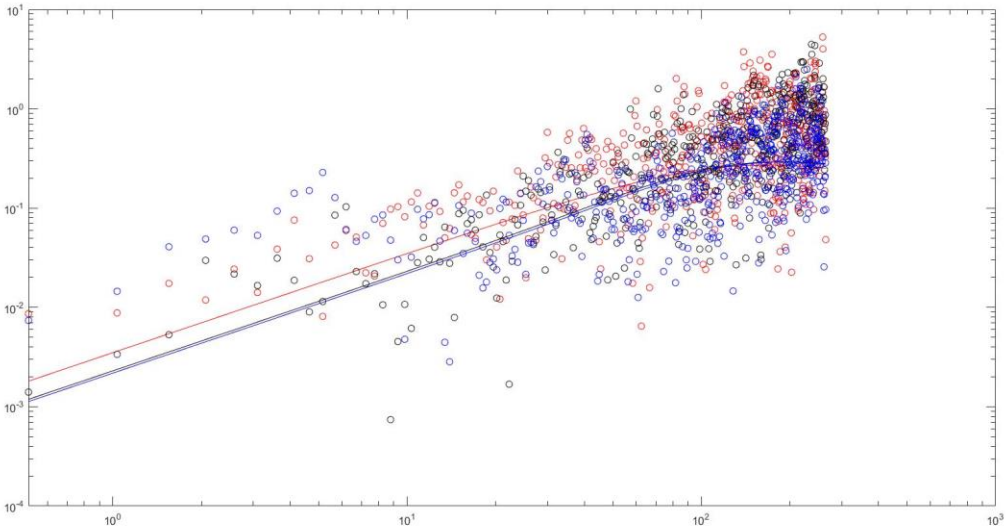

3-4-3-500

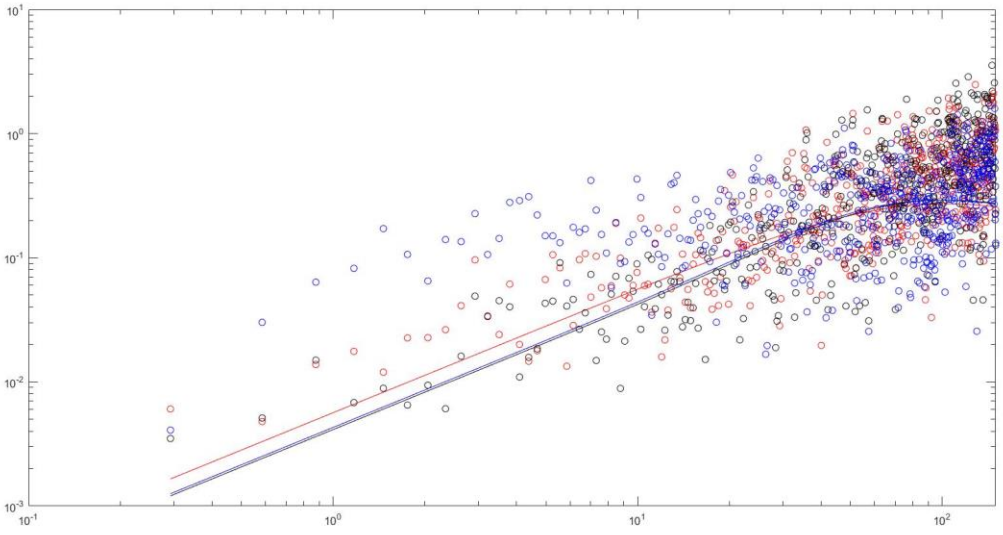

3-4-4-500

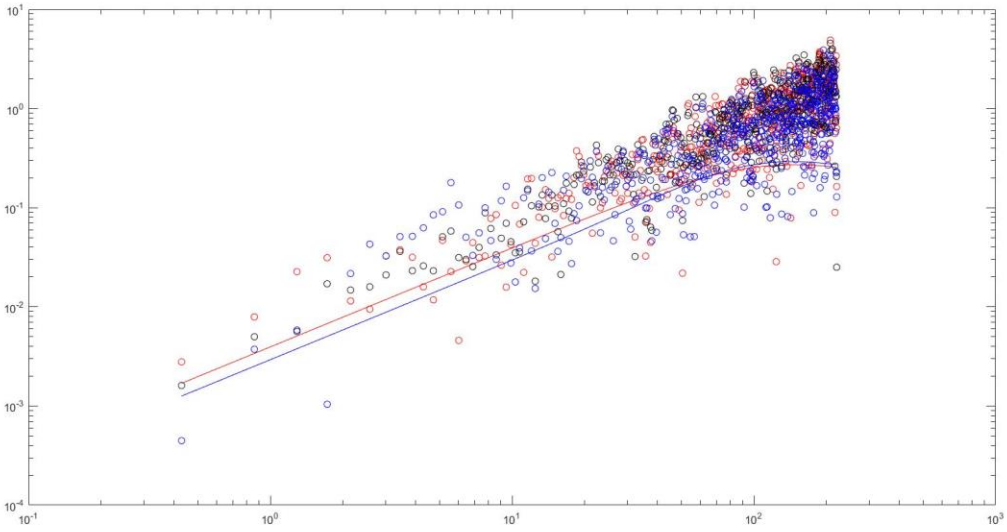

3-4-5-500

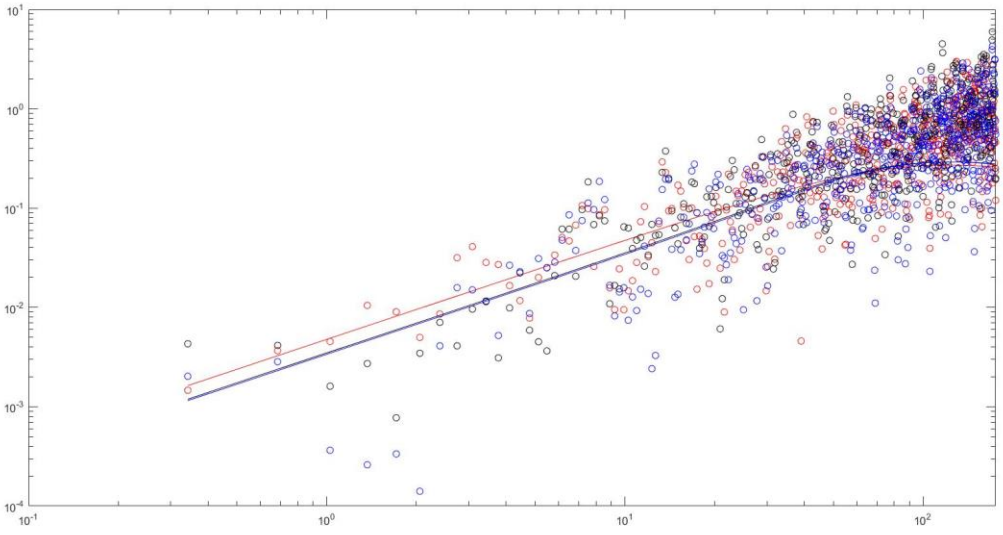

3-4-1-600

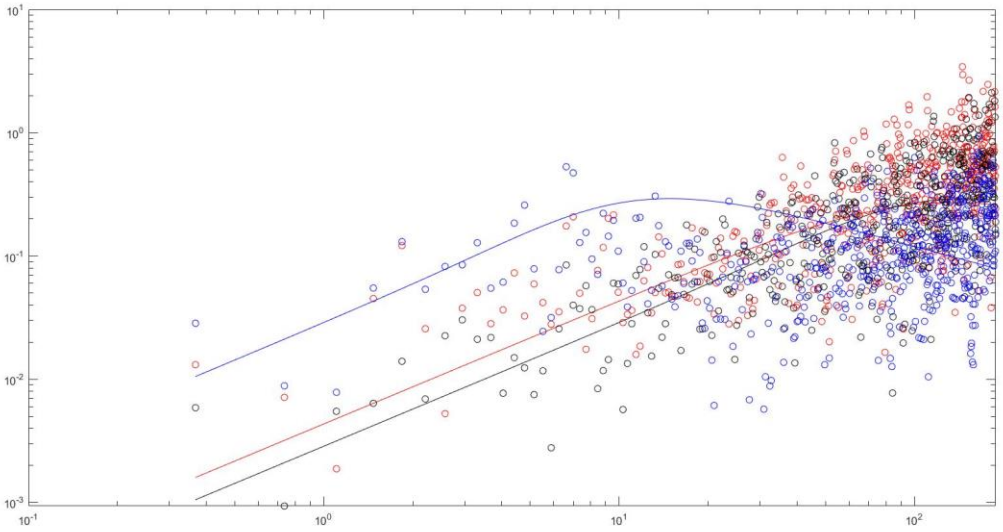

3-4-3-600

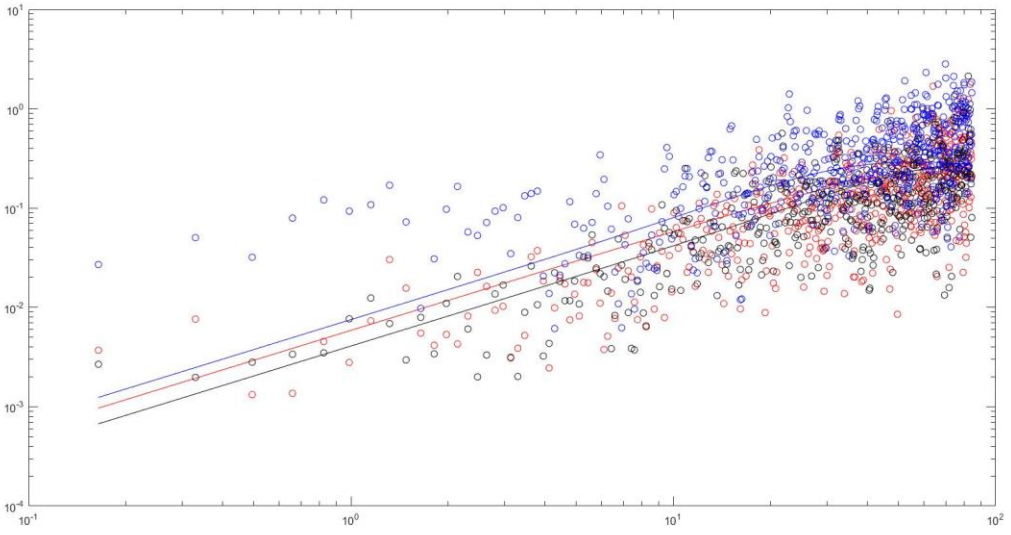

3-4-4-600

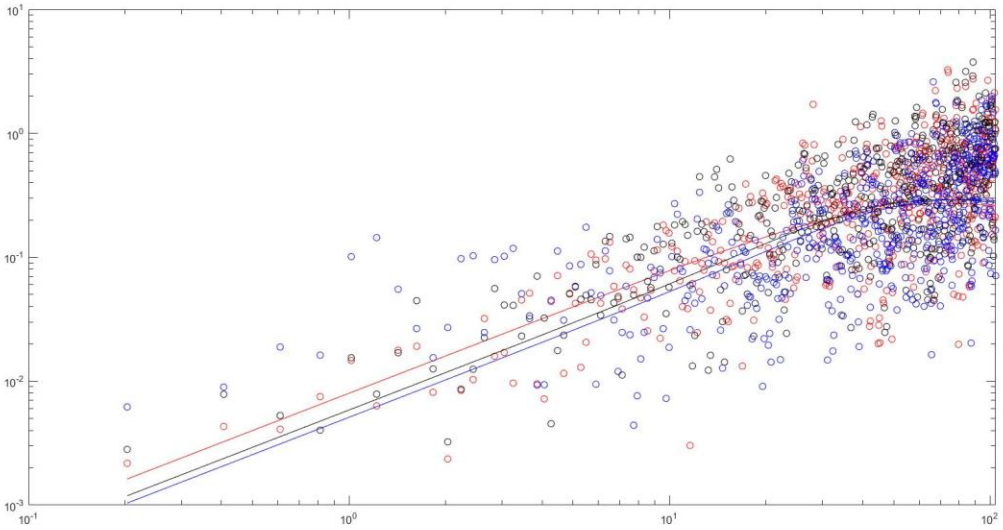

3-4-5-600

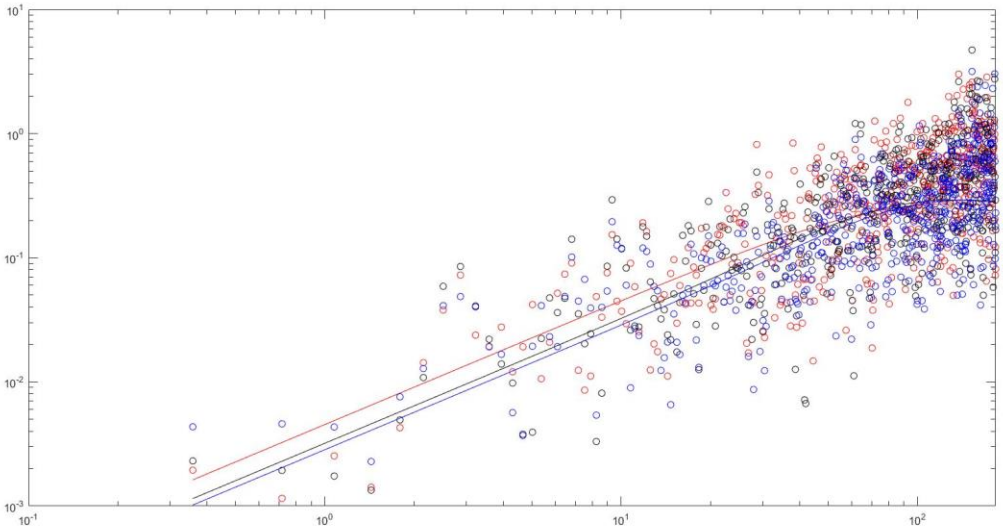

3-4-1-700

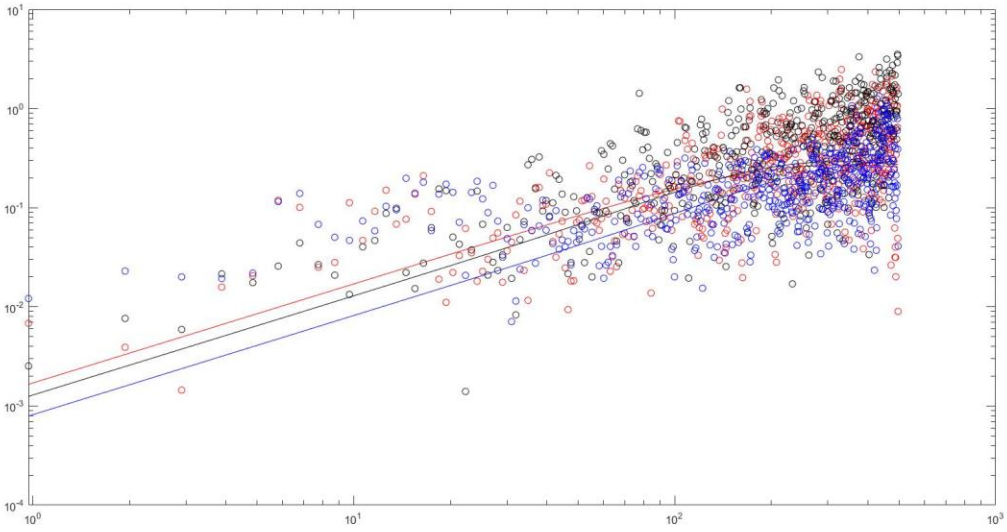

3-4-3-700

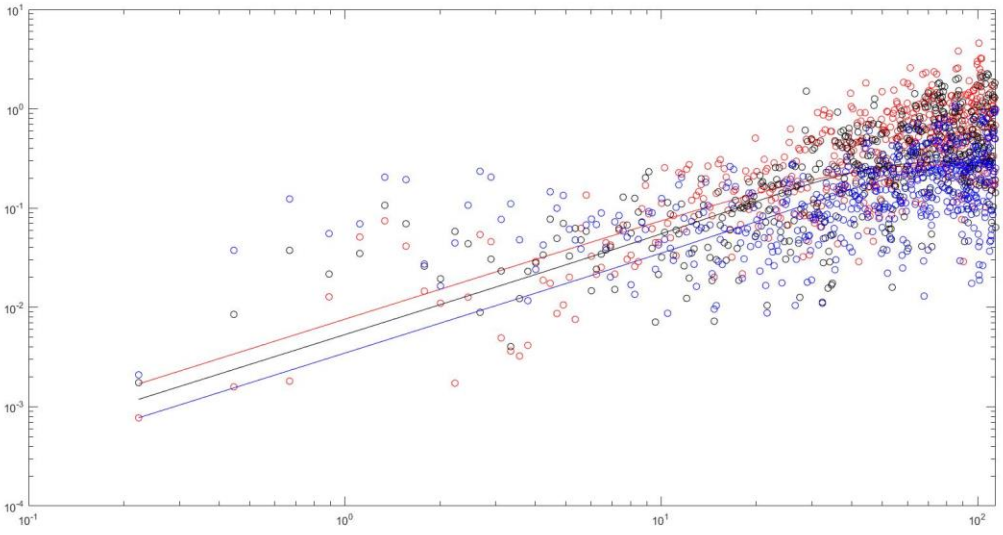

3-4-4-700

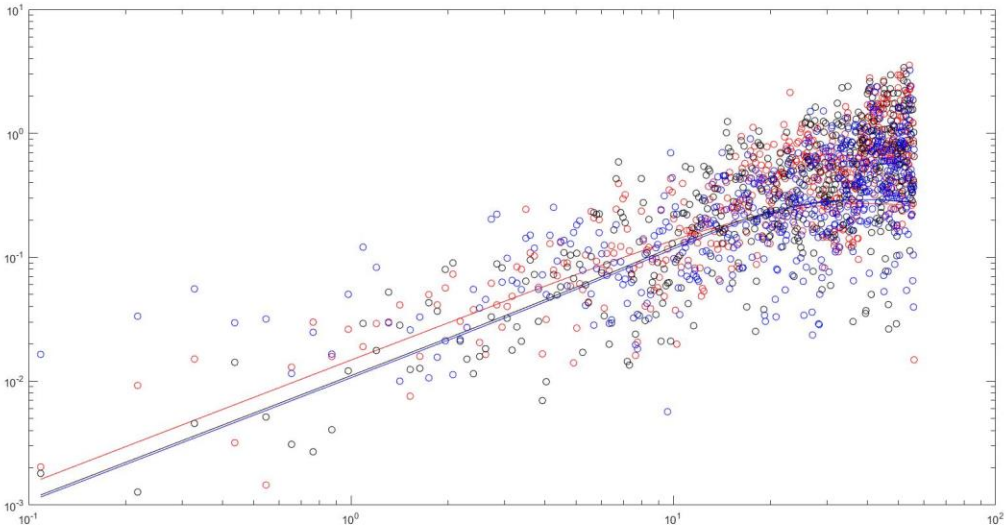

3-4-5-700

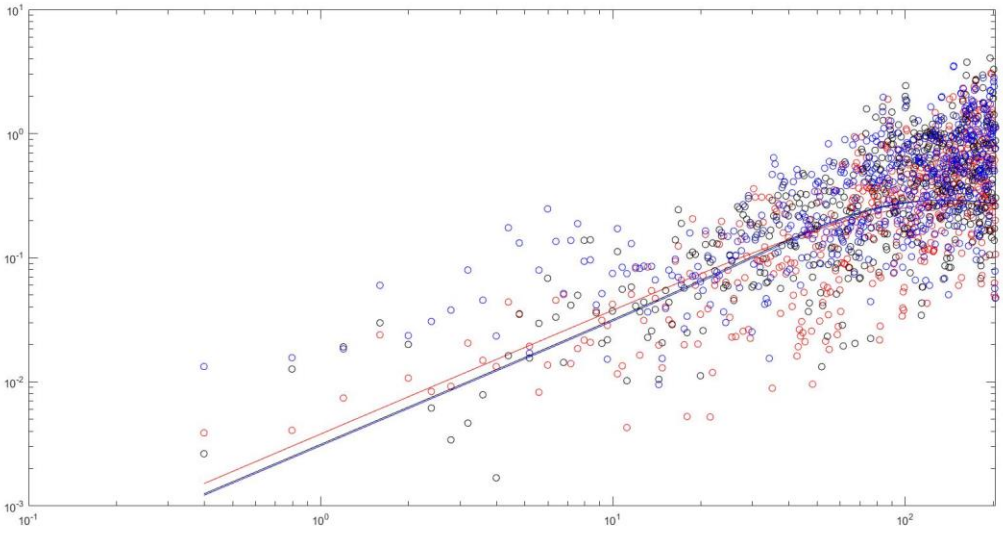

3-4-3-800

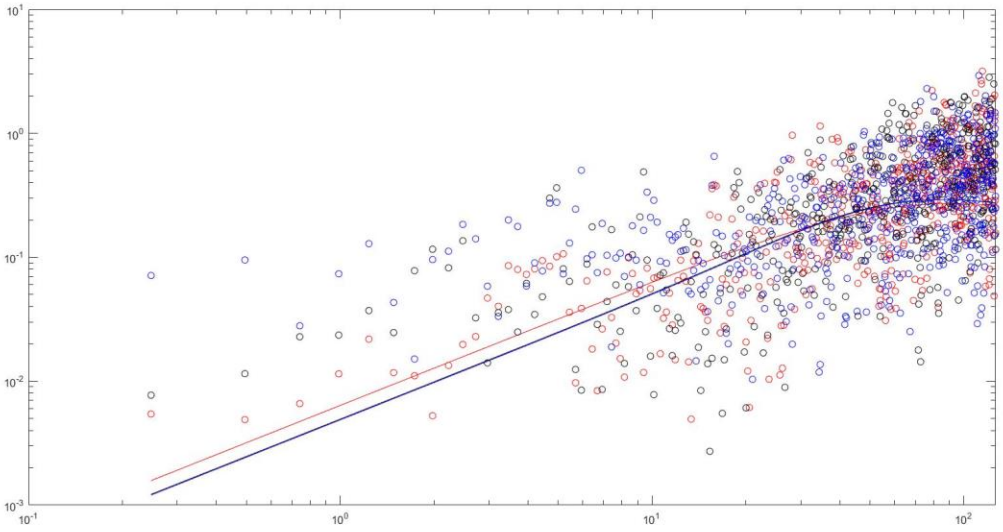

3-4-4-800

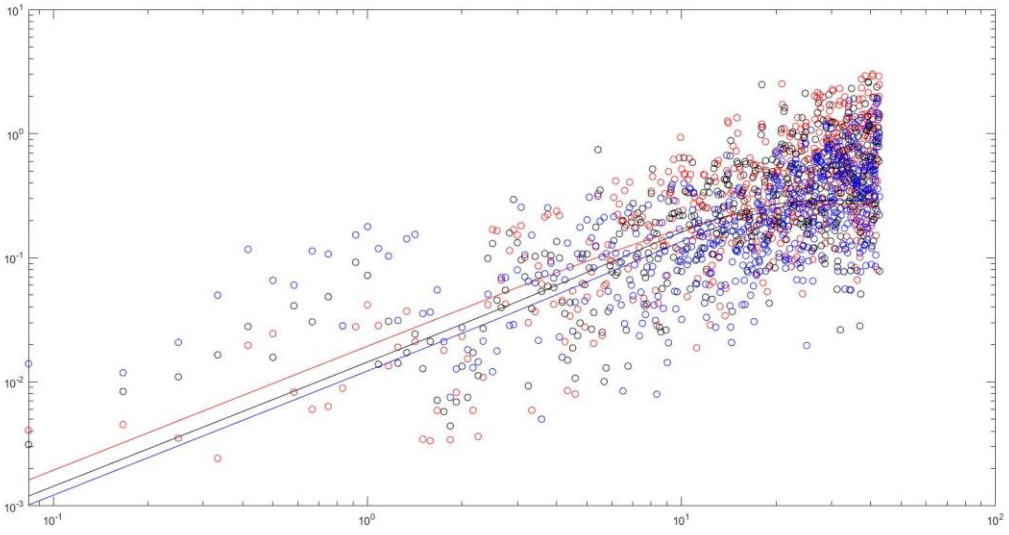

3-4-5-800

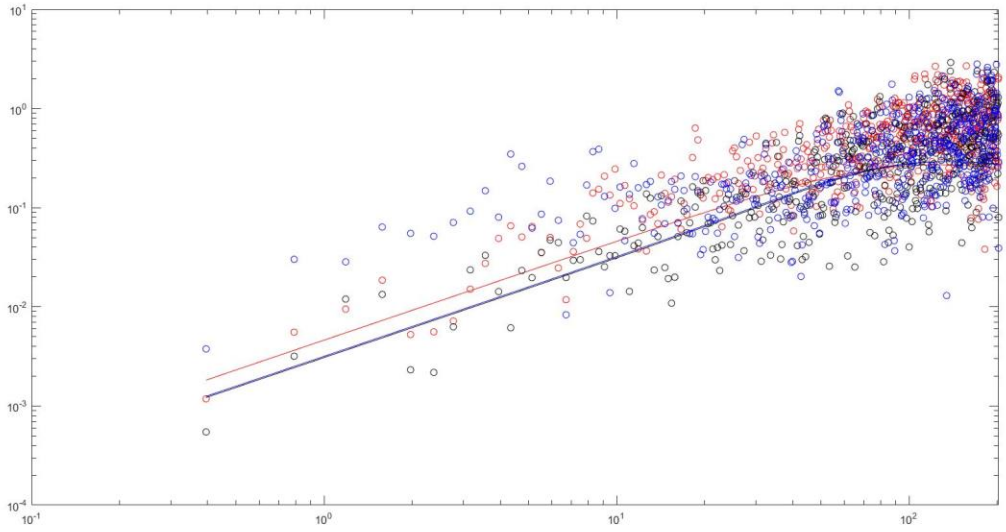
$10^{1}$
$10^{0}$
$10^{-1}$
$10^{-2}$
$10^{-3}$
$10^{-4}$
$10^{-1}$
$10^{0}$
$10^{1}$
$10^{2}$

# Appendix B: CP, velocity time history and wind speed profiles

Same Location Different RPMS

Case 1

Location 1

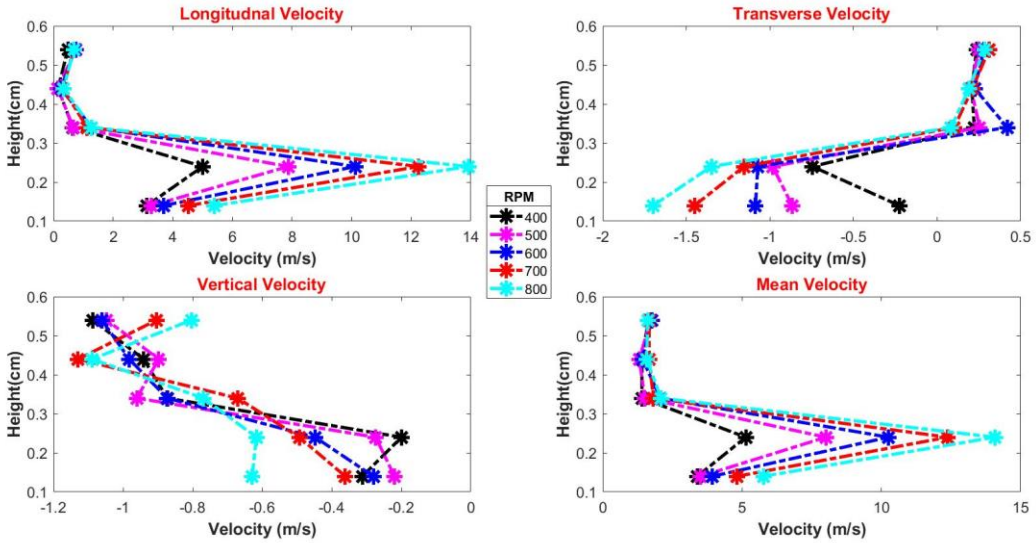


Location 2

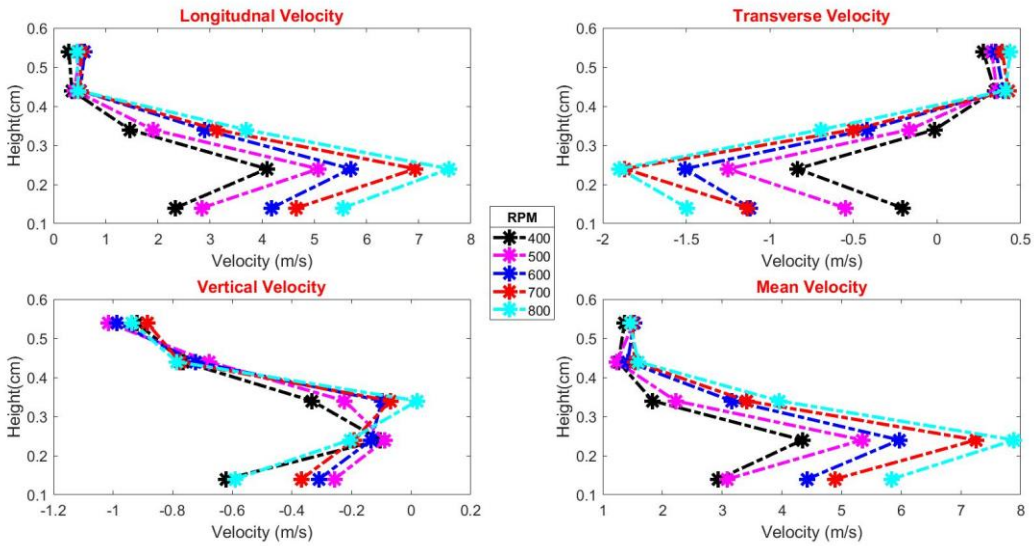


Location 4

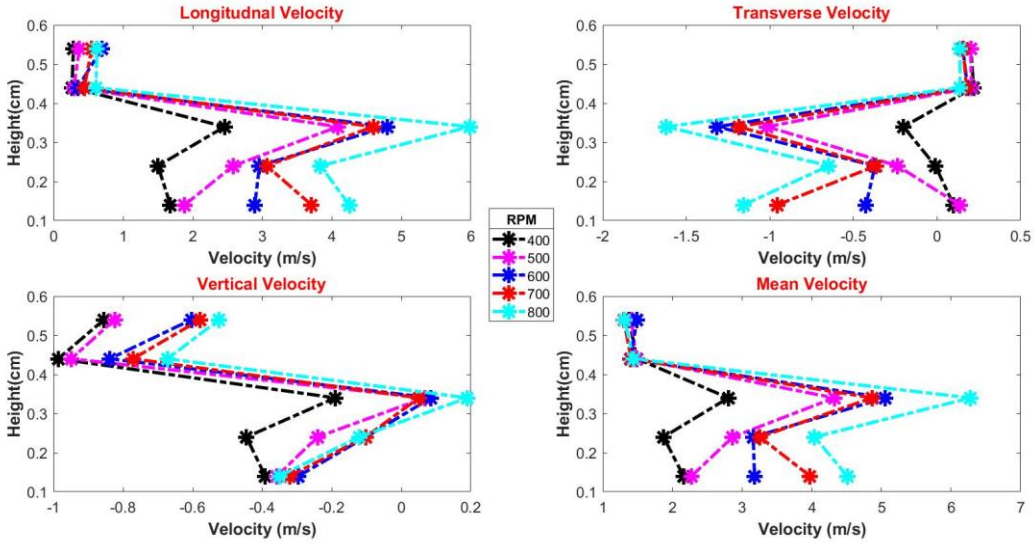


Case 3

Location 1

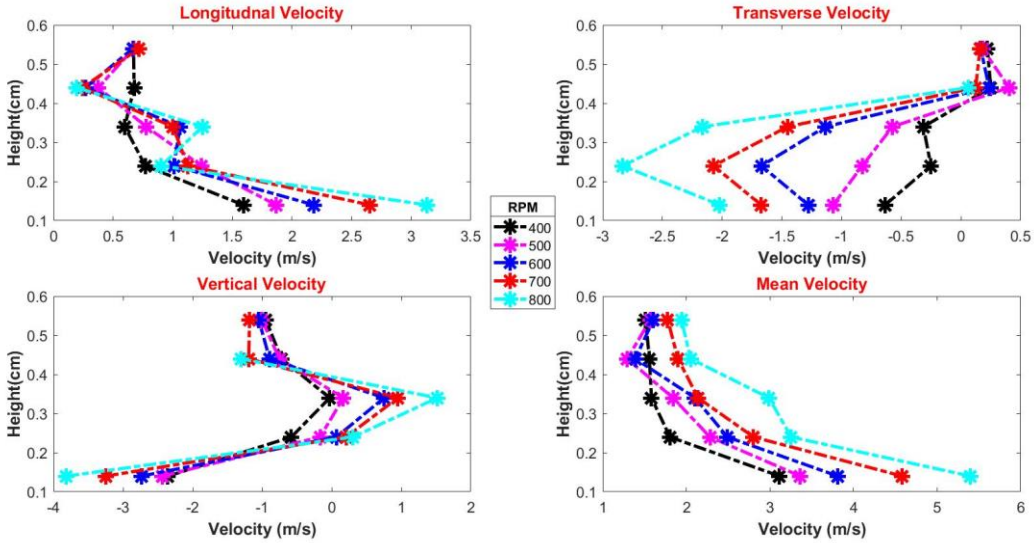


Location 2

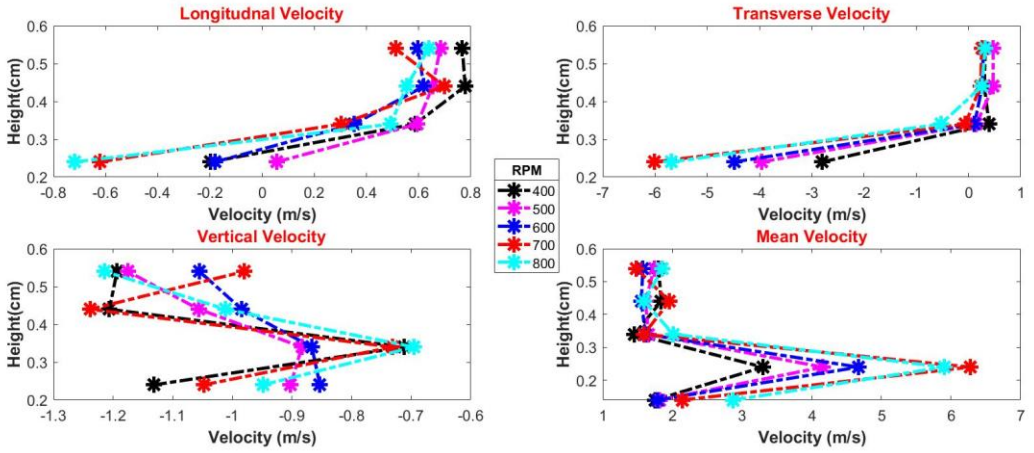


Location 4

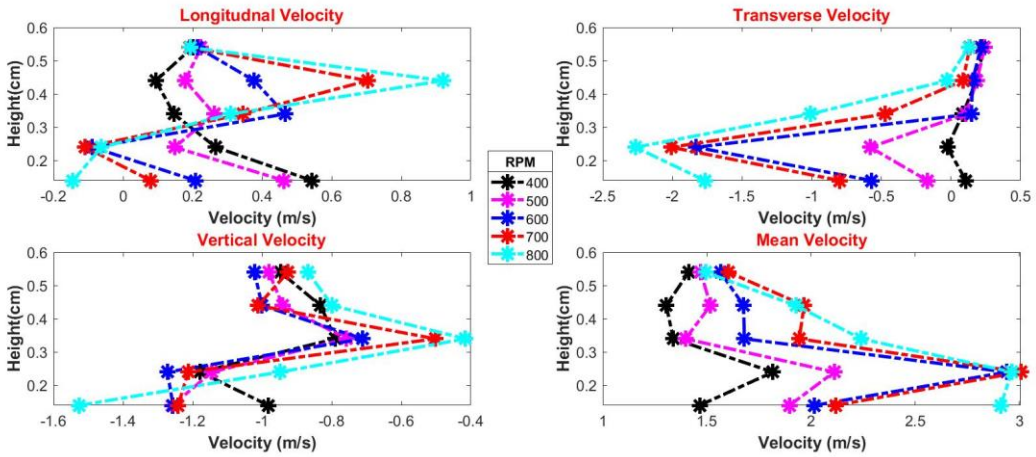


Different Locations same rpm

Case 1

400 rpm

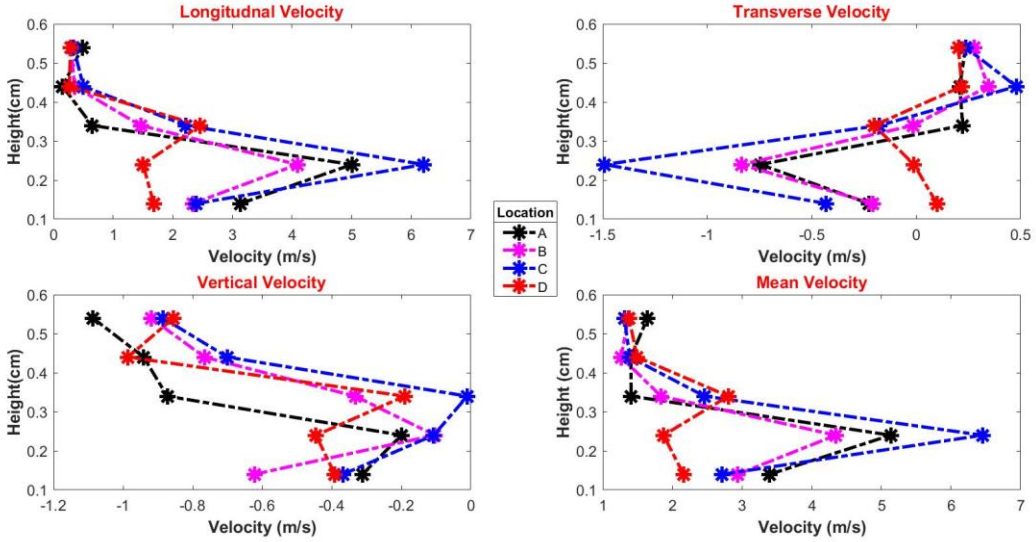


500 rpm

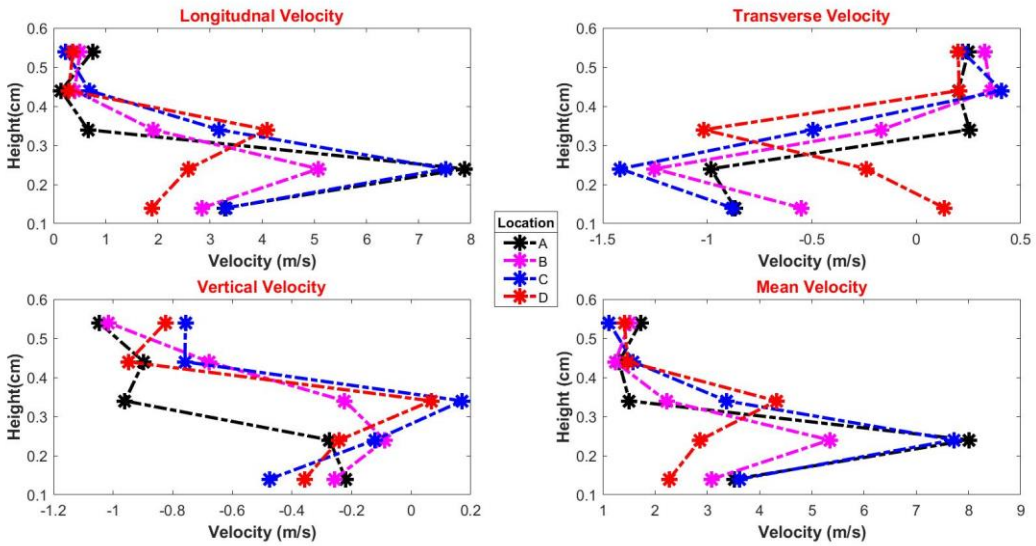


600 RPM

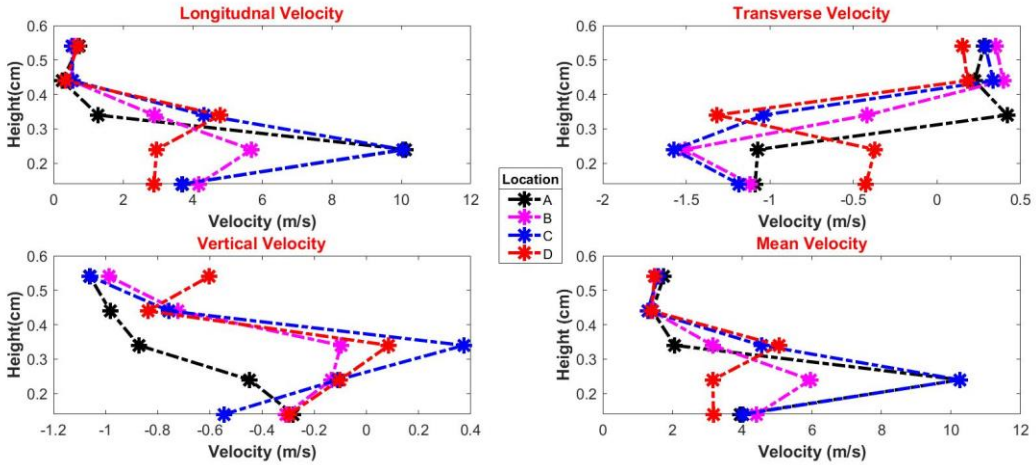


700 RPM

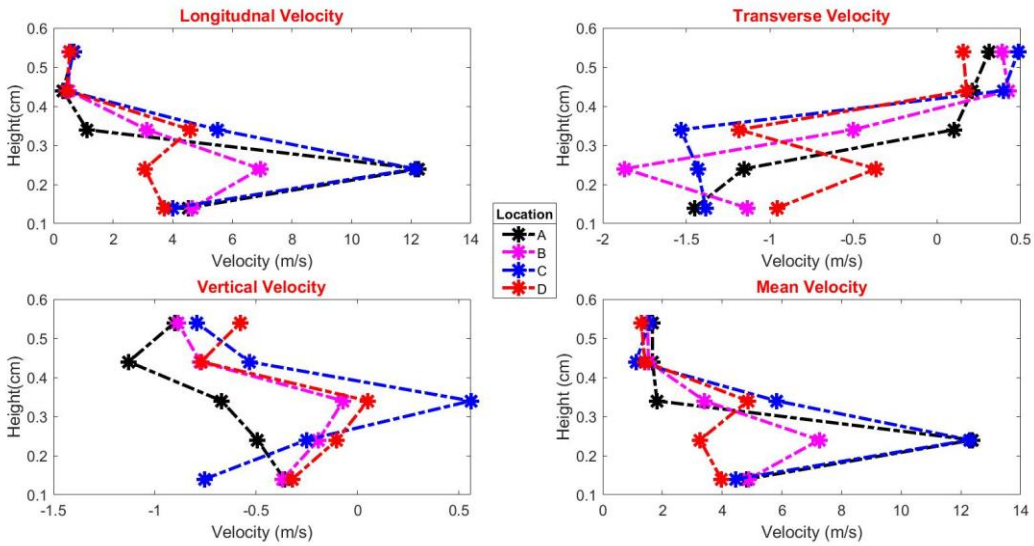


800 RPM

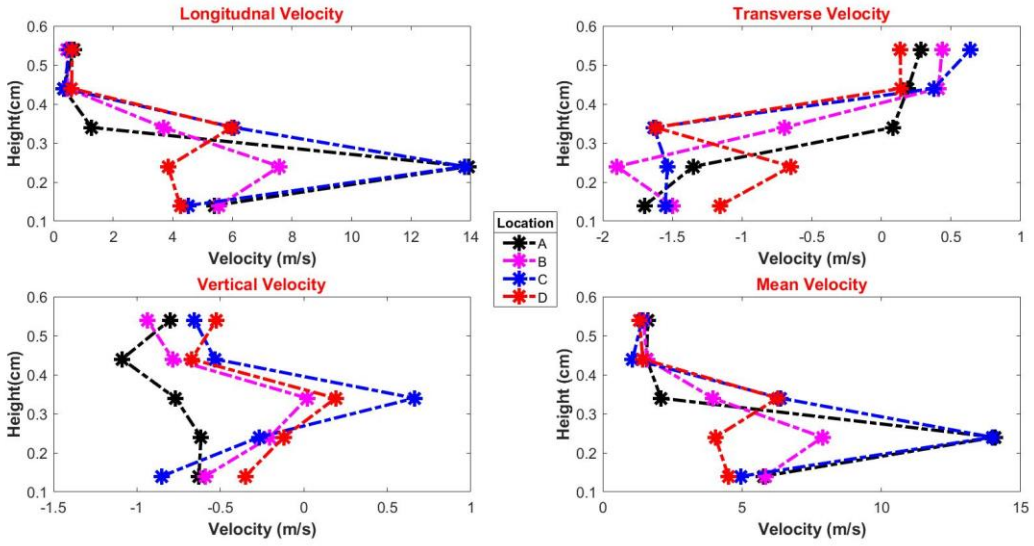


Case 3

400 RPM

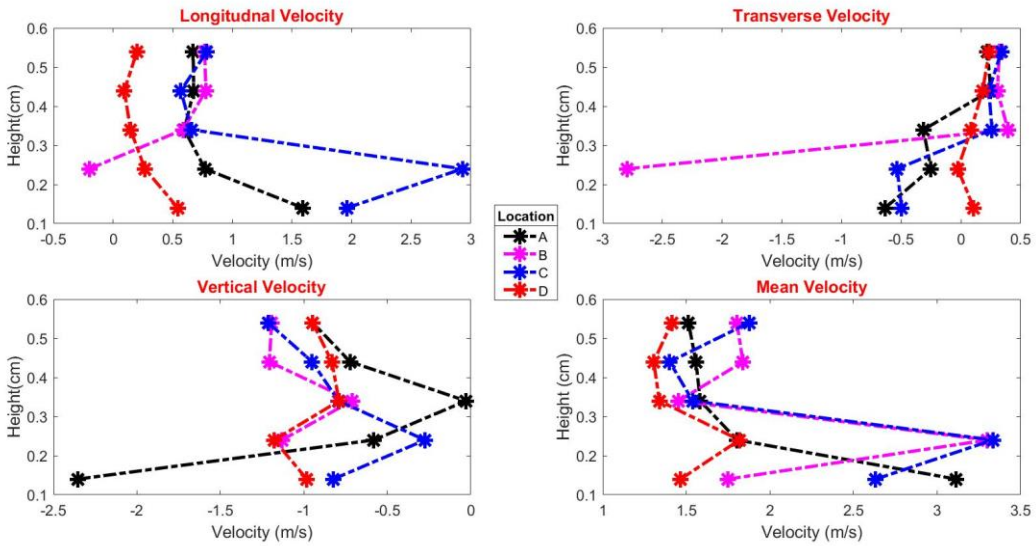


500 RPM

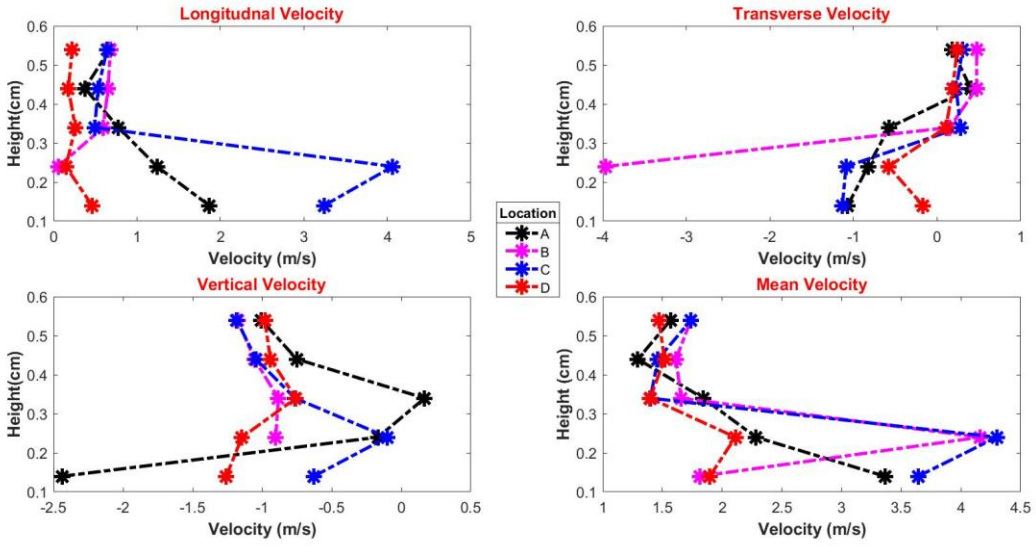


600 RPM

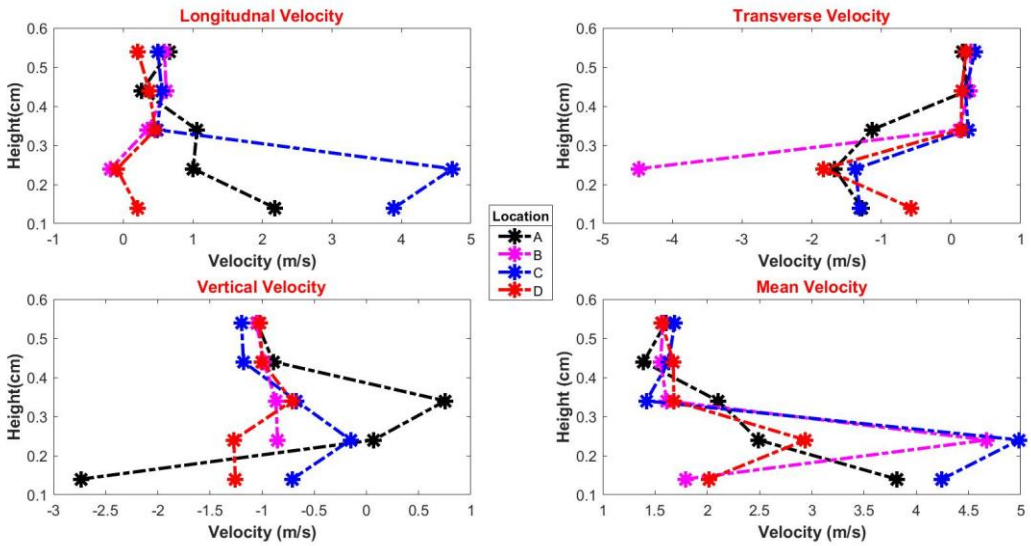


700 RPM

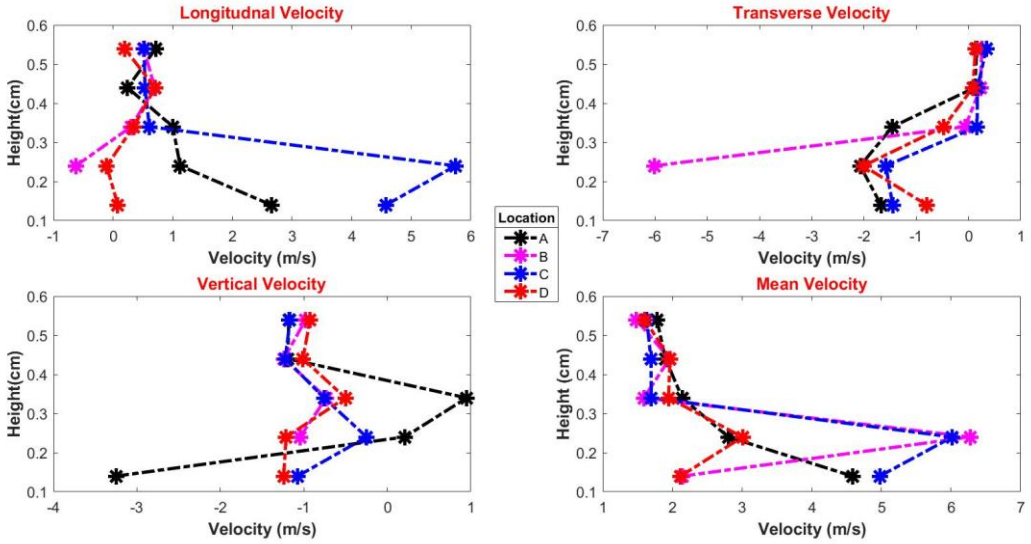


800 RPM

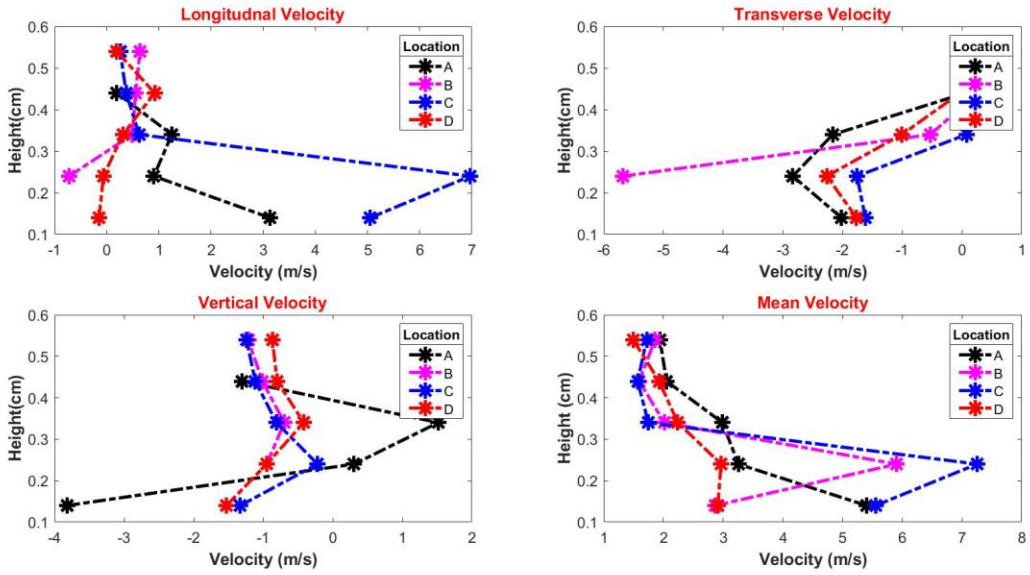


Case 2 location 1 2nd height 600 rpm

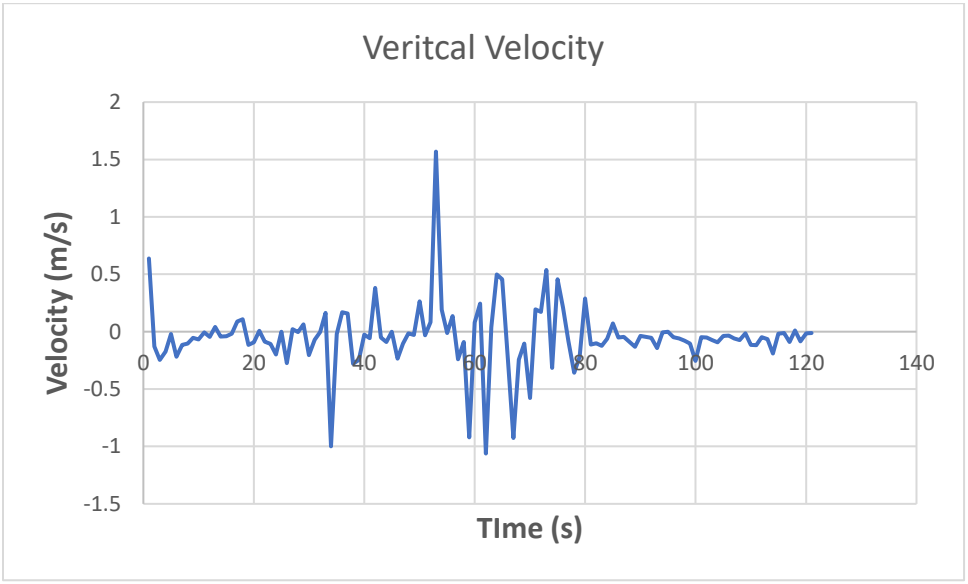

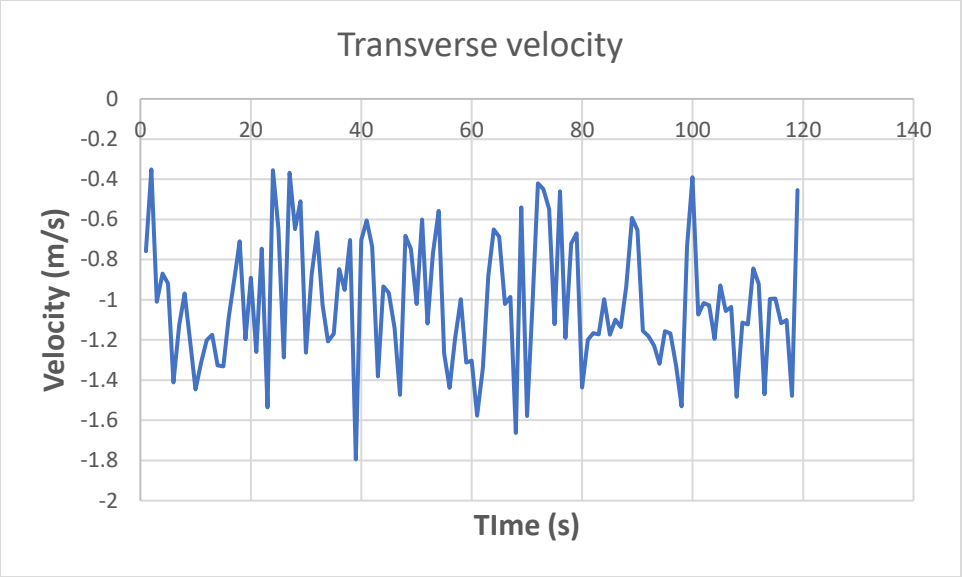


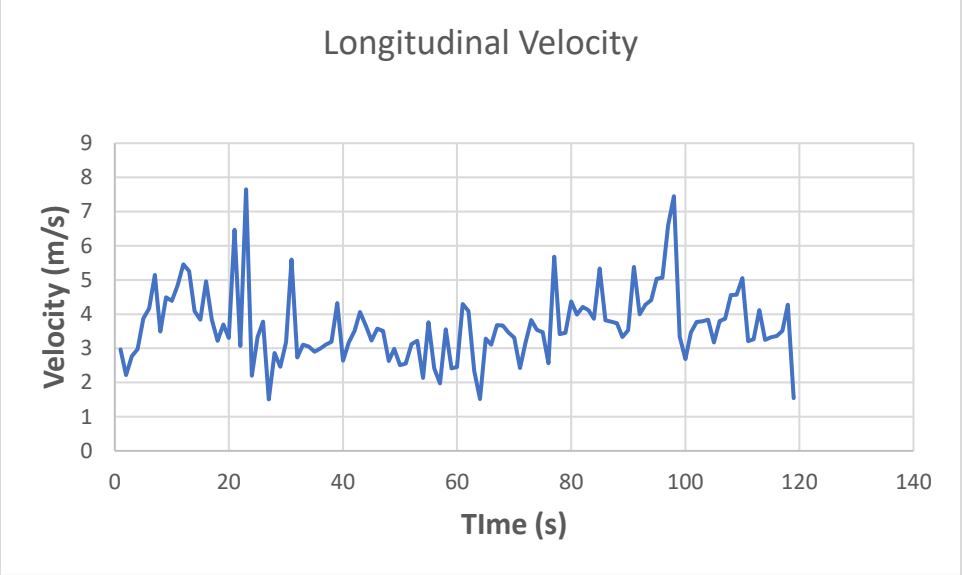


Case 3, location 1, 2nd height, 600 RPM

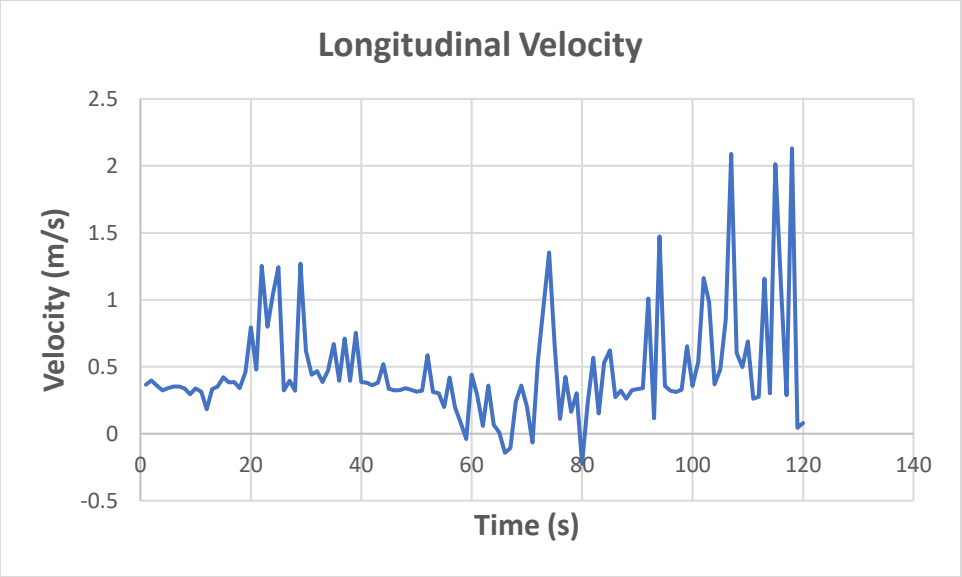
Longitudinal Velocity
Velocity (m/s)
2.5
2
1.5
1
0.5
0
-0.5
0
20
40
60
80
100
120
140
Time (s)

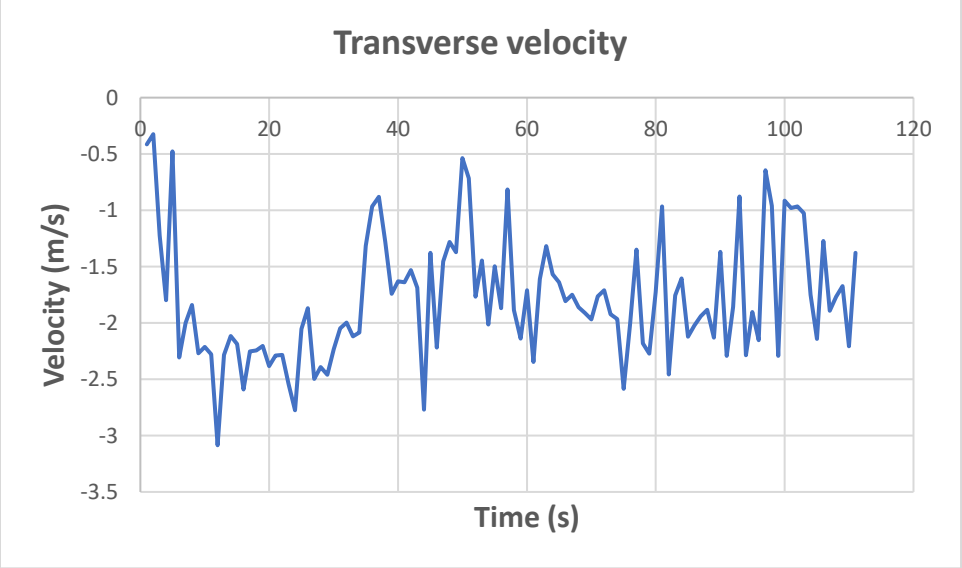
Transverse velocity
Velocity (m/s)
0
-0.5
-1
-1.5
-2
-2.5
-3
-3.5
0
20
40
60
80
100
120
Time (s)

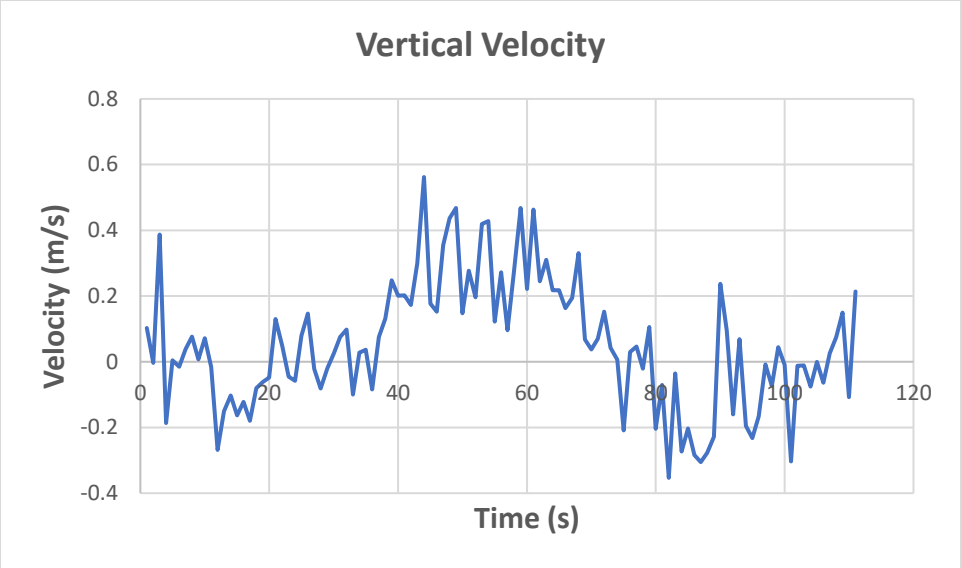


1:20 model 600 RPM

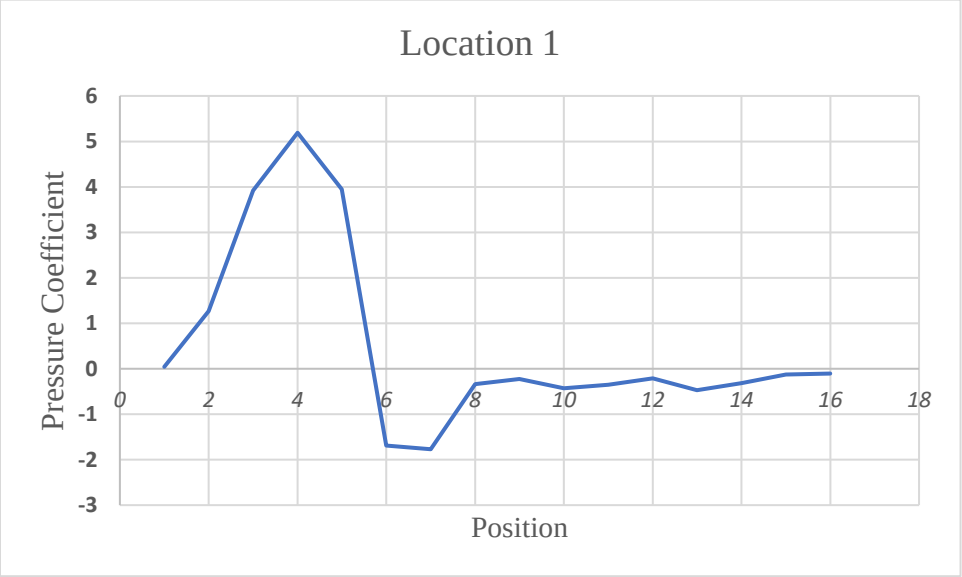

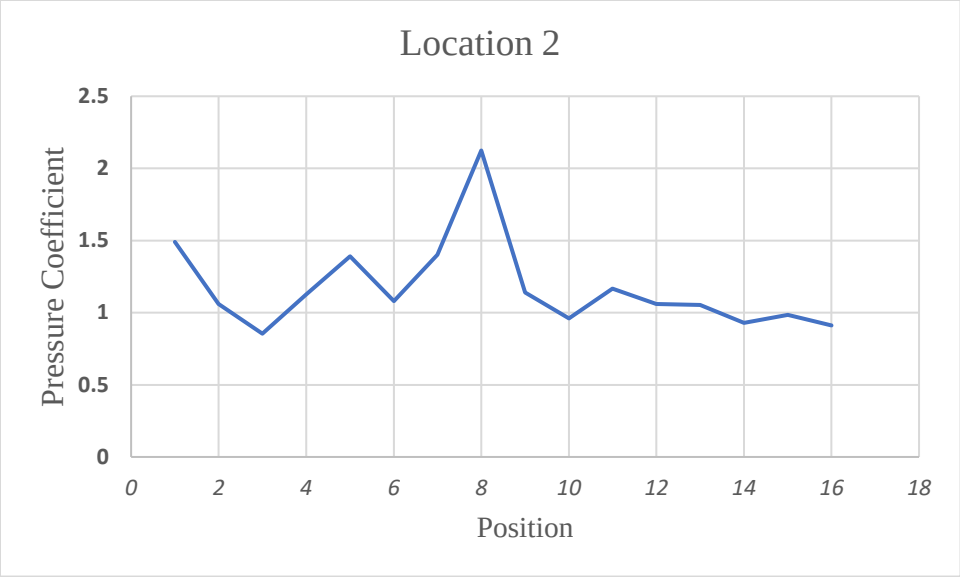
Location 2
Pressure Coefficient
2.5
2
1.5
1
0.5
0
0
2
4
6
8
10
12
14
16
18
Position

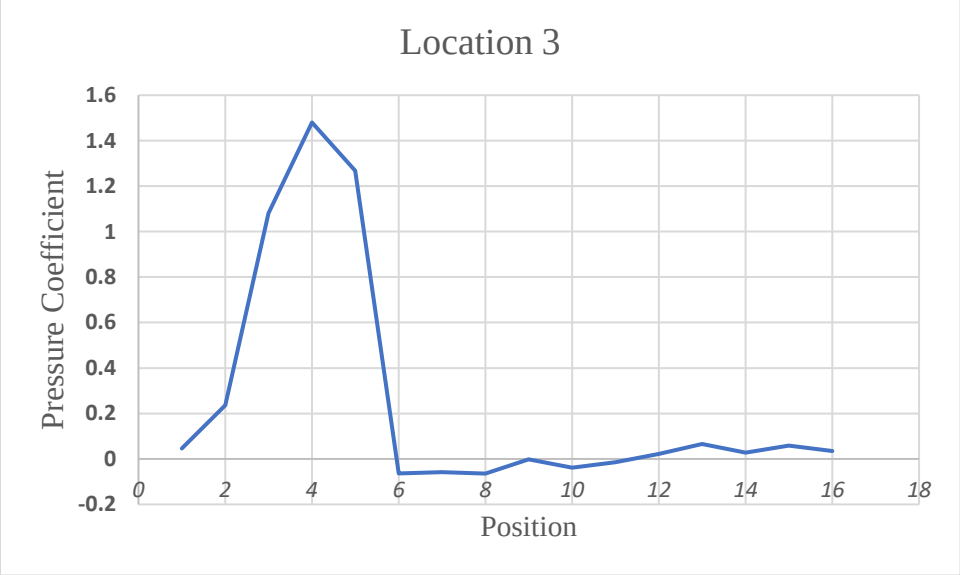
Location 3
Pressure Coefficient
1.6
1.4
1.2
1
0.8
0.6
0.4
0.2
0
-0.2
0
2
4
6
8
10
12
14
16
18
Position

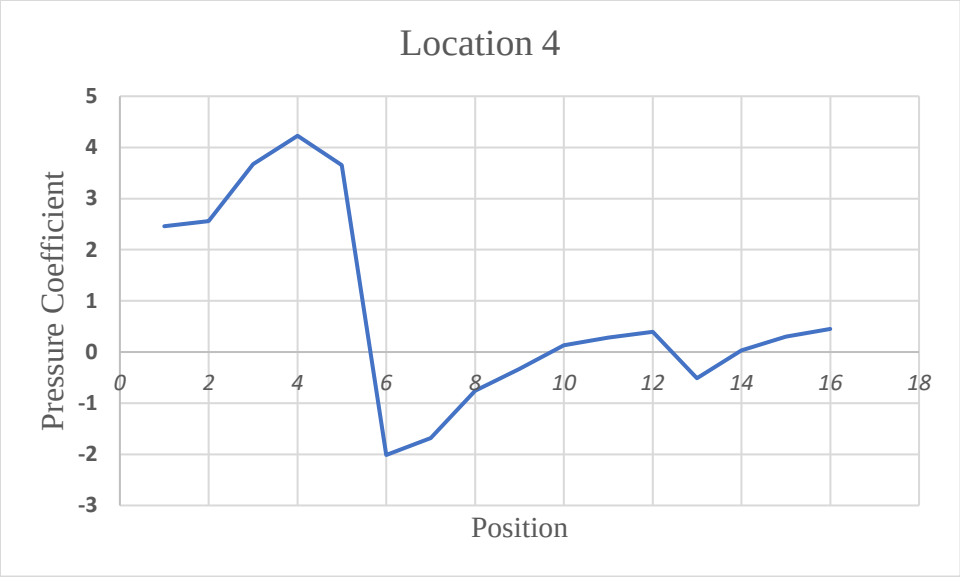
Location 4
Pressure Coefficient
5
4
3
2
1
0
-1
-2
-3
0
2
4
6
8
10
12
14
16
18
Position